Analysis of HIV-1 cell-to-cell transfer to macrophages

Lucie Bracq

UNIVERSITY PARIS DESCARTES-SORBONNE PARIS CITE / INSTITUT COCHIN

UNIVERSITY OF CHINESE ACADEMY OF SCIENCE / INSTITUT PASTEUR OF SHANGHAI

PhD THESIS

Thesis to obtain the degree of PhD of University Paris Descartes and University of Chinese Academy of Sciences

Major: Biology

Specialty: Cellular biology and virology

Presented publicly by Lucie Bracq

17 November 2017

Analysis of HIV-1 cell-to-cell transfer to macrophages.

Committee members:

Dr Alexandre Benmerah	President of committee
Pr Quentin Sattentau	Principal referee
Dr Helene Dutartre	Principal referee
Pr Xia Jin	Referee
Dr Delphine Muriaux	Referee
Pr Andres Alcover	Referee
Dr Serge Benichou	PhD Supervisor
Pr Paul Zhou	PhD Co-supervisor

Analysis of HIV-1 Cell-to-cell transfer to macrophages

Abstract:

Macrophages are important targets of HIV-1 and play crucial roles in physiopathology of infection. Because of their long term survival capacity, infected macrophages participate in virus dissemination and establishment of persistent virus reservoirs in numerous tissues. *In vitro*, macrophage infection and analysis of the different steps of the virus cycle have been largely documented using cell-free virus infection. However, there is a paucity in knowledge of the mechanisms that control infection and dissemination to macrophages by cell-to-cell transfer. In the work presented here, we establish a model of HIV-1 cell-to-cell transfer from infected T cells to macrophages. We observed that infected T cells are able to interact with macrophages leading to cell fusion for transfer of viral material to macrophages targets. This cell-to-cell fusion transfer, very fast and efficient, is restricted to CCR5-tropic viruses, and mediated by viral envelope-receptor interactions. Transferred viruses can then accumulate in cytoplasmic compartments of newly formed lymphocyte/macrophages fused cells but we also observed early viral assembly and budding events at the plasma membrane of these fused cells, resulting from the merging of viral material between infected T cells and macrophages. These cells then acquire the ability to fuse with neighboring non-infected macrophages for virus dissemination. Together, these two-sequential envelope-dependent cell fusion process lead to the formation of highly virus-productive multinucleated giant cells reminiscent of the infected multinucleated giant macrophages detected *in vivo* in lymphoid organs and the central nervous system of HIV-1 infected patients and simian immunodeficiency virus-infected macaques. These mechanisms may represent an original mode of virus transmission for viral spreading and formation of macrophage virus reservoirs during HIV-1 infection.

Keywords : HIV-1, T cell, Macrophages, Cell-to-cell transfer, Cell fusion

Laboratories :

- Virus et trafic intracellulaire.
Institut Cochin – InsermU1016 – CNRS UMR8104 –Université Paris-Descartes, Sorbonne Paris-Cité.
- Antiviral immunity and genetic therapy
Institut Pasteur of Shanghai – Chinese académie of sciences.

Analyse du transfert intercellulaire du VIH-1 vers les macrophages.

Résumé :

Les macrophages sont une cible particulièrement importante de l'infection par le VIH-1 et jouent un rôle crucial dans la physiopathologie de l'infection. Lorsqu'ils sont infectés, leur capacité de survie dans les tissus leur permet de jouer un rôle essentiel dans la dissémination virale et l'établissement de réservoirs viraux au niveau des différents territoires tissulaires. *In vitro*, les étapes précoces et tardives du cycle de réplication virale dans les macrophages ont été analysées dans le cadre de l'infection par des virus libres. Cependant, les modalités d'infection des macrophages lors d'une transmission intercellulaire restent largement inexplorées. Les travaux présentés ici ont permis d'établir un modèle de transmission intercellulaire du VIH-1 des lymphocytes T infectés vers les macrophages. Nous avons montré que les lymphocytes T infectés sont capables d'interagir étroitement avec les macrophages, conduisant ainsi à la fusion cellulaire de ces deux cellules et permettant le transfert de matériel viral dans les macrophages cibles. Ce transfert viral par fusion cellulaire, rapide et efficace, est restreint aux virus utilisant le corécepteur CCR5 et dépend de l'interaction entre l'enveloppe virale et le récepteur CD4. Les virus transférés sont alors stockés au sein de compartiments cytoplasmiques dans les cellules fusionnées mais nous observons également des évènements précoces d'assemblage et de bourgeonnement du VIH-1 à la membrane plasmique des cellules fusionnées, résultant de la fusion des membranes des lymphocytes T infectés et des macrophages cibles. Ces cellules fusionnées acquièrent alors la capacité de fusionner avec les macrophages non infectés environnants permettant la dissémination du VIH-1. L'ensemble de ces résultats met en évidence un nouveau mécanisme de transmission intercellulaire entre lymphocytes T et macrophages via un mécanisme de double fusion cellulaire dépendant de l'enveloppe virale et des récepteurs CD4 et CCR5. Ces évènements successifs de fusion entre lymphocytes T et macrophages puis entre macrophages permettent la formation de cellules géantes multinucléées capables de produire de grande quantité de virus infectieux. Ces cellules multinculéees pourraient correspondre aux macrophages multinucléees observés *in vivo* dans les organes lymphoïdes et le système nerveux central de patients infectés par le VIH-1 ou de singes infectés par le VIS. Ce mécanisme représente donc un modèle de transmission intercellulaire original permettant la dissémination virale et la formation de macrophages réservoirs durant l'infection par le VIH-1.

Mots clés : VIH-1, Lymphocytes T, Macrophages, Transfert intercellulaire, Fusion cellulaire.

Laboratoires :
- Virus et trafic intracellulaire.
Institut Cochin – InsermU1016 – CNRS UMR8104 –Université Paris-Descartes, Sorbonne Paris-Cité.
- Antiviral immunity and genetic therapy
Institut Pasteur of Shanghai – Chinese académie of sciences.

HIV-1向巨噬细胞的细胞到细胞传播分析

摘要：

巨噬细胞是人类免疫缺陷病毒I型（HIV-1）重要的靶细胞并在HIV-1感染病理生理学起着重要作用。由于他们的长期存活性，感染的巨噬细胞在多数组织中参与了病毒传播和长期病毒库的建立。在体外，巨噬细胞的感染和病毒周期的不同阶段分析经由游离病毒颗粒的形式感染早有充分记载。然而，关于病毒向巨噬细胞的细胞到细胞传播控制传播和感染的机理却知之甚少。在本研究中，我们建立了一个HIV-1从感染淋巴细胞到巨噬细胞的细胞到细胞传播模型。我们观察到感染的T细胞能够同巨噬细胞相互作用从而导致细胞融合以实现病毒物质向巨噬细胞靶细胞的转移。这种细胞到细胞的融合传播，非常迅速而且高效，仅限于CCR5嗜性的病毒株，并通过病毒的包膜受体相互作用所介导。被传递的病毒之后能够在新形成的淋巴细胞/巨噬细胞融合细胞的胞质区室中累积，但我们也观察到在融合细胞包膜上的早期病毒组装和出芽过程，这源自于感染淋巴细胞和巨噬细胞的病毒物质的整合。这些细胞进而获得了同相邻未感染巨噬细胞融合的能力以实现病毒传播。总之，这两步连续的依赖包膜的细胞融合过程导致的高病毒产量的多核合胞体的形成令人联想到在体内淋巴器官和HIV-1感染病人和猴免疫缺陷病毒（SIV-1）感染猕猴的中枢神经系统检测到的多核合胞体巨噬细胞。这些机制可能代表了在HIV-1感染中病毒传播散布和巨噬细胞病毒库形成的一种原始的模型。

关键词：HIV-1，淋巴细胞，巨噬细胞，细胞到细胞传播，细胞融合

实验室：

-病毒和细胞内膜泡运输研究组

科钦研究所 - 国家健康与医学研究院Inserm U1016 - 法国国家科研中心CNRS UMR8104 -巴黎笛卡尔大学, 索邦巴黎西贷大学

-抗病毒免疫与遗传治疗研究组

中国科学院上海巴斯德研究所

Acknowledgments

Opening these acknowledgments, I warmly thank Pr Quentin Sattentau, Dr Hélène Dutartre and Pr Xia Jin for their careful reviewing of my thesis manuscript. I am also very thankful to Dr Alexandre Benmerah, president of my thesis jury, and to Prof Andres Alcover and Dr Delphine Muriaux, examinators, for their interest in my thesis project.

J'ai eu la chance durant cette thèse en cotutelle de faire partie de deux équipes dont celle de Serge Benichou à l'institut Cochin et celle de Paul Zhou à l'Institut Pasteur de Shanghai. J'ai donc fait de nombreuses rencontres en France et en Chine à la fois sur le plan professionnel que personnel. Cette cotutelle m'a permis de voyager et de découvrir ce nouveau pays que j'affectionne désormais tant. Je tiens donc particulièrement a remercié Serge Benichou pour m'avoir donné l'opportunité de faire partie de cette aventure mais aussi Paul Zhou qui m'a accueilli dans son équipe et dont j'ai beaucoup appris.

Depuis mon arrivée dans son équipe en 2014 pour mon stage de master, Serge m'a accordé une grande confiance, et une liberté qui m'ont permis de pleinement m'épanouir durant ma thèse. Merci à toi Serge pour les nombreuses discutions scientifiques, opportunités que tu m'as donné mais aussi pour d'un point de vue plus personnel pour les nombreux fous rires (notamment au cours de chinois), les déjeuners au Cafelito, et tous les (très nombreux) bons moments passés qui ont fait que venir travailler au labo chaque matin était un véritable plaisir.

Je pense aussi à tous les membres de l'équipe de Serge Benichou et de Paul Zhou. Merci à Lihong Liu et Weiming Wang d'avoir partagé leurs savoirs avec moi et de m'avoir si bien intégré à mon arrivée à Shanghai. Je remercie aussi Maorong, Marie-christine, Trang, Héloise et Amandine pour avoir partagé de nombreux moments ensemble à l'institut Cochin. Un merci tout particulier à Jérôme Bouchet pour tous tes conseils, pour ton aide et d'avoir partagé avec moi ton expérience mais aussi tous les discutions (pas forcement scientifique) que l'on a eu aux pauses café, dans nos nombreux trajets en train (et parfois en Uber) ou autour d'une bière.

Je souhaite également remercier toutes les personnes qui ont participé à ma formation et permis de réaliser ce travail de thèse. Merci à Julie Matz qui a fait preuve d'une grande douceur et gentillesse à mon arrivée en Master à Cochin et qui a su me donner gout à ce projet sur lequel j'ai tant aimé travailler. Je tiens également à remercier Cécile

Hérate et Clarisse Vigne qui étaient également présente à mon arrivée et qui sont devenus de très bonnes amies depuis et ont beaucoup manqué après leur départ.

Au-delà des membres de l'équipe, je voudrais remercier de nombreuses personnes au sein des deux Instituts. Merci donc aux membres des équipes d'Isabelle Dusanter et Ralf Jockers mais aussi à l'équipe de microscopie électronique pour tous les déjeuners et moments passés ensemble. Du côté chinois, je remercie particulièrement l'équipe de Xia Jin dont Jiayi et Ranran ainsi que Fernando et Laure qui m'ont beaucoup aidé lorsque ma compréhension plus que limité du chinois me limitait énormément.

J'ai eu la chance lors de cette thèse de collaborer avec plusieurs équipes qui ont ainsi partagé leur savoir et leurs bonne humer avec moi. Je remercie donc toute l'équipe de Clotilde Randriamampita mais aussi l'équipe de Christel Vérollet et particulièrement Maeva qui est venu passé quelques mois à Cochin avec qui se fut un plaisir de travailler.

Je remercie aussi les membres des plateformes scientifiques de l'Institut Cochin et de l'Institut Pasteur de Shanghai qui m'ont aidé et conseiller durant ces quatres années. Mais également les différentes gestionnaires, Véronique Chauvin et Xiaoyu pour leur aide et leur bonne humeur.

Si j'ai eu le courage de partir passé de nombreux mois à Shanghai c'est grâce au soutien de ma famille et particulièrement de mes parents et mes sœurs que je remercie pour tout, mais aussi de mes amis. Un grand merci donc à Anthony, Kim, Juliette, Clara et tous les autres, de m'avoir tout d'abord poussé à partir, d'avoir toujours été présent a chacun et mes retours mais aussi d'avoir supporté mes longues tirades sur la chine a mes retours en France. Merci particulier à Kim, Clara et à ma famille qui sont venus me rendre visite à Shanghai.

Pour finir merci à tous ceux qui ont fait que chaque moment passé à Shanghai était un réel plaisir. Un immense merci à Antoine qui a été le premier que j'ai rencontré, qui m'a permis de rencontrer tant d'amis, avec qui j'ai passé tant de bons moments et qui restera le meilleur coloc que j'ai pu avoir. Merci à Clara, Cécile, Victoria Oliver et tant d'autres avec qui j'ai partagé mon quotidien, mes galères et mes bonheurs pendant ces années et qui sont devenus ma deuxième famille à l'autre bout du monde. Enfin je tiens à remercier Marie, qui suit le même parcours que le miens et avec qui nous nous sommes beaucoup soutenus pendant les moments plus compliqués mais aussi dans les bons lorsque nous allions « zapater » autour d'une marguarita. Je te souhaite bon courage pour la fin de ta thèse et espère te revoir rapidement à Shanghai.

`

Table of Contents

Table of Figures

Abreviations

AIDS : Acquired immunodeficiency syndrome

AMP : Adenosine monophosphate

APC : Antigen presenting cell

ART : Anti-retroviral therapy

APOBEC : *Apolipoprotein BmRNA-editing catalytic polyprotein*

AP1 : *Adaptator protein complex 1*

AZT : Azidothymidine

BST2 : *Bone marrow stromal antigen 2*

CCR5 : *C-C Chemokine receptor 5*

CD4 : Cluster of differentiation 4

CXCR4 : CXC Chemokine receptor 4

CDC42 : Cell division control protein 42

CNS : Central nervous system

DC : Dendritic cell

DAP12 : DNAX activation protein of 12kb

DC-SIGN : *Dendritic cell-specific intracellular adhesion molecule grabbing non-integrin*

DC-STAMP : Dendrocyte expressed seven transmembrane protein

dNTP : Deoxynucleoside triphosphate

DNA : Deoxyribonucleoside acid

DNM2 : Dyanamin 2

EEA-1 : Early endosomal antigen 1

ELISA : Enzyme-linked immunosorbent assay

EM : Electron microscopy

GMCSF : Granulocyte macrophage colony-stimulation factor

HAART : *Highly active retroviral therapy*

HCK : Hematopoietic cell kinase

HIV : Human immunodeficiency virus

HTLV : Human T-cell leukemia-lymphoma virus

IL-4 : Interleukin-4

ICAM-1 : *Intracellular adhesion molecule 1*

IN : Integrase

IFN : Interferon

IFITM : Interferon-induced transmembrane protein

KIR : Killer-cell immunoglobulin like receptor

LAMP-1 : *Lysosomal-associated membrane protein 1*

LFMC : Lymphocyte/macrophage fused cell

LFA-1 : *Lymphocyte function associated antigen 1*

MA : Matrix

MDM : Monocyte derived macrophage

MHC : Major histocompatibility complex

MMP9 : Matrix metallopeptidase

MLV : Murine leukemia virus

MGC : Multinucleated giant cell

MTOC : Microtubule organizing center

NC : Nucleocapsid

Nef : Negative factor

NK : Natural killer

NRTI : Nucleosidic reverse transcriptase inhibitor

NNRTI : Non-nucleosidic reverse transcriptase inhibitor

OC : Osteoclast

PtdSer : Phosphatidyl Serine

PAMP : Pathogen-associated molecular pattern

PIC : Pre integration complex

RANKL : Receptor activator of nuclear factor kappa-B ligand

Rev : Regulator of expression of virion proteins

RNA : Ribonucleic acid

RT : Reverse transcriptase

SIV : Simian immunodeficiency virus

SAMHDI : Sterile alpha motif and HD domain-containing protein- 1

SIRPa : Signal regulated protein alpha

STAT6 : Signal transducer and activator or transcription 6

SYK : Spleen tyrosine kinase

TRAIL : Tumor-necrosis-factor related apoptosis inducing ligand

TNF : Tumor-necrosis factor

Tat : Trans-activator

TCR : T-cell receptor

TSP : Surface-bound thrombospondin

TSPAN : Tetraspanin

VCC : Virus containing compartment

Vif : Viral infectivity factor

Vpr : Viral protein R

Vpu : Viral protein U

VS : Virological synapse

INTRODUCTION

1. The Human immunodeficiency virus

1.1. Physiopathology of HIV-1 infection

The Human Immunodeficiency Virus (HIV) is the causative agent of the acquired immunodeficiency syndrome (AIDS). In 2016, 36.7 million people were living with HIV, with 1.8 million people newly infected in 2016 (World Health Organization website). Two types of HIVs are known to cause AIDS: HIV-1 and HIV-2, exhibiting distinct biological and epidemiological attributes. Whereas HIV-1 has world wild distribution, HIV-2 remains confined to West Africa and is characterized by low transmission and slow progression to AIDS (Gilbert *et al*, 2003). The Sub-Saharan region of Africa is the most affected region with approximatively two thirds of HIV-1 infected people living in this area (Tebit & Arts, 2011). Therefore, HIV is a major global public health issue since more than 35 million people died so far from AIDS since the beginning of the epidemic in 1980. Until now, no cure or vaccine are available but the appearance and development of antiretroviral therapy in the early 1990s led to a significant decrease of AIDS related death and morbidity in HIV-infected patients (Figure 1).

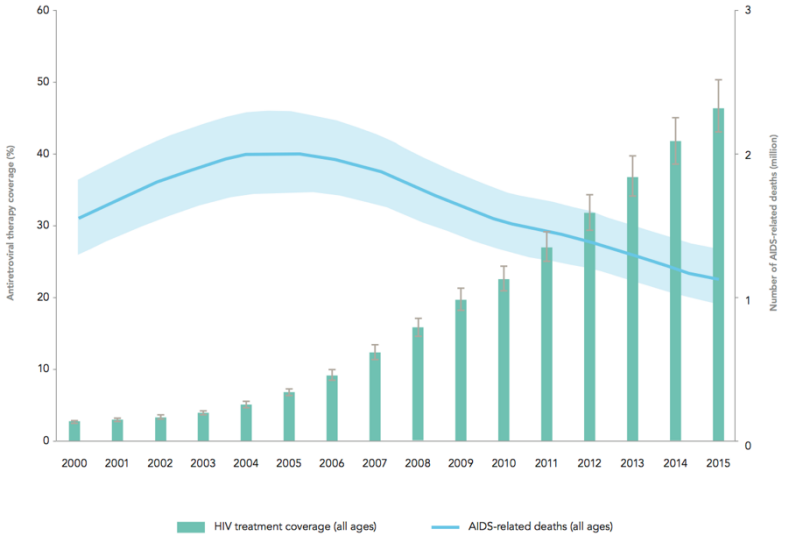

Figure 1: Antiretroviral therapy coverage and number of AIDS-related deaths.
Representation of HIV-1 treatment coverage and AIDS-related deaths from 2000 to 2015. From UNAIDS 2016.

HIV-1 is a lentivirus transmitted through mucosa or blood. In infected patients, a common pattern of three different stages is observed with an extended incubation period (median of 10 years) varying among patients. Each stage is characterized by the viral load (number of viral RNA copy/mm^3 of plasma) and the number of circulating CD4+ T cells (Figure 2).

The first stage of HIV-1 infection is an acute phase, which generally develops within 3 to 6 weeks after the initial infection and is characterized by a high viral load due to viral replication of HIV-1 in peripheral blood mononuclear cells (Pantaleo *et al*, 1993). This active replication leads to a rapid but transient decrease of the number of circulating CD4+ T cells. 50 to 70% of infected patients have flu-like symptoms during this phase, such as fever, headache and/or rash. This phase is also characterized by the development of an HIV-specific immune response leading to a rapid decrease of viral load after several weeks. However, this immunity is not sufficient to suppress viral replication completely since HIV-1 expression persists in lymph nodes even when plasma viral load is very low or when viral RNA is undetectable in peripheral blood mononuclear cells (Pantaleo *et al*, 1993).

The second stage of HIV infection is the chronic phase, and is also called asymptomatic phase or clinical latency. During this stage of infection, the virus continues to replicate in lymph nodes but at very low levels. This low viral replication is related to both humoral and cellular immune responses. During clinical latency, high levels of HIV-1 specific antibodies and cytotoxic CD8+ T cells are observed, and this immune response leads to the killing of infected CD4+ T cells, responsible, at least in part, for the progressive decrease of circulating CD4+ T cells (McCune, 2001). Without treatment with antiretroviral therapy, chronic HIV infection usually progresses to AIDS in 10 years or longer, though it may take less time for some patients. The USA centers for disease control and prevention defined this chronic stage by a CD4+ T cell number between 200 and 499 cells/mm^3. The world health organization recommends starting antiretroviral therapy if the number of CD4+ T cells goes below 350 cells/mm^3.

When the number of CD4+ T cells is below 200 cells/mm^3, the patient is in the clinical stage of AIDS. Loss of cytotoxic CD8+ T cells and immune response are thus observed whereas the viral load increases rapidly. Severe immunodeficiency leads to severe symptoms and opportunistic infections such as pneumonia, tuberculosis, cancer or neurologic diseases leading to the death of infected patients.

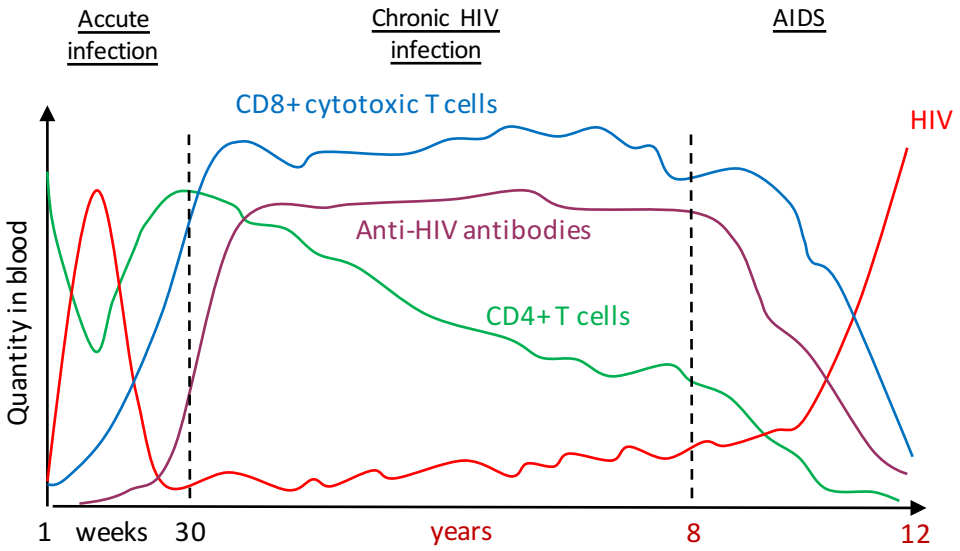

Figure 2: Evolution of HIV-1 infection.
During the first week after HIV-1 infection, virus multiplies actively (red line) and the level of HIV-1 increases whereas the number of CD4+ lymphocyte decreases (green line). 6 weeks after infection, the immune response leads to the presence of HIV-1 targeting antibodies (purple line) and activation of CD8+ cytotoxic T lymphocytes (blue line). During chronic infection, the viral load is low, because of immune response of cytotoxic T cells however the number of CD4+ T cells decrease progressively leading to AIDS where the immune system collapses and viral load increases dramatically. From (Pantaleo *et al*, 1993).

1.2. General presentation of HIV-1

1.2.1. Structure and genome

HIV is an enveloped virus that belongs to the *Retroviridae* family and *Lentivirus* genus. HIV-1 particles are spherical with an average diameter of 100 nm and are coated by the viral envelope membrane. The viral membrane is a lipid bilayer derived from the membrane of the host cell containing the viral envelope glycoproteins, the surface gp120 and the transmembrane gp41, generated from the cleavage of the viral glycoprotein precursor gp160 encoded by the *env* gene (Freed, 2001). These envelope glycoproteins are present on the cell surface of infected cells as the envelope complex, a trimer of heterodimers of gp120 and gp41, and are incorporated into the lipid bilayer through the transmembrane region of gp41 (White *et al*, 2010). During viral budding from the plasma membrane of the host cell, around 7 to 14 trimers of envelope are incorporated in a single virus particle (Chertova *et al*, 2002; Cosson, 1996). The inner leaflet of the envelope lipid membrane is lined with the matrix protein p17 which surrounds a conical capsid composed

of the capsid protein p24. This capsid encloses two copies of the viral single-stranded RNA, approximatively 10,000 bases long, that are linked together through non-covalent interactions. The HIV-1 RNA is part of a nucleoprotein complex, which is composed of the nucleoprotein p7 and the reverse transcriptase p66 (RT). The viral particle also contains all the enzymatic equipment that is necessary for replication: the reverse transcriptase (RT), the integrase p32 and the protease (Figure 3).

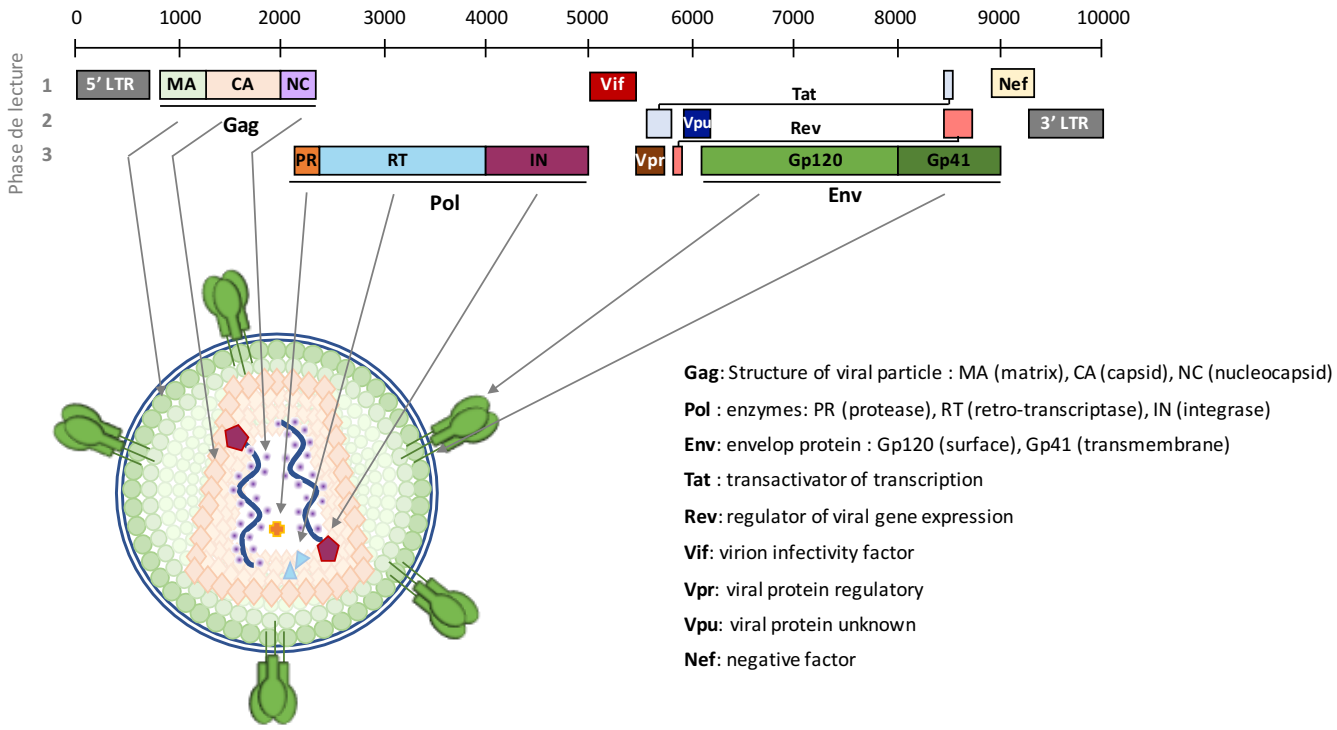

Figure 3: Genomic and structural organization of HIV-1.
The HIV-1 genome contains three major genes (*Gag, Pol* and *Env*) encoding for structural polyproteins, enzyme and envelope proteins. In addition, HIV-1 encodes for regulatory and auxiliary proteins (Tat, Rev, Vif, Vpr, Vpu and Nef). From (Ganser-Pornillos *et al*, 2008).

The HIV-1 genome contains the three major genes that are found in all retroviruses, *gag*, *pol* and *env* encoding respectively for structural proteins of the viral core and matrix, enzymes and envelope glycoproteins. These proteins are first synthesized as polyproteins and then cleaved resulting in all the viral proteins present in virions. The HIV-1 genome also contains nonstructural genes (or accessory) encoding for auxiliary proteins (Vif, Vpr, Vpu and Nef) and regulatory proteins (Tat and Rev) (Figure 3 and Table 1).

Class	Gene name	Primary protein products	Processed protein products
Viral structural proteins	*Gag*	Gag polyprotein	MA, CA, SP1, NC, SP2, P6
	Pol	Pol polyprotein	RT, Rnase H, IN, PR
	Env	Gp160	Gp120, Gp41
Essential regulatory proteins	*Tat*	Tat	
	Rev	Rev	
Accessory regulatory proteins	*Nef*	Nef	
	Vpr	Vpr	
	Vif	Vif	
	Vpu	Vpu	

Table 1: Proteins encoded by the HIV-1 genome.
The HIV-1 genome encodes for structural, regulatory and auxiliary proteins as well as enzymes. The viral proteins can be directly synthesized as primary protein products or first synthesized as polyproteins and then cleaved resulting in processed protein products.

1.2.2. Target cells of HIV-1

1.2.2.1. T lymphocytes

One major characteristics of the HIV-1 infection is the loss of CD4+ T lymphocytes which are thus the main targets of the virus and have been the most studied target cells. HIV-1 infection and replication are highly efficient in activated CD4+ T cells compared to resting CD4+ T cells. CD4+ T lymphocytes express CD4 as well as the coreceptor CXCR4 and CCR5 leading to their infection by a large amount of viral strains (Jolly *et al*, 2004). CD4+ T cells can be directly infected by cell-free viruses, but they can also be infected through cell-to-cell transmission of viruses from other infected donor T cells (Jolly & Sattentau, 2005; Jolly *et al*, 2004), dendritic cells (DC) (Dong *et al*, 2007) or macrophages (Duncan *et al*, 2014; Giese & Marsh, 2014).

1.2.2.2. Monocytes/Macrophages

Macrophages derived from blood monocytes are important targets for HIV-1 infection since they also express the CD4 receptor and the CXCR4 and CCR5 coreceptor. However, whereas CD4+ T lymphocytes die quickly after infection (within 48 h) (Perelson *et al*, 1996), macrophages are more resistant to the cytopathic effect of HIV-1 and thus may participate in the establishment of viral reservoirs in host tissues (see 3.3.1 section – viral reservoirs). Furthermore, monocytes can migrate in a lot of different tissues where they differentiate into macrophages allowing efficient dissemination of HIV-1 in the organism (Kumar & Herbein, 2014). Differentiated macrophages can be infected by cell-free viruses but are less permissive, at least *in vitro*, than T cells, and they can also transmit the virus to T cells through cell-to-cell contacts. However, only a single study describing cell-to-cell

infection of macrophages from infected T cell was reported so far in the literature (see 2.4 section – Engulfment of infected T cells by macrophages).

1.2.2.3. Dendritic cells.

Dendritic cells (DCs) have either myeloid or lymphoid origins and are divided in different subsets depending on their anatomical distribution and functions. The main dendritic cell subset includes myeloid DCs, derived from the same cell progenitors as macrophages, plasmocytoid DCs (pDC) present in low frequency in blood, and Langerhans cells present in tissues (skin, mucosa and other stratified squamous epithelia). In the mucosa, dendritic cells as well as macrophages are present and may correspond to the first cells infected during HIV-1 infection. Myeloid DCs, pDCs and Langerhans cells are all susceptible to HIV-1 infection (Wu & KewalRamani, 2006) but HIV-1 replication in DCs is generally less productive compared to T cells, and the frequency of HIV-1 infected DCs *in vivo* is often 10 to 100-fold lower (McIlroy *et al*, 1995).

Early studies suggested that DCs are able to bind and capture HIV-1 in mucosal tissues through the interaction between HIV-1 envelope glycoprotein and C-type lectin receptor DC-SIGN (Geijtenbeek *et al*, 2000; McDonald *et al*, 2003), which will be thus stored for weeks and maybe months in a nonacidic internal compartment without any replication (Smith *et al*, 2001). DCs then migrate to lymph nodes where they interact and transfer HIV-1 to CD4+ T cells. More recently, another receptor, Siglec-1 (or CD169) has been identified as a new receptor able to bind HIV-1 for capture of HIV-1 in DCs and transfer to CD4+ T cells (Izquierdo-Useros *et al*, 2012). Through this process, DCs can then efficiently transmit HIV-1 to CD4+ T for virus dissemination. This transfer will be described later in detail (see 2.4.1 section - The infectious synapse).

1.2.3. Viral entry and tropism

CD4+ T cells, DCs, monocytes and macrophages, which are target cells of HIV-1, all express the CD4 receptor at the cell surface required for virus entry (Klatzmann *et al*, 1984). The first step of viral entry is the binding of HIV-1 envelope glycoprotein gp120 to CD4 receptor expressed on target cells (Figure 4). The binding of CD4 with gp120, which contains five conserved domains (C1-C5) and five variable loops (V1-V5), induces rearrangement of V1/V2 and subsequently V3 loop of gp120 that favors exposure of a co-receptor binding surface on gp120. Co-receptor binding to the binding site of gp120 leads to the exposure of the hydrophobic gp41 fusion peptide which inserts into the host cell

membrane thus tethering the viral and host membrane resulting in the formation of a fusion pore and efficient fusion between viral membrane and plasma membrane of the cell.

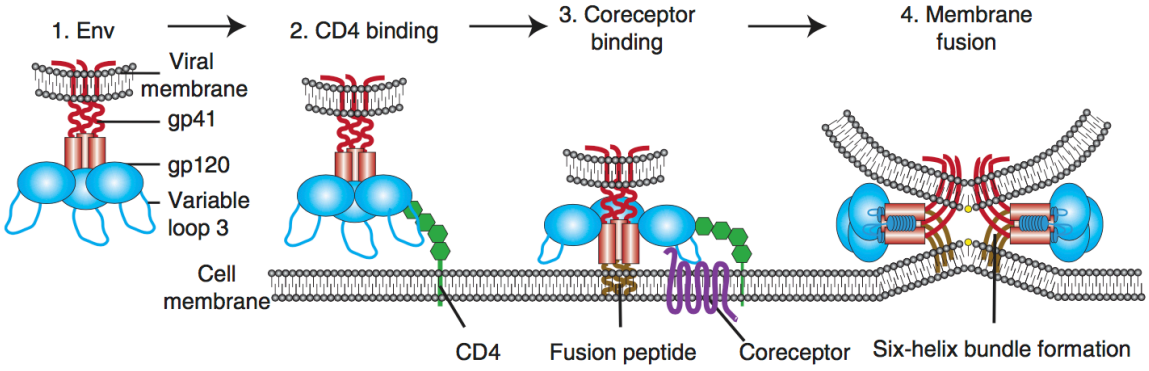

Figure 4: Schematic representation of HIV-1 binding and fusion.
During HIV-1 entry, the viral envelope (Env) binds CD4 receptor on the plasma membrane of target cells. Conformational changes in Env result in the engagement of the co-receptor, insertion of the fusion peptide and ultimately membrane fusion. From (Wilen *et al*, 2012).

In addition to CD4, HIV-1 also uses two chemokines receptors as co-receptor for virus entry: CXCR4 and/or CCR5. These receptors are seven-transmembrane G-protein coupled receptors and are involved in different cell-signaling pathways (Alkhatib, 2009). CXCR4 is a ubiquitously expressed protein while CCR5 in only expressed on immune cells such as macrophages, DCs and T cells. HIV-1 strains are divided according to their co-receptor usage: while X4 viruses use CXCR4 as co-receptor, R5 viruses use CCR5, and R5X4 strains use both co-receptors. The cell-tropism of the viral strains, X5, R5 or R5X4 was defined regarding the ability of the HIV-1 envelope glycoprotein gp120 to recognize respectively CXCR4, CCR5 or both (Berger *et al*, 1998). Usually, most of the viruses involved in primary infection are R5-tropic whereas most of the viruses during the symptomatic AIDS stage are X4-tropic viruses (Connor *et al*, 1997; Scarlatti *et al*, 1997).

1.2.4. HIV-1 life cycle

HIV enters the cell through initial interactions between viral surface glycoproteins gp120 and cellular receptors CD4 and CXCR4 or CCR5. This binding leads to the fusion of the viral envelope with the host cell plasma membrane. Once in the cytoplasm, the viral core is uncoated, leading to the release in the cytoplasm of the viral genome and the enzyme required for the reverse transcription of viral RNA into double-strand viral DNA. As the first DNA strand is synthesized, the viral RNA is degraded by the enzyme RNase H, allowing synthesis of the complementary DNA. The newly synthesized double-stranded viral DNA, together with the integrase enzyme, and auxiliary proteins such as Vpr, form the pre-integration complex (PIC). This PIC is translocated from the cytoplasm to the nucleus

through the nuclear pore complex by an active mechanism. Once in the nucleus, viral DNA is integrated into the host cell genome by the integrase enzyme. The integrated viral genome will be then transcribed upon transcription of the host genome. The mRNAs and genomic RNA are transported to the cytoplasm where mRNAs are translated into viral proteins. After synthesis of viral proteins, HIV-1 proteins and viral genomic RNA are trafficked to the plasma membrane where they are assembled into new immature viral particles leading to budding and release of immature virions. In macrophages, assembly and budding does not take place at the plasma membrane but in internal compartments continuous with the plasma membrane. This specific step of viral replication in macrophages will be described later in more details (see 3.4 section – HIV-1 replication in macrophages). In the newly released viral particles the cleavage of the gag-pol polyprotein by the viral enzyme protease results in the maturation of the viral particles (Figure 5).

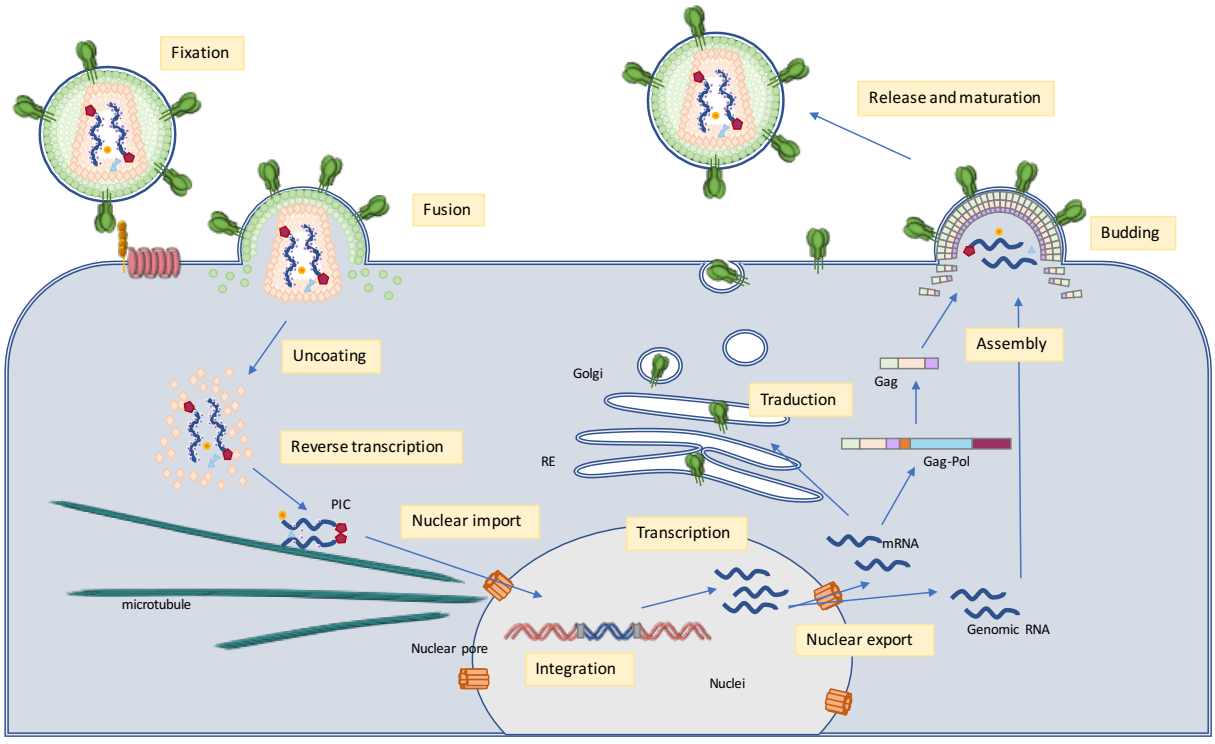

Figure 5: Simplified representation of HIV-1 life cycle.
The envelope glycoprotein (Env) recognizes the CD4 receptor and co-receptor at the surface of the target cell. Viral envelope fuses with the plasma membrane leading to the release of the HIV-1 capsid into the cytoplasm. Viral RNA is then uncoated, reverse transcribed into double-stranded cDNA, and imported into the nuclei where viral DNA is integrated in the genomic DNA of the target cell. It is then transcribed into mRNA and genomic RNA is exported back to the cytoplasm. mRNAs are translated into viral proteins which assemble at the plasma membrane with genomic RNA for budding of new immature viral particle. Once released into the extracellular space, HIV-1 becomes mature. From (Ganser-Pornillos *et al*, 2008).

2. Mechanisms of cell-to-cell transmission of HIV-1

2.1. Cell-free and cell-to-cell infection

It is now well documented by numerous studies that in addition to cell-free infection, HIV-1 is able to infect target cells through cell-to-cell contacts with a virus infected-donor cell (Sattentau, 2008). At least *in vitro*, the establishment of cell-to-cell contacts between infected donor CD4+ T cells and target T cells leads to a massive and very efficient infection that may be 100-1000 times more efficient than cell-free infection (Carr *et al*, 1999; Chen *et al*, 2007; Dimitrov *et al*, 1993; Martin & Sattentau, 2009; Phillips, 1994). It is difficult to quantify the contribution of cell-free and cell-to-cell infection by HIV-1 *in vivo*, but some reports show that cell-to-cell infection could be the main route of HIV-1 infection *in vivo* (Sourisseau *et al*, 2007; Zhong *et al*, 2013). Recently, using mathematical models, Iwami et al. estimated that viral cell-to-cell transfer may correspond to about 60% of total HIV-1 infection in infected patients (Iwami *et al*, 2015) showing the relevance of HIV-1 cell-to-cell transmission studies.

The efficiency of cell-to-cell infection between CD4+ T cells has been related to the high multiplicity of infection (MOI) at the cell-cell contact site probably leading to the integration of multiple proviruses in the target cell (Agosto *et al*, 2014; Zhong *et al*, 2013). The high efficiency of cell-to-cell infection was also proposed to be responsible for partial escape to antiretroviral therapy (ART) and neutralizing antibodies (Sigal *et al*, 2011) but these results are controversial and will be discussed below in the manuscript (Agosto *et al*, 2015; Chen *et al*, 2007; Permanyer *et al*, 2012) (see 2.3 section - Virological synapses).

Several different structures have been described over the past years for cell-to-cell transmission of HIV-1 *in vitro*. Intercellular transfer of viral material can occur through cytoplasmic protrusions (tunneling nanotubes), membrane exchange (trogocytosis), establishment of infectious or virological synapses, cell fusion or cell engulfment. These different cell-to-cell structures will be described below.

2.2. Nanotubes and trogocytosis

2.2.1. Nanotubes and filopodia

In a physiological context, cells can communicate through different pathways including cytoplasmic protrusions. Different types of membrane protrusions between two cells have been described in a large variety of cells such as neurons, glial cells and cells of the immune system (B, T and Natural Killer cells, neutrophils, dendritic cells and macrophages) both *in vitro* (Aggarwal *et al*, 2012; Rustom *et al*, 2004; Sherer *et al*, 2007) and *in vivo* (Chinnery *et al*, 2008; Lou *et al*, 2012; Pasquier *et al*, 2013; Seyed-Razavi *et al*, 2013).

Two different types of nanotubes have been described corresponding to close-ended nanotubes and open-ended nanotubes (also called tunneling nanotubes) (Kimura *et al*, 2013; Marzo *et al*, 2012; Onfelt *et al*, 2004). Intercellular communications involving tunneling nanotubes were first observed in 2004 and were described as a F-actin-containing membrane extension able to connect distant cells during minutes to hours (Rustom *et al*, 2004). Tunneling nanotubes are fragile and dynamic structures extended up to 100 µm in length with diameters ranging from 50 to 200 nm, and are not attached to the substratum (Rustom *et al*, 2004). Tunneling nanotubes can mediate and facilitate the transfer of cytoplasmic and cell-surface molecules and components between cells, but also cellular organelles (mitochondria)(Marzo *et al*, 2012).

Several studies showed that HIV-1 is able to use tunneling nanotube networks to move from one cell to another leading to virus cell-to-cell transfer. HIV-1 can thus be transferred through intracellular vesicles or by surfing along tunneling nanotubes (Eugenin *et al*, 2009; Sowinski *et al*, 2008) (Figure 6). The frequency of tunneling nanotube formation is not affected by HIV-1 in T cells (Sowinski *et al*, 2008) whereas, in macrophages, it was reported that the HIV-1 auxiliary protein Nef, together with the scaffolding protein M-Sec, may promote tunneling nanotubes formation (Eugenin *et al*, 2009; Hashimoto *et al*, 2016).

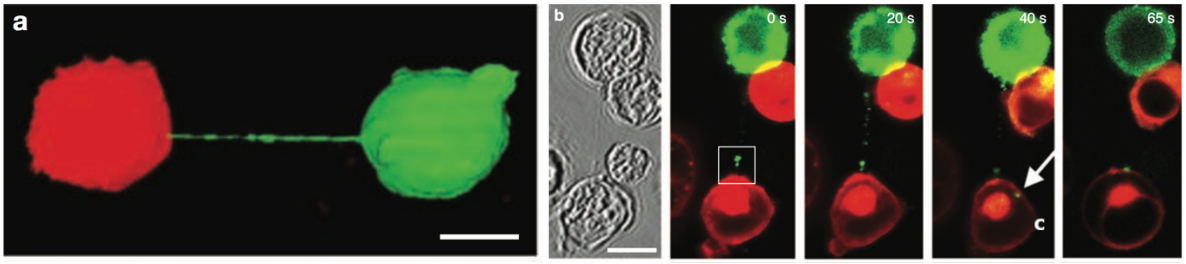

Figure 6: HIV-1 transfer across nanotubes in T cells.
a) Long membrane tethers, or membrane nanotubes, readily form between Jurkat T cells labelled with DiO (green) and DiD (red), *n* >500. b) Time-lapse imaging of Gag-GFP (green), expressed in the context of the fully infectious virus, along a membrane nanotube connecting infected with uninfected Jurkat T cells (stained with membrane dye DiD; red; *n* = 8). (Sowinski *et al*, 2008)

Another way of viral cell-to-cell transmission through membrane extension involving formation of filopodia was first described for transmission of the retroviral murine leukemia virus (MLV) (Sherer *et al*, 2007). Filopodia are F-actin-rich thin plasma membrane extensions, in contact with the substrate, that are involved in several cellular functions, such as chemo-migration, growth of nerve cones and formation of cell-cell contacts. Filopodia have been observed in HIV-1 infected cells expressing CD4 and CXCR4 where virus can "surf" on the outside of filopodia, and this process is dependent on the interaction between Env and the CD4 receptor (Lehmann *et al*, 2005; Sherer *et al*, 2007). Thus, unlike nanotubes, filopodia are attached with the substratum and dependent on the interaction between the receptor CD4 and HIV-1 envelope glycoprotein gp120.

2.2.2. Trogocytosis

During the formation of the immunological synapse with antigen-presenting cells (APCs), membrane patches containing transmembrane proteins can be bi-directionally transferred from the surface of one cell to another one (Figure 7). This mechanism of membrane exchange is called trogocytosis (from the greek *trogo* meaning "gnaw"). Using trogocytosis, CD4+, CD8+ T cells or natural killer (NK) cells are able to capture membrane fragments from APC during antigen presentation (Joly & Hudrisier, 2003). Indeed CD4+, and CD8+ T cells are able to capture major histocompatibility complex class I or class II (MHC-I-and MHC-II), respectively, as well as the intracellular adhesion molecule ICAM-1 and the costimulatory molecules B7-1 (CD80), B7-2 (CD86), (Caumartin *et al*, 2006). Natural killer cells can also perform trogocytosis and thus acquire MHC-I or -II and transfer of the killer-cell immunoglobulin like (KIR) receptor expressed on natural killer cells, to T cells. One study reported that these membrane exchanges could also be involved in HIV-1 cell-to-cell transfer by increasing viral transfer during contacts between infected cells and

target cells (Blanco *et al*, 2004). Another study also reported some cases of trogocytosis between CD4+ and CD8+ T cells enabling the transfer of the CD4 receptor to CD8+ T cells (Aucher *et al*, 2010), suggesting that CD8+ T cells, expressing CD4 after trogocytosis from CD4+ T cells can acquire the ability to bind to HIV-1 leading to syncytia formation. The mechanism of trogocytosis is not well understood in the context of HIV-1 infection but may have important implications during the virological synapse process (described below).

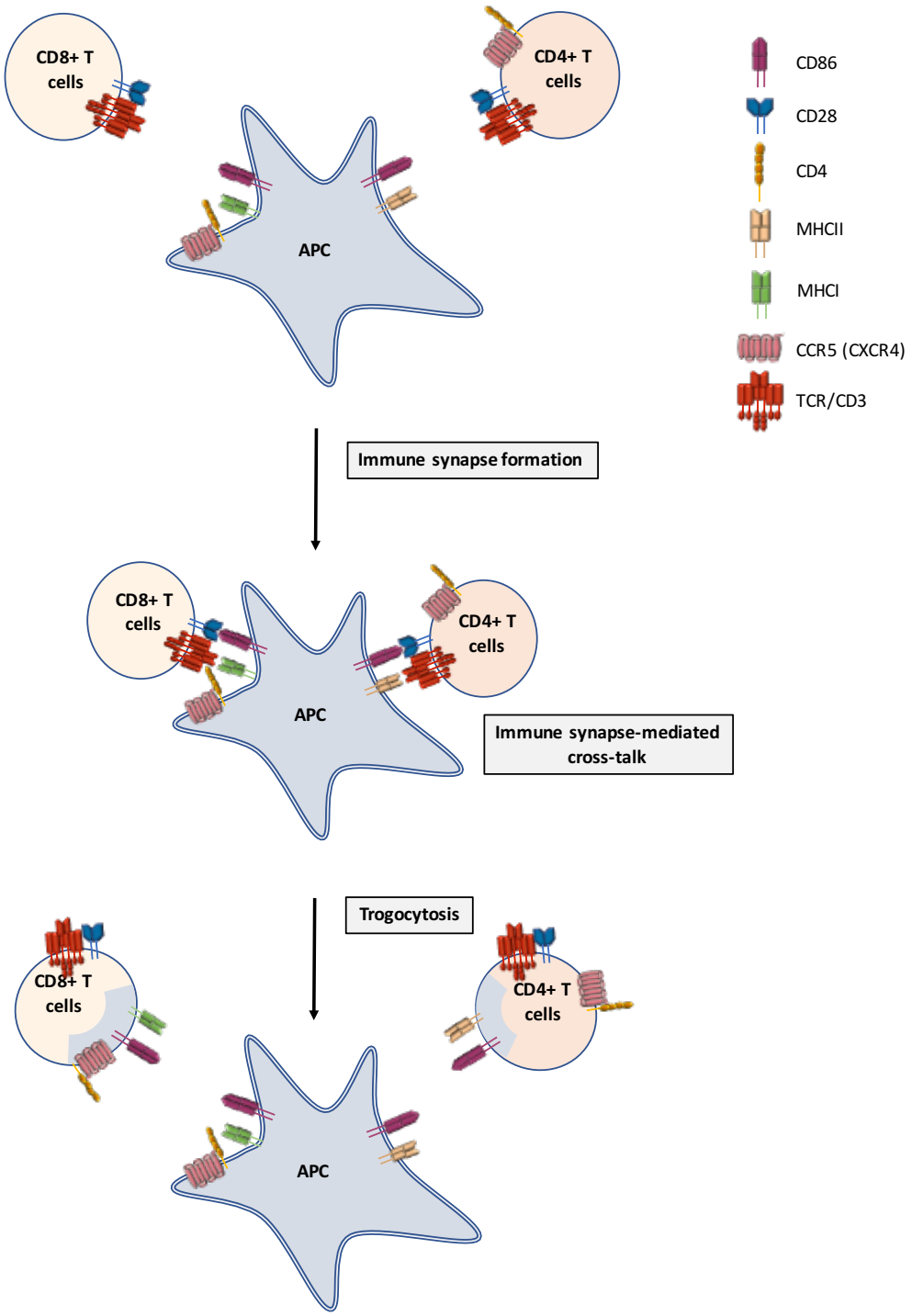

Figure 7: Schematic illustration of a trogocytosis process between an antigen-presenting cell (APC) and $CD4^+$ and $CD8^+$ T cells.

During antigen presentation, APC, $CD4^+$ and $CD8^+$ T cells form immunological synapses, and upon dissociation of these synapses uproot membrane patches from APC. Thus, after immunological synapse dissociation, $CD4^+$ and $CD8^+$ T cells acquire APC specific components. (Caumartin *et al*, 2006)

2.3. The Virological synapses

The formation of a so-called virological synapse is the major and well-established route for viral cell-to-cell infection, and was first described in the context of HTLV-1 (Human T-lympho-tropic virus) infection as a close and organized cell-to-cell contact between an infected donor cell and a target cell, enabling the transfer of viral material between the two cells (Igakura *et al*, 2003). The virological synapse has been named from some homologies with the immunological synapse formed between APCs and T cells for antigen presentation. During the formation of the immunological synapse, binding of the T-cell receptor (TCR) to the MHC-peptide complex expressed at the surface of APCs leads to T cell activation by transducing signals that cause transcriptional up-regulation of numerous genes and cell-proliferation (Huppa & Davis, 2003). The immunological synapse is very stable due to the interaction between the integrin Lymphocyte Function-Associated Adhesion molecule (LFA-1) and its ligand Intracellular Adhesion Molecule-1 (ICAM-1) but also through the interaction between the costimulatory receptor CD28 and its ligand CD86. The virological synapse has also been described in the context of HIV-1 infection and will be described in detail here.

2.3.1. Structure of the virological synapse

The virological synapse between HIV-1 infected cells was defined by the group of Quentin Sattentau as a cytoskeleton-dependent, stable adhesive junction across which virus is transmitted by directed transfer (Jolly & Sattentau, 2004). The virological synapse shares several common features with the immunological synapse. Indeed, formation of both virological and immunological synapses involves the recruitment of receptors and cell adhesion molecules to an adhesive interface in an actin-dependent manner. I will here focus on the structure of the virological synapse established between a donor infected CD4+ T cell and a T cell target which has been the best documented. The specific synapses formed between T cells and DCs or macrophages will be described after (see 2.4 – heterogeneity of the virological synapses).

The virological synapse is a dynamic structure initiated by the recognition of the CD4 receptor at the surface of the target T cell by the HIV-1 envelope-surface glycoprotein gp120 expressed at the surface of the infected T cell (Figure 8). This interaction allows the recruitment of the Gag precursor to the intercellular interface (Jolly *et al*, 2004). The interaction between gp120 and CD4 is essential for the formation of the virological synapse

since a total inhibition of the formation of cell- cell conjugates and viral transfer was observed when gp120/CD4 interactions were blocked (Chen *et al*, 2007; Puigdomènech *et al*, 2008). This first step induces the recruitment of co-receptors CXCR4 or CCR5, adhesion molecules LFA-1, ICAM-1, actin, and other cell surface proteins such as tetraspanins to the contact site for stabilization of the virological synapse and efficient viral transfer. While some studies suggested that the formation of the virological synapse and virus transfer between CD4+ T cells at the virological synapse was independent of the co-receptor usage (Blanco *et al*, 2004; Chen *et al*, 2007; Jolly *et al*, 2004; Puigdomènech *et al*, 2008), other reports showed that the formation of the virological synapse and virus transfer required co-receptor expression and was inhibited by co-receptor antagonists (Dale *et al*, 2011; Felts *et al*, 2010, 2009; Hübner *et al*, 2009; Martin *et al*, 2010). This discrepancy could be explained by different assays since some teams looked at viral transfer when others analyzed viral production following virological synapse transfer. In this case co-receptor usage could have no effect on virological synapse formation but could be required for efficient infection after HIV-1 transfer across the virological synapse.

Similarly, the implication of LFA-1 and ICAM-1 is still a matter of debate. Initially, interaction between LFA-1 and ICAM-1, has been proposed to stabilize the virological synapse for efficient viral transfer. Jolly et al. first demonstrated that antibodies against LFA-1 and ICAM-1 were able to partially block the formation of the virological synapse (Jolly *et al*, 2007b). However, the percentages of inhibition were very different depending on the antibody used (40 to 90% inhibition for LFA-1 antibodies and 30% inhibition for ICAM-1 antibodies). Rudnicka et al. then confirmed the importance of adhesion molecules for the formation of the virological synapse and viral transfer (Rudnicka *et al*, 2009). They showed a significant three-fold decrease in virus transfer using T cells lacking the α subunit of LFA-1. Finally, a third group obtained opposite results showing that virus transfer through the virological synapse between T cells did not require LFA-1 binding to ICAM-1. Using antibodies blocking adhesion molecules LFA-1, ICAM-1 and ICAM-3, or 293T cells lacking LFA-1, no change in viral transfer through the virological synapse was observed in this study (Puigdomènech *et al*, 2008). The different assays used to analyze viral transfer and viral production could also explain this discrepancy. In the study by Puigdomènech et al., the LFA-1/ICAM-1 interaction could poorly affect viral transfer but seems to inhibit viral production after HIV-1 transfer through the virological synapse.

Finally, specific rearrangements of the cytoskeleton are required for the formation of the virological synapse and efficient viral transfer. Both actin and microtubules are indeed required for polarization of the Gag precursor and envelope glycoproteins to the site of cell-

cell contact (Jolly *et al*, 2007a; Rudnicka *et al*, 2009). During the immunological synapse the T cell receptor (TCR) interaction with its ligand, MHC molecules expressed at the surface of an antigen-presenting cell (APC), triggers a cascade of intracellular signals leading to cytokine gene expression, proliferation, and execution of the T cell effector functions. This cascade of events requires the activation of several protein tyrosine kinases such as ZAP-70 and cytoskeleton rearrangements. Using ZAP-70 deficient T cells, Blanchard et al, (2002) demonstrated that ZAP-70 signaling drives the T cell polarization through reorientation of the microtubule-organizing center (MTOC) at the cell-to-cell contact site (Blanchard *et al*, 2002). Similarly, polarization of MTOC at the virological synapse has been observed in 30 to 60% of the conjugated formed between infected donor T cells and target T cells (Jolly *et al*, 2011; Sol-Foulon *et al*, 2007; Vasiliver-Shamis *et al*, 2009). An intracellular compartment containing the viral envelope glycoproteins associates with the polarized MTOC during MTOC reorientation to the virological synapse, suggesting an active role of the microtubule network in the recruitment of the viral envelope at the virological synapse (Starling & Jolly, 2016). Polarization of organelles such as mitochondria, lysosomes, lipid bodies has also been observed at the site of cell-cell contact in 75% of the virological synapse (Jolly *et al*, 2011). Polarization of the cells can be mediated by ICAM1/LFA-1 signaling, which in addition to its effect on stabilizing virological synapse formation, induces a ZAP70-dependant signaling pathway for cytoskeleton remodeling, T cell polarization and efficient HIV-1 transfer across the virological synapse (Sol-Foulon *et al*, 2007; Starling & Jolly, 2016).

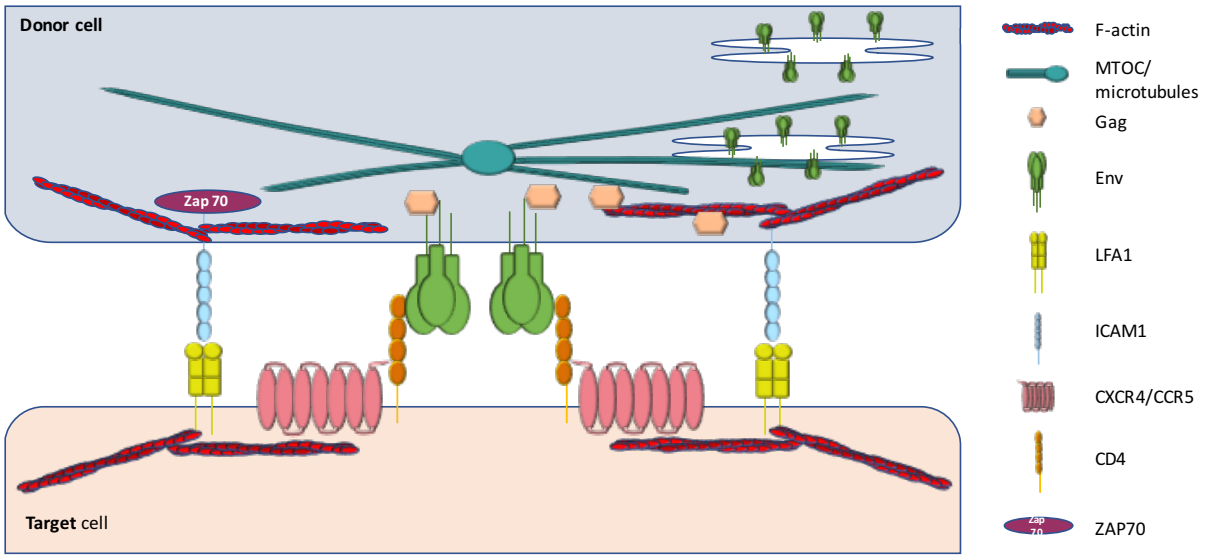

Figure 8: Schematic illustration of virological synapse formation.
HIV-1 envelope glycoproteins (Env) are expressed on the infected cell plasma membrane and interact with the receptors CD4 and CCR5 or CXCR4 on the target cell. The adhesion molecule intercellular adhesion molecule 1 (ICAM1) and lymphocyte function-associated antigen 1 (LFA1) stabilize the synapse. LFA-1/ICAM-1 interaction leads to ZAP70 signaling inducing the microtubule organizing center (MTOC) polarization to the cell-cell contact site. Microtubule and filamentous actin (F-actin) leads to recruitment of Env and Gag at the virological synapse for efficient viral transfer. (Sattentau, 2008)

2.3.2. Viral entry downstream of the virological synapse.

The exact mechanisms of viral transfer through the virological synapse are still debated since some groups described that the virus enters in the target T cells through fusion with the plasma membrane in the inter-synaptic space, when others described endocytic-uptake of virus particles and then membrane fusion in an intracellular compartment (Blanco *et al*, 2004; Jolly & Sattentau, 2004) (Figure 9).

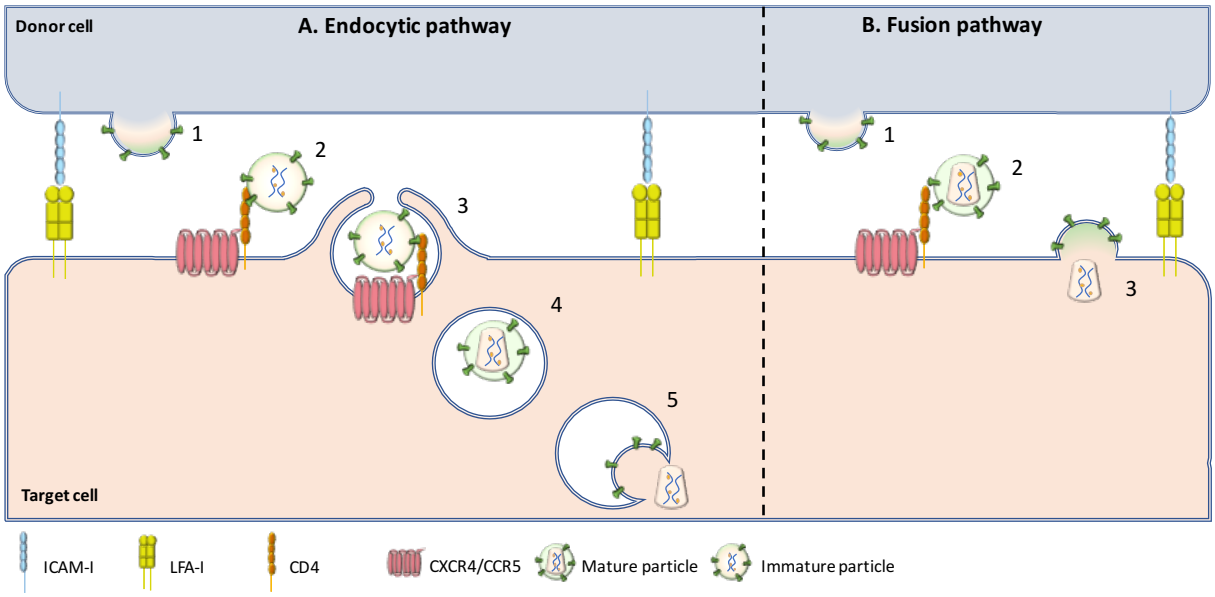

Figure 9: Hypothetical mechanisms of HIV-1 entry across Virological synapse.
(A) Endocytic pathway: HIV-1 budding from an infected T cell leads to the production of immature virus particles at a virological synapse (1). Immature virions then interact with the CD4 receptor but are incompetent for viral fusion (2). Immature particles are thus internalized by endocytosis (3). Maturation happens in internal compartments (4) leading to viral fusion and release of viral capsid into the cytoplasm of the target cell (5). (B) Fusion pathway: HIV-1 budding from an infected T cell leads to the production of mature, fusion- competent virions (1). Mature viruses can thus bind to CD4 (2) and leads to viral-cell fusion for release of viral material in the cytoplasm of the target cells for viral transfer (3)(Sattentau, 2010).

The first observation of the virological synapse by electron microscopy by Jolly et al. showed that mature HIV-1 particles were found in the synaptic space (Jolly & Sattentau, 2004), suggesting that mature viruses released from the donor T cells at the virological synapse could fuse directly with the plasma membrane of the target cells. Another group also observed HIV-1 particles in the synaptic space but suggested that these particles can be internalized by lamellipodia-like structures (Blanco *et al*, 2004). They also showed that HIV-1 was endocytosed in a trypsin-resistant compartment observed by electron microscopy. Several groups confirmed the mechanism of endocytosis of HIV-1 at the virological synapse. It has been shown that immature HIV-1 particles can be transferred across the virological synapse through dynamin- and clathrin-dependent endocytosis leading to productive infection of target T cells (Hübner *et al*, 2009; Miyauchi *et al*, 2009; Ruggiero *et al*, 2008; Sloan *et al*, 2013). HIV-1 particles contained in intracellular compartments colocalized with the early-endosomal marker EEA1 but not with the lysosomal-associated membrane protein LAMP1 suggesting that viruses are internalized in endosomal compartments but are not addressed to lysosomal degradation (Bosch *et al*, 2008). In accordance with these results, Dale et al demonstrated that after HIV-1 endocytosis, the

cleavage of gag polyprotein by the viral protease induced maturation of viral particles in endosomal compartments (Dale *et al*, 2011). This cleavage restores the viral membrane fusion activity and thus leads to viral-cell membrane fusion in these compartments (Figure 10).

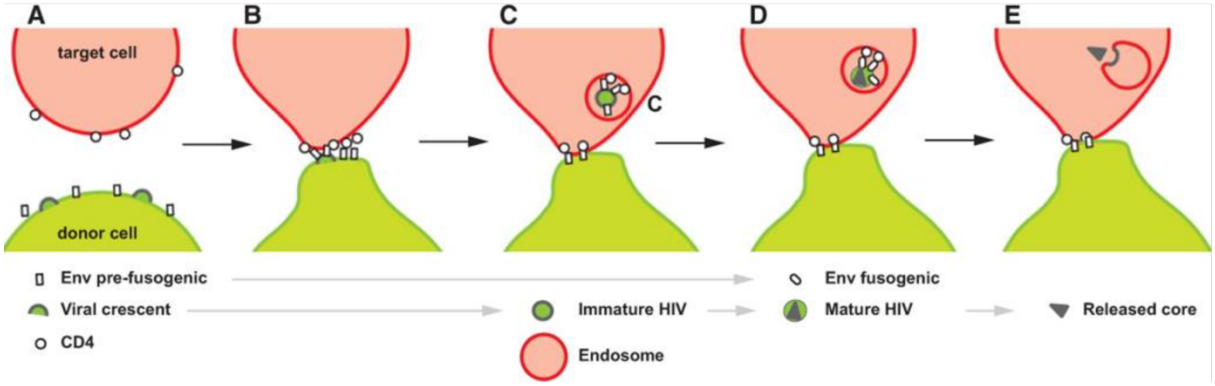

Figure 10 : Model for Maturation-Induced Fusion at the Virological Synapse.
(A) In the steady state, an HIV-1 infected T cell has a diffuse distribution of Env and Gag. (B) The engagement of Env on the infected donor cell, with CD4 on the target cell, induces an adhesion event and results in the recruitment of Gag, Env, and CD4 to the virological synapse. (C) An endocytic event is triggered resulting in CD4-dependent uptake of immature virus into acceptor cell intracellular compartments. (D) Bound to CD4, virus particles undergo protease-dependent maturation over time. (E) Viral particle maturation triggers viral membrane fusion, releasing the capsid to the cytoplasm. (Dale *et al*, 2011)

Finally, the group of Sattentau, who first described the formation of the virological synapse for HIV-1 transfer failed to observe endocytosis of HIV-1 across the virological synapse using confocal microscopy, electron microscopy or electron microscopy coupled with tomography (Jolly & Sattentau, 2004; Martin *et al*, 2010). Puigdomenèch et al. hypothesize that these different results could be explained by different experimental systems and the use of primary or immortalized cell lines (Puigdomènech *et al*, 2009). They suggest that the differences observed between primary CD4 T cells and cell lines might be associated with the kinetics of fusion events. Delayed fusion at the cell membrane may increase endocytosis in primary cells. In contrast, rapid fusion kinetics at the cell membrane in cell lines may favor transmission of HIV infection with lower levels of endocytosis. Thus they suggest that the endocytosis of HIV particles is the main mechanism of HIV transfer in primary CD4 T cells.

2.3.3. Viral transfer across the virological synapse and resistance to neutralizing antibodies and antiretroviral drugs

As described above (see 2.1 section, Cell free and cell-to-cell infection), viral transfer of HIV-1 across the virological synapse between an infected donor T cell and a recipient T cells is more efficient than cell-free infection for productive infection of the target T cells. Like for other viruses (Herpesviruses, poxviruses and Hepatitis C viruses), it has been proposed that HIV-1 could escape, at least partially, neutralization by specific antibodies targeting the viral envelope when it is transferred across the virological synapse. This was already suggested in 1995 by Pantaleo et al. who described that neutralizing antibodies against the glycan V3-loop of gp120 were unable to block cell-to-cell viral transfer (Pantaleo *et al*, 1995). However, after characterization of the virological synapse for HIV-1 cell-to-cell transfer in 2004, several different groups tried to elucidate the mechanisms of neutralizing antibody escape in virological synapse-mediated viral transfer. There is a general agreement that the potency of neutralizing antibodies is reduced during cell-to-cell transmission compared to cell-free infection and that only a subset of neutralizing antibodies can efficiently inhibit cell-to-cell transmission (Abela *et al*, 2012; Blanco *et al*, 2004; Jolly & Sattentau, 2004; Jolly *et al*, 2004; Malbec *et al*, 2013; Massanella *et al*, 2009). For example, Abela et al. demonstrated that several specific anti-CD4 binding site antibodies lost considerable potency (10- to 100-fold decrease) when HIV-1 was transferred by cell-to-cell transmission (Abela *et al*, 2012). However, if some antibodies are still able to block cell-to-cell transmission at high concentration, VRC01, which is one of the most potent antibodies for inhibition of cell-free infection, is particularly ineffective for blocking cell-to-cell viral transfer. While most anti-gp120-directed antibodies, and in particular those directed against the CD4 binding site of gp120, displayed a reduced activity during viral cell-to-cell transmission, the same group reported that gp41-directed inhibitor T20 and neutralizing antibodies targeting gp41 maintained their activity and are thus able to block both cell-free and cell-to-cell infection with the same efficiency. However, other groups showed that anti-gp41 antibodies failed to inhibit cell-to-cell transmission (Blanco *et al*, 2004; Chen *et al*, 2007; Massanella *et al*, 2009). Globally, efficiency of neutralizing antibodies for neutralization of the VS-mediated viral transfer is variable and some epitopes of the viral envelope glycoproteins seem more susceptible than others to neutralization of VS-mediated viral transfer.

Similarly, activities of entry inhibitors and antiretroviral drugs on HIV-1 transmission through the virological synapse is still a matter of debate. A lot of opposite results have been published regarding the effect of entry inhibitors. Whereas Chen et al. initially reported that the peptide entry inhibitor of Env-mediated membrane fusion T20, targeting the gp41 transmembrane glycoprotein, was unable to block VS-mediated viral transfer using flow cytometry analysis (Chen *et al*, 2007), Martin et al., then showed that cell-free and cell-to-cell infection across the virological synapse were equivalently susceptible to T20, using qPCR for detection of infection (Martin *et al*, 2010). These different results can be explained by the different experimental approaches used since the first study was looking for viral transfer of viral material when the other study analyzed *de-novo* synthesized viral DNA after viral transfer. Thus, we can hypothesize that the T20 entry inhibitor does not affect viral transfer across the virological synapse but inhibits HIV-1 infection in the target cell after the VS-mediated viral transfer. Fusion inhibitors, such as T20, could have no effect on endocytosis of HIV-1 (viral transfer) but could then block viral fusion in the endosomal compartments leading to the inhibition of the productive infection.

Other studies reported that protease inhibitors inhibited HIV-1 VS-mediated infection similarly to cell-free infection (Agosto *et al*, 2014; Sigal *et al*, 2011). Regarding reverse transcriptase inhibitors, it seems that non-nucleoside-analog reverse transcriptase inhibitors (NNRTI) could block VS-mediated infection (Agosto *et al*, 2014; Sigal *et al*, 2011) whereas nucleoside-analog reverse transcriptase inhibitors (NRTI) were unable to do it (Agosto *et al*, 2014). However, other results from Sigal et al showed that NRTI were also able to block cell-to-cell infection even if the level of inhibition is lower than for cell-free infection (Sigal *et al*, 2011). Finally, it seems that the idea that the cell-to-cell viral transfer through the VS can escape from neutralizing antibodies and antiretroviral therapies is not so clear and is probably dependent on the inhibitors used.

2.4. Heterogeneity of virological synapses

Most of the studies regarding HIV-1 transmission through the virological synapse have been done between an infected donor T cell and a recipient target T cell. However, dendritic cells and macrophages can also perform cell-to cell transmission to target T cells through the formation of a related virological synapse. Thus, several groups investigated virological synapses formation using dendritic cells (DCs) or macrophages as infected donor cells. If cell-to-cell transfer between DCs and T cells, and between macrophages and

T cells, show similarities with the virological synapse observed between T cells, they also showed some differences which will be developed here.

2.4.1. The DC infectious synapse

Regarding DCs, two types of cell-to-cell transfer have been proposed. In cis-infection, DCs are productively infected whereas in trans-infection DCs are able to capture HIV-1 independently of CD4 and then transfer viruses to CD4+ T cells through the "infectious synapse". Early studies demonstrated that DCs can capture HIV-1 through the binding of HIV-1 envelope glycoprotein to the mannose specific C-type lectin receptor (DC-SIGN) and store viruses into tetraspanin-enriched compartments, in continuity with the plasma membrane without viral replication. More recently, it has been demonstrated that the immunoglobulin(I)-type lectin Siglec-1 (or CD169) can also bind to HIV-1 through the recognition of sialyllactose gangliosides present in the viral membrane (Izquierdo-Useros *et al*, 2012). After capturing HIV-1, DCs are able to transfer these viruses to CD4+ T cells, independently of viral replication through the formation of infectious synapse (Dutartre *et al*, 2016; McDonald, 2010; Piguet & Steinman, 2007) (Figure 11).

If virological synapse formation depends on the interaction between HIV-1 envelope glycoprotein gp120 and the receptor CD4, the infectious synapse observed during trans-infection does not rely upon CD4/gp120 interaction since Rodriguez-Plata et al demonstrated that the number of conjugates between DCs and CD4+ T cells was not increased in presence of HIV-1 (Rodriguez-Plata *et al*, 2013). However, they also demonstrated that the formation of the infectious synapse was decreased by 60% when interactions between the adhesion molecules ICAM-1 and LFA-1 were disrupted. Furthermore, interaction between the T-Cell receptor (TCR) and the major histocompatibility complex, both present at the immunological synapse during antigen presentation significantly enhance HIV-1 transfer across the infectious synapse (Rodriguez-Plata *et al*, 2013). Thus, the formation of the infectious synapse is not triggered by the virus but is related to the hijacking of the immunological synapse which is switched into an infectious synapse for HIV-1 transfer to CD4+ T cells (Dutartre *et al*, 2016).

Even if the formation of the infectious synapse does not rely on CD4/gp120 interaction, this interaction is still required for efficient productive infection of CD4+ T cells following infectious synapse formation. Indeed, after the formation of the infectious synapse, HIV-1 receptor CD4, and co-receptors CXCR4 and CCR5, are recruited at the cell-cell contact site. Furthermore, HIV-1 transfer from DCs harboring HIV and CD4+ T cells

could be blocked using neutralizing antibodies targeting gp41 and, at high concentration, gp120 (Sagar *et al*, 2012).

Rearrangements of the actin cytoskeleton also play a key role in HIV-1 transfer across the infectious synapse. Indeed, a recent study showed that tetraspanins 7 (TSPAN7) and dynamin-2 (DNM2) control nucleation and cortical stabilization of actin to maintain viruses on dendrites for efficient cell-to-cell transfer to T cells (Ménager & Littman, 2016). Furthermore, it has been shown that large sheet-like membrane structures derived from infected DCs wrap around T cells leading to a large interface at the infectious synapse (Felts *et al*, 2010). Within this interface, filopodia extensions from T cells are able to interact with HIV-1-containing compartments in continuity with the plasma membrane of DCs for efficient cell-to-cell transmission (Felts *et al*, 2010). Together, these results show that in DCs, HIV-1, by hijacking the immunological synapse can efficiently transfer HIV-1 without productive infection of DCs.

Some studies suggest that macrophages, which also express DC-SIGN and/or Siglec-1 are able to use the same mechanism of trans-infection for efficient viral cell-to-cell transfer to CD4+ T cells (Carr *et al*, 1999; Rinaldo, 2013; Sewald *et al*, 2012; Wu & KewalRamani, 2006).

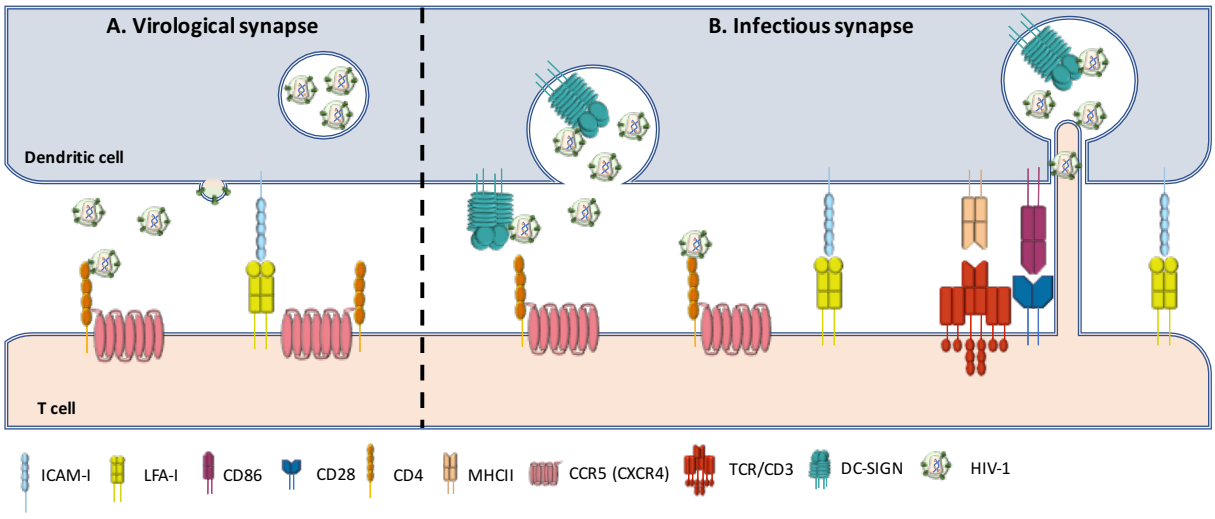

Figure 11: Schematic illustration of virological and infectious synapses formed between infected DCs and T cells.
(A) Productively infected DCs use the classical virological synapse for HIV-1 transfer characterized by CD4, CCR5/CXCR4, LFA1 and ICAM interaction. (B) DCs can capture HIV-1 through DC-SIGN and transfer captured-viruses to CD4+ T cells across an infectious synapse. This phenomenon called Trans-infection depends first on antigen presentation using MHCII and TCR and is dependent on DC-SIGN and LFA1/ICAM-1 interactions but not on CD4/gp120 interactions. During these contacts CD4+ T cells are also able to induce filopodia inside HIV-1 containing compartment in DCs for efficient cell-to-cell transfer. (Dutartre *et al*, 2016).

2.4.2. Transfer of HIV-1 at the virological synapse formed with macrophage targets

Compared to virological or infectious synapses involving T cell or DC as infected-donor cells, little is known about the formation of virological synapses between infected macrophages and target T cells. In infected macrophages, viral particles accumulate both at the plasma membrane and in tetraspanins-enriched compartments called virus-containing compartments (VCC) (described below in 3.4 section – HIV-1 replication in macrophages). Infected macrophages can efficiently transfer viruses to uninfected T cells or uninfected macrophages across the virological synapse but the mechanisms involved in the formation of the MDM/T cell virological synapse are not completely characterized (Carr *et al*, 1999; Groot *et al*, 2008) (Figure 12). During the formation of the conjugates, VCCs could move rapidly to the virological synapse (Gousset *et al*, 2008) through a cytoskeleton-dependent remodeling (Duncan *et al*, 2014). Similarly, to the virological synapse involving T cells, the virological synapse involving macrophages leads to the recruitment of CD4, CCR5, LFA1, ICAM-1, HIV-1 Gag polyproteins and envelope glycoproteins at the site of contact (Duncan *et al*, 2014; Groot *et al*, 2008). In contrast to the virological synapse formed between two T cells, which is dependent of CD4, it seems that the formation of the virological synapse between infected macrophages and T cells is independent of CD4 (Gousset *et al*, 2008), while the viral transfer is dependent of gp120/CD4 and LFA1/ICAM1 interactions (Duncan *et al*, 2014). Through the formation of the virological synapse, infected macrophages can transfer a high-multiplicity of HIV-1 to CD4+ T cells, promoting reduced viral sensitivity to reverse transcriptase inhibitors as well as to some neutralizing antibodies (Duncan *et al*, 2014; Gousset *et al*, 2008). If virological synapse formation between infected macrophage and uninfected T cells has been described and shows several differences with the virological synapse between T cells (Waki & Freed, 2010), to our knowledge, no virological synapse has been described so far between infected T cells and uninfected macrophages.

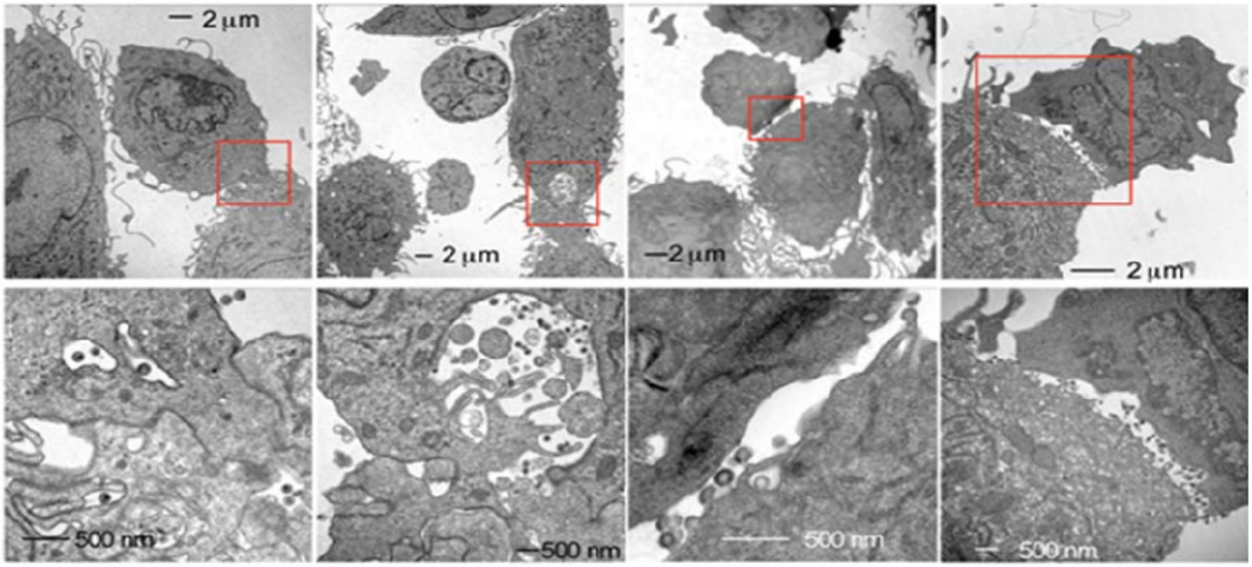

Figure 12: Recruitment and accumulation of Gag at the macrophage/macrophage and macrophages/T cell synapse.
Electron microscopy images show the accumulation of virions in intracellular compartments near the plasma membrane and the contact between infected macrophages and uninfected macrophages or T cells. (Gousset *et al*, 2008).

2.5. Engulfment of infected T cells by macrophages

If HIV-1 infection of T cells by viral cell-to-cell transfer has been largely documented, cell-to-cell infection of macrophages remains poorly investigated, and only one study addresses this process. Recently, the group of Quentin Sattentau reported, for the first time, a new mechanism for specific cell-to-cell transfer of HIV-1 from infected T cells to macrophages (Baxter *et al*, 2014). In this study, the authors showed that macrophages can engulf infected T cells leading to productive infection of the macrophage targets. The engulfment of infected/dead/dying T cells was significantly higher compared to uninfected/healthy cells demonstrating that cell death and HIV-1 independently promotes T cell engulfment by macrophages. This preferential uptake of infected dying T cells is independent of gp120/CD4 interaction but is dependent of the actin cytoskeleton remodeling. Since this phenomenon is dependent of actin remodeling and since the macropinocytosis inhibitor amiloride did not affect uptake of infected T cells, the authors suggested that this engulfment/uptake of infected T cells by macrophages rather results from phagocytosis and not from micropinocytosis

If the uptake of infected T cell by macrophages is independent of the interaction between HIV-1 envelope glycoprotein gp120 and the receptor CD4, the infection of

macrophages following the uptake of the T cell is dependent of this interaction. Productive infection of macrophages is also dependent of the tropism of the viruses. Indeed, the engulfment of T cells infected with CCR5-tropic viruses led to productive infection of the macrophages demonstrated by a cytoplasmic diffuse signal of Gag in macrophages and release of p24 in the supernatant. By contrast, after engulfment of T cells CXCR4-tropic viruses, no diffuse signal of Gag was observed. Only concentrated Gag signal was observed in association with the T-cell specific marker CD3, suggesting internalized T cells.

2.6. Cell-to-cell fusion

2.6.1. Formation of T cell-syncytia

Cell-to-cell fusion between T cells has been initially proposed to be another mechanism for HIV-1 infection and dissemination between T cells. Early studies suggested that HIV-1 infected T cells could fuse with uninfected T cells to form giant syncytia, 5 to 100 times bigger than individual cells. In this context, cell-to-cell fusion occurs through cytoskeleton rearrangements, is dependent on LFA1 and mediated through interaction between envelope glycoproteins expressed at the cell surface of infected cells and CD4 expressed on fusing cells (Hildreth & Orentas, 1989; Schols *et al*, 1989; Sylwester *et al*, 1993). These T cell syncytia, initially observed only *in vitro* with immortalized cell lines, have been shown to rapidly die through mitochondrion-dependent apoptosis (Roumier et al., 2003). Formation of HIV-1 T cell-syncytia leads to activation of the target of rapamycin mTOR which mediates phosphorylation of p53. Thus, p53 induces upregulation of Bax expression leading to mitochondrial permeabilization and release of pro-apoptotic mitochondrial proteins. These pro-apoptotic proteins activate caspase-3 leading to apoptosis (Ahr *et al*, 2004). Several groups thus proposed that this could be the mechanism of CD4+ T cells loss observed *in vivo* in infected patients (Hildreth & Orentas, 1989; Sylwester *et al*, 1997).

However, formation of T cell syncytia has been a controversial subject since other groups did not observed formation of T cell syncytia using primary CD4+ T cells (Carr *et al*, 1999; Chen *et al*, 2007; Sourisseau *et al*, 2007). Since no *in vivo* evidence of T cell syncytia in tissue were demonstrated, it has been suggested that these giant syncytia could be *in vitro* artefacts only observed with immortalized cell lines and restricted to CXCR4-viruses (Moore & Ho, 1995). Actually, viral strains were initially classified as syncytia-inducing (SI) or non-syncytia inducing (NSI) strains, referring to their capacity to induce

syncytia *in vitro*, and then to the ability of viral strains to use CXCR4 or CCR5 for virus entry, respectively. However, NSI viruses can readily form syncytia with CCR5-positive cells, and a new classification of viral strains based on CXCR4 or CCR5-usage was adopted (Berger *et al*, 1998).

However, small T cell syncytia, containing no more than 5 nuclei, have been observed *in vivo* in lymph nodes (Orenstein, 2000). More importantly, some more recent studies using HIV-1-infected humanized mouse models demonstrated the presence of motile infected syncytia in lymph nodes, smaller than those observed *in vitro* (Murooka *et al*, 2012). These motile small T cell syncytia can establish tethering interactions with uninfected T cells that may facilitate cell-to-cell transmission through the formation of a virological synapse (Murooka *et al*, 2012; Symeonides *et al*, 2015). Interestingly, these interactions between small syncytia and uninfected T cells do not lead to cell-to-cell fusion suggesting that this mechanism of cell fusion is finely regulated (Murooka *et al*, 2012).

2.6.2. Inhibition of cell-cell fusion at the virological synapse.

The numerous studies describing the formation of conjugates between infected and uninfected T cells for viral transfer across the virological synapse did not show observation of cell-cell fusion, confirming that this process is finely regulated during the formation of the virological synapse between T cells (Figure 13). A first mechanism of regulation of cell-cell fusion between T cells could be related to interferon-induced transmembrane proteins (IFITM). IFITM-1, 2 and 3 are antiviral factors interfering with a large spectrum of viruses including filoviruses, coronaviruses, dengue viruses or HIV-1. During HIV-1 infection, they could be involved in different steps. For example it has been demonstrated that IFITM-1 decrease the production of infectious particles by inhibiting the expression of Gag, and the auxiliary proteins Vif and Nef (Chutiwitoonchai *et al*, 2013; Tartour *et al*, 2014). IFITM also have an important role in the early steps of infection. IFITM are incorporated into viral particles and inhibit the fusion capacity of membranes in which they reside by increasing the curvature of cell membranes and reducing their fluidity thus resulting in the inhibition of the formation of a fusion pore (Tartour *et al*, 2014).

Second, inhibition of envelope-mediated cell fusion could be related to the presence at the cell-to-cell contact site of immature viral particles in which the Gag precursor inhibits env-mediated fusion by interacting with the gp41 cytoplasmic tail. After maturation of viral particles and cleavage of the Gag precursor, the fusion activity of gp41 is restored. Indeed, truncation of the gp41 cytoplasmic tail has been shown to increase T cell syncytia formation

(Freed & Martin, 1995). More recently, the group of Markus Thali showed that, through ezrin signaling, cellular components, such as regulatory tetraspanins CD9, CD63, CD81 or CD82, were targeted to the T cell virological synapse to inhibit cell-cell fusion (Roy *et al*, 2014; Weng *et al*, 2009). Together, these studies confirm that during virological synapse formation, cell-cell fusion is probably highly regulated by different mechanisms.

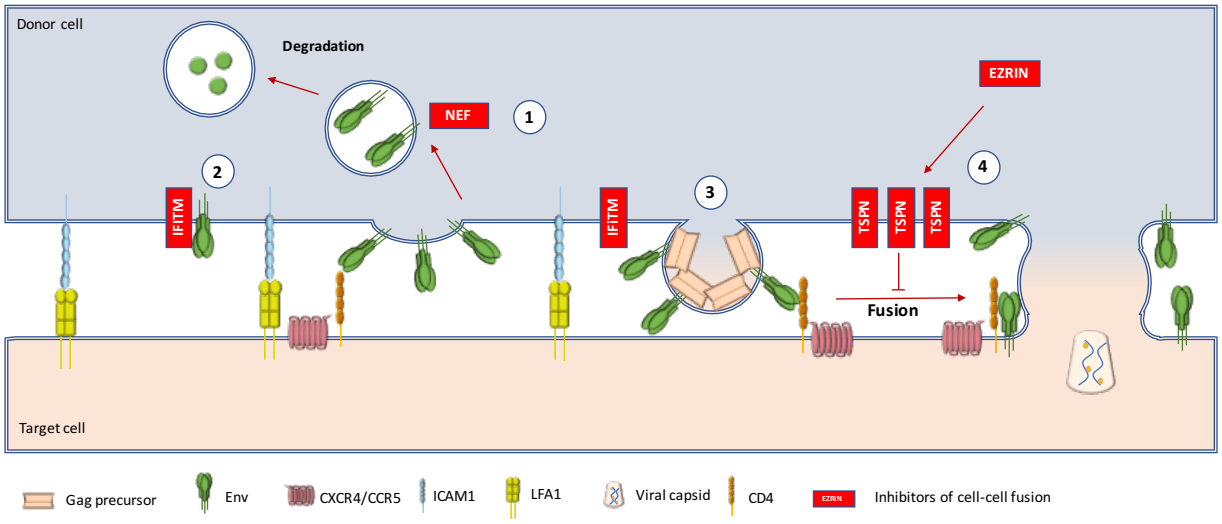

Figure 13: inhibition of cell-cell fusion across virological synapse.
(1) In infected cells, the auxiliary protein Nef downregulate CD4 and env, essential for cell-cell fusion at the plasma membrane by inducing degradation. **(2)** IFITM are able to interact with env, incorporate into viral particles and prevent the formation of the fusion pore **(3)** Immature particles need maturation to restore fusion activity inhibited by gag precursor. **(4)** Ezrin leads to tetraspanins recruitment to the site of contact to inhibits cell-cell fusion induced by HIV-1.

2.6.3. Presence of multinucleated giant cells in infected tissue

If the mechanism of T cell syncytia formation has been largely documented *in vitro* and discussed for its *in vivo* relevance, it seems that cell-to-cell fusion for HIV-1 infection and dissemination is not restricted to T cells. Numerous studies showed that multinucleated macrophages, as well as multinucleated DCs, can be found in different tissues *in vivo* in HIV-1-infected patients. Indeed, multinucleated syncytia expressing DCs markers S100 and p55 were found 20 years ago at the surface of the nasopharyngeal tonsil in infected patients (Frankel *et al*, 1996). The same group suggested that infected T cells could fuse with skin-derived dendritic cells (Pope *et al*, 1994) thus leading to multinucleated cell formation between T cells and DCs. Similarly, multinucleated giant HIV-1-infected macrophages have been found *in vivo* during infection in several different tissues, including lymph nodes, spleen, lungs, genital and digestive tracts, and the central nervous system (CNS) (Costiniuk & Jenabian, 2014; Dargent *et al*, 2000; Fischer-Smith *et al*, 2008; Frankel *et al*, 1996; Geny *et al*, 1991; Koenig *et al*, 1986; Lewin-Smith *et al*, 1999; Orenstein & Wahl, 1999; Teo *et al*,

1997; Vicandi *et al*, 1999). While several groups showed the presence of infected multinucleated macrophages in tissues, and more specifically in the brain of HIV-1 infected patients and SIV-infected monkeys, the cellular and molecular mechanisms related to their formation remain poorly investigated.

In summary (Table 2), cell-to-cell infection of T cells and dendritic cells has been largely investigated and can occur, at least in *in vitro* experimental systems, through different structures such as the virological synapse, infectious synapse, nanotubes, trogocytosis or syncytia formation. However, to our knowledges, only one study showed productive infection macrophages through a cell-to-cell mechanism, by engulfment of infected T cells (Baxter *et al*, 2014).

	T cells	**DC**	**macrophages**
nanotubes/folpodia	between T cells (Sowinsky et al, 2008)	between DCs and T cells (during trans-infection) (Felts et al, 2010)	between macrophages (Eugenin et al, 2009)
trogocytosis	between T cells (Jolly et al, 2003)	between DC and T cells (Caumartin et al, 2016)	-
virological synapse	between T cells (Jolly et al, 2004)	between infected T cells and DC (Dutarte et al, 2016)	between infected macrophages and T cells (Groot et al, 2008)
infectious synapse	between infected DC and T cells (trans-infection) (Dutarte et al, 2016)	between infected DC and T cells (trans-infection) (Dutarte et al, 2016)	between infected macrophages and T cells (trans-infection) (Wu and Kewalramani, 2006)
syncytia	between T cells (Orenstein et al, 2000)	between Dc and T cells Suggestion from (Pope et al, 1994)	-
engulfment	-	-	between infected T cells and macrophages (Baxter et al, 2014)

Table 2: Summary of the different cell-to-cell transmission mechanisms according to the cell type.

3. Macrophages: Targets of HIV-1

As evidenced by the presence of infected macrophages in different tissues of infected patients, macrophages are cellular targets of HIV-1 and probably play an important role in HIV-1 pathogenesis. As describe above, they participate in cell-to-cell transmission of HIV-1 and may be important for HIV-1 spread in infected patients. Replication of cell-free HIV-1 in macrophages, and the relevant role of macrophage in HIV-1 infection, as well as the impairment of macrophages functions during HIV-1 infection have been largely documented and will be reviewed here.

3.1. Origins and tissue distribution of macrophages

Differentiated macrophages are myeloid cells of the immune system present in all tissues in the organism. Macrophages come from different origins, since they can either derived from primitive embryonic precursors (tissue-resident macrophages) or from monocytes (infiltrating macrophages) (Haldar & Murphy, 2014). Depending on their anatomical localization and functions, macrophages have been divided in different subpopulations. For example, specialized tissue-resident macrophages include osteoclasts (bone), alveolar macrophages (lung), histiocytes (interstitial connective tissue) or Kupffer cells (liver). Macrophages are also found in brain (microglia) or in lymph nodes, gut and other tissues. All these macrophages have been divided in two subsets: classically activated macrophages (M1 macrophages) and alternatively activated macrophages (M2 macrophages). M1 macrophages have pro-inflammatory functions, induce by interferon gamma (IFNγ) and mediate defense of the host from a variety of bacteria, protozoa or viruses, and also play a role in antitumor immunity. Conversely, M2 macrophages have anti-inflammatory functions and regulate wound healing and fibrosis. The activation state of macrophages is important for inflammation regulation depending on their localization. For example, in mucosal tissues such as respiratory and gastrointestinal tracts, macrophages minimize inflammation-mediated organ damage in response to repeated exposure to foreign material. In contrast, in internal organs less exposed to microbial constituents, macrophages rather induce inflammation in response to pathogens (Gordon & Martinez-Pomares, 2017; Murray & Wynn, 2011).

3.2. Functions of macrophages and impairment by HIV-1

Macrophages exhibit a large panel of specialized functions depending on their localization. For example, osteoclasts regulate bone formation and degradation, bone marrow macrophages promote erythropoiesis and iron recycling, alveolar macrophages regulate lung homeostasis, and microglial cells regulate brain development (Gordon & Martinez-Pomares, 2017; Murray & Wynn, 2011). In all tissues, macrophages perform an important immune surveillance, respond to signs of tissue damage, and induce uptake of dying cells. The main mechanism used by macrophages to participate in these functions is phagocytosis which will be described in detail below. For example, alveolar macrophages facilitate removal of allergens from the lungs, whereas Kupffer cells in liver participate in the clearance of pathogens and toxins from the circulation.

3.2.1. Phagocytosis

3.2.1.1. Phagocytosis under physiological condition

Internalization of particles (pathogens, cellular debris or apoptotic cells) is initiated by the interaction of specific receptors on the surface of macrophages and ligands on the surface of the particle. This interaction leads to high polymerization of actin at the site of ingestion and internalization of the particle. After internalization, particles are sequestered in a phagosome. Maturation of the phagosome, through a series of fusion and fission events with components of the endocytic pathway, will then results in the degradation of the particles in a phagolysosome (Aderem & Underhill, 1999).

During phagocytosis of apoptotic cells, receptors on the macrophage recognize ligands found on apoptotic cells but not present on healthy cells, including phosphatidylserine in the outer leaflet of the plasma membrane, changes in the pattern of glycosylation of cell surface proteins and surface-bound thrombospondin (TSP). Binding of these ligands to specific receptors (CD14, CD36 and lectins for example) induce phagocytosis of the apoptotic cells without activating the pro-inflammatory responses of the macrophage (Figure 14).

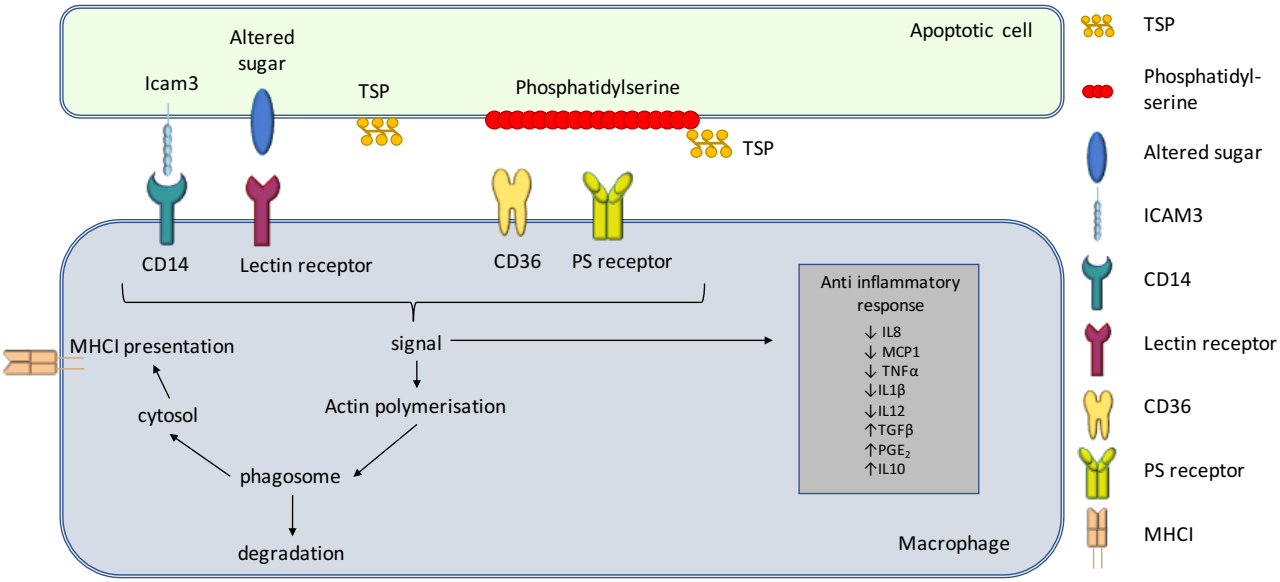

Figure 14: Phagocytosis of apoptotic cells by macrophages.
A large variety of receptors is involved in the recognition of apoptotic cells (CD14, lectin receptor, CD36 and PS receptor for example). They induce different cellular pathways leading to actin remodeling, phagocytosis of dying cells and anti-inflammatory response.

During phagocytosis of pathogens, macrophages recognize conserved motifs on pathogens that are not found in higher eukaryotes called "pathogen-associated molecular patterns" (PAMPs) (Janeway, 1992). Cellular receptors that recognize these patterns include Fc receptors, mannose receptor, integrin and scavenger receptors (Sastry & Ezekowitz, 1993; Stahl & Ezekowitz, 1998). The recognition mechanisms leading to phagocytosis occur through either cellular or humoral immune responses with opsonization of the infectious agent before being recognized by a phagocytic receptor. Pathogens are then internalized using different cellular pathways though Fc-receptor-, mannose-receptor-, or complement-receptor-mediated phagocytosis (Aderem & Underhill, 1999). Maturation of the phagosome finally leads to degradation of the pathogens. Pathogens are either completely degraded or peptide antigens from the degradation of these particles are preserved for presentation in association with major histocompatibility complex (MHC) class I or class II molecules in order to stimulate antigen-specific T cells and specific immune responses (Mantegazza *et al*, 2013).

3.2.1.2. Impairment of phagocytosis by HIV-1

HIV-1 infection of macrophages leads to defective function of these specialized cells, including impairment of Fc-receptor, complement-receptor, and mannose-receptor dependent phagocytosis (Biggs *et al*, 1995; Crowe *et al*, 1994). These defects could be important for the immuno-pathogenesis of AIDS, contributing to the development and reactivation of opportunistic infections, and significant morbidity and mortality. For

example, infection of alveolar macrophages leads to impairment of phagocytosis resulting in defective pulmonary immune responses and higher risk of respiratory tract infections than HIV-1-uninfected individuals (Jambo *et al*, 2014).

During complement-receptor mediated phagocytosis, recognition of particles by complement-receptor induces a signaling pathway leading to activation of the RhoA small GTPase for cytoskeleton rearrangements allowing efficient internalization. RhoA activation can be inhibited by intracellular cyclic AMP. During HIV-1 infection, complement-receptor mediated phagocytosis is strongly inhibited (Azzam *et al*, 2006), and this inhibition is due to the increase of intracellular cyclic AMP levels suggesting that by increasing intracellular cyclic AMP, HIV-1 inhibits RhoA activation leading to impairment of complement-receptor-mediated phagocytosis (Figure 15).

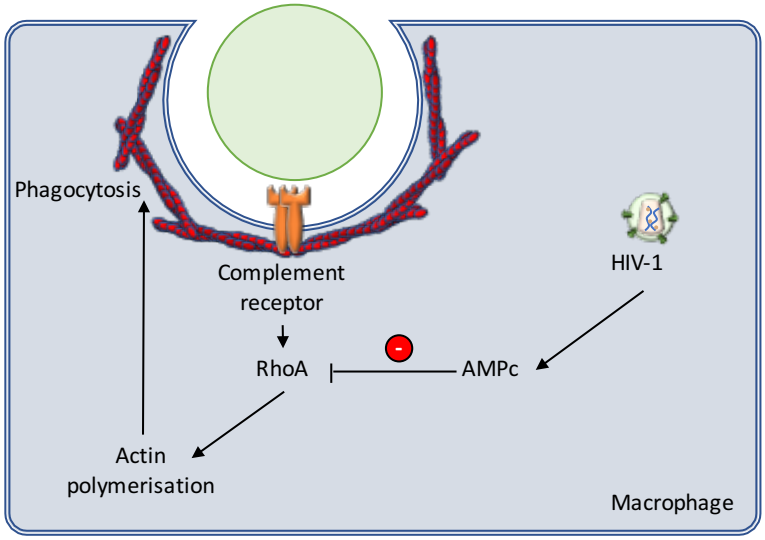

Figure 15: HIV-1 impairs complement-receptor mediated phagocytosis.
During complement-receptor mediated phagocytosis, activation of RhoA induces actin polymerization for efficient phagocytosis. In the presence of HIV-1, levels of AMPc are increased, leading to inhibition of RhoA and thus inhibition of phagocytosis.

Fc-receptor-mediated phagocytosis is also strongly inhibited by HIV-1 through different processes. During Fc-receptor-mediated phagocytosis, Fc-receptor mediates intracellular signaling through the kinase SYK inducing the recruitment of the small GTPase CDC42 and the adaptor protein AP1 in the phagocytic cup for cytoskeleton remodeling and formation of pseudopodia required to induce efficient internalization of particles. During HIV-1 infection, HIV-1 downregulates the expression of γ-chain of the Fc receptor leading to inhibition of SYK and therefore inhibition of phagocytosis (Kedzierska *et al*, 2002; Leeansyah *et al*, 2007). Furthermore, the HIV-1 auxiliary protein Nef, and also the regulatory protein Tat, inhibit Fc-receptor mediated phagocytosis by inhibiting the

recruitment of AP1 (Mazzolini *et al*, 2010) and CDC42 (Debaisieux *et al*, 2015) in the phagocytic cup (Figure 16).

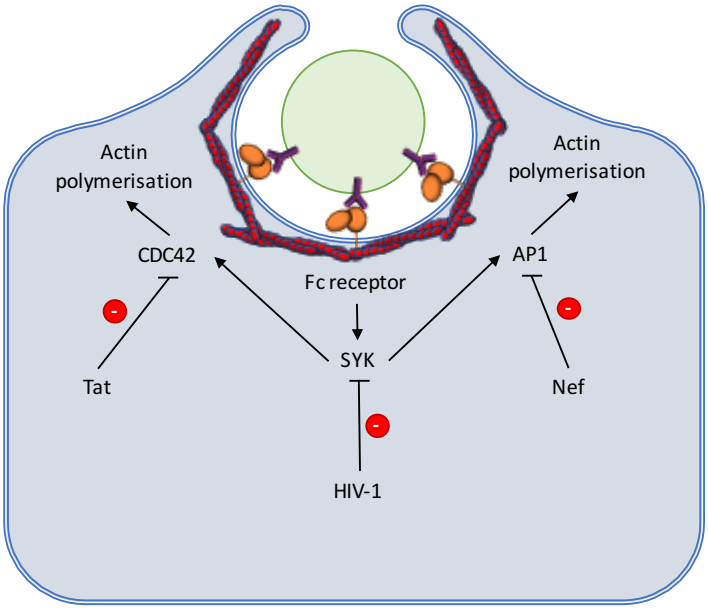

Figure 16: HIV-1 impairs Fc-receptor mediated phagocytosis.
During Fc-receptor mediated phagocytosis, activation of tyrosine kinase SYK induces the recruitment of CDC42 and AP1 in the phagocytic cup leading to actin polymerization for efficient phagocytosis. In the presence of HIV-1, SYK is inhibited, and the auxiliary proteins Tat and Rev inhibit the recruitment of AP1 and CDC42, leading to inhibition of phagocytosis.

3.2.2. Cell-cell fusion

3.2.2.1. Cell-cell fusion for osteoclast formation

The propensity of macrophages to fuse together seems to be an important process for macrophage functions. Indeed, in bones, macrophages have the ability to fuse together to generate multinucleated osteoclasts which are essential for bone resorption. Fused macrophages can also be found in other tissues where they are termed as multinucleated giant cells (MGCs), first described in pulmonary granulomas formed during tuberculosis infection. The formation of osteoclasts is induced by RANKL, macrophage colony-stimulating factor 1 (GM-CSF), or IL4 (Novack & Teitelbaum, 2008). In contrast, multinucleated giant cells seem to form in response to different cytokines and other stimuli such as IL-4 and IL-13, GM-CSF, IL-17A, interferon-γ (IFN-γ) and lectins (Helming & Gordon, 2009). To trigger the cell-cell fusion process, macrophages must first become fusion-competent (Figure 17). Cytokines IL-4 and IL-13, which are secreted by immune cells and macrophages themselves induce this fusion-competent state through involvement of the signal transducer and activator of transcription 6 (STAT6) (Moreno *et al*, 2007). DAP12-mediated signaling is also important in programming of macrophages into a fusion-

competent state, since it mediates transcription of other fusion mediators through the kinase Syk (Helming *et al*, 2008). When macrophages acquire the fusion-competent state, IL-4 signaling leads to upregulation of fusion mediators such as E-cadherin or dendritic cell-specific transmembrane protein DC-STAMP and induces the release of metalloproteinases such as MMP9 (Helming *et al*, 2008; Yagi *et al*, 2007). Macrophages fusion may be also regulated by the CD36 scavenger receptor and tetraspanins CD9 and CD81(Parthasarathy *et al*, 2009; Takeda *et al*, 2003). The lipid composition of the fusing membranes is also important for fusion. Indeed, macrophages display changes in their lipid composition during fusion, and phosphatidylserine (PtdSer), which is normally present in the inner leaflet of the plasma membrane, is re-localized in the outer leaflet during fusion where it can bind to CD36 to induce macrophages fusion (Helming *et al*, 2009). Together, these processes lead to strong interactions and adhesion between individual macrophages to induce cell-cell fusion, essential for osteoclast formation and functions in bone resorption.

Interestingly, osteoclasts can also be infected by HIV-1 *in vitro* (Gohda *et al*, 2015), even if evidence is missing regarding the presence of HIV-1 infected osteoclasts *in vivo*. Moreover, osteoclast functions seem to be important in the physiopathology of AIDS, since reduced bone mineral density is a frequent complication observed in HIV-1 infected patients that often progresses to osteoporosis and high prevalence of fractures. A 6-fold increased risk of low bone mineral density is observed in HIV-1-positive individuals compared to the general population, and it has been proposed that osteoclasts, as cells specialized in bone degradation, have a major contribution in this process (Aziz *et al*, 2014; Titanji *et al*, 2014).

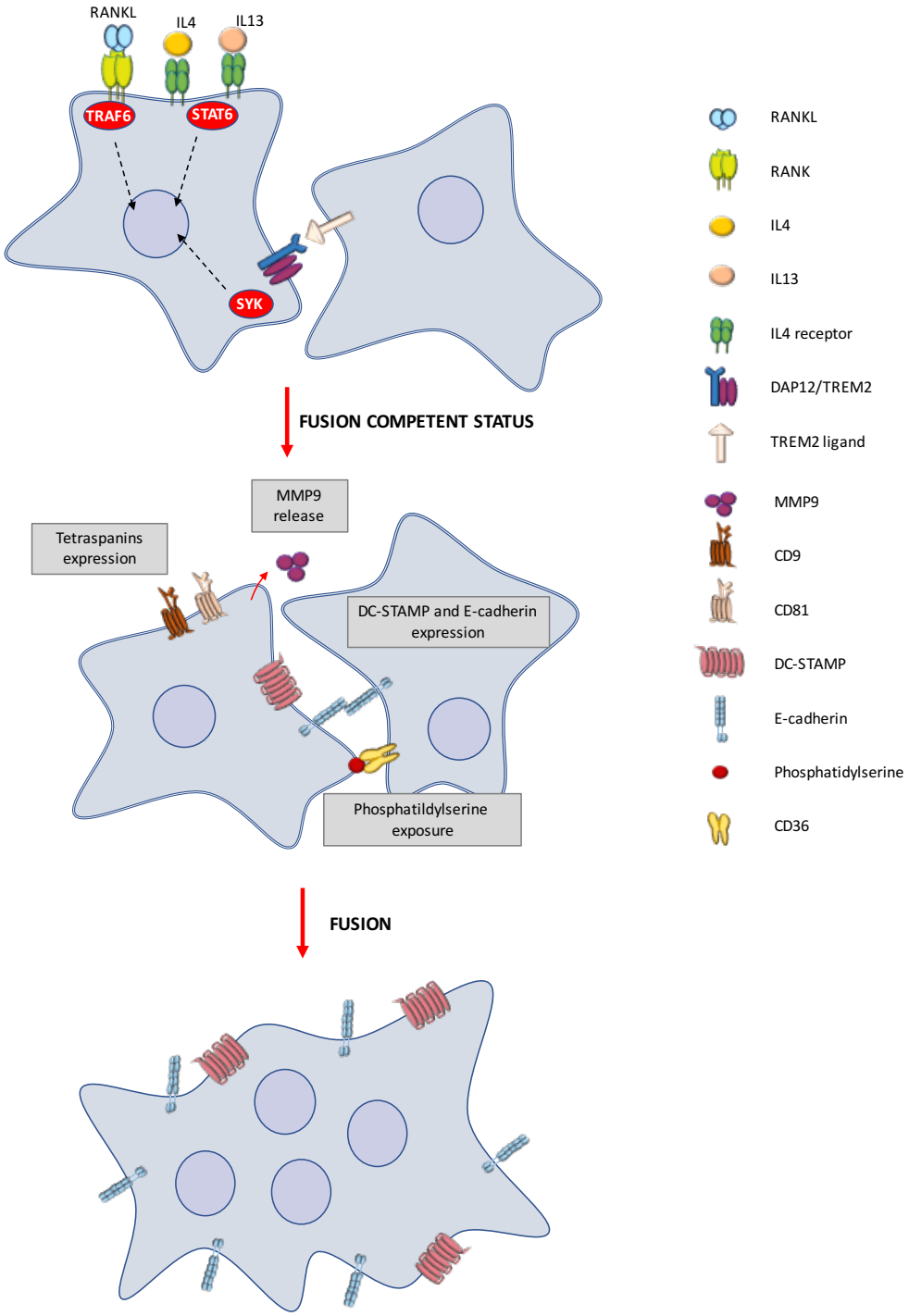

Figure 17: formation of multinucleated giant cells (osteoclasts).
RANKL, IL4 and IL13 induce signaling pathways through STAT6 and the kinase SYK leading to the fusion competent state of macrophages. Fusion competent macrophages thus release MMP9, express higher levels of tetraspanins, and fusion proteins (E-cadherin, DC-STAMP…), and present phosphatidylserine in the outer leaflet of the plasma membrane resulting in cell-cell fusion. (Helming & Gordon, 2009).

3.2.2.2. Cell-cell fusion and HIV-1

During HIV-1 infection, the formation of multinucleated giant cells (MGCs) is enhanced suggesting that HIV-1 is able to regulate cell-cell fusion in macrophages. It has been reported by Verollet et al that the Nef HIV-1 auxiliary protein is able to induce cell-cell fusion between macrophages after cell-free infection through a mechanism related to activation of the Hck tyrosine kinase (Vérollet *et al*, 2010) (Figure 18). After 8 days of infection with cell-free viruses, 70% of infected macrophages contained several nuclei whereas this percentage decreased to 45% with viruses deleted for the Nef protein. By interacting directly with the SH3 domain of Hck, Nef is able to activate this phagocyte-specific kinase in macrophages, thus leading to macrophages fusion (Vérollet *et al*, 2010). Similarly, treatment of macrophages with Interferon-γ activates Hck and leads to similar macrophages fusion.

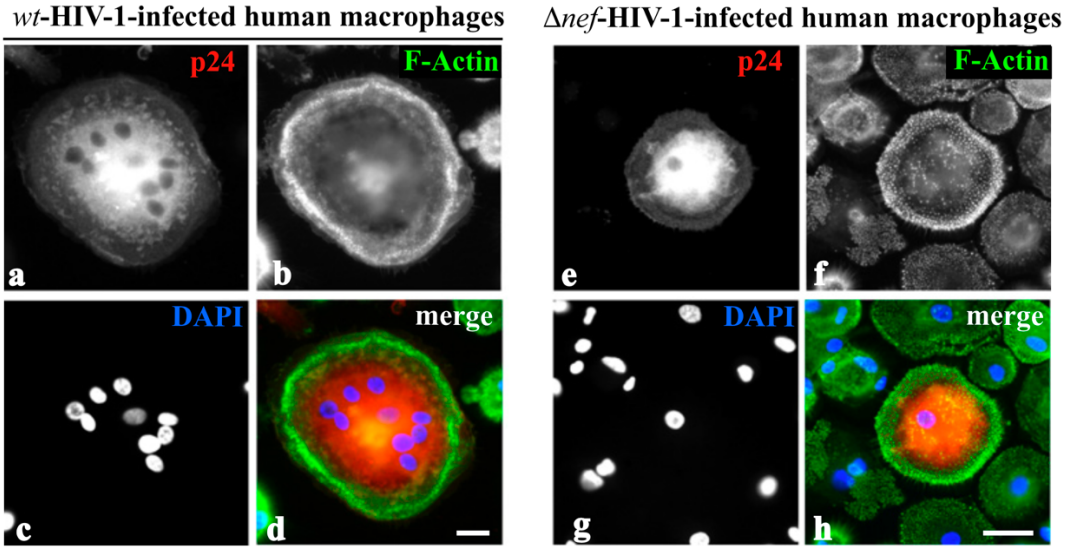

Figure 18: HIV-1 infection induce formation of multinucleated macrophages.
Δnef HIV-1–infected human macrophages form fewer MGCs than wt-HIV-1–infected human macrophages. Immunofluorescence microscopy of human monocyte-derived macrophages at day 8 postinfection with wt-HIV-1 or Δnef HIV-1.Scale bars, 10 mm. (Vérollet *et al*, 2010).

3.3. Implication of macrophages in HIV-1 infection.

3.3.1. Viral reservoirs

Because HIV-1-infected macrophages have been detected in numerous tissues, it was proposed that they could constitute important viral reservoirs during HIV-1 infection. Unlike CD4+ T cells, macrophages are long-lived cells that are indeed resistant to the cytopathic effects of HIV-1 replication observed for infected T cells, and could be maintained in host tissues for a long period of time. Different mechanisms for resistance of macrophages to HIV-1 infection have been proposed.

It was established that HIV-1 infection differentially regulates the telomerase activity in immune cells, and especially in infected macrophages where the telomerase activity is increased. This increase in telomerase activity was specific to HIV-1 infection and correlated with p24 antigen production (Lichterfeld *et al*, 2008; Ojeda *et al*, 2014; Reynoso *et al*, 2012). Moreover, increase in telomerase activity by HIV-1 infection results in higher resistance of macrophages against oxidative stress and DNA damage. Thus HIV-1-infected long-lived macrophages and formation of resistant viral reservoirs could be due to this resistance (Abbas *et al*, 2015).

Another model proposed by Swingler et al suggests that HIV-1-infected macrophages are able to resist apoptosis through involvement of the death ligand TRAIL (tumor necrosis factor–related apoptosis-inducing ligand). In HIV-1–infected macrophages, the viral envelope protein induces the release of macrophage colony-stimulating factor (M-CSF), and this pro-survival cytokine downregulates the expression of the TRAIL receptor and upregulates the anti-apoptotic genes Bfl-1 and Mcl-1 leading to a protective effect against TRAIL-induced apoptosis (Swingler *et al*, 2007). Similarly, another study showed that the HIV-1 regulatory protein Tat can induce expression of the anti-apoptotic protein Bcl-2 resulting in inhibition of TRAIL-induced apoptosis in macrophages during infection (Zheng *et al*, 2007).

3.3.2. Multinucleated giant macrophages in the neurophysiopathology of AIDS.

As mentioned above, HIV-1-infected multinucleated giant macrophages have been found in numerous tissues in HIV-1 infected patients, including lymphoid tissues (Dargent

et al, 2000), hyperplastic tonsils and adenoids (Figure 19)(Orenstein & Wahl, 1999), lungs (Costiniuk & Jenabian, 2014), colon (Lewin-Smith *et al*, 1999), paratoid glands (Vicandi *et al*, 1999) and especially brain (Fischer-Smith *et al*, 2008; Geny *et al*, 1991; Koenig *et al*, 1986; Teo *et al*, 1997). Similarly, infected multinucleated giant cells were also observed in many studies related to SIV-infected rhesus macaques (Calantone *et al*, 2014; DiNapoli *et al*, 2017; Harbison *et al*, 2014; Soulas *et al*, 2011).

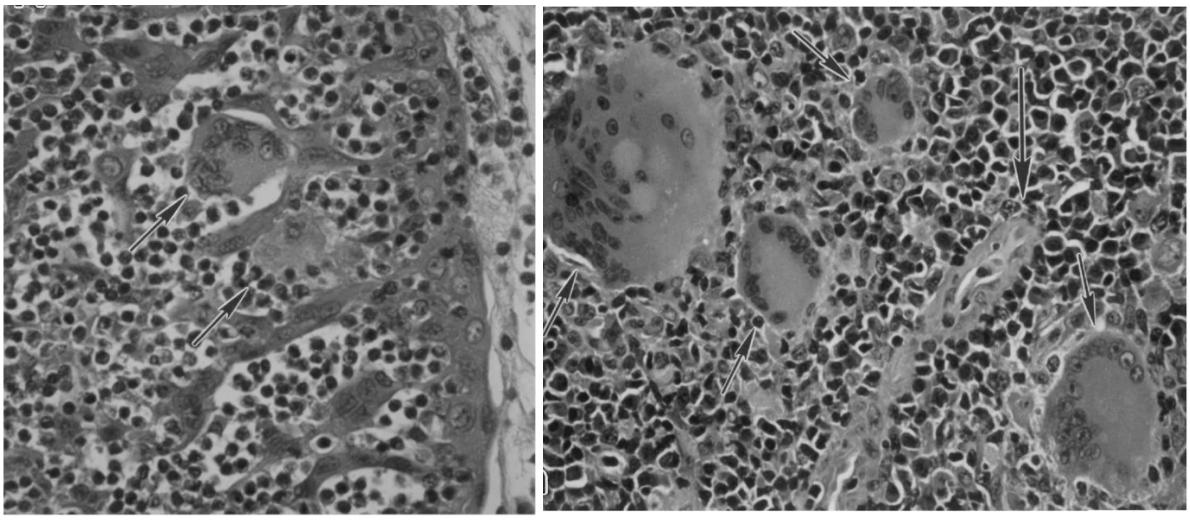

Figure 19: Presence of multinucleated giant macrophages in HIV-1 infected patients.
HIV multinucleated giant cell (black arrow) present in hyperplastic tonsil and adenoids from HIV+ infected patients. From (Orenstein & Wahl, 1999).

The presence of infected multinucleated giant cells in brain correlates with AIDS-associated neurological disorders and has been proposed as a neuropathological hallmark of HIV-1 infection in the brain. Indeed, macrophages are the only resident cells that can be productively infected by HIV-1 in the central nervous system and play a crucial role in HIV-1-associated dementia.

Infected multinucleated giant macrophages could release cytokines, viral proteins and neurotoxic molecules, such as quinolic acid, glutamate, nitric oxide and other reactive oxygen species, that contribute to neuronal damage and apoptosis through direct or indirect mechanisms (Brew *et al*, 1995; Giulian *et al*, 1990; Kaul *et al*, 2001; Nardacci *et al*, 2005). Among cytokines, interleukin-1β (IL-1b) and TNF-α have been shown to be overexpressed in the nervous system of infected patients with associated dementia (Yeh *et al*, 2000). Similarly, release of viral proteins Tat, Nef, Vpr, Rev and gp120 have been shown to cause neuronal injuries (Gendelman *et al*, 1994; Meucci *et al*, 1998).

As demonstrated by the presence of infected macrophages in numerous tissues and their implication in physiopathology of AIDS especially in brain, macrophages are

important targets of HIV-1. Furthermore, one recent study investigated the role of macrophages in HIV-1 infection by using a model of humanized mice generated by reconstituting immune-deficient mice with human $CD34^+$ hematopoietic stem cells that were devoid of human T cells (myeloid-only mice [MoM]). Using myeloid-only mice, they demonstrated that macrophages can sustain HIV replication in the absence of T cells demonstrating that macrophages represent an important target of HIV-1 that can sustain and transmit HIV-1 *in vivo* (Honeycutt *et al*, 2016, 2017).

3.4. HIV-1 replication in Macrophages

Infection of macrophages by cell-free virus has been well documented and presents some substantial differences compared to the life cycle of HIV-1 in CD4+ T cells.

3.4.1. Early steps of the viral replication cycle in macrophages

HIV-1 entry into target host cells involves the viral surface glycoprotein gp120 and its interaction with the CD4 receptor followed by the fusion of the viral envelope with the host cell membrane which is governed by the engagement of the co-receptors (CCR5 or CXCR4) both expressed on macrophages as well as in T cells *in vivo*.

After HIV-1 entry the ribonucleoprotein complex containing the viral RNA is released into the cytoplasm where reverse transcription takes place. However, the rate of reverse transcription is clearly slower in macrophages than what is observed in T cells. As non-dividing cells, macrophages have limited dNTP concentrations and express high level of SAMHD1, a specific cellular host restriction factor highly expressed in myeloid cells such as macrophages. SAMHD1 has a triphosphohydrolase activity resulting in hydrolysis of dNTPs, and thus reduces the dNTP pool available in macrophages resulting in a slower reverse transcription of the viral genomic RNA into proviral DNA (Lahouassa *et al*, 2012) (Figure 20).

The newly synthesized viral DNA is then imported into the nucleus within the nucleoprotein pre-integration complex (PIC). Unlike in activated proliferative CD4+ T cells, transport of the pre-integration complex to the nucleus is independent of cell division in terminally-differentiated macrophages. Therefore, several viral constituents of the PIC could, through interactions with host cell proteins, participate in the nuclear import of the viral DNA in macrophages, including the viral matrix (MA), viral capsid CA (p24),

nucleocapsid protein (NC), integrase (IN) and/or the auxiliary protein Vpr (Ambrose & Aiken, 2014; Fassati, 2006). However, the precise role of these viral proteins in the nuclear import of the PIC in non-dividing cells, such as macrophages, is still discussed.

After nuclear import of the viral DNA, its integration into the genome is dependent on the cellular factor p75/LEDGF (Llano *et al*, 2006). In macrophages, an additional factor is required for efficient integration: the integral nuclear inner membrane protein emerin. This protein plays an indispensable role in the integration of the viral DNA into the chromatin since infection of primary macrophages lacking emerin was abortive in that viral cDNA localized to the nucleus but integration into chromatin was inefficient (Jacque & Stevenson, 2006). This role of the emerin protein is specific to macrophages since no defect in the integration step was observed in CD4+ T cells lacking emerin (Shun *et al*, 2007).

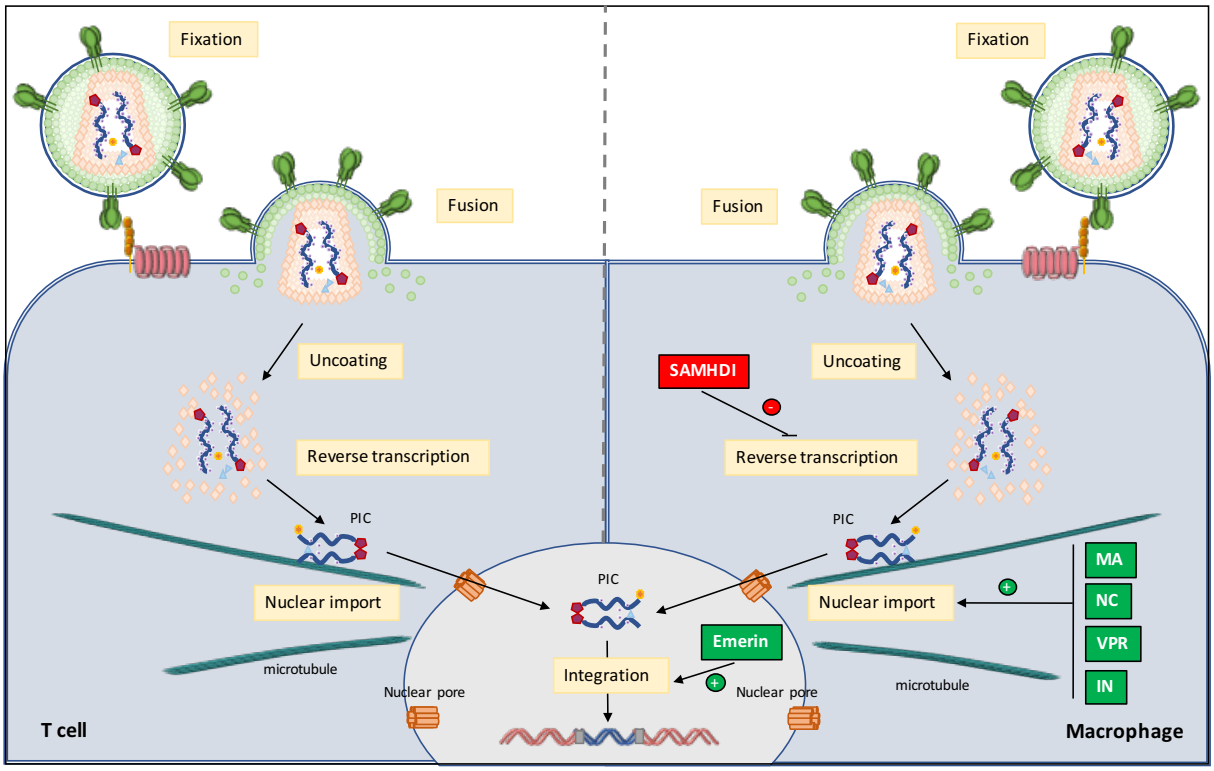

Figure 20: Early steps of the HIV-1 life cycle in T cell and macrophages.
In macrophages, the level of reverse transcription is reduced by the SAMHDI restriction factor. Nuclear import in macrophages requires matrix the viral matrix protein (MA), nucleocapsid protein (NC), integrase (IN) or the auxiliary protein Vpr. Finally, Integration in macrophages in dependent on the emerin protein.

3.4.2. Late steps of the viral life cycle in macrophages

One major difference in the HIV-1 life cycle between T cells and macrophages is related to the assembly and budding steps of new viral particles. In primary CD4+ T cells, it is well established that viral assembly takes place at the plasma membrane (Frank *et al*, 1996), while in macrophages, the site of assembly has been a matter of debate. Early electron microscopy (EM) experiments showed that virus assembly in macrophages took place in an internal, vesicle-like compartment. This membrane compartment was characterized by the presence of the tetraspanins CD63 and CD81, and was thus proposed to correspond to late endosomes or multivesicular bodies (Ono & Freed, 2004; Orenstein *et al*, 1988; Pelchen-Matthews *et al*, 2003). A few years later, several groups demonstrated that these internal virus-containing compartments (VCC) were in fact connected to the extracellular space by thin channels and was in continuity with the plasma membrane (Bennett *et al*, 2009; Deneka *et al*, 2007; Welsch *et al*, 2007). These results, in addition with the observation of the neutral pH of this compartment (Jouve *et al*, 2007), indicate that this compartment does not exhibit the same characteristics than endosomes or multivesicular bodies and has been defined as "virus-containing compartment". Viruses thus assembles in a protected compartment and are then released in the extracellular environment (Figure 21).

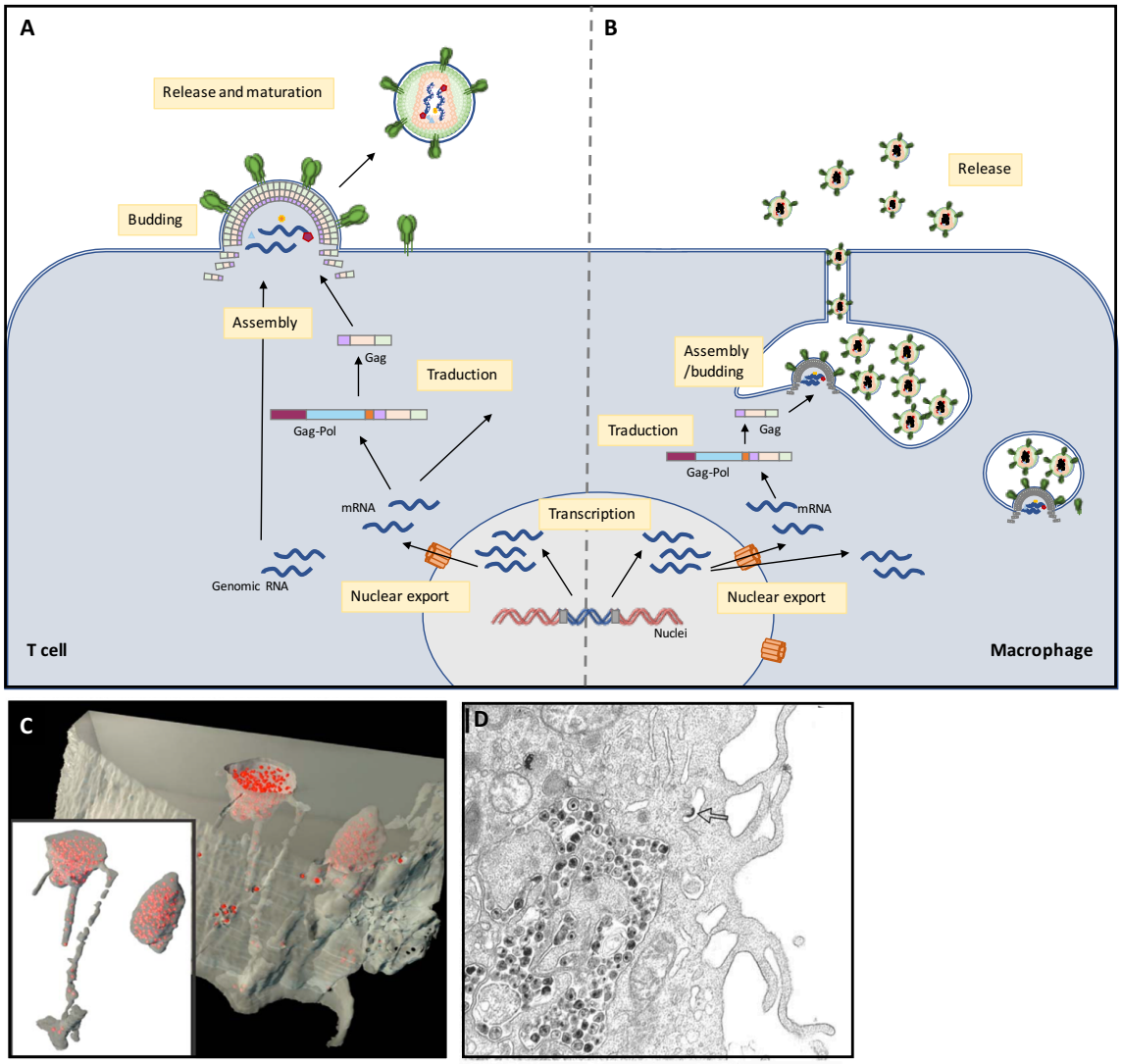

Figure 21: Late step of the HIV-1 life cycle in T cells and macrophages.
(A-B) Schematic representation of HIV-1 late steps in T cells and macrophages. In T cells (A) HIV-1 assembles and buds at the plasma membrane whereas in macrophages (B) HIV-1 assembles and buds in virus-containing compartments continuous with the plasma membrane follow by viral release. (C) Reconstruction of a 3D image from IA-SEM, showing internal HIV-1 particles (red) and virion channels (Bennett *et al*, 2009) (D) Electron microscopy of virus-containing compartment showing intracellular virions and budding profiles (open arrow) (Welsch *et al*, 2007).

3.4.3. Implication of HIV-1 auxiliary proteins.

The HIV-1 auxiliary proteins (Nef, Vif, Vpu, Vpr) play primordial role *in vivo* for virus infectivity and replication, as well as in AIDS pathogenesis. *In vitro*, a lot of functions have been attributed to these regulatory proteins during virus replication in the target cells of HIV-1. While it was known for many years that these proteins utilize and perturb basic cellular pathways for optimization of essential steps of the virus life cycle, more recent reports have shown that they are also involved in the counteraction of innate antiviral cellular restriction

factors that partially inhibit virus infectivity and dissemination in the virus target cells, especially in macrophages.

3.4.3.1. The auxiliary proteins Nef.

Nef is a protein expressed early during the viral life cycle and affects vesicular trafficking and signal transduction leading to prevention of superinfection, protection of infected cells from recognition by the immune system and enhancement of the infectivity and replication of released virus particles (Abraham et al, 2012; Basmaciogullari et al, 2014). Nef is a multifunctional protein able to interact with cellular components involved in vesicular transport between membrane compartments of the endocytic pathway, and in the control of several signaling pathways in HIV-1 infected cells (Mazzolini et al, 2010). The positive impact of Nef on virus infectivity is related to its ability to prevent incorporation of the SERINC3 and SERINC5 host cell restriction factors from virus particles released from the virus-producer cell (Usami et al, 2015; Rosa et al, 2015). The mechanism by which the SERINC proteins impair virus particle infectivity and how Nef counteracts this restriction remain to be defined, but recent studies suggested that SERINC proteins could negatively modulate the fusogenicity of virus particles by altering the conformation of HIV-1 envelope glycoproteins (Sood *et al*, 2017).

3.4.3.2. The auxiliary proteins Vpr

Vpr, an essential player of the early steps of virus replication. Vpr is the only auxiliary protein specifically incorporated into viral particles. Vpr has been shown to influence the accuracy of the reverse transcription through modulation of the mutation rate, and this activity is more pronounced in infected macrophages. This role of Vpr was related to the recruitment of the uracil DNA glycosylase (UNG2), a DNA repair enzyme, into virus particles. While some results suggest that virion incorporation of UNG2 has a positive impact on virus replication in macrophages and positively influences the reverse transcription process (Guenzel et al, 2014; Chen et al, 2004; Herate et al, 2016), conflicting findings have been reported arguing that UNG2 has rather a detrimental impact on virus replication and may act as a restriction factor (for review: Guenzel et al, 2014). In addition, Vpr could be involved in the transport of viral DNA into the nucleus. Through interaction with some proteins of the nuclear pore complex (for review: Guenzel et al, 2014), Vpr accumulates at the nuclear envelope and may participate in the nuclear import of the PIC in non-dividing cells, such as macrophages.

3.4.3.3. The auxiliary protein Vif and APOBEC3

Vif, an essential factor for virus replication. Vif expression is absolutely required for virus replication *in vitro* in all primary target cells (lymphocytes, macrophages and dendritic cells). This restriction is related to the expression of the cellular restriction factors of the APOBEC3 family which are counteracted by Vif (Opi *et al*, 2007; Sheehy *et al*, 2002). The seven members of the APOBEC3 family are cellular cytidine deaminase enzymes that catalyze sequence specific cytidine deamination of single-stranded DNA (Yu *et al*, 2004). APOBEC3G and APOBEC3F displays the most potent restriction activity against HIV-1 and are able to remove the amino group from the cytosine bases creating uracil residues in the viral DNA leading to the insertion of mutations (Jónsson et al, 2013). As mentioned above, the UNG2 enzyme could introduce a-basic sites in place of deoxyuridine created by APOBEC3 proteins leading to the degradation of the neo-synthesized viral DNA (Jónsson & Andrésdóttir, 2013; Wissing *et al*, 2010). Even if the restriction activity of APOBEC3 proteins is mainly related to their cytidine deaminase activity, some studies reported that APOBEC3G and 3F proteins may also exert antiviral activity independently of cytidine deamination through direct action on the reverse transcription process (Strebel et al, 2013). Vif counteracts APOBEC3 proteins through ubiquitination and proteasomal degradation of APOBEC3, and thus prevents its incorporation into virions released from virus-producer cells (Münk *et al*, 2012; Wissing *et al*, 2010).

3.4.3.4. The auxiliary protein Vpu and BST-2

Vpu, an essential protein for virus budding. Vpu is a transmembrane protein expressed later during the viral life cycle suggesting that it is playing a role during the late stages. Indeed, the two main functions assigned to Vpu are the downregulation of the CD4 expression through proteasomal degradation of the receptor and the enhancement of virion release from the plasma membrane (Malim et al, 2008). Vpu-induced CD4 degradation is believed to block interaction of CD4 with envelope glycoproteins insuring the release of infectious viruses (Van Damme et al, 2008). Vpu also enhances virus release from the plasma membrane by counteracting the cellular restriction factor BST-2 (or tetherin). BST-2 is upregulated in response to type-I IFN, and express at the plasma membrane where it tether the virus thus inhibiting the release of new virions. The mechanism of Vpu antagonism appears to rely on misdirection of BST-2 from the plasma membrane to intracellular compartments followed by its degradation (Tokarev et al, 2011; Roy et al 2014).

3.4.3.5. The auxiliary protein Vpx and SAMHDI

SAMHD1, a cellular protein that restricts HIV-1 replication in non-dividing cells. SAMHD1 is an interferon-induced enzyme displaying a deoxynucleosidetriphosphate (dNTP) phosphohydrolase activity recently identified has HIV-1 restriction factors in non-divinding cells such as macrophages, dendritic cells, and resting T cells (Hrecka *et al*, 2011; Laguette *et al*, 2011). By maintaining the levels of the cellular dNTP pool below the levels required for efficient reverse transcription, SAMHDI strongly inhibit the synthesis of viral genomic RNA (Baldauf *et al*, 2012; Lahouassa *et al*, 2012). In viruses from the HIV-2 or SIV lineages, SAMHD1 is counteracted by the auxiliary protein Vpx through degradation by the proteasome machinery allowing very efficient replication of these viruses in myeloid cells, including macrophages.

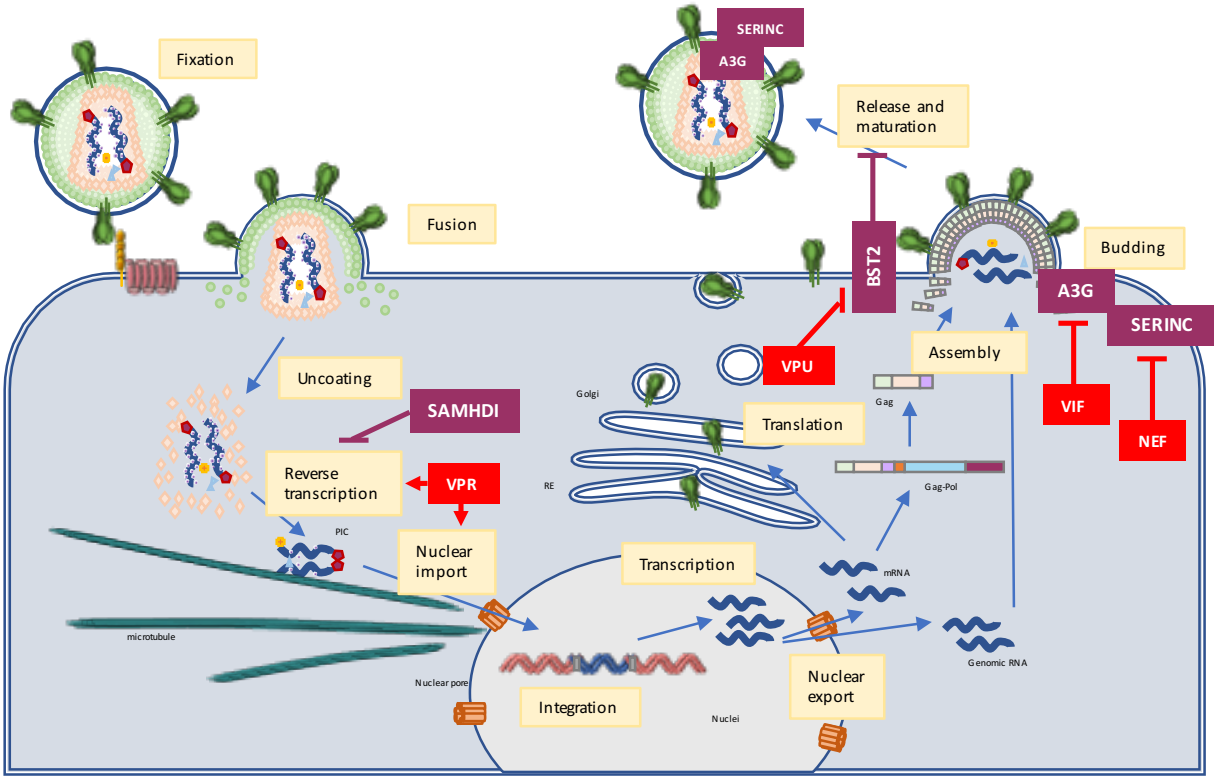

Figure 22: Effect of auxiliary proteins and cellular restriction factors of HIV-1.
SAMHDI, APOBEC3G (A3G), SERINC and BST2 are cellular restriction factor of HIV-1 inhibiting reverse transcription, or release and infectivity of new viral particles. The HIV-1 auxiliary proteins are able to counteract these restriction factors and to act directly on the different step of the viral replication cycle like reverse transcription or nuclear import.

3.5. Macrophages and HIV-1: conclusions

In summary, macrophages play an important role in the physiopathology of AIDS since infected macrophages participate in virus dissemination and establishment of persistent virus reservoirs in numerous host tissues, including lymph nodes, spleen, lungs, genital and digestive tracts, and the central nervous system (CNS) of infected patients and leads to the development of the HIV-1-associated neurologic disorders and especially HIV-associated dementia. Specific characteristics of cell-free infection in macrophages have been well documented (virus-containing compartments, restriction factors, nuclear import…) and the implication of HIV-1 in some specialized macrophages functions has been evidenced by inhibition of phagocytosis or increase of cell-to-cell fusion in infected macrophages. However, mechanisms of cell-to-cell infection of macrophages through cell-to-cell contacts remain poorly investigated with only one study concerning engulfment of infected dying T cells leading to macrophage infection having been published so far.

4. Aims of the experimental work

Thus, during my PhD, I focused my work on investigating cellular and molecular mechanisms of HIV-1 cell-to-cell transfer in macrophages.

Cell-to-cell infection has been largely documented for HIV-1 transmission between T cells but the mechanisms of cell-to-cell infection of macrophages and osteoclast remains poorly investigated. Given the importance of macrophages in HIV-1 infection, the aim of my PhD was to analyze HIV-1 cell-to-cell transfer to macrophages. Additionally, in collaboration with the team of Isabel Maridonneau-Parini, I also investigated cell-to-cell infection of osteoclasts.

4.1. Analysis of HIV-1 cell-to-cell transmission between infected T cells and macrophages

Macrophages, which express both CD4 and the CCR5 and CXCR4 co-receptors required for virus entry, are targets of HIV-1 and important for the physiopathology of AIDS. Indeed, infected multinucleated giant macrophages are present in different tissues of infected patients, especially in the brain where it leads to the development of the HIV-1-associated neurologic disorders and even dementia. However, almost all the data reported so far regarding macrophage infection and analysis of the different steps of the virus life cycle in this cell type were performed using cell-free infection. Only one study regarding productive infection of macrophages via selective capture of healthy or rather dying HIV-1-infected CD4+ T lymphocytes was recently reported (Baxter *et al*, 2014).

In contrast, efficient virus dissemination in T lymphocytes by HIV-1 cell-to-cell transfer between T cells or from infected macrophages or dendritic cells to T cells has been documented, mainly through the formation of the so-called virological or infectious synapse but also using other membrane structures such as filopodia, nanotubes or trogocytosis. These intercellular routes of infection are, at least *in vitro*, several orders of magnitude more efficient than T cell infection with cell-free virus particles. Importantly, this mode of virus dissemination may enable virus to escape elimination by the immune system and antiretroviral drugs.

While few data are available about HIV-1 cell-to-cell transmission between infected T cells and macrophages, it is obvious that macrophages can establish tight intercellular contacts with infected T lymphocytes as observed in some tissues, such as lymphoid organs, colon and brain, in HIV-infected patients and in SIV-infected monkeys. Thus, the main aim of my PhD work was to investigate whether and how HIV-1 is transferred from infected T cells to macrophages through cell-to-cell contacts for virus dissemination and productive infection of macrophage targets.

4.2. Analysis of HIV-1 infection of osteoclasts.

Since osteoclasts share a common myeloid origin with macrophages, it has been proposed that osteoclasts are targets for HIV-1 and that infected osteoclasts would contribute to bone loss disorders observed in HIV-1-infected patients. Reduced bone mineral density is a frequent complication of HIV-1 infected patients and often progresses to osteoporosis and high prevalence of fractures. Multiple factors are believed to contribute to bone loss in infected patients. HAART is one of these factors, especially during the first years of therapy. In addition, there is evidence of bone deficit in non-treated patients, showing that the virus alone alters bone homeostasis (Bruera *et al*, 2003; Gibellini *et al*, 2007; Grijsen *et al*, 2010; Titanji *et al*, 2014). Indeed, it has recently been shown that HIV-1 may replicate *in vitro* in human monocyte-derived osteoclasts and enhance their bone resorption activity (Gohda *et al*, 2015). However, the relevance of this observation has to be tested *in vivo* and both cellular and viral mechanisms involved in osteoclast infection or bone resorption processes remain to be characterized.

In this context, the group of Isabel Maridonneau-Parini (IPBS, Toulouse, France) investigated HIV-1 infection in osteoclasts, *in vitro* and *in vivo* and the mechanism of bone resorption in HIV-1 infected osteoclasts. In order to investigate these phenomena, the second aim of my phD was, in collaboration with Christel Verollet and Brigitte Raynaud-Messina, to study osteoclast HIV-1 infection through cell-to-cell transmission of HIV-1 between infected T cells and osteoclasts.

RESULTS

Article 1: T cells-macrophages fusion triggers multinucleated giant cell formation for HIV-1 spreading.

1. Abstract

HIV-1-infected macrophages participate in virus dissemination and establishment of virus reservoirs in host tissues, but the mechanisms for virus cell-to-cell transfer to macrophages remain poorly investigated. Here, we reveal the mechanisms for cell-to-cell transfer from infected T cells to macrophages and virus spreading between macrophages. We show that contacts between infected T lymphocytes and macrophages lead to cell fusion for fast and massive transfer of CCR5-tropic viruses to macrophages. Through the merging of viral material between T cells and macrophages, these newly formed lymphocyte/macrophage fused cells acquire the ability to fuse with neighboring non-infected macrophages. Together, these two-step envelope-dependent cell fusion processes lead to the formation of highly virus-productive multinucleated giant cells reminiscent of the infected multinucleated giant macrophages detected in HIV-1-infected patients and SIV-infected macaques. These mechanisms represent an original mode of virus transmission for viral spreading and a new model for the formation of macrophage virus reservoirs during infection.

2. Presentation of the article

First, we have investigated whether HIV-1-infected CD4+ T cells (primary and T-cell lines) were able to transfer viral material to monocyte-derived macrophages. T cells were infected with different viral strains of HIV-1 (CCR5-using viruses or CXCR4-using viruses) and co-cultured with macrophages for different periods of time. Using flow cytometry, we evaluated the number of macrophages positive for viral Gag material, and then analyzed whether these Gag-positive macrophages were productively infected by quantifying viral production by p24 ELISA and analyzing the effect of antiretroviral drugs on viral production.

In order to visualize and characterize HIV-1 cell-to-cell transfer from infected T cells to macrophages, we then performed immunofluorescence and electron microscopy on fixed cells and live-cell imaging on living cells. Using these techniques, we observed that infection of macrophages by cell-to-cell transfer from infected T cells led to the formation of infected multinucleated giant cells. We then investigated the mechanisms related to the

formation of these multinucleated giant cells by immunofluorescence microscopy or by using different inhibitors against the viral envelope, and against the CD4 receptor and CCR5 co-receptor. Finally, we analyzed the role of these infected multinucleated giant macrophages in viral dissemination by quantifying viral production over extended periods.

3. Article

Revised manuscript (JVI01237-17)

T cell-macrophage fusion triggers multinucleated giant cell formation for HIV-1 spreading

Lucie Bracq[1,2,3,4,5], Maorong Xie[1,2,3,5*], Marie Lambelé[1,2,3,5*], Lan-Trang Vu[1,2,3,5], Julie Matz[1,2,3], Alain Schmitt[1,2,3], Jérôme Delon[1,2,3], Paul Zhou[4,5], Clotilde Randriamampita[1,2,3], Jérôme Bouchet[1,2,3,5#], and Serge Benichou[1,2,3,5#]

[1]Inserm U1016, Institut Cochin, Paris, France;

[2]CNRS, UMR8104, Paris, France;

[3]Université Paris-Descartes, Sorbonne Paris-Cité, Paris, France.

[4]Institut Pasteur Shanghai-Chinese Academy of Sciences, Shanghai, China.

[5]International Associated Laboratory (LIA VirHost), CNRS, Université Paris-Descartes, and Institut Pasteur Shanghai-Chinese Academy of Sciences.

Running title: Fusion of HIV-1-infected T cells with macrophages

#To whom correspondence should be addressed:

Serge Benichou and Jérôme Bouchet

Institut Cochin, 22 Rue Méchain, 75014 Paris, France;

Tel.: (33) 1 40 51 65 78; Fax: (33) 1 40 51 65 70;

e-mail: serge.benichou@inserm.fr; jerome.bouchet@inserm.fr

Keywords: HIV-1, T lymphocytes, macrophages, cell-to-cell transfer, cell fusion

*These authors equally contributed to this work

Abstract

HIV-1-infected macrophages participate in virus dissemination and establishment of virus reservoirs in host tissues, but the mechanisms for virus cell-to-cell transfer to macrophages remain unknown. Here, we reveal the mechanisms for cell-to-cell transfer from infected T cells to macrophages and virus spreading between macrophages. We show that contacts between infected T lymphocytes and macrophages lead to cell fusion for fast and massive transfer of CCR5-tropic viruses to macrophages. Through the merge of viral material between T cells and macrophages, these newly formed lymphocyte/macrophage fused cells acquire the ability to fuse with neighboring non-infected macrophages. Together, these two-step envelope-dependent cell fusion processes lead to the formation of highly virus-productive multinucleated giant cells reminiscent of the infected multinucleated giant macrophages detected in HIV-1-infected patients and SIV-infected macaques. These mechanisms represent an original mode of virus transmission for viral spreading and a new model for the formation of macrophage virus reservoirs during infection.

44 **Importance**

45

46 We reveal a very efficient mechanism involved in cell-to-cell transfer from infected T cells to
47 macrophages and subsequent virus spreading between macrophages by a two-step cell fusion
48 process. Infected T cells first establish contacts and fuse with macrophage targets. The newly
49 formed lymphocyte/macrophage fused cells then acquire the ability to fuse with surrounding
50 uninfected macrophages leading to the formation of infected multinucleated giant cells that
51 can survive for a long time as evidenced *in vivo* in lymphoid organs and the central nervous
52 system. This route of infection may be a major determinant for virus dissemination and the
53 formation of macrophage virus reservoirs in host tissues during HIV-1 infection.

54

55 **Introduction**

56

57 Besides CD4+ T lymphocytes and dendritic cells, macrophages are cellular targets of
58 HIV-1 and play crucial roles in the physiopathology of infection (1–5). The presence of
59 infected macrophages has been evidenced *in vivo* in HIV-1-infected patients and SIV-infected
60 macaques, as well as in "Humanized" mice where macrophages can sustain HIV-1 productive
61 infection and HIV-1 can persist in tissue macrophages even in mice treated with antiretroviral
62 therapy (6–8). Several specialized functions of macrophages, such as cytokine production,
63 phagocytosis and migration are affected by HIV-1 infection (9–14). In addition to latently
64 infected CD4+ T cells, infected macrophages also participate in virus dissemination and
65 establishment of persistent virus reservoirs in numerous host tissues, including lymph nodes,
66 spleen, lungs, genital and digestive tracts, and the central nervous system (CNS) (4, 5, 15).
67 Virus access to the CNS is indeed mainly related to migration of infected perivascular
68 monocytes/macrophages through the blood brain barrier and can result in a massive
69 infiltration of macrophages and microglial cells often detected as multinucleated giant cells
70 (MGCs) (1, 16–19).

71 *In vitro*, macrophages derived from blood monocytes, which express both CD4 and the
72 CCR5 and CXCR4 co-receptors required for virus entry, can be productively infected by
73 HIV-1 (2, 20). However, almost all the data reported so far regarding macrophage infection
74 and analysis of the different steps of the virus life cycle in this cell type were performed using
75 cell-free virus particles. Only one study regarding the possibility of productive infection of
76 macrophages via selective capture of healthy or rather dying HIV-1-infected CD4+ T
77 lymphocytes was recently reported (21).

78 In contrast, efficient virus dissemination in T lymphocytes by cell-to-cell transfer of virus
79 particles between T cells or from infected macrophages or dendritic cells to T cells has been

documented, mainly through the formation of the so-called virological synapse (22–26) but also using other membrane structures such as filopodia or nanotubes (27–31). This ability of HIV-1 to spread toward T cells by cell-to-cell contacts is the major determinant for virus dissemination as evidenced *in vivo* in animal models (32, 33). Moreover, these intercellular routes of infection are, at least *in vitro*, several orders of magnitude more efficient than T cell infection with cell-free virus particles (24, 25). Importantly, this mode of virus dissemination may enable virus to escape elimination by the immune system and antiretroviral drugs (15, 20, 22, 34–37).

Whereas infection of T lymphocytes via cell-to-cell transfer was largely investigated, there is a paucity in knowledge of the mechanisms that control infection and dissemination to macrophages by cell-to-cell transfer (21). However, it is obvious that macrophages can establish tight intercellular contacts with infected T lymphocytes as observed in some tissues, such as lymphoid organs, colon and brain, in HIV-infected patients and in SIV-infected monkeys (2, 19, 38). The aim of the present study is to investigate how HIV-1 is transferred from infected T cells to macrophages through cell-to-cell contacts for virus dissemination and productive infection of macrophage targets. We show here, for the first time, that the establishment of close contacts between infected T lymphocytes and macrophage targets leads to heterotypic cell fusion for fast and efficient transfer of viral material that subsequently triggers viral envelope-dependent homotypic fusion of macrophages able to generate new infectious particles for intercellular dissemination of HIV-1. Altogether, our data reveal a new mechanism employed by HIV-1 for spreading between its different cell targets and an original model for the formation of macrophage virus reservoirs during HIV-1 infection.

Results

Productive infection of macrophages through HIV-1 cell-to-cell transfer from infected T cells.

To analyze whether infected T lymphocytes could mediate cell-to-cell virus transfer to macrophages, we used Jurkat cells or purified primary CD4+ T cells as donor infected T cells and macrophages derived from blood monocytes (MDMs) as target cells (Fig. 1A). Jurkat or primary T cells were infected with CCR5- (YU2 and NLAD8 strains) or CXCR4-tropic (NL4.3 strain) viruses (Fig. 1B-D, green bars). 36 h later, infected T cells were co-cultured for 6 h with MDMs using different MDM/T-cell ratios. After elimination of T cells by extensive washing (98.5% of T cell removal, data not shown), MDMs were fixed and stained for intracellular Gag and cell surface CD11b and CD3, and the percentage of Gag+ cells among the CD11b+ cells was quantified by flow cytometry to assess the transfer of viral material in MDMs. After 6 h of co-culture with YU2- and NLAD8-infected Jurkat or primary T cells, transfer of viral material was detected in a significant percentage (10-40%) of MDMs (Fig. 1B-D, blue bars). By comparison, a very low percentage of transfer of the YU2 and NLAD8 viruses was detected when infected T cells were separated from MDMs by a virus-permeable Transwell membrane (Fig. 1C-D, red bars) or when MDMs were infected with cell-free viruses produced by T cells during the 6 h of co-culture (Fig. 1C, yellow bars). Since viral transfer in CD11b+ MDMs was optimal at the 1:2 MDM/T-cell ratio (Fig 1B and 1D), this ratio was used in subsequent experiments.

Interestingly, the NLAD8 CCR5-tropic viral strain, which differs from the NL4.3 CXCR4-tropic strain only by substitution of a fragment of the gp120 envelope glycoprotein from the ADA CCR5-tropic strain (39, 40) was efficiently transferred to MDMs whereas the NL4.3 viral strain was not (Fig. 1C, blue bars). This indicates that the process for virus

transfer to MDMs is related to a mechanism dependent of the tropism and co-receptor usage of the viral envelope (Env). To confirm that HIV-1 Env contributed to virus transfer, we tested various viral entry inhibitors, such as anti-gp120 neutralizing antibodies, the anti-CD4 Leu3 antibody, the T20 fusion inhibitor, and the Maraviroc CCR5 antagonist. As shown in Fig. 1E-F, all the entry inhibitors blocked virus transfer to MDMs, demonstrating that virus cell-to-cell transfer to MDMs is Env-dependent.

We next investigated whether the transfer of viral material led to productive infection of MDMs. Infected Jurkat or primary CD4+ T cells were co-cultured for 6 h with MDMs as previously, eliminated by washing, and the percentage of Gag+ MDMs was evaluated 1, 6, 9, 12 and 15 days later (Fig. 2A and 2D). Again, a very low viral transfer was observed with NL4.3-infected Jurkat cells, whereas both YU2 and NLAD8 macrophage-tropic strains propagated efficiently in MDMs, as evidenced by the level of Gag+ MDMs detected during the 15-day observation period after the initial transfer from infected T cells. As expected, high levels of viral p24 production were detected in the supernatants from MDMs co-cultured with YU2- and NLAD8-infected T cells (Fig. 2B and 2E). We checked that the virions produced by MDMs were fully infectious by infecting the TZM-Bl reporter cell line (Fig. 2C and 2F). Additionally, virus dissemination and production in MDMs were inhibited by the AZT reverse-transcriptase inhibitor (Fig. 2G, day 6, and Fig. 2H) without affecting the initial virus transfer to MDMs (Fig. 2G, 6 h).

Visualization of cell contacts and viral transfer between infected T cells and macrophages.

To visualize virus transfer, fluorescence microscopy was performed first using infected Jurkat cells co-cultured for 30 min, 2 h or 6 h with MDMs preloaded with the CellTrace dye before fixation and intracellular Gag staining. As shown in Fig. 3A-B, infected T cells established

153 contacts with MDMs leading to visualization of Gag+ dots in the cytoplasm of the MDMs
154 after 30 min of co-culture (Fig. 3A, upper images, 0.5 h). Virus transfer subsequently resulted
155 in accumulation of larger Gag+ puncta (Fig. 3A, middle images, 2 h). Intriguingly, a diffuse
156 cytoplasmic staining was observed in almost all Gag+ MDMs after 6 h of co-culture (lower
157 images, 6 h); at this time point, all the Gag+ MDMs contained at least 2 nuclei. In agreement,
158 fluorescence quantification from images showed significant increase of the intracellular Gag
159 staining of MDMs from 0.5 h to 6 h of co-culture (Fig. 3B). Similarly, infected primary CD4+
160 T cells also established contacts with autologous MDMs leading to accumulation of
161 intracytoplasmic Gag+ dots in MDMs after 2 h of co-culture (data not shown), and exhibited a
162 diffuse cytoplasmic Gag staining and contained several nuclei after 6 h of co-culture with
163 infected T cells (see Fig. 6G).

164 We also performed live-cell imaging using Jurkat cells infected with fluorescent HIV-1-
165 GFP and co-cultured with MDMs preloaded with CellTrace. As shown in Fig. 3C (Movie S1),
166 we could visualize contacts between infected T cells and MDMs allowing a continuous
167 discharge of fluorescent viral material (white arrows) into MDMs during the first hour of co-
168 culture. Interestingly, longer live-cell experiments showed a rapid and massive diffusion of
169 the virus-associated fluorescence from infected T cells to the cytoplasm of MDMs, strongly
170 suggesting that these cell contacts lead to the fusion of infected T cells with MDMs targets
171 (Fig. 3D and Movies S2). Since our experiments were carried out 36 h after T cell infection,
172 when less than 2% of infected T cells were apoptotic (data not shown), we did not observe
173 phagocytosis of infected T cells by MDMs as recently reported (21). In addition, virus
174 transfer from infected T cells to macrophages was not significantly affected by high
175 concentrations of latrunculin A, an actin-binding drug preventing F-actin polymerization and
176 known to totally inhibit phagocytosis at low concentration, in our experimental system (data

not shown). Of note, we did not observe formation of Gag+ T cell syncytia in our experimental system.

Transmission electron microscopy was also used to visualize the contacts between infected T cells and MDMs after 6 h of co-culture. As shown in Fig. 4A, electron-dense material corresponding to viral buds protruding from the plasma membrane of the donor T cell (blue arrows), as well as mature virions (red arrow), were observed at the site of contact with MDMs. Interestingly, we also observed the accumulation of mature viruses in cytoplasmic membrane compartments of MDMs (Fig. 4B, white arrows). More surprisingly, electron-dense material reminiscent of Gag assembly and virus budding (blue arrows) and mature virions (red arrows) were observed at the plasma membrane of MDMs as well as between MDMs which established tight contacts (Fig. 4B-C), suggesting that virus assembly and budding took place at the cell surface of MDMs only 6 h after co-culture with infected T cells, before *de novo* virus production. In agreement, virus-containing cytoplasmic compartments as well as plasma membrane viral buds were still observed when MDMs were treated with AZT during co-culture with infected T cells (Fig. 4D-E). In contrast, we could not observe such virus-containing compartments and viral buds 6 h after infection of MDMs with cell-free viruses (data not shown). These observations could result from the cell fusion of infected T cells with MDMs revealed by live-cell imaging, suggesting plasma membrane exchanges and the merge of Gag and Env material between infected T cells and MDM targets.

Viral transfer to macrophages through heterotypic cell-fusion with infected T cells.

Because we observed from immunofluorescence images that almost all Gag+ MDMs contained at least 2 nuclei after virus transfer (see Fig. 3A, lower images, 6 h), we first quantified the number of nuclei in MDMs after co-culture with infected Jurkat cells (Fig. 5A). Before co-culture, more than 90% of the MDMs contained 1 nucleus, whereas about 50% of

Gag+ MDMs contained at least 2 nuclei (mean nucleus number=1.83) after 2 h of co-culture, and this percentage increased to 99% (mean nucleus number=3.24) after 6 h (Fig. 5A). Similarly, MDMs co-cultured for 6 h with autologous infected primary CD4+ T cells contained several nuclei (mean nucleus number=5.36, Fig. 5B), suggesting that these Gag+ multinucleated MDMs are generated through cell fusion events with infected T cells as documented by live-cell imaging analysis (see Fig. 3D and Movies S2).

To test this hypothesis, infected Jurkat cells were preloaded with the CellTracker dye and co-cultured as previously with MDMs. After 6 h of co-culture, all Gag+ MDMs contained several nuclei, including at least 1 CellTracker-stained nucleus (Fig. 5C-D), demonstrating cell fusion between infected T cells and MDMs. This cell fusion between infected T cells and MDMs is mediated by viral envelope-receptor interactions, since it was totally blocked by anti-gp120 neutralizing antibodies and the T20 fusion inhibitor (Fig. 5E-F). Finally, immunofluorescence staining confirmed that all Gag+ MDMs contained membrane and cytoplasmic specific T cell markers, such as CD3, CD2 and Lck after 6 h of co-culture with infected Jurkat (Fig. 6A-F) or primary CD4 T cells (Fig. 6G-H).

Together, these results demonstrate that HIV-1 is mainly transferred from infected T cells to macrophages through a heterotypic envelope-dependent cell fusion process leading to the formation of lymphocyte/macrophage fused cells (LMFCs).

Virus dissemination through homotypic cell-fusion between macrophages.

Interestingly, since we observed that a large majority of the Gag+ newly formed LMFCs contained more than 2 nuclei after 6 h of co-culture (see Fig. 5A-B), we explored whether LMFCs could fuse with surrounding MDMs leading to the formation of Gag+ multinucleated giant cells. After co-culture for 6 h with infected Jurkat cells to allow initial cell fusion and virus transfer, LMFCs cultured for 1 or 5 days after elimination of infected T cells indeed

contained more than 2 nuclei with an average nucleus number of 4.8 and 7.9, respectively (Fig. 7A-C). To confirm LMFC/MDM fusion, infected T cells were co-cultured for 6 h with MDMs, eliminated, and autologous non-infected MDMs preloaded with the CellTrace dye were added. 24 h later, Gag+ MDMs with several nuclei were also labeled with CellTrace (Fig. 7D), resulting from the fusion of Gag+ LMFCs with neighboring uninfected MDMs to form Gag+ multinucleated giant cells (MGCs). Fusion of Gag+ MDMs with surrounding MDMs was also observed when pre-labeled non-infected MDMs were added 5 days after co-culture and elimination of infected T cells (data not shown). Since the initial fusion with infected T cells led to the presence of T cell specific markers at the cell surface of LMFCs (see Fig. 6), we hypothesized that these latter could also express the viral envelope, and explored whether the fusion of Gag+ LMFCs with MDMs was mediated by viral envelope-receptor interactions. Following the 6 h co-culture to allow initial cell fusion and virus transfer, infected T cells were eliminated and MDMs were cultured in the presence of the T20 fusion inhibitor and the Maraviroc CCR5 antagonist. As expected, about 60% of Gag+ LMFCs cultured without inhibitors contained at least 3 nuclei 1 day later, but this percentage decreased to 20 and 10% when LMFCs were cultured with Maraviroc and T20, respectively (Fig. 7E). Importantly, inhibition of LMFC fusion with neighboring MDMs by T20 after initial virus transfer led to a net decrease in virus dissemination (Fig. 7F) and virus production by LMFCs (Fig. 7G). In agreement, infected MGCs with many nuclei could be still detected after 26 days of culture (Fig. 8A), and were indeed still able to produce high levels of p24 30 days after elimination of infected T cells (Fig. 8B). These results show that the LMFC/MDM cell fusion is required for optimal virus spreading and production by long-lived multinucleated giant cells.

Discussion

In the present study, we reveal the mechanisms involved in a rapid and massive HIV-1 cell-to-cell transfer from infected T cells to MDMs and the subsequent virus spreading between MDMs by a two-step cell fusion process leading to the productive infection of MDM targets. Both cell fusion steps are mediated by viral envelope-receptor interactions at the cell surface of T cells and MDMs, and are completed in less than 2 h. This route of infection may be a major determinant *in vivo* for virus dissemination to macrophages.

As evidenced by fluorescence microscopy analyses including live-cell imaging, the first step is related to the establishment of contacts with infected T cells resulting in the fusion of infected T cells with MDM targets. This cell fusion process is evidenced by the massive and rapid transfer of Gag+ material as well as membrane and cytosolic T cell specific markers such as CD2, CD3 and Lck, then ensuring efficient virus dissemination between these two important target cells of HIV-1. We did not observe, in our experimental system, formation of HIV-1-induced T cell syncytia, either using Jurkat cells or CD4+ primary T cells as virus donor cells, suggesting that HIV-1 induced cell-to-cell fusion could be restricted to myeloid cell targets such as macrophages, and inhibited between T cells (41-45). In agreement with this first step of T cell-to-MDM fusion for viral transfer, it was shown that myeloid cells from lymphoid tissues of SIV-infected macaques, such as spleen and lymph nodes, contain T cell markers and viral RNA and DNA originating from infected T cells (47, 46).

Electron microscopy analysis confirmed that infected T cells establish contacts with macrophages, with evidences of virus assembly at the site of cell-to-cell contacts, leading to virus transfer and accumulation of mature virus particles in cytoplasmic membrane compartments in macrophages after only 6 h of co-culture with infected T cells, before *de novo* virus production by the macrophage targets. We could hypothesize that the mature and

immature viruses found in these early-formed virus-containing compartments (VCCs) result from the initial discharge of viral material, before cell fusion, observed by fluorescence microscopy on both fixed and lived cells. Such early-formed VCCs have been observed in target T cells following virus cell-to-cell transfer in enclosed endocytic compartments from infected donor T cells (48–51). Formation of VCCs has been also largely documented when macrophages were infected with cell-free viruses, but they appeared later at least 5-6 days after infection, and contained neo-synthesized virus particles (52–57). While the exact mechanisms for the formation of these early and late VCCs need to be further investigated, such VCCs could participate in long term storage of HIV-1 in tissue macrophages and lead to establishment of viral reservoirs for virus maintenance and spreading (1–5). Interestingly, some events of assembly and budding of virus particles were detected at the plasma membrane of the macrophage targets before *de novo* virus production after only 6 h of co-culture with infected T cells, suggesting that the newly formed Gag+ lymphocyte/macrophage fused cells also expose viral envelope at their cell surface. These cells then acquire the ability to fuse with neighboring uninfected MDMs leading to the formation of multinucleated giant cells that can survive and produce high amount of fully infectious viruses even after 30 days of cell-culture. Similarly, formation of HIV-1-infected giant cells was reported when macrophages were infected with cell-free viruses (14, 58), but they appeared several days after infection. Despite their large size, these infected multinucleated macrophages migrate faster than their infected mononucleated counterpart and may participate in virus dissemination (13). More importantly, these Gag+ multinucleated giant cells observed *in vitro* are reminiscent of the infected multinucleated giant macrophages detected *in vivo* in lymphoid organs and the CNS of HIV-1-infected patients and SIV-infected macaques (3, 17, 59-64).

We found that virus transfer to macrophages through initial T cell fusion and subsequent virus dissemination in multinucleated giant macrophages were restricted to macrophage-tropic

CCR5-using viral strains. In contrast, Baxter et al. (21) reported that internalization of healthy or dying infected T cells by MDMs was related to a non-conventional mechanism independent of the viral envelope and showed that the NL4.3 CXCR4-tropic strain could be efficiently transferred to macrophages using GFP-tagged NL4.3-infected T lymphocytes as donor cells. This discrepancy could be related to the use of non-dying T cells infected with the untagged wild-type replication-competent NL4.3 strain to analyze transfer in our experimental system. While initial studies suggested that virus transfer between CD4+ T cells at the virological synapse was independent of the co-receptor usage (65, 66), subsequent reports showed that this transfer required co-receptor expression and was inhibited by co-receptor antagonists (24, 49, 67, 68). Here, we found that the initial virus transfer to macrophages was inhibited by neutralizing monoclonal antibodies targeting the HIV-1 gp120 envelope glycoprotein as well as by the Leu3a antibody targeting the CD4 receptor, indicating that early interactions between T cells and recipient macrophages involve recognition of CD4 by gp120. Virus transfer to macrophages leading to the formation of infected lymphocyte/macrophage fused cells was also blocked by the T20 fusion inhibitor targeting the viral transmembrane gp41 envelope glycoprotein and the Maraviroc CCR5 antagonist. These results indicate that virus transfer and T cell fusion with macrophages are mediated by initial viral envelope-receptor and -coreceptor interactions. In addition, we show that the second cell fusion step between Gag+ lymphocyte/macrophage fused cells and neighboring MDMs, required for virus dissemination and virus production by multinucleated giant cells, is also dependent of the viral envelope, since it is inhibited by T20 and Maraviroc. While our data clearly show that both cell fusion processes for virus transfer and dissemination in macrophages are dependent of the viral envelope, we cannot exclude that other mechanisms related to the propensity of macrophages to mediate homotypic cell fusion could also participate in the cell fusion processes for viral transfer and dissemination. It would be

interesting to investigate the potential role in HIV-1-mediated T-cell/MDM and MDM/MDM fusions, of some effector proteins known to be involved in programming of macrophages into a fusion-competent state and then in cell fusion for formation of multinucleated giant macrophages (for review, see Ref 69).

Our analyses indicate that this virus cell-to-cell from infected T cells to macrophages is largely more efficient than virus infection with cell-free viruses, and is certainly the most potent experimental system described so far to infect macrophage *in vitro* (1–5). Indeed, we failed to detect significant transfer of viral material when macrophages were directly infected with the cell-free virus particles released by infected donor T cells during the time of co-culture with macrophages. In sharp contrast, virus transfer from infected CD4+ T cells evaluated here resulted in a robust productive infection of macrophages, as evidenced by the 30-days monitoring of high virus production in the supernatant of the multinuclear giant macrophages.

In summary, our results show that HIV-1 can be transferred efficiently to macrophages from infected donor T cells without implying internalization of infected CD4+ T cells by the macrophage targets (21). While the two mechanisms are not mutually exclusive, we reveal a novel fast and very efficient mechanism involved in cell-to-cell transfer from non-dying infected T cells to macrophages and subsequent virus spreading between macrophages by a two-step cell fusion process (model on Fig. 9). In the first step, infected T cells establish tight contacts and initially discharge viral material to MDMs, resulting in the fusion of infected T cells with MDM targets. The newly formed Gag+ lymphocyte/macrophage fused cells then acquire the ability to fuse with surrounding non-infected MDMs leading to the formation of infected multinucleated giant cells that could survive for a long time in host tissues to produce infectious virus particles as shown *in vivo* in lymphoid organs and the CNS of HIV-1-infected patients and SIV-infected macaques (3, 17, 59-64). Similarly, the first step related to the

initial T cell-to-MDM fusion agrees with results showing that myeloid cells from lymphoid tissues of SIV-infected macaques contain T cell markers and viral DNA originating from infected T cells (46, 47). These *in vivo* observations support the importance of the molecular mechanisms revealed here, which contribute to a better understanding of virus dissemination from infected T cells toward macrophages and formation of long-lived macrophage viral reservoirs in host tissues.

358 **Materials and Methods**

359

360 **Plasmids and reagents.** The proviral plasmids pNL4-3 and pNLAD8 were obtained from the
361 AIDS Research and Reference Reagent Program, Division of AIDS, NIAID. The proviral
362 plasmid HIV-1R5-GFP is a gift of Dr. Michael Schindler (Munich, Germany) (70) while the
363 pYU-2 and the plasmid encoding the VSV-G envelope glycoprotein (pVSVg), have been
364 described (71). The following antibodies were used: PE- or FITC-conjugated anti-CD11b
365 (clone ICRF44, BD Biosciences), PE-Cy7-conjugated anti-CD11b (clone ICRF44, Biolegend),
366 RD1- or FITC-conjugated anti-Gag (clone KC57, Beckman coulter), anti-CD4 (clone Leu3a,
367 Biolegend), anti-CD3 (clone UCHT1, Biolegend), anti-CD2 (TS2/18 clone) was a gift from
368 Dr. Andres Alcover (Paris, France) (72); Alexa647-conjugated phalloidin (Life Technologies)
369 was used. The following reagents were obtained from the AIDS Research and Reference
370 Reagent Program, Division of AIDS, NIAID: the anti-gp120 antibodies (PG16 and NIH45-
371 46), HIV-1 CAp24 Hybridoma (183-H12-5C), HIV-IG, Maraviroc, T20, and AZT. Anti-
372 gp120 antibodies (10-1074 and PGT128) were a gift from Pr. Paul Zhou (Shanghai, China).

373

374 **Cell culture.** HEK293T, TZM-bl and Jurkat cell-lines were obtained from the ATCC
375 Collection. HEK293T and TZM-bl cells were maintained in Dulbecco minimal essential
376 medium (DMEM) supplemented with 10% heat-inactivated fetal calf serum (FCS), 100 IU of
377 penicillin/ml, and 100 µg of streptomycin/ml (ATB, Invitrogen). Jurkat cells were maintained
378 in RPMI 1640 complete culture medium supplemented with 10% FCS and ATB. Peripheral
379 blood mononuclear cells (PBMCs) were isolated from blood of healthy anonymous donors by
380 density gradient sedimentation using Histopaque (Sigma), and monocytes were purified using
381 the CD14-positive selection kit (CD14 microbeads, Miltenyi) according to manufacturer's
382 guidelines. Blood samples from anonymous healthy donors were purchased from

"*Etablissement Français du Sang Paris-Saint-Antoine-Crozatier, 21 rue Crozatier, 75012 Paris, France*". The monocytes were differentiated into macrophages for 8 days in RPMI 1640 culture medium supplemented with 20% FCS, ATB, and 25 ng/ml of GM-CSF and M-CSF (Miltenyi). Human primary CD4+ T cells were isolated from PBMCs by density gradient sedimentation using Histopaque and then purified by negative selection (CD4+ T cell isolation kit, Miltenyi) following manufacturer's recommendation. CD4+ T cells were activated for 3 days in RPMI medium containing 20% FBS, interleukin-2 at 10 u/ml (IL-2, Miltenyi), and phytohemagglutinin-P at 5 µg/ml (PHA-P, Sigma-Aldrich). After activation, CD4+ T cells were kept in RPMI medium supplemented with 20% FBS and IL-2. All cells were grown at 37°C under 5% CO_2.

Viral production, titration, and infection. Replication-competent HIV-1 YU2, NL4.3, NLAD8 and HIV-1R5-GFP strains were produced in HEK293T cells by cotransfection of the proviral plasmid in combination with pVSVG using calcium phosphate precipitation technique as described (71). Amounts of CAp24 produced were determined by enzyme-linked immunosorbent assay (ELISA; Innogenetics). Viral titer was determined using Jurkat cells (J77 clone) by flow cytometry (Accuri C6, BD Biosciences) as described (71).

Viral transfer and dissemination. To study the transfer from Jurkat or primary CD4+ T cells to MDMs, T cells were infected using a multiplicity of infection (MOI) of 0.5 for 16 h. Cells were then washed and cultured for 20 h. After washing, T cells were co-cultured at a ratio 2:1 (except if otherwise stated in the text/figure legend) with MDMs seeded at a density of $0.5x10^6$ cells/well, respectively, during 0.5-6 h. To remove T cells, MDMs were then washed extensively with PBS once, PBS containing 10 mM EDTA, and 2 more washes with PBS were performed. MDMs were harvested or cultured during several days and then collected.

Cells were then surface stained using anti-CD11b and anti-CD3 antibodies, then fixed with 4% PFA, permeabilized and stained with an anti-Gag (KC57, 1/500) using permeabilization buffer (Beckman Coulter). The percentage of Gag+ cells among CD11b+ cells corresponding to the MDM population was determined by flow cytometry. To analyze viral production, MDM culture supernatants were collected, and the amount of CAp24 produced was determined by ELISA. For MDM infection with cell-free viruses, T cells were infected as previously and incubated with MDMs for 6 h through a 0.4 µm-Transwell membrane. Alternatively, the supernatant of producer Jurkat cells corresponding to the 6 h co-culture was added to the MDMs, and the percentage of Gag+ was analyzed by flow cytometry as described above.

Infectivity assay. $2x10^5$ TZM-bl (HeLa-CD4 cells stably expressing CD4 and CCR5) cells were incubated with viral supernatants (200 ng of CAp24) during 18 h. TZM-bl were then cultured during 2 days, fixed with formaldehyde 3.7% (Sigma), and treated with permeabilization buffer. Cells were stained with an anti-Gag and the percentage of Gag+ cells was determined by flow cytometry.

Effect of inhibitors on viral transfer and dissemination. To analyze the effect of inhibitors on virus transfer, infected donor T cells or MDM targets were pre-treated for 1 h with anti-gp120 neutralizing antibodies (PGT128, 10-1074, NIH 45-46, and PG16) or anti-CD4 (Leu3a), respectively, using 3 concentrations (0.1, 1, or 10 µg/ml) of antibodies in the presence of 10 µg/ml of Fc-Block (Sigma). Infected T cells were then co-cultured for 6 h with MDMs, removed by washings, and the percentage of Gag+/CD11b+ MDMs was determined by flow cytometry. Results were expressed as the percentage of Gag+ MDMs relative to that determined without antibodies. The effect of the CCR5 receptor antagonist Maraviroc as well

as the fusion inhibitor T20 were also tested on virus transfer. Infected donor T cells or MDM targets were pre-treated for 1 h with T20 or Maraviroc at 10 μM and 10 μg/ml, respectively. Infected T cells were then co-cultured for 6 h with MDMs, removed, and the percentage of Gag+/CD11b+ MDMs was determined by flow cytometry. Results were expressed as the percentage of Gag+ MDMs relative to that determined without inhibitors. To show that virus transfer from infected T cells to MDMs led to productive infection, MDM targets were pretreated with AZT (5 μM) 2 h prior to the co-culture for 6 h with infected T cells. After removal of infected T cells, the percentage of Gag+/CD11b+ MDMs was determined by flow cytometry either directly after the 6 h of co-culture or 6 days later, while the viral p24 production from MDMs was determined by ELISA after 6 days of culture. Results were expressed as the percentage of Gag+ MDMs or as the amount of p24 relative to those determined without AZT. To analyze the effect of inhibitors on virus dissemination between MDMs, infected T cells were first co-cultured for 6 h with MDMs, removed by washings, and MDMs were cultured for 1, 5, 8, or 12 days in the presence of 10 μM of T20. The percentage of Gag+/CD11b+ MDMs was then determined by flow cytometry, while the CAp24 production from MDMs was determined by ELISA. Results were expressed as the percentage of Gag+ MDMs or as the amount of CAp24 relative to those determined without T20.

Fluorescence microscopy analysis. To visualize cell contacts and virus transfer, 10^6 Jurkat or primary CD4+ T cells infected with NLAD8 as described above were pre-labeled with 2 μM CellTrace Far Red (Life Technologies) and co-cultured for 0.5, 2 or 6 h with $0.5x10^6$ MDMs plated onto coverslips. MDMs were then fixed with 4% PFA, blocked for 10 min in PBS containing 1% BSA, stained with 2 μM DRAQ5 (eBioscience) for 20 min in PBS, permeabilized and stained using KC57 FITC-conjugated antibody and Phalloidin-Alexa647 (Molecular Probes) diluted in permeabilization buffer for 1 h. Coverslips were washed with

458 PBS and mounted on slide using 10 µl of Fluoromount (Sigma). Images were acquired on a
459 spinning disk (CSU-X1M1, Yokogawa) inverted microscope (DMI6000, Leica), and then
460 processed using Fiji (ImageJ, NIH) (73). Quantitative image analysis was performed using
461 Fiji software by defining a region of interest using the actin staining and measuring the whole
462 fluorescence intensity of the Gag staining, with respect to non-infected cells. To analyze
463 fusion between infected T cells and MDMs, infected Jurkat or primary CD4+ T cells were co-
464 cultured for 6 h with MDMs. Cells were then fixed with 4% PFA and blocked in PBS
465 containing 1% BSA. Anti-CD2 (TS2/18, 1/200 dilution) surface staining was performed on
466 non-permeabilized cells in PBS-BSA during 1 h. Coverslips were then rinsed in PBS-BSA
467 and incubated for 1 h with anti-mouse Alexa Fluor 555 in PBS-BSA. Anti-CD3 (10 µg/mL), -
468 Lck (2 µg/mL) and -Gag (KC57-FITC, 1/200 dilution), and F-actin intracellular staining were
469 done by incubating coverslips with the indicated primary antibody and Phalloidin-Alexa647
470 diluted in the permeabilization buffer. Coverslips were then rinsed with PBS-BSA and
471 incubated for 1 h with the corresponding fluorescent-coupled secondary antibody. After three
472 washes, coverslips were mounted on microscope slides, using 10 µl of Fluoromount mounting
473 medium with DAPI (Sigma-Aldrich). Cells were examined under an epifluorescence
474 microscope (Leica DMI6000), and quantitative image analysis was performed using Fiji
475 software by defining a region of interest using the actin staining and measuring the whole
476 fluorescence intensity of the indicated marker (i.e. CD3, CD2 or Lck) in Gag+ cells, with
477 respect to non-infected cells. For the CellTracker experiment, NLAD8-infected Jurkat cells
478 were labeled with 5 µM CellTracker CMAC (Life technologies) for 30 min, and then co-
479 cultured for 6 h with MDMs. Cells were then fixed in 4% PFA for 20 min, blocked for 10 min
480 in PBS containing 1% BSA, stained with 2 µM DRAQ5 for 20 min in PBS, permeabilized
481 and stained using KC57 FITC-conjugated antibody and Phalloidin-Alexa555 (Molecular
482 Probes) diluted in permeabilization buffer for 1 h. Coverslips were washed with PBS and

mounted on slide using 10 µl of Fluoromount media. Images were acquired and then processed as described above. To analyze the effect of inhibitors on fusion between T cells and macrophages, infected donor T cells or MDM targets were pre-treated for 1 h with anti-gp120 neutralizing antibodies (PGT128, 10-1074) or T20, using a concentration of 10 µg/ml in the presence of 10 µg/ml of Fc-Block (Sigma). Infected T cells were then labeled with 5 µM CellTracker CMAC and co-cultured for 6 h with MDMs in the presence of inhibitors. Cells were then fixed and stained as previously using KC57 FITC-conjugated antibody and Phalloidin-Alexa647. Images were acquired and then processed as described above. To analyze fusion between MDMs, infected T cells were initially co-cultured with MDMs for 6 h. After elimination of T cells by extensive washing, autologous MDMs pre-labeled with CellTrace Far red or CellTracker were added to the MDMs just after the 6 h-co-culture or 4 days later, respectively, and cultured for 1 more day. Coverslips were then washed, and mounted with Fluoromount media containing DAPI or NucRed. Images were acquired and processed as previously. To analyze the effect of T20 and Maraviroc on fusion between MDMs, infected T cells were initially co-cultured with MDMs for 6 h. After removal of T cells by extensive washings, MDMs were cultured for 1 more day with or without T20 (10 µg/ml) or Maraviroc (10 µM), and cells were stained for nuclei, Gag and F-actin following fixation and blocking steps as previously. The number of nuclei per cell was analyzed from images on at least 50 cells. To analyze the survival of infected giant multinucleated cells in culture, infected Jurkat cells and MDMs were co-cultured for 6 h, and MDMs were then cultured for up to 30 days after removal of T cells by extensive washings as previously. Cells were then collected, fixed and stained for Gag and F-actin as previously. Coverslips were washed with PBS and mounted on slide using 10 µl of Fluoromount medium containing DAPI. Images were acquired on a spinning disk inverted microscope and then processed using Fiji as previously.

508

509 **Live-cell imaging of HIV-1 transfer.** 2x10^6 Jurkat cells infected with HIV-1R5-GFP were
510 co-cultured for 1 h with 10^6 MDMs pre-labeled with CellTrace Far Red, and plated onto 35
511 mm Ibidi dish in RPMI without Phenol Red and containing 10% FBS and ATB. Images were
512 recorded using a 20x air objective every 1 or 2.5 min for 1, 2 or 3 h on a spinning disk (CSU-
513 X1M1, Yokogawa) confocal inverted microscope (DMI6000, Leica) equipped with a heated
514 chamber. Z-stack optical section were acquired at 0.5 µm depth increments, and movies were
515 analyzed using Fiji.

516

517 **Transmission electron microscopy analysis.** 2x10^6 Jurkat cells infected with NLAD8 as
518 described above were co-cultured for 6 h with 10^6 MDMs plated onto coverslips with or
519 without AZT (5 µM). In parallel, MDMs were infected by cell-free NLAD8 for 6 h. The
520 coverslips were then fixed using glutaraldehyde 2.8% and 2% PFA for 20 min. After 2 washes
521 in PBS, cells were dehydrated and embedded into epoxy (Electron Microscopy Sciences).
522 Ultrathin sections of 90 nm were cut with an ultra-microtome, stained with uranyl acetate and
523 Reynold's lead and observed with a transmission electron microscope (JEOL 1011).
524 Acquisition was performed with a Gatan ES1000W CCD camera.

525

Acknowledgements. We thank Drs Michael Schindler and Andres Alcover for the gift of reagents. We thank the members of the Flow Cytometry (Cybio), and the Cellular Imaging core facilities of the Cochin Institute for their technical help. We thank Clarisse Vigne for technical help. We thank Andres Alcover, Georges Bismuth, Clarisse Berlioz-Torrent and Mark Scott for discussion and critical reading of the manuscript. This work was supported in part by INSERM, the CNRS and the University Paris-Descartes. It is also funded by Grants from the *Agence Nationale de Recherche sur le SIDA et les Hépatites virales* (ANRS). LB is supported by grants from the Institut Pasteur International Network and the Chinese Academy of Sciences. ML is supported by a grant from the European HIVERA Program. MX is supported by a grant from the China Scholarship Council. JB is supported by a grant from Sidaction. The research was conducted within the context of the International Associated Laboratory (LIA) VIRHOST between CNRS, Institut Pasteur, Université Paris-Descartes, and the Institut Pasteur Shanghai – Chinese Academy of Sciences.

541 **References**

542

543 1. Burdo TH, Lackner A, Williams KC. 2013. Monocyte/macrophages and their role in
544 HIV neuropathogenesis. Immunol Rev 254:102–113.

545 2. Carter CA, Ehrlich LS. 2008. Cell biology of HIV-1 infection of macrophages. Annu
546 Rev Microbiol 62:425–443.

547 3. Harbison C, Zhuang K, Gettie A, Blanchard J, Knight H, Didier P, Cheng-Mayer C,
548 Westmoreland S. 2014. Giant cell encephalitis and microglial infection with mucosally
549 transmitted simian-human immunodeficiency virus SHIVSF162P3N in rhesus macaques.
550 J Neurovirol 20:62–72.

551 4. Tan J, Sattentau QJ. 2013. The HIV-1-containing macrophage compartment: a perfect
552 cellular niche? Trends Microbiol 21:405–412.

553 5. Watters SA, Mlcochova P, Gupta RK. 2013. Macrophages: the neglected barrier to
554 eradication. Curr Opin Infect Dis 26:561–566.

555 6. Honeycutt JB, Wahl A, Baker C, Spagnuolo RA, Foster J, Zakharova O, Wietgrefe S,
556 Caro-Vegas C, Madden V, Sharpe G, Haase AT, Eron JJ, Garcia JV. 2016. Macrophages
557 sustain HIV replication in vivo independently of T cells. J Clin Invest 126:1353.

558 7. Araínga M, Edagwa B, Mosley RL, Poluektova LY, Gorantla S, Gendelman HE. 2017.
559 A mature macrophage is a principal HIV-1 cellular reservoir in humanized mice after
560 treatment with long acting antiretroviral therapy. Retrovirology 14:17.

8. Honeycutt JB, Thayer WO, Baker CE, Ribeiro RM, Lada SM, Cao Y, Cleary RA, Hudgens MG, Richman DD, Garcia JV. 2017. HIV persistence in tissue macrophages of humanized myeloid-only mice during antiretroviral therapy. Nat Med.

9. Dumas A, Lê-Bury G, Marie-Anaïs F, Herit F, Mazzolini J, Guilbert T, Bourdoncle P, Russell DG, Benichou S, Zahraoui A, Niedergang F. 2015. The HIV-1 protein Vpr impairs phagosome maturation by controlling microtubule-dependent trafficking. J Cell Biol 211:359–372.

10. Kedzierska K, Ellery P, Mak J, Lewin SR, Crowe SM, Jaworowski A. 2002. HIV-1 Down-Modulates γ Signaling Chain of FcγR in Human Macrophages: A Possible Mechanism for Inhibition of Phagocytosis. J Immunol 168:2895–2903.

11. Koppensteiner H, Brack-Werner R, Schindler M. 2012. Macrophages and their relevance in Human Immunodeficiency Virus Type I infection. Retrovirology 9:82.

12. Mazzolini J, Herit F, Bouchet J, Benmerah A, Benichou S, Niedergang F. 2010. Inhibition of phagocytosis in HIV-1-infected macrophages relies on Nef-dependent alteration of focal delivery of recycling compartments. Blood 115:4226–4236.

13. Vérollet C, Souriant S, Bonnaud E, Jolicoeur P, Raynaud-Messina B, Kinnaer C, Fourquaux I, Imle A, Benichou S, Fackler OT, Poincloux R, Maridonneau-Parini I. 2015. HIV-1 reprograms the migration of macrophages. Blood 125:1611–1622.

14. Vérollet C, Zhang YM, Cabec VL, Mazzolini J, Charrière G, Labrousse A, Bouchet J, Medina I, Biessen E, Niedergang F, Bénichou S, Maridonneau-Parini I. 2010. HIV-1 Nef Triggers Macrophage Fusion in a p61Hck- and Protease-Dependent Manner. J Immunol 184:7030–7039.

583 15. Costiniuk CT, Jenabian M-A. 2014. The lungs as anatomical reservoirs of HIV infection.
584 Rev Med Virol 24:35–54.

585 16. Fischer-Smith T, Bell C, Croul S, Lewis M, Rappaport J. 2008. Monocyte/macrophage
586 trafficking in acquired immunodeficiency syndrome encephalitis: Lessons from human
587 and nonhuman primate studies. J Neurovirol 14:318–326.

588 17. Geny C, Gherardi R, Boudes P, Lionnet F, Cesaro P, Gray F. 1991. Multifocal
589 multinucleated giant cell myelitis in an AIDS patient. Neuropathol Appl Neurobiol
590 17:157–162.

591 18. González-Scarano F, Martín-García J. 2005. The neuropathogenesis of AIDS. Nat Rev
592 Immunol 5:69–81.

593 19. Gras G, Kaul M. 2010. Molecular mechanisms of neuroinvasion by monocytes-
594 macrophages in HIV-1 infection. Retrovirology 7:30.

595 20. Gorry PR, Francella N, Lewin SR, Collman RG. 2014. HIV-1 envelope–receptor
596 interactions required for macrophage infection and implications for current HIV-1 cure
597 strategies. J Leukoc Biol 95:71–81.

598 21. Baxter AE, Russell RA, Duncan CJA, Moore MD, Willberg CB, Pablos JL, Finzi A,
599 Kaufmann DE, Ochsenbauer C, Kappes JC, Groot F, Sattentau QJ. 2014. Macrophage
600 Infection via Selective Capture of HIV-1-Infected CD4+ T Cells. Cell Host Microbe
601 16:711–721.

602 22. Agosto LM, Uchil PD, Mothes W. 2015. HIV cell-to-cell transmission: effects on
603 pathogenesis and antiretroviral therapy. Trends Microbiol 23:289–295.

604 23. Alvarez RA, Barría MI, Chen BK. 2014. Unique features of HIV-1 spread through T cell
605 virological synapses. PLoS Pathog 10:e1004513.

606 24. Dale BM, Alvarez RA, Chen BK. 2013. Mechanisms of enhanced HIV spread through
607 T-cell virological synapses. Immunol Rev 251:113–124.

608 25. Schiffner T, Sattentau QJ, Duncan CJA. 2013. Cell-to-cell spread of HIV-1 and evasion
609 of neutralizing antibodies. Vaccine 31:5789–5797.

610 26. Law KM, Komarova NL, Yewdall AW, Lee RK, Herrera OL, Wodarz D, Chen BK.
611 2016. In Vivo HIV-1 Cell-to-Cell Transmission Promotes Multicopy Micro-
612 compartmentalized Infection. Cell Rep 15:2771–2783.

613 27. Lehmann MJ, Sherer NM, Marks CB, Pypaert M, Mothes W. 2005. Actin- and myosin-
614 driven movement of viruses along filopodia precedes their entry into cells. J Cell Biol
615 170:317–325.

616 28. Llewellyn GN, Hogue IB, Grover JR, Ono A. 2010. Nucleocapsid promotes localization
617 of HIV-1 gag to uropods that participate in virological synapses between T cells. PLoS
618 Pathog 6:e1001167.

619 29. Ménager MM, Littman DR. 2016. Actin Dynamics Regulates Dendritic Cell-Mediated
620 Transfer of HIV-1 to T Cells. Cell 164:695–709.

621 30. Sherer NM, Lehmann MJ, Jimenez-Soto LF, Horensavitz C, Pypaert M, Mothes W.
622 2007. Retroviruses can establish filopodial bridges for efficient cell-to-cell transmission.
623 Nat Cell Biol 9:310–315.

624 31. Sowinski S, Jolly C, Berninghausen O, Purbhoo MA, Chauveau A, Köhler K, Oddos S,
625 Eissmann P, Brodsky FM, Hopkins C, Onfelt B, Sattentau Q, Davis DM. 2008.

626 Membrane nanotubes physically connect T cells over long distances presenting a novel
627 route for HIV-1 transmission. Nat Cell Biol 10:211–219.

628 32. Murooka TT, Deruaz M, Marangoni F, Vrbanac VD, Seung E, von Andrian UH, Tager
629 AM, Luster AD, Mempel TR. 2012. HIV-infected T cells are migratory vehicles for viral
630 dissemination. Nature 490:283–287.

631 33. Sewald X, Gonzalez DG, Haberman AM, Mothes W. 2012. In vivo imaging of
632 virological synapses. Nat Commun 3:1320.

633 34. Abela IA, Berlinger L, Schanz M, Reynell L, Günthard HF, Rusert P, Trkola A. 2012.
634 Cell-cell transmission enables HIV-1 to evade inhibition by potent CD4bs directed
635 antibodies. PLoS Pathog 8:e1002634.

636 35. Agosto LM, Zhong P, Munro J, Mothes W. 2014. Highly active antiretroviral therapies
637 are effective against HIV-1 cell-to-cell transmission. PLoS Pathog 10:e1003982.

638 36. Malbec M, Sourisseau M, Guivel-Benhassine F, Porrot F, Blanchet F, Schwartz O,
639 Casartelli N. 2013. HIV-1 Nef promotes the localization of Gag to the cell membrane
640 and facilitates viral cell-to-cell transfer. Retrovirology 10:80.

641 37. Sigal A, Kim JT, Balazs AB, Dekel E, Mayo A, Milo R, Baltimore D. 2011. Cell-to-cell
642 spread of HIV permits ongoing replication despite antiretroviral therapy. Nature 477:95–
643 98.

644 38. Orenstein JM. 2001. The Macrophage in HIV Infection. Immunobiology 204:598–602.

645 39. Theodore TS, Englund G, Buckler-White A, Buckler CE, Martin MA, Peden KW. 1996.
646 Construction and characterization of a stable full-length macrophage-tropic HIV type 1

molecular clone that directs the production of high titers of progeny virions. AIDS Res Hum Retroviruses 12:191–194.

40. Freed EO, Englund G, Martin MA. 1995. Role of the basic domain of human immunodeficiency virus type 1 matrix in macrophage infection. J Virol 69:3949–3954.

41. Krementsov DN, Weng J, Lambelé M, Roy NH, Thali M. 2009. Tetraspanins regulate cell-to-cell transmission of HIV-1. Retrovirology 6:64.

42. Weng J, Krementsov DN, Khurana S, Roy NH, Thali M. 2009. Formation of syncytia is repressed by tetraspanins in human immunodeficiency virus type 1-producing cells. J Virol 83:7467–7474.

43. Roy NH, Lambelé M, Chan J, Symeonides M, Thali M. 2014. Ezrin is a component of the HIV-1 virological presynapse and contributes to the inhibition of cell-cell fusion. J Virol 88:7645–7658.

44. Symeonides M, Murooka T, Bellfy L, Roy N, Mempel T, Thali M. 2015. HIV-1-Induced Small T Cell Syncytia Can Transfer Virus Particles to Target Cells through Transient Contacts. Viruses 7:6590–6603.

45. Compton AA, Schwartz O. 2017. They Might Be Giants: Does Syncytium Formation Sink or Spread HIV Infection? PLoS Pathog 13:e1006099.

46. Calantone N, Wu F, Klase Z, Deleage C, Perkins M, Matsuda K, Thompson EA, Ortiz AM, Vinton CL, Ourmanov I, Loré K, Douek DC, Estes JD, Hirsch VM, Brenchley JM. 2014. Tissue myeloid cells in SIV-infected primates acquire viral DNA through phagocytosis of infected T cells. Immunity 41:493–502.

668 47. DiNapoli SR, Ortiz AM, Wu F, Matsuda K, Twigg HL, Hirsch VM, Knox K, Brenchley
669 JM. 2017. Tissue-resident macrophages can contain replication-competent virus in
670 antiretroviral-naive, SIV-infected Asian macaques. JCI Insight 2:e91214.

671 48. Bosch B, Grigorov B, Senserrich J, Clotet B, Darlix J-L, Muriaux D, Este JA. 2008. A
672 clathrin-dynamin-dependent endocytic pathway for the uptake of HIV-1 by direct T cell-
673 T cell transmission. Antiviral Res 80:185–193.

674 49. Hübner W, McNerney GP, Chen P, Dale BM, Gordon RE, Chuang FYS, Li X-D,
675 Asmuth DM, Huser T, Chen BK. 2009. Quantitative 3D video microscopy of HIV
676 transfer across T cell virological synapses. Science 323:1743–1747.

677 50. Sloan RD, Kuhl BD, Mesplède T, Münch J, Donahue DA, Wainberg MA. 2013.
678 Productive entry of HIV-1 during cell-to-cell transmission via dynamin-dependent
679 endocytosis. J Virol 87:8110–8123.

680 51. Wang L, Eng ET, Law K, Gordon RE, Rice WJ, Chen BK. 2017. Visualization of HIV T
681 Cell Virological Synapses and Virus-Containing Compartments by Three-Dimensional
682 Correlative Light and Electron Microscopy. J Virol 91.

683 52. Pelchen-Matthews A, Kramer B, Marsh M. 2003. Infectious HIV-1 assembles in late
684 endosomes in primary macrophages. J Cell Biol 162:443–455.

685 53. Deneka M, Pelchen-Matthews A, Byland R, Ruiz-Mateos E, Marsh M. 2007. In
686 macrophages, HIV-1 assembles into an intracellular plasma membrane domain
687 containing the tetraspanins CD81, CD9, and CD53. J Cell Biol 177:329–341.

688 54. Jouve M, Sol-Foulon N, Watson S, Schwartz O, Benaroch P. 2007. HIV-1 buds and
689 accumulates in “nonacidic” endosomes of macrophages. Cell Host Microbe 2:85–95.

690 55. Bennett AE, Narayan K, Shi D, Hartnell LM, Gousset K, He H, Lowekamp BC, Yoo TS,
691 Bliss D, Freed EO, Subramaniam S. 2009. Ion-abrasion scanning electron microscopy
692 reveals surface-connected tubular conduits in HIV-infected macrophages. PLoS Pathog
693 5:e1000591.

694 56. Welsch S, Keppler OT, Habermann A, Allespach I, Krijnse-Locker J, Kräusslich H-G.
695 2007. HIV-1 Buds Predominantly at the Plasma Membrane of Primary Human
696 Macrophages. PLoS Pathog 3:e36.

697 57. Chu H, Wang J-J, Qi M, Yoon J-J, Chen X, Wen X, Hammonds J, Ding L, Spearman P.
698 2012. Tetherin/BST-2 is essential for the formation of the intracellular virus-containing
699 compartment in HIV-infected macrophages. Cell Host Microbe 12:360–372.

700 58. Kadiu I, Ricardo-Dukelow M, Ciborowski P, Gendelman HE. 2007. Cytoskeletal Protein
701 Transformation in HIV-1-Infected Macrophage Giant Cells. J Immunol 178:6404–6415.

702 59. Dargent JL, Lespagnard L, Kornreich A, Hermans P, Clumeck N, Verhest A. 2000.
703 HIV-associated multinucleated giant cells in lymphoid tissue of the Waldeyer's ring: a
704 detailed study. Mod Pathol Off J U S Can Acad Pathol Inc 13:1293–1299.

705 60. Lewin-Smith M, Wahl SM, Orenstein JM. 1999. Human immunodeficiency virus-rich
706 multinucleated giant cells in the colon: a case report with transmission electron
707 microscopy, immunohistochemistry, and in situ hybridization. Mod Pathol Off J U S
708 Can Acad Pathol Inc 12:75–81.

709 61. Ryzhova EV, Crino P, Shawver L, Westmoreland SV, Lackner AA, González-Scarano F.
710 2002. Simian immunodeficiency virus encephalitis: analysis of envelope sequences from
711 individual brain multinucleated giant cells and tissue samples. Virology 297:57–67.

712 62. Soulas C, Conerly C, Kim W-K, Burdo TH, Alvarez X, Lackner AA, Williams KC.
713 2011. Recently infiltrating MAC387(+) monocytes/macrophages a third macrophage
714 population involved in SIV and HIV encephalitic lesion formation. Am J Pathol
715 178:2121–2135.

716 63. Teo I, Veryard C, Barnes H, An SF, Jones M, Lantos PL, Luthert P, Shaunak S. 1997.
717 Circular forms of unintegrated human immunodeficiency virus type 1 DNA and high
718 levels of viral protein expression: association with dementia and multinucleated giant
719 cells in the brains of patients with AIDS. J Virol 71:2928–2933.

720 64. Vicandi B, Jiménez-Heffernan JA, López-Ferrer P, Patrón M, Gamallo C, Colmenero C,
721 Viguer JM. 1999. HIV-1 (p24)-positive multinucleated giant cells in HIV-associated
722 lymphoepithelial lesion of the parotid gland. A report of two cases. Acta Cytol 43:247–
723 251.

724 65. Blanco J, Bosch B, Fernández-Figueras MT, Barretina J, Clotet B, Esté JA. 2004. High
725 Level of Coreceptor-independent HIV Transfer Induced by Contacts between Primary
726 CD4 T Cells. J Biol Chem 279:51305–51314.

727 66. Chen P, Hübner W, Spinelli MA, Chen BK. 2007. Predominant Mode of Human
728 Immunodeficiency Virus Transfer between T Cells Is Mediated by Sustained Env-
729 Dependent Neutralization-Resistant Virological Synapses. J Virol 81:12582–12595.

730 67. Felts RL, Narayan K, Estes JD, Shi D, Trubey CM, Fu J, Hartnell LM, Ruthel GT,
731 Schneider DK, Nagashima K, Bess JW, Bavari S, Lowekamp BC, Bliss D, Lifson JD,
732 Subramaniam S. 2010. 3D visualization of HIV transfer at the virological synapse
733 between dendritic cells and T cells. Proc Natl Acad Sci U S A 107:13336–13341.

734 68. Martin N, Welsch S, Jolly C, Briggs JAG, Vaux D, Sattentau QJ. 2010. Virological
735 Synapse-Mediated Spread of Human Immunodeficiency Virus Type 1 between T Cells
736 Is Sensitive to Entry Inhibition. J Virol 84:3516–3527.

737 69. Helming L, Gordon S. 2009. Molecular mediators of macrophage fusion. Trends Cell
738 Biol 19:514–522.

739 70. Koppensteiner H, Banning C, Schneider C, Hohenberg H, Schindler M. 2012.
740 Macrophage Internal HIV-1 Is Protected from Neutralizing Antibodies. J Virol 86:2826–
741 2836.

742 71. Herate C, Vigne C, Guenzel CA, Lambele M, Rouyez M-C, Benichou S. 2016. Uracil
743 DNA glycosylase interacts with the p32 subunit of the replication protein A complex to
744 modulate HIV-1 reverse transcription for optimal virus dissemination. Retrovirology
745 13:26.

746 72. Bouchet J, Del Río-Iñiguez I, Lasserre R, Agüera-Gonzalez S, Cuche C, Danckaert A,
747 McCaffrey MW, Di Bartolo V, Alcover A. 2016. Rac1-Rab11-FIP3 regulatory hub
748 coordinates vesicle traffic with actin remodeling and T-cell activation. EMBO J.

749 73. Schindelin J, Arganda-Carreras I, Frise E, Kaynig V, Longair M, Pietzsch T, Preibisch S,
750 Rueden C, Saalfeld S, Schmid B, Tinevez J-Y, White DJ, Hartenstein V, Eliceiri K,
751 Tomancak P, Cardona A. 2012. Fiji: an open-source platform for biological-image
752 analysis. Nat Methods 9:676–682.

753

754 **Figure Legends**

755

756 **Figure 1. HIV-1 cell-to-cell transfer from infected T cells to macrophages.** (A)
757 Experimental protocol. (B) Jurkat cells were infected with the NLAD8 strain and the
758 percentage of infected cells was evaluated 36 h later by flow cytometry after Gag staining
759 (green bars). Infected Jurkat cells were co-cultured for 6 h with MDMs at the indicated cell
760 ratio (1:1, 1:2, or 1:3 MDM/Jurkat ratios). After elimination of Jurkat cells, the percentage of
761 CD11b+/Gag+ MDMs was quantified by flow cytometry. As a negative control (NI), non-
762 infected Jurkat cells were co-cultured with MDMs. (C) Jurkat cells were infected with the
763 NL4.3, YU2, or NLAD8 strains and the percentage of infected cells was evaluated 36 h later
764 by flow cytometry (green bars). Infected Jurkat cells were then co-cultured with MDMs
765 directly (blue bars) or through a Transwell membrane (red bars) for 6 h. In parallel, culture
766 supernatants from Jurkat cells collected during the 6 h-co-culture with MDMs was used to
767 infect autologous MDMs (yellow bars). The percentage of CD11b+/ Gag+ MDMs was
768 evaluated by flow cytometry. (D) Purified primary CD4+ T cells were infected with the YU2
769 strain and the percentage of infected cells was evaluated 36 h later by flow cytometry (green
770 bar). Infected T cells were then co-cultured either directly (blue bars) or through a Transwell
771 membrane (red bars) with autologous MDMs using different cell ratios (1:1, 1:2, 1:3, or 1:4
772 MDM/T cell ratios) for 6 h. After elimination of T cells, the percentage of CD11b+/Gag+
773 MDMs was quantified by flow cytometry. As a negative control (NI), non-infected CD4+ T
774 cells were co-cultured with MDMs. (E and F) NLAD8-infected Jurkat cells were pretreated
775 with anti-gp120 antibodies or T20, while MDMs were pretreated with anti-CD4 or Maraviroc.
776 Infected T cells were co-cultured with MDMs for 6 h, and viral transfer to MDMs was
777 quantified as previously. Results are expressed as the percentage of Gag+ MDMs relative to
778 that determined without antibodies or inhibitors. The results are the means of 5 independent

779 experiments performed with MDMs of 5 donors. Error bars represent 1 SEM. Statistical
780 significance was determined using paired Students *t* test (ns, p>0.05; **p<0.01; ***p<0.001).
781
782 **Figure 2. Productive infection of macrophages by virus cell-to-cell transfer from infected**
783 **T cells.** NLAD8-infected Jurkat cells (A-C) or primary CD4+ T cells (D-F) were co-cultured
784 with MDMs for 6 h, eliminated, and the percentage of CD11b+/Gag+ MDMs was then
785 evaluated 1, 6, 9, 12 or 15 days later by flow cytometry (A and D). In parallel, cell culture
786 supernatants from MDMs were collected and p24 was quantified (B and E). Culture
787 supernatants (100 ng of p24) from MDMs collected 9 days (C) or 12 days (F) after the co-
788 culture with YU2- or NLAD8-infected Jurkat (C) or CD4+ T (F) cells were used to infect
789 TZM-bl cells, and the percentage of Gag+ TZM-bl was evaluated 48 h later by flow
790 cytometry. (G and H) NLAD8-infected Jurkat cells were co-cultured for 6 h with MDMs
791 pretreated with or without AZT. The percentage of CD11b+/Gag+ MDMs was then evaluated
792 just after co-culture (6 h) and 6 days (D6) later (G). In parallel, culture supernatants of MDMs
793 were collected 6 days after co-culture and p24 was quantified (H). The results shown (A-B,
794 D-E, and G-H) are the means of 5 independent experiments performed with MDMs of 5
795 donors, while the results shown in (C and F) are representative of 3 independent experiments.
796 Error bars represent 1 SEM. Statistical significance was determined using Anova One-way
797 test (ns, ****p<0.0001).
798
799 **Figure 3. Fluorescence microscopy analysis of intercellular contacts and viral transfer**
800 **between infected T cells and macrophages.** (A-B) NLAD8-infected Jurkat cells were co-
801 cultured for 0.5, 2 or 6 h with MDMs pre-stained with CellTrace. Cells were then fixed,
802 stained with anti-Gag, phalloidin and DRAQ5, and analyzed by confocal microscopy. A 5
803 µm-thick medial stack is shown (A). Infected donor T cells and MDM targets are drawn with

804 yellow and red dashed lines, respectively. Scale bar, 25 µm. Intracellular Gag mean
805 fluorescence intensity was quantified as indicated in the Methods Section (B). Each dot
806 corresponds to 1 cell, and the number of cells analyzed is indicated (n). Horizontal bars
807 represent the mean ± 1 SEM. Statistical significance was determined with unpaired T-test (ns,
808 $p>0.05$, *$p>0.05$, ****$p<0.0001$). (C) Jurkat cells infected with HIV-1R5-GFP (green) were
809 co-cultured with MDMs previously plated onto IBIDI dish and labeled with CellTrace (red).
810 Fluorescence images were acquired using a 20x air objective on a spinning disk microscope
811 every 2.5 min for 145 min. A 5 µm-thick medial stack of representative images is shown, and
812 the time-lapse is indicated. Scale bar, 25 µm. Discharge of viral material (arrows) into MDMs
813 (dashed line) from infected T cells is shown. (D) Jurkat cells infected with HIV-1R5-GFP
814 (green) were co-cultured with MDMs previously labeled with CellTrace (red). Fluorescence
815 images were then acquired using a 20x air objective on a spinning disk microscope every 2.5
816 min during 100 min. A 5 µm-thick medial stack of representative images is shown, and the
817 time-lapse is indicated. Scale bar, 25 µm. The labeled MDM target is drawn with a dashed
818 line.
819
820 **Figure 4. Transmission electron microscopy analysis of viral transfer to macrophages.**
821 NLAD8-infected Jurkat cells were co-cultured for 6 h with MDMs with (D and E) or without
822 (A-C) AZT (5 µM). Cells were then fixed and dehydrated. Ultrathin sections were cut, stained
823 and observed with a transmission electron microscope. Assembling and budding viruses are
824 indicated by blue arrows, while mature virions are indicated by red arrows. White arrows
825 indicate MDM cytoplasmic membrane compartments containing mature viruses (B and D). In
826 (A), the right image (black scale bar, 100 nm) corresponds to higher magnification of the area
827 selected on the left image (black scale bar, 1 µm). In B), the right and left (black scale bar, 1
828 µm) images correspond to higher magnification of the areas selected on the middle image

(black scale bar, 1 μm). In C), the right and left images (black scale bar, 100 nm) correspond to higher magnification of the areas selected on the middle image (black scale bar, 1 μm). In D), the right image (black scale bar, 1 μm) corresponds to higher magnification of the area selected on the left image (black scale bar, 1 μm). In E), black scale bar, 100 nm. Images shown are representative images obtained from analysis of MDMs of 3 independent donors.

Figure 5. Viral transfer to macrophages by cell fusion with infected T cells. (A-B) NLAD8-infected Jurkat (A) or primary CD4+ T (B) cells were co-cultured with MDMs for 0.5, 2 or 6 h. After elimination of T cells, MDMs were stained with anti-Gag, phalloidin and Dapi. Cells were analyzed by confocal microscopy, and the number of nuclei per cell was analyzed from images on at least 50 cells. Results are expressed as the percentages of cells with 1, 2, 3 or more than 3 nuclei (left panels), and as the mean nucleus number per cell (right panels). Error bars represent 1 SEM. Statistical significance was determined with the Mann-Whitney U-test (ns, $p>0.05$, ***$p<0.001$, ****$p<0.0001$). (C and D) NLAD8-infected Jurkat cells pre-labeled with CellTracker were co-cultured for 6 h with MDMs. After elimination of T cells, MDMs were fixed and stained with anti-Gag, phalloidin, and Draq5, and analyzed by confocal microscopy (scale bar, 25 μm) (C). In D), the number of CellTracker+ nuclei per cell was analyzed from images on at least 50 cells. Results are expressed as the percentages of cells with 1, 2 or more than 2 CellTracker+ nuclei. (E and F) NLAD8-infected Jurkat cells pre-labeled with CellTracker were pretreated with anti-gp120 antibodies (PGT128 or 10-1074) or T20 for 1 h and co-cultured with MDMs for 6 h in the presence of the inhibitors. Cells were then fixed, permeabilized, stained with anti-Gag, phalloidin and DRAQ5, and analyzed by confocal microscopy (scale bar, 25 μm). Images were acquired and processed as previously (E). In F), the number of CellTracker+ nuclei per DRAQ5+ MDMs was analyzed from images on at least 1200 cells for each condition. Results are expressed as the fusion

854 index corresponding to the percentages of cells containing at least 1 CellTracker+ nucleus
855 relative to that corresponding to NLAD8-infected Jurkat cells co-cultured with MDMs
856 without drugs. The results shown are representative of 4 independent experiments performed
857 with MDMs from 4 donors. NI, non-infected Jurkat or primary CD4+ T cells were co-cultured
858 with MDMs.
859
860 **Figure 6. Macrophages express T cell specific marker after cell fusion with infected T**
861 **cell.** NLAD8-infected Jurkat cells (A-F) or primary CD4+ T cells (G, H) were co-cultured for
862 6 h with MDMs. After elimination of T cells, MDMs were stained with anti-CD2 (A, B) and
863 anti-CD3 (G, H) before permeabilization. Cells were then permeabilized and stained with
864 anti-Gag, anti-CD3 (C, D), anti-Lck (E-F) and Dapi. Representative images of cell surface
865 CD2 (A), CD3 (C and G) and Lck (E) staining are shown (scale bars, 25 μm). Cell surface
866 CD2 (B) or CD3 (H) and intracellular CD3 (D) or Lck (F) mean fluorescence intensities were
867 quantified as indicated in the Methods Section. Each dot corresponds to 1 cell, and the
868 number of cells analyzed is indicated (n). Horizontal bars represent the mean ± 1 SEM.
869 Statistical significance was determined with the Mann-Whitney U-test (****$p<0.0001$).
870
871 **Figure 7. Viral dissemination between macrophages by homotypic cell fusion.** (A-C)
872 NLAD8-infected Jurkat cells were co-cultured with MDMs for 6 h. After elimination of T
873 cells, MDMs were cultured for 1 or 5 more days, and then stained with anti-Gag, phalloidin
874 and Dapi. Cells were analyzed by confocal microscopy (scale bar, 25 μm) (A). In B and C),
875 the number of nuclei per MDM was quantified from images on at least 50 cells. Results are
876 expressed as the percentages of cells with 1, 2, 3 or more than 3 nuclei (B), and as the mean
877 nucleus number per cell (C). Error bars represent 1 SEM. Statistical significance was
878 determined with the Mann-Whitney U-test (****$p<0.0001$). (D) Infected Jurkat cells were co-

cultured with MDMs for 6 h. After elimination of T cells, autologous MDMs pre-labeled with CellTrace were added and cultured for 1 day. MDMs were then stained with anti-Gag, phalloidin and Dapi. Cells were analyzed by confocal microscopy (scale bar, 25 µm). (E) Infected Jurkat cells were co-cultured with MDMs for 6 h. After elimination of T cells, MDMs were cultured for 1 day with or without T20 (10 µg/ml) or Maraviroc (10 µM) before staining with anti-Gag, phalloidin and Dapi. Cells were analyzed by confocal microscopy. The number of nuclei was analyzed from images on at least 50 cells. Results are expressed as the percentages of cells with 2, 3 or more than 3 nuclei. (F and G) Infected Jurkat cells were co-cultured with MDMs for 6 h. After elimination of T cells, MDMs were cultured for 1, 5, 8 or 12 days with or without T20 (10 µg/ml). The percentage of Gag+ MDMs was then evaluated by flow cytometry (F). In parallel, culture supernatants from MDMs were collected and p24 was quantified (G). The results shown in (A-E) are representative of 4 independent experiments performed with MDMs of 4 donors, while the results shown in (F, G) correspond to the means of 3 independent experiments performed with MDMs of 3 donors. NI, non-infected Jurkat cells were co-cultured with MDMs.

Figure 8. Formation and survival of infected multinucleated giant cells. NLAD8-infected Jurkat cells were co-cultured with MDMs for 6 h, eliminated, and MDMs were then cultured for the indicated period of time. In A), cells were fixed, permeabilized and stained with anti-Gag, phalloidin and DAPI. Cells were analyzed by confocal microscopy and images were acquired and processed as previously. Scale bar, 25 µm. In B), culture supernatants of MDMs were collected at the indicated days after co-culture and p24 was quantified. The results correspond to the means of 3 independent experiments. Error bars represent 1 SEM. Non infected, non-infected Jurkat cells were co-cultured with MDMs.

Figure 9. Model for virus cell-to-cell transfer from infected T cells to MDMs and virus spreading between MDMs. Initial virus transfer and subsequent virus spreading are mediated by a two-step cell fusion process. In a first step, infected T cells establish contacts, initially discharge viral material to MDMs [1], and then fuse with MDM targets [2] with accumulation of viruses in intracytoplasmic compartments and virus assembly and budding at the cell surface. Gag+ newly formed LMFCs [3] then acquire the ability to fuse with surrounding uninfected MDMs leading to the formation of Gag+ multinucleated giant cells [4] that could survive for a long time to produce infectious viruses [5].

Figure 1

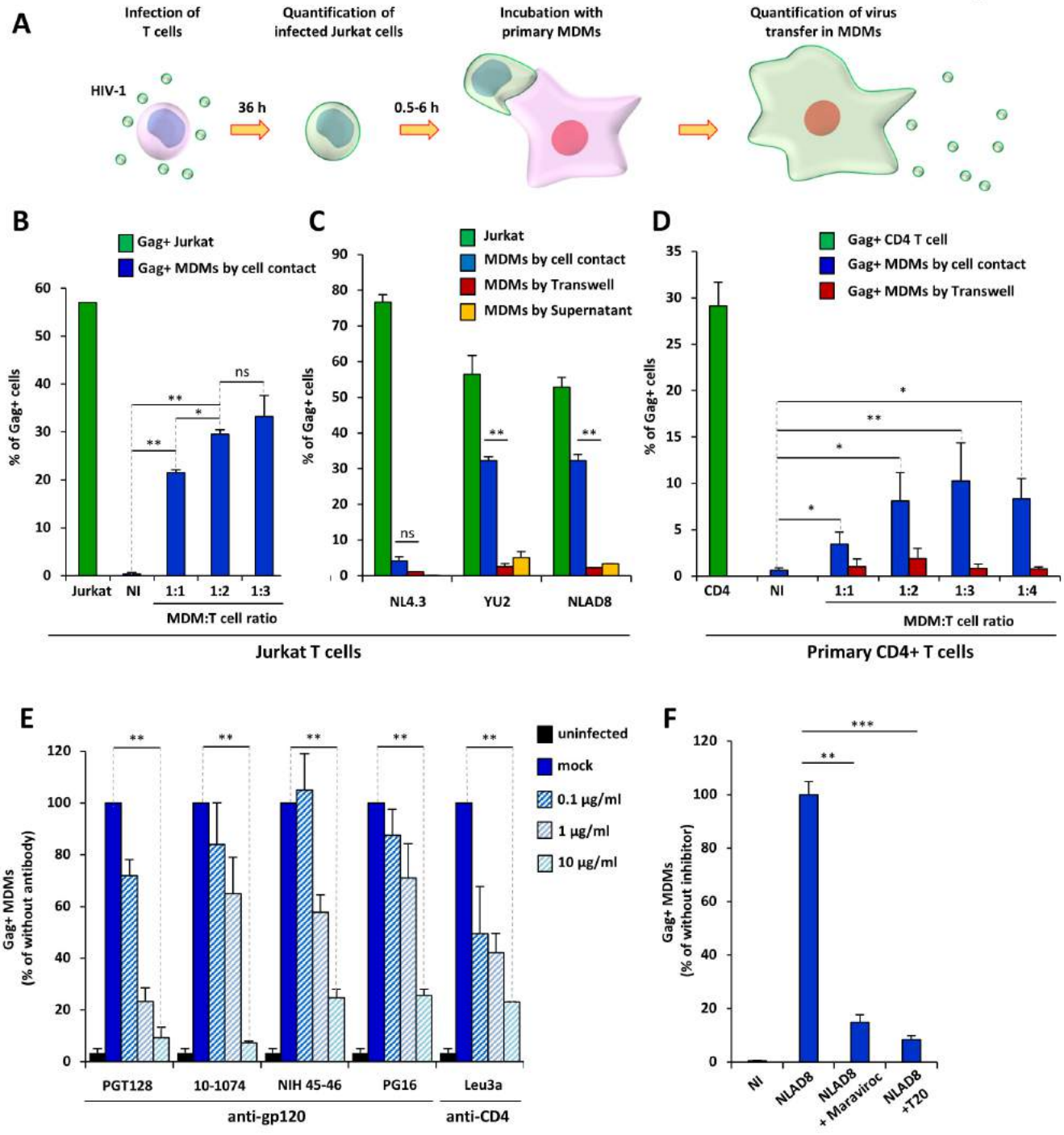

Figure 2

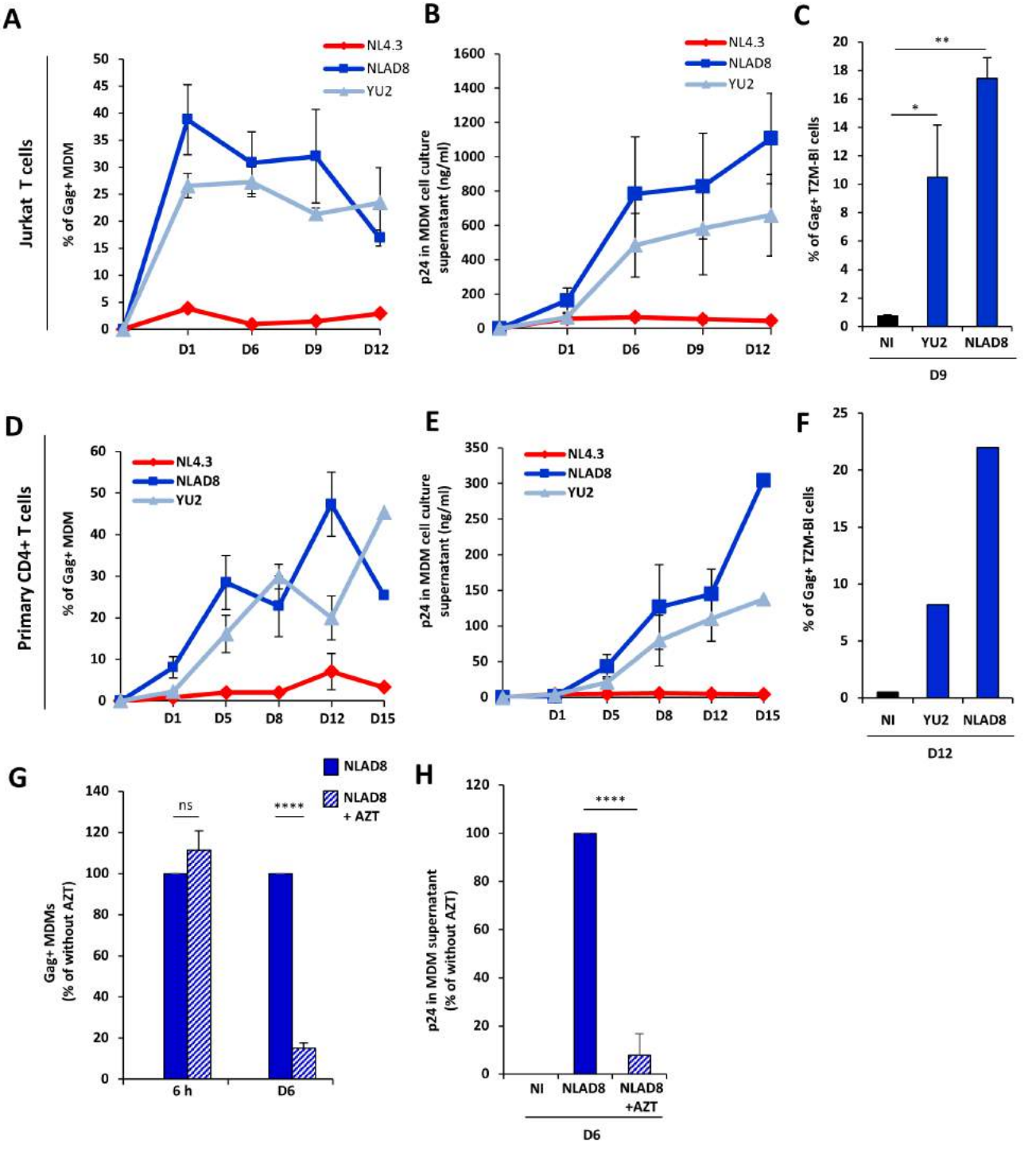

Figure 3

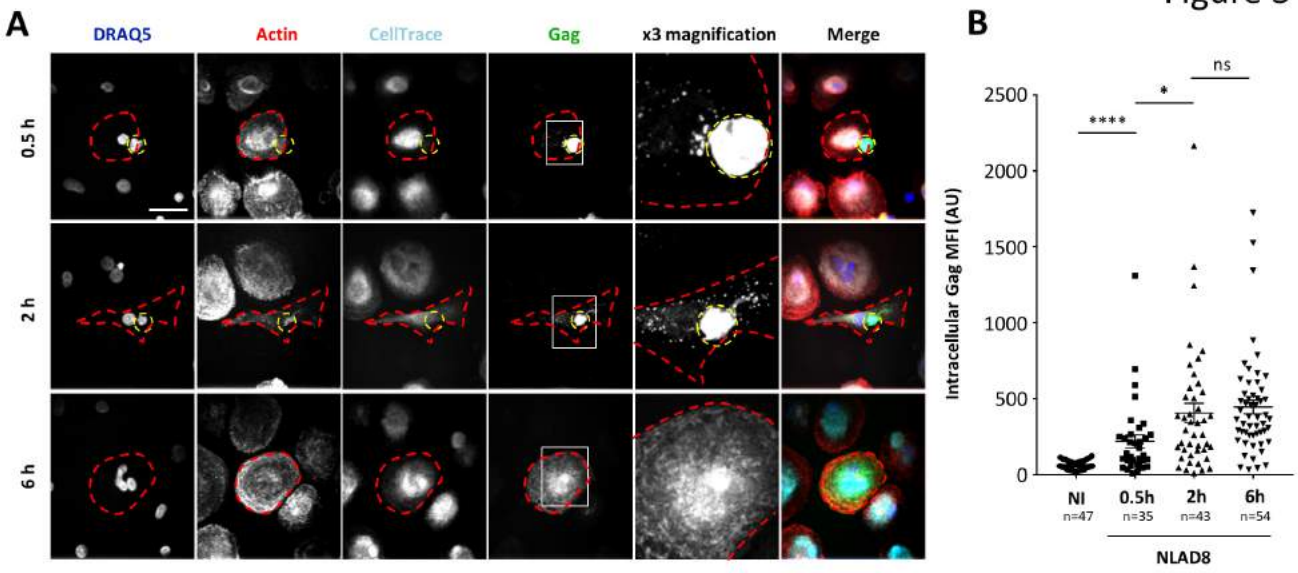

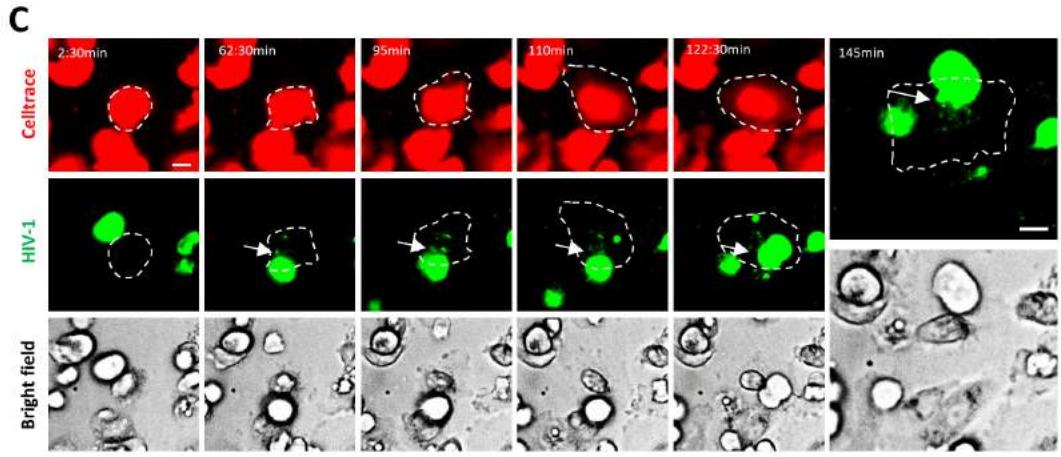

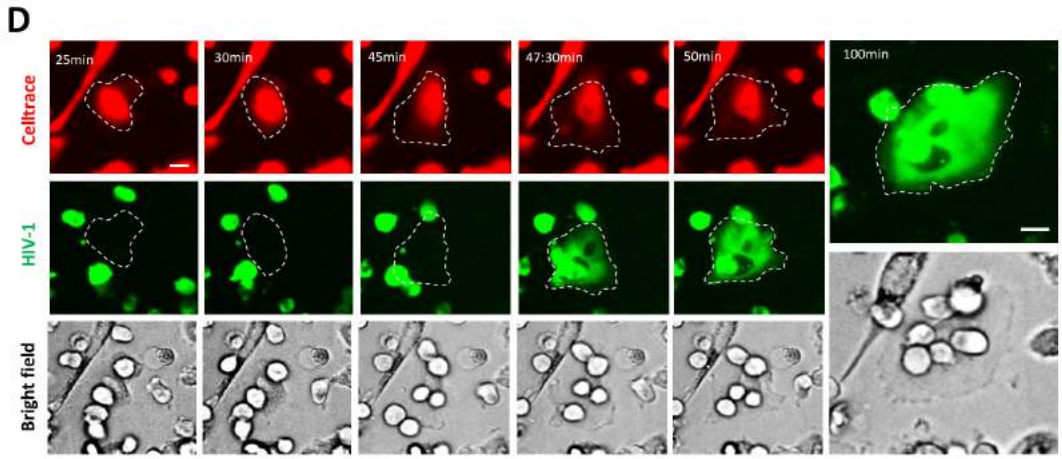

Figure 4

Figure 5

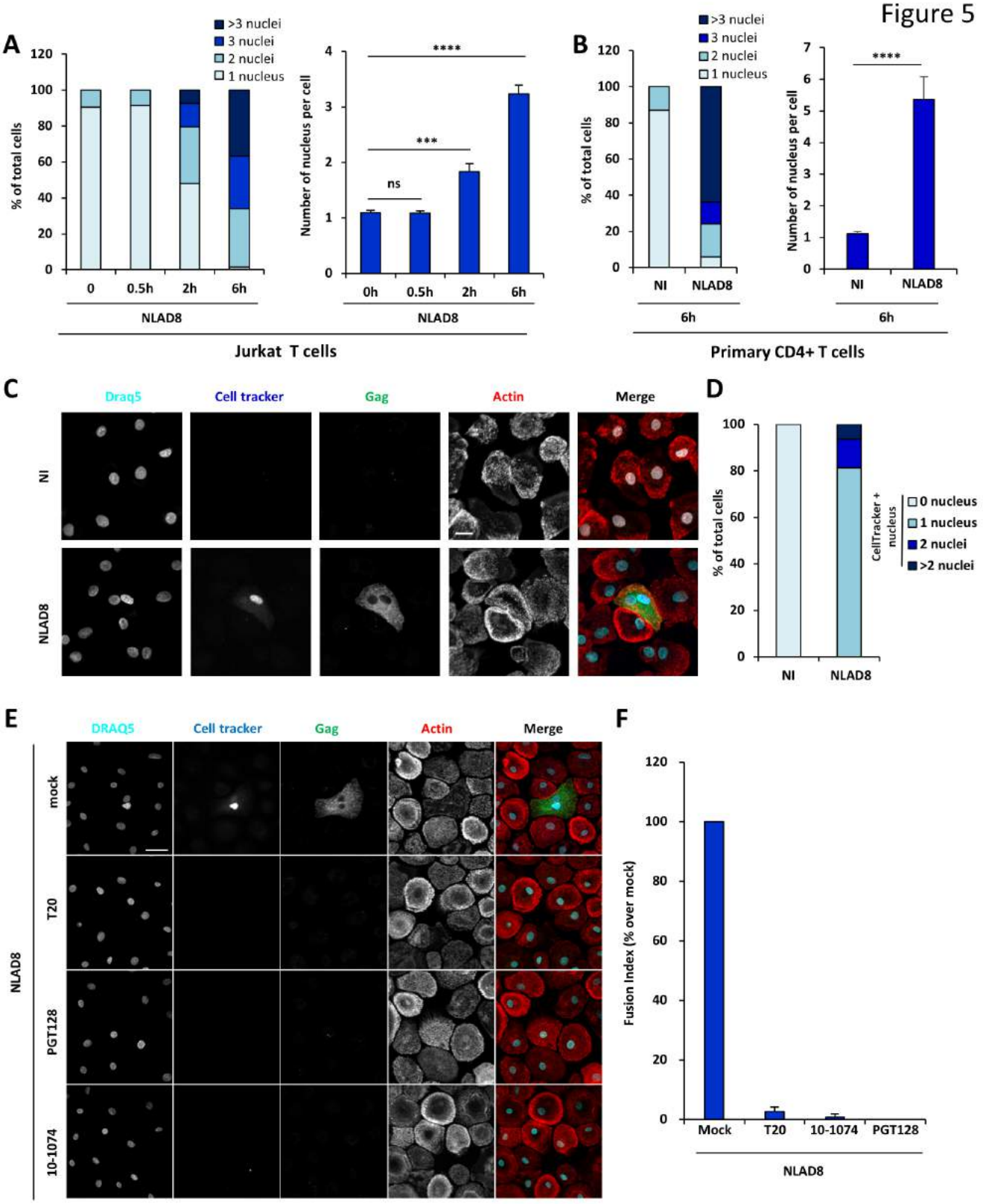

Figure 6

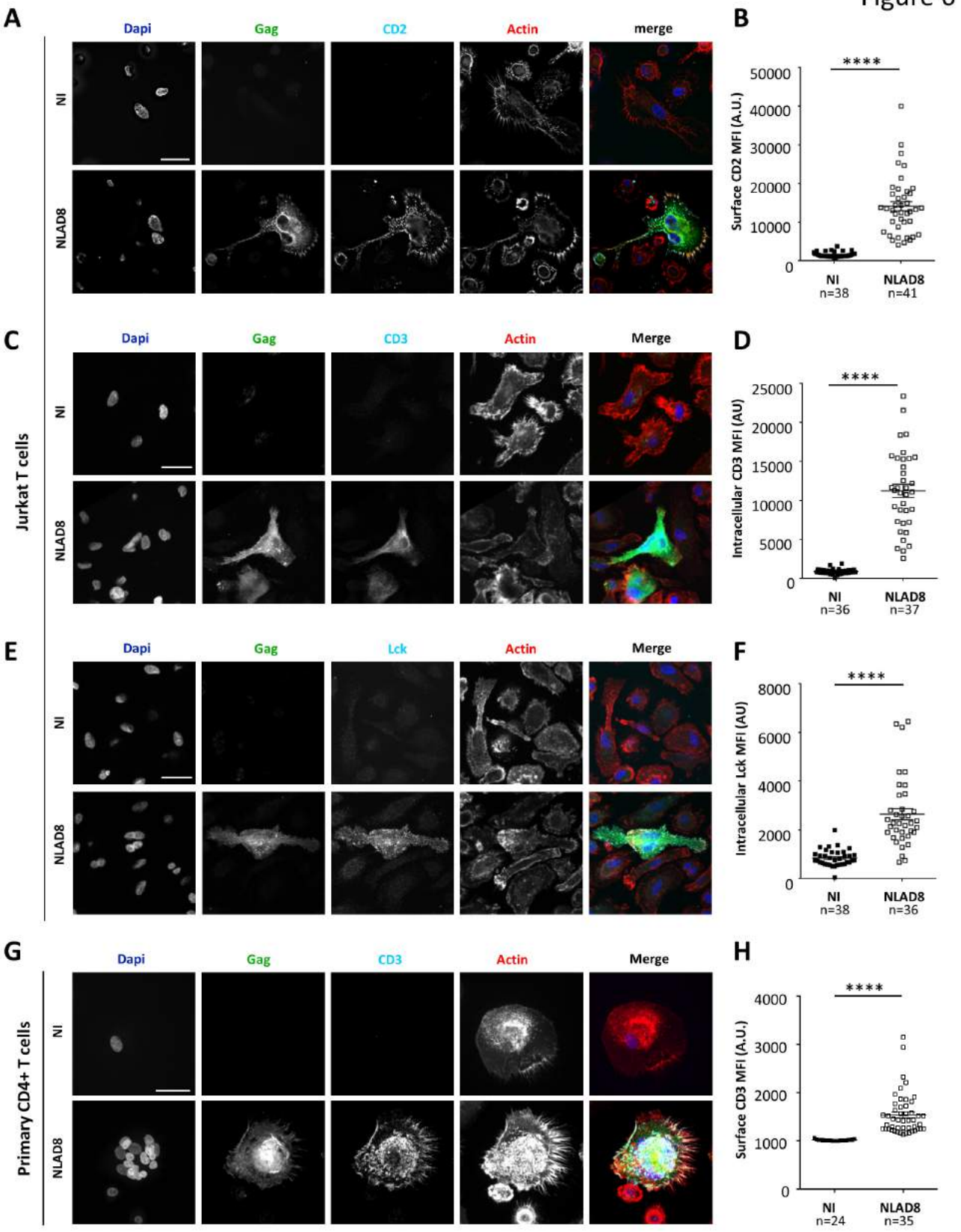

Figure 7

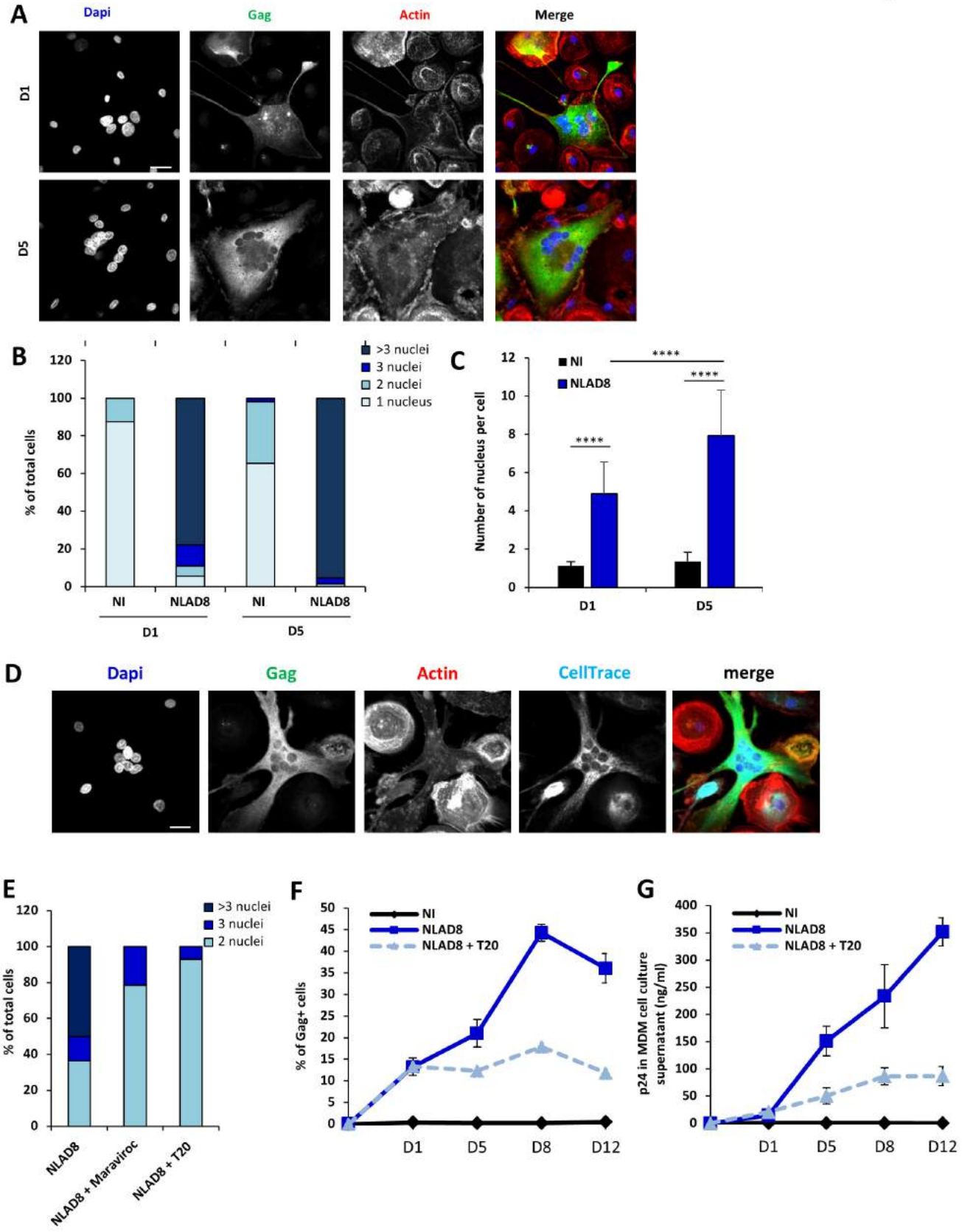

Figure 8

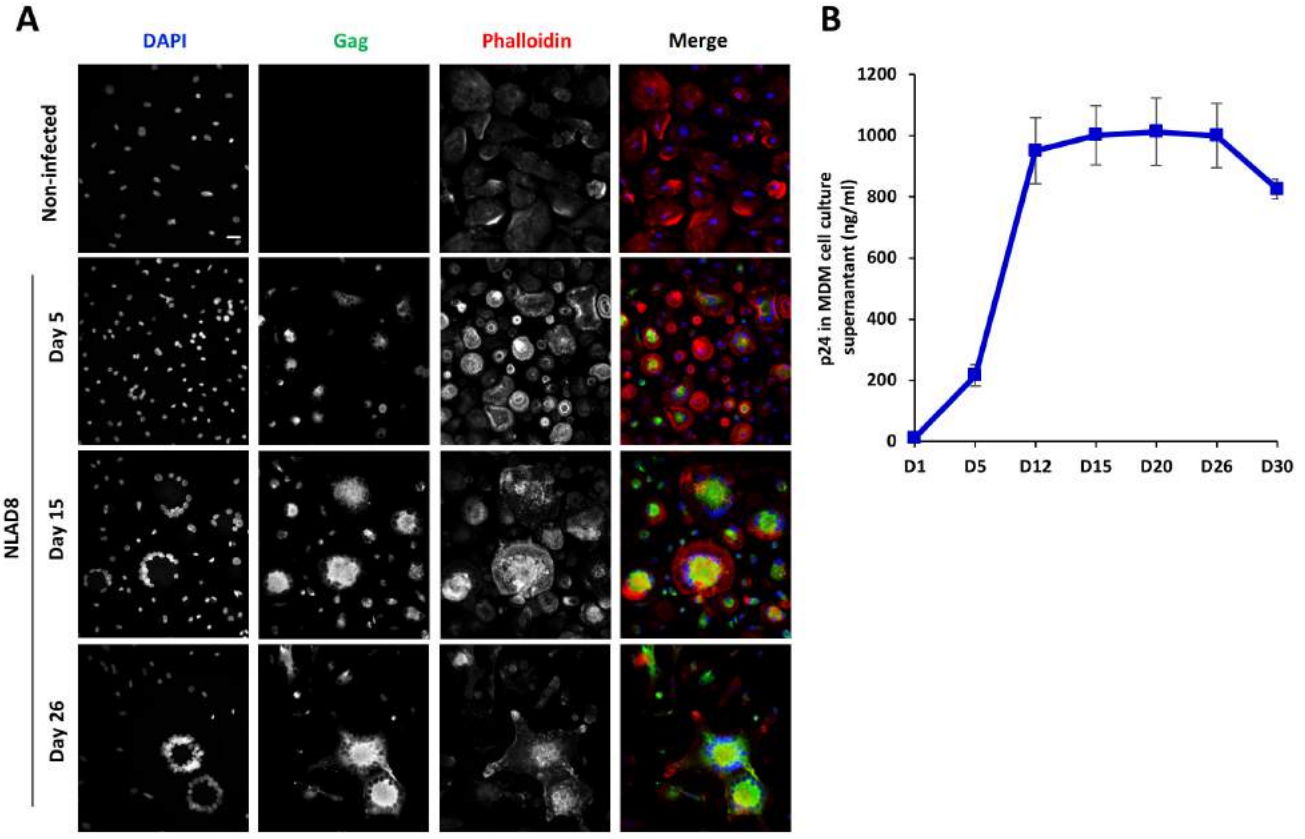

Figure 9

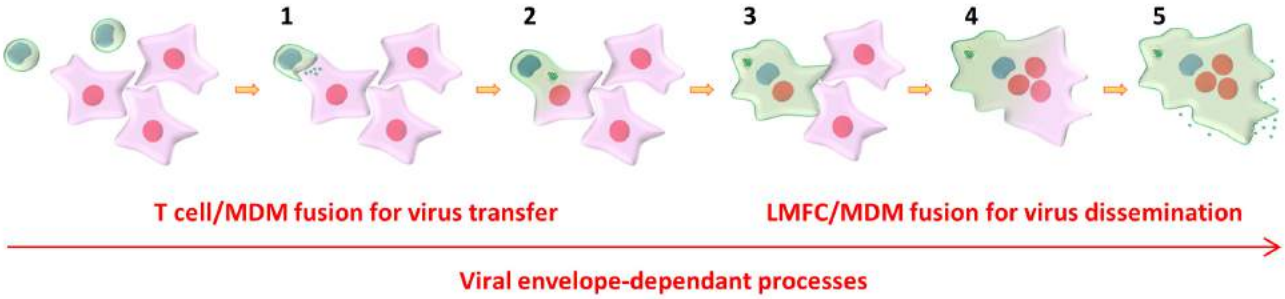

4. Conclusion

In this article, we show that infected CD4+ T cells efficiently transmit HIV-1 to macrophages leading to productive infection and viral spreading in macrophages through a two-step cell-cell fusion process. First, infected T cells interact with macrophages and fuse together for massive and fast transfer of viral material. Then, the newly formed lymphocyte/macrophage fused cells fuse with surrounding uninfected macrophages for HIV-1 spreading. Both cell fusion steps are mediated by viral envelope-receptor interactions at the cell surface of T cells and MDMs, and are completed in less than 2 h of co-culture since Gag+ multinucleated MDMs were already detected at this time. Infected multinucleated giant macrophages are long live cells and their formation may be a major determinant *in vivo* for virus dissemination to macrophages.

Article 2: The bone degradation machinery of osteoclasts: a novel HIV-1 target that contributes to bone loss

1. Abstract

While osteoclasts (OC), the cells specialized in bone degradation, can be infected by HIV-1 *in vitro*, evidence is missing regarding the presence of infected OC *in vivo* and the mechanisms by which they could contribute to bone loss frequently observed in HIV-1 infected patients. Here we report that infected OC are found in the bones of HIV-1-infected humanized mice as well as in human synovial explants exposed to HIV-1. Regarding the infection of OC *in vitro*, we show that it occurs at different stages of osteoclastogenesis *via* cell-free viruses and, more efficiently, by transfer from infected T cells. HIV-1 infection enhances the adhesion and the bone degradation activity of OC, by modifying the structure and function of the sealing zones, the F-actin structures responsible for bone resorption. The viral protein Nef is involved in all HIV-1-induced effects *in vitro*, in part through activation of Src kinase. Remarkably, OC differentiated *in vitro* from transgenic mice expressing Nef display high osteolytic activity, and these mice exhibit numerous OC along with bone defects, supporting a critical role of Nef in OC- dependent bone homeostasis *in vivo.*

Altogether, our data show that OC are host cells for HIV-1 and provide strong evidence for the contribution of infected OC to bone disorders induced by the virus.

2. Presentation of the article

In order to investigate HIV-1 infection of osteoclasts, especially through viral cell-to-cell transfer, we collaborated with the group of Isabel Maridonneau-Parini (IPBS, Toulouse, France). First, this group investigated the presence of HIV-1 infected osteoclast *in vivo* in the bones of HIV-1-infected humanized mice and in human synovial explants. The mechanisms of HIV-1 infection of osteoclasts were then analyzed *in vitro* using cell-free or cell-associated viruses. In order to analyze virus transfer from infected T cells to differentiated osteoclasts, we used the same experimental system previously used to analyze virus cell-to-cell transfer to macrophages (see Article 1). Viral cell-to-cell infection from infected CD4+ T cells and dissemination in osteoclasts was thus evaluated using immunofluorescence microscopy, flow cytometry and p24 ELISA techniques.

The group of Isabel Maridonneau-Parini then analyzed the impact of infection on osteoclast functions (i.e. migration of osteoclast precursors, and osteoclast bone resorption activity). Finally, the role of the Nef auxiliary viral protein in the functional defects observed in infected osteoclasts was analyzed *in vitro* using *nef*-deleted HIV-1 strains *in vivo* using Nef-transgenic mice.

3. Article

The bone degradation machinery of osteoclasts: a novel HIV-1 target that contributes to bone loss

Brigitte Raynaud-Messina[1,2], Lucie Bracq[4,5,6,$], Maeva Dupont[1,2,3,$], Shanti Souriant[1,2,$], Shariq M. Usmani[7,8], Amsha Proag[1], Karine Pingris[1,2], Christophe Thibault[9,10], Florence Capilla[11], Talal Al Saati[11], Isabelle Gennero[12,13], Pierre Jurdic[14], Paul Jolicoeur[15,16,17], Jean-Luc Davignon[12,13], Serge Benichou[4,5,6], Thorsten R. Mempel[7,8], Isabelle Maridonneau-Parini[1,2,*,#] & Christel Vérollet[1,2,*,#]

[1] *Institut de Pharmacologie et Biologie Structurale, IPBS, Université de Toulouse, CNRS, UPS, Toulouse, France*

[2] *International associated laboratory (LIA) CNRS "IM-TB/HIV" (1167), Toulouse, France, and Buenos Aires, Argentina*

[3] *Institute of Experimental Medicine-CONICET, National Academy of Medicine, Buenos Aires, Argentina*

[4] *Inserm U1016, Institut Cochin, Paris, France*

[5] *CNRS UMR8104, Université Paris Descartes, Paris, France*

[6] *Institut Pasteur Shanghai-Chinese Academy of Sciences, Shanghai, China*

[7] *Massachusetts General Hospital, Center for Immunology and Inflammatory Diseases, Charlestown, MA 02129*, USA

[8] *Harvard Medical School, Boston, MA 02115, USA*

[9] *LAAS, CNRS, Toulouse, France*

[10] *Université de Toulouse, INSA, Toulouse, France.*

[11] *INSERM/UPS/ENVT- US006/CREFRE, Service d'Histopathologie, Toulouse, France*

[12] *Centre de Physiopathologie de Toulouse-Purpan (CPTP), INSERM-CNRS UMR 1043, Université Paul Sabatier, Toulouse, France*

[13] *Institut Fédératif de Biologie, Centre Hospitalier Universitaire Toulouse, France*

[14] *Institut de génomique fonctionnelle de Lyon, CNRS UMR3444, Université de Lyon, Ecole Normale Supérieur de Lyon, Lyon, France*

[15] *Division of Experimental Medicine, McGill, University, Montreal H3G 1A4, Quebec, Canada*

[16] *Department of Microbiology and Immunology, University of Montreal, Montreal, Quebec, Canada*

[17] *Laboratory of Molecular Biology, Clinical Research Institute of Montreal, Montreal, Quebec, Canada*

$Co-authors *Co-last authors # Co-corresponding authors

Phone: 33- (0)5 61 17 54 58 FAX number: 33- (0)5 61 17 59 94 E-mail address: Christel.Verollet@ipbs.fr and Isabelle.Maridonneau-Parini@ipbs.fr

Short title: HIV-1 exacerbates osteoclast functions

Abstract

While osteoclasts (OC), the cells specialized in bone degradation, can be infected by HIV-1 *in vitro*, evidence is missing regarding the presence of infected OC *in vivo* and the mechanisms by which they could contribute to bone loss frequently observed in HIV-1$^+$ patients. Here, we report that infected OC are found in the bones of HIV-1-infected humanized mice as well as in human synovial explants exposed to HIV-1. Regarding the infection of OC *in vitro*, we show that it occurs at different stages of osteoclastogenesis *via* cell-free viruses and, more efficiently, by transfer from infected T cells. HIV-1 infection enhances the adhesion and the bone degradation activity of OC, by modifying the structure and function of the sealing zones, the F-actin structures responsible for bone resorption. The viral protein Nef is involved in all HIV-1-induced effects *in vitro*, in part through activation of Src kinase. Remarkably, OC differentiated *in vitro* from transgenic mice expressing Nef display high osteolytic activity, and these mice exhibit numerous OC along with bone defects, supporting a critical role of Nef in OC- dependent bone homeostasis *in vivo.* Altogether, our data show that OC are host cells for HIV-1 and provide strong evidence for the contribution of infected OC to bone disorders induced by the virus.

Significance Statement:

Bone deficits are frequent complications observed in HIV-1 infected patients. Our study demonstrates that HIV-1 infects osteoclasts, the cells specialized in bone degradation, using different models including HIV-1 infected humanized mice. We decipher the cellular mechanisms by which HIV-1 contributes to enhanced bone degradation in human osteoclasts, showing that the virus modifies the structure and function of the sealing zone, the bone resorption machinery of osteoclasts. We identify the viral protein Nef as the key factor responsible for such effects. As a proof of concept, we correlate bone deficit in Nef-expressing mice with enhanced osteoclast activity. Thus, our findings provide formal evidence that osteoclasts constitute novel HIV-1 host cells, contributing to bone deficits *in vivo*.

Introduction

Reduced bone mineral density is a frequent complication of HIV-1 infected patients and often progresses to osteoporosis and high prevalence of fractures. A 6-fold increased risk of low bone mineral density is observed in HIV-1-positive individuals compared to the general population (1). The use of highly active antiretroviral therapy (HAART) has significantly improved the lifespan of patients, revealing these long-term effects of the infection and the persistence of latent proviruses in reservoir cells (2). Multiple factors are believed to contribute to bone loss in infected patients. HAART is one of these factors, especially during the first years of therapy. In addition, there are evidence of bone deficit in non-treated patients, showing that the virus alone alters bone homeostasis (3-6).

Bones undergo continual remodeling, which mainly relies on the sequential actions of bone- resorbing

osteoclasts (OC) and bone-forming osteoblasts, under the control of osteocytes (7, 8). In the case of aging or HIV-1 infection, this balance can be disrupted in favor of bone loss. HIV-1-induced bone disorders are associated with an increase of blood biomarkers for bone resorption and little or no change in markers specific to bone formation, suggesting a major contribution of OC in this process (6, 9). OC are multinucleated cells derived from the monocytic lineage, which have the unique ability to resorb bone matrix. They terminally differentiate by fusion from mononucleated precursors, including blood-circulating monocytes and bone-resident precursors (10). This process is regulated by Macrophage Colony-Stimulating Factor (M- CSF) and the key osteoclastogenic cytokine, Receptor Activator of Nuclear factor Kappa-B Ligand (RANKL), mainly secreted by osteocytes but also by osteoblasts, activated B- and T- cells (10, 11). Terminally-differentiated OC express high levels of the αvβ3 integrin adhesion receptor and enzymes involved in resorption including cathepsin K, Matrix MetalloProtease 9 (MMP9) and Tartrate Resistant Acidic Phosphatase (TRAP). Bone attachment and resorption are mediated by an OC-specific structure called sealing zone (SZ). It is composed of a dense array of inter-connected F-actin structures, the podosomes. The SZ anchors the cells to the bone surface and creates a confined resorption environment where protons and osteolytic enzymes are secreted (11-14). Alteration in SZ formation and dynamics are linked to defective bone resorption, and ultimately to bone disorders as demonstrated by knocking out regulators or constituents of the SZ (14-17).

To explain the increase in osteolytic activity associated to HIV-1-induced bone loss, only a few mechanisms have been proposed: they include an increase in the production of proinflammatory cytokines (18), disruption of the immune system(6, 19) and the infection of OC(20). Regarding the immune system, studies from the HIV-1-transgenic rat model revealed that bone damage results, in part, from an altered production by B cells of regulator factors of osteoclastogenesis(19). This modified cytokine profile correlates with some bone mineral defects in non-treated HIV-1-infected patients (6). Along with CD4 T lymphocytes, macrophages serve as primary host cells for HIV-1 *in vivo* (21-23). Since OC share a common myeloid origin with macrophages, the last proposed hypothesis is that OC are targets for HIV-1 and that infected OC would contribute to bone loss. Indeed, it has recently been shown that HIV-1 may replicate *in vitro* in human monocyte-derived OC and enhance their bone resorption activity (20). However, the relevance of this observation has to be tested *in vivo* and both cellular and viral mechanisms involved in the bone resorption process remain to be characterized.

Here, we report the occurrence of infected OC in bones of HIV-1-infected humanized mice and in human synovial explants exposed to HIV-1. We further show that the exacerbated osteolytic activity of infected OC results from modified structure and function of the SZ, correlates with Src activation, a regulator of the SZ, and is dependent on the viral protein Nef.

Results

Infected OC are found in the bones of HIV-1-infected humanized mice and in human synovial explants exposed to HIV-1

Our first attempt has been to study whether OC are infected *in vivo*. Since bone marrow/Liver/Thymus (BLT) humanized mice infected with HIV-1 reproduce most hallmarks of infection in humans (22, 24, 25), we used these mice infected for 14-21 days (2.10^4-8.10^4 RNA copies/ml in blood, n=4) to examine the growth plate of femurs and tibias, zones rich in OC. In each bone section, one or two cells that presented OC characteristics (multiple nuclei, TRAP activity and localization at bone surface) were positive for the viral protein p24 (Fig. 1A), used as an indicator of productive viral infection. Negative controls were included for each sample by omitting the primary antibody (not shown). The moderated viremia of the animals, the short time of infection and the low sensitivity of the IHC detection approach could explain the fact that, in our experimental conditions, infected OC appeared as a rare event. Nevertheless, this mouse model provided the first evidence that OC can be infected *in vivo* by HIV-1.

We then determined whether OC can be infected in human tissue using synovial membrane explants, which contain fibroblasts, macrophages, lymphocytes, dendritic cells and OC, in abundant extracellular matrix (26). Fresh human synovial tissues were incubated *ex vivo* with the HIV-1 macrophage R5-tropic ADA strain and maintained in culture with osteoclastogenic cytokines to keep resident OC and OC precursors alive throughout the experiment. Fifteen days post-infection, OC were characterized by multiple nuclei, TRAP- and cathepsin K-positivity and we observed that about 10% of these cells were positive for viral p24 (n=5 synovial explants examined) (Fig. 1B).

Altogether, these data show for the first time that infection of OC occurs both *in vivo* in humanized mice and *ex vivo* in humans.

Human osteoclasts are permissive to HIV-1 infection by cell-free viruses, at different stages of differentiation

To examine the stage of differentiation at which the cells become permissive, we turned to human OC derived from primary monocytes differentiated *in vitro* in the presence of M-CSF and RANKL. The OC differentiation process was assessed by measuring OC protein level: TRAP and β3 integrin appeared at day 1 while cathepsin K, a late-stage differentiation marker, was significantly expressed only at day 6. All these proteins increased until day 10, when cells presented characteristics of mature OC including high fusion index and bone degradation activity (Supplemental Fig. 1A-E). Of note, at day 10, monocyte-derived macrophages (MDM) from the same donors differentiated with M-CSF only exhibited undetectable or low levels of these OC proteins, low fusion index and lacked osteolytic activity (Supplemental Fig. 1B-E). Cells were infected with the HIV-1 ADA strain at day 0, 1, 6 or 10 of differentiation (Fig. 2A). The extent of HIV-1 infection and replication was evaluated, at day 10 post-infection, by immunofluorescence (IF) analysis of p24 and quantified by measuring the concentration of p24 released in the supernatant. While monocytes (day 0) were unable to sustain infection, cells became increasingly permissive to infection from

day 1 to day 10 of differentiation (Fig. 2B-C, black bars); this correlated with the increased expression of the CCR5 entry co-receptor from day 1 (Supplemental Fig. 1F), CD4 being non-limitative (data not shown). HIV-1 ADA strain entered in OC mainly *via* CCR5 as OC virus production quantified by the p24 concentration in the supernatant was significantly reduced when cells were pre-treated with the CCR5 antagonist, Maraviroc (20±5 pg/ml *versus* 150 ± 15 pg/ml in control cells, n=5). We noticed that MDM and OC equally sustained infection (Fig. 2B-C), which is consistent with similar levels of CD4 and CCR5 receptors expressed during differentiation (Supplemental Fig. 1F) and at day 10 (data not shown and (20)). Moreover, the viral particles produced by infected OC or MDM had comparable infectivity, as assessed using the TZM-bl reporter cell line (27 ± 5% of p24-positive TZM-bl for OC-produced particles *versus* 26 ± 7% for MDM, n=5), indicating that both cell types released infectious virions. Importantly, HIV-1 did not affect OC viability, as cell density was not altered even at day 20 post-infection (1580 ± 276 nuclei/mm^2 for non-infected OC *versus* 1560 ± 352 for infected OC, n=6 donors, ≥3000 cells/condition).

Collectively, these results show that HIV-1 infects and replicates in OC and their precursors, without significant cytotoxic effect.

Human osteoclasts are preferentially infected by transmission from infected T cells

HIV-1 spreads by infecting target cells either as cell-free particles or more efficiently *via* cell-to- cell transmission, both *in vitro* and *in vivo* (27-30). We thus examined whether mature OC could be infected by contact with infected CD4$^+$ T lymphocytes, using Jurkat T cells infected with the HIV-1 macrophage R5-tropic NLAD8 strain (> 50% of infected T cells, n=8). After 6 hours of contact with OC, T cells were washed out and OC were harvested either immediately (day 0) or 5 days later (day 5) and stained for intracellular viral p24 by IF (Fig. 2D-E). We observed that 6 hours contact (day 0) was sufficient for T cell-to-OC virus transfer with about 15% of p24- positive OC while no detectable infection was observed at this time point when OC were cultured with cell-free virions produced by T cells. The difference was maintained at day 5. At this time point, the high rate of infected OC could result from the initial infection by T cell-to-OC transmission and from enhanced OC cell fusion. Virus transfer *via* infected T cells led to a productive infection by OC as shown by the amount of p24 detected in the supernatant at day 5 of co-culture (Fig. 2F), which is higher than in the case of infection with cell-free virions. Of note, the virus particles were equally infectious in both cases using the TZM-bl assay (data not shown).

We show that OC are infected by virus cell-to-cell transfer *via* T cells and that this infection route is more efficient than infection by cell-free virions.

HIV-1 infection enhances OC precursor migration and OC bone resorption activity

In HIV-1 transgenic rats, severe bone loss has been correlated to an increase in the number and size of OC (19). This increase could reflect an enhanced recruitment of OC precursors and/or a stimulated OC differentiation. We tested both hypotheses.

Since *in vivo*, migration of OC precursors from blood to bones requires proteases (31) and defect in the 3D protease- dependent mesenchymal migration of these cells *in vitro* correlates with lower recruitment of OC to bones *in vivo* (16), we assessed whether HIV-1 infection alters OC precursor mesenchymal migration (32, 33). Human OC precursors were infected at day 1 of differentiation (see Supplemental Fig. 1A and 1F), seeded at day 2 on Matrigel and migration was measured 48h later (Fig. 3A-C). Of note, OC precursors inside Matrigel exhibited the characteristic elongated shape of the mesenchymal migration. The percentage of migrating cells and the distance covered by the cells were both significantly increased upon HIV-1 infection.

Next, we examined the consequences of HIV-1 infection on the extent of OC fusion and bone resorption activity. HIV-1 infection significantly enhanced cell fusion, as measured by the fusion index and the area covered by infected *versus* non-infected OC (Fig. 4A), the percentage of TRAP-positive multinucleated cells and the number of nuclei per multinucleated cell (Supplemental Fig. 2A-B). When cells were treated with Maraviroc before infection, the fusion index was similar to controls (Supplemental Fig. 2C). Then, to explore the effects of OC infection on bone resorption activity, we characterized the morphology of the resorption lacunae. The total bone resorption area increased upon HIV-1 infection (Fig. 4B and D) and resorption pits presented profound morphological modifications (Fig. 4B-F). Infected OC generated resorption pits that appeared deeper (28 ± 1.2 µm *versus* 17 ± 0.7 µm for controls, $p<0.0001$ ****, Fig. 4C) and less elongated (Fig. 4E) than those of non-infected OC, which form resorption trails reminiscent of "inchworm-like migration" (34). These modifications correlated with a significant up-regulation of the bone volume resorbed per pit in the HIV-1 infection context (Fig. 4F). We also found a significant increase in the concentration of the C-terminal telopeptide of type 1 collagen (CTX) released in the supernatants and used as an additional marker of bone resorption (Fig. 4G).

Osteolytic activity is mediated by acidic dissolution of the minerals and enzymatic digestion of the organic components (35). HIV-1 infection enhanced these two activities as evidenced by the increase in the capacity of OC to dissolve minerals (Fig. 4H) and release TRAP (Fig. 4I). No variation in protein expression and activity was noticed regarding secreted cathepsin K and MMP9 (Fig. 4J-K).

Finally, we examined OC attachment/detachment to bone, a critical factor for bone degradation (12), since OC resorption, at least in part, proceeds through a succession of migratory phases alternating with bone resorption stationary phases(12, 36). When infected, OC were more resistant to detachment induced by Accutase treatment than non-infected counterparts (Fig. 4L). This increased adhesion likely slows down OC motility on bone, which should contribute to the modified morphology of resorption lacunae and to the higher bone degradation activity.

These results indicate that HIV-1 infection enhances the 3D migration of OC precursors, which may favor recruitment of OC to bones, and the adhesion and bone resorption activity of mature OC.

HIV-1 infection alters the architecture of the sealing zone and activates Src kinase

Since the SZ has been related to

adhesion and bone degradation capacities of OC (11, 37), we sought to characterize the architecture of this structure in infected OC. We observed that in OC seeded on bones, the number of cells harboring SZ and the size of SZ were increased (Fig. 5A-C). SZ delineated an area corresponding to 25 ± 1% of the cell surface of infected OC *versus* 18 ± 2% in control cells (Fig. 5D). In addition, we noticed that the fluorescence intensity of F- actin was significantly higher in SZ of infected cells (Fig. 5A and E) and the F-actin core of podosomes, the basal element of the SZ, was larger (Fig. 5F-G). The tyrosine kinase Src plays a key role in bone homeostasis by controlling the formation and stability of the SZ and the rate of actin turnover within OC podosomes (14, 16, 38). Consequently, OC from $Src^{-/-}$ mice do not assemble functional SZ and the mice exhibit a strong osteopetrotic phenotype (15). Interestingly, we showed that in the context of HIV-1-infected OC, the activity of Src kinase family was significantly enhanced as measured by phosphorylation of the regulatory tyrosine (Fig. 5H).

These results show that the increase in bone adhesion and resorption observed in infected OC is associated with larger and more numerous SZ as well as higher Src kinase activity.

The viral factor Nef is involved in HIV-1-induced effects on OC both *in vitro* and *in vivo*

Finally, we looked for the viral mechanisms involved in HIV-1-induced effects in OC. We focused on the viral accessory factor Nef because it is known, among other functions, to modulate F-actin organization and to stimulate both the kinase activity of Src (39-44) and cell fusion (45). To this end, wild type (*wt* ADA) HIV-1 and *nef*-deleted HIV-1 (HIV-1*Δnef* ADA) strains were used (33). As reported in Fig. 6A, the 3D mesenchymal migration of OC precursors infected with HIV- 1*Δnef* was similar to non-infected cells. Regarding mature OC, Src kinase phosphorylation, the bone resorption activity, the number of cells with SZ, the fusion index, and the SZ area were reduced in HIV-1*Δnef*-infected OC compared to cells infected with the *wt* virus (Fig. 6B-F). Of note, the viral particles produced by OC infected with the *wt* or mutant strains showed the same level of infectivity (26 ± 7% of p24-positive TZM-bl cells for *wt* strain *versus* 22 ± 5% for HIV- 1*Δnef*, n=4).

Next, we considered performing ectopic expression of Nef-GFP in OC but we faced a technical challenge as we failed to obtain more than 5% of Nef-expressing cells, precluding a rigorous quantification of SZ size and bone resorption activity. Nonetheless, we observed that a fraction of Nef-GFP localized at the SZ on bones (Fig. 6G). When the transfected cells were plated on glass, podosomes of Nef-expressing OC occupied a larger area than those of control cells (Fig. 6H), mimicking the results obtained with OC infected with the *wt* virus (see Fig. 5 F-G).

To address the role of Nef on OC-dependent bone remodeling *in vivo*, we took advantage of transgenic (Tg) mice expressing Nef under the regulatory sequence of the human CD4C gene, in $^{CD4+}$ T cells, macrophages and dendritic cells (46, 47). To verify that CD4C regulatory elements also drove protein expression in OC, in the absence of any available Nef antibody for IHC, we used CD4C-HIV^{GFP} Tg mice and showed that GFP was expressed in all OC (Supplemental Fig. 3A). Interestingly, the Nef Tg-mice

exhibited bone defects as evidenced by abnormal bone fragility during dissection and by an overall decrease in bone density (Supplemental Fig. 3B). To analyze alteration of bone remodeling, we examined the tibia growth plates of 7-week-old female mice, a zone that is indicative of OC activity (48, 49). We observed a decrease in bone area in Nef Tg-mice compared to non Tg-mice (Fig 7A-B, in grey), associated to a disorganized hypertrophic chondrocyte zone (Fig 7A, delimited by the red line), which appeared thinner and irregular. Moreover, a marked increase in TRAP-positive signal was noticed (Fig. 7A-B, in purple), indicating that OC were larger and/or more numerous in Nef Tg-mice compared to control littermates. Next, we examined whether Nef expression in OC modifies their differentiation and function. To this end, bone marrow precursors were isolated from Nef Tg and non Tg-mice and differentiated into OC *in vitro* (50). In OC derived from Nef Tg mice, fusion rate was not modified compared to OC derived from control mice (Fig. 7C) but bone resorption (Fig. 7D) and the width of F-actin staining in the SZ were enhanced (Fig 7E-F). Thus, modified SZ and enhanced osteolysis in OC from Nef Tg-mice could contribute to the observed bone loss in these mice.

Altogether, these results support that the viral protein Nef expressed in mouse OC reproduces the effect of the virus in human cells as it impacts the bone degradation machinery of OC and thereby may contribute to bone loss.

Discussion

Bone defects resulting from HIV-1 infection have long been described, but the causes remain poorly investigated (1). We report that HIV-1 infects OC *in vivo*, *ex vivo* and *in vitro*. In infected OC, the structure and function of the SZ are modified, impacting bone attachment and resorption and the viral protein Nef is instrumental in these processes. Hence, OC are a cell targets for HIV-1, which is, to our knowledge, the first pathogen able to manipulate the SZ.

Using HIV-1 infected BLT-humanized mice, which provide information on HIV-1 infection in human cells, we obtained the first evidence of the presence of infected OC in bones. OC can also be infected *in situ* in fresh human synovial explants. In both cases, cell infection was detected by IHC of the viral p24, which is suggestive of viral replication. *In vitro*, virus production by OC was similar to that of macrophages (see Fig. 2B-C), a known HIV host cell (21, 22, 51). Infection of OC occurred at different time points along the differentiation process, starting at day 1 in OC precursors and correlating with CCR5 expression. This suggests that circulating OC precursors, which encounter the virus in blood, could become infected and migrate to bones where they terminally differentiate (52, 53). Whether mature OC can be infected in bones is difficult to explore. Up to now, the presence of HIV-1 in bones has not been documented. We showed that direct contact of OC with infected T cells leads to productive infection of OC and even more efficiently compared to infection by cell-free viruses. This might be a way to infect OC *in situ,* which would be consistent with data showing that cell-to-cell infection is critical for efficient viral spread (25, 29, 54-56). Altogether, these results show that OC are novel host cells for HIV-1.

Regarding the consequence of HIV-

1 infection on OC function, we and others observed that the bone resorption activity of infected OC is exacerbated (this report and (20)). Herein, we provided information regarding the mechanisms involved in enhanced bone resorption which concern the structure and function of the SZ, the cell structure instrumental for bone resorption. SZ are larger in HIV-1 infected OC and, consequently, they can degrade larger bone areas. This is in line with the formation of giant OC, which contain twice more nuclei when they are infected. This exacerbated bone degradation by HIV-1 infected OC also resulted from an increased demineralization process combined with an enhanced secretion of TRAP. The SZ is made of densely connected podosomes, F-actin-rich cell structures involved in cell adhesion, mechanosensing and cell migration (57). SZ assembly and patterning are under the control of Src (14, 38). Interestingly, we report that the Src kinase activity was activated in infected OC and that podosomes were enlarged, as visualized by an increase of F-actin staining. In human macrophages, modifications of the F-actin content in individual podosomes has been correlated with fluctuations of protrusion forces exerted onto the extracellular matrix by these cell structures (58). In OC, these modified podosomes may promote more efficient sealing to bone surface. Indeed, we observed stronger adhesion for HIV-1-infected OC compared to non- infected OC. Since the SZ is a barrier that limits the diffusion of acidic and proteolytic molecules released in the resorption lacunae (11-14), increased adhesion would likely enhance the efficiency of containment and favor bone resorption (59). From these results, we propose that modification of several parameters of the SZ (*i.e.* increased size, adhesion and degradative activity) contribute to the enhanced osteolytic activity and to the modifications of the topography of resorption pits on infection (Fig. 4B-G) (12, 36, 60). Pharmacological destabilization of the SZ would reduce the impact of HIV-1 on bone degradation. Several ongoing therapeutic strategies, including the inhibition of the SZ component DOCK5 or cathepsin K activity are being developed to reduce osteoporotic syndromes while preserving OC viability and differentiation and thus bone homeostasis (17, 61, 62). We also noticed that OC precursors displayed an enhanced ability to migrate when infected with HIV-1. Interestingly, the efficiency of OC precursor migration has been correlated to OC density in bones (10, 16). Thus, in addition to enhanced bone resorption activity of infected OC, increased migration of OC precursors should favor OC recruitment to bones, as depicted in Fig. 8, contributing to bone disorders in infected patients.

Nef is a crucial determinant of viral pathogenesis and disease progression. It is known to physically interact with several host proteins to control their activity at the benefit of the virus. Namely, it regulates the intracellular protein trafficking (63), actin cytoskeleton (41), cell-cell fusion (45), cell migration (33, 42, 64, 65) and the kinase activity of several members of the Src family (40). In infected OC, all these effects could contribute to the enhanced bone resorption activity that is observed in the present study. *In vitro* experiments show that Nef, in part located at the SZ, was necessary for all the HIV-induced effects. The role of Nef was also revealed *in vivo* in CD4C-Nef-Tg mice which

exhibit reduced bone density and an increase of the surface occupied by OC-TRAP staining, suggesting an increase in recruitment, and/or differentiation of OC. Similarly, in HIV-1-Tg rats, a model involving the global transgenic expression of a non- replicative HIV-1, reduced bone mass is reported, which correlates with a high OC-TRAP staining (19). OC derived from the bone marrow of CD4C-Nef-Tg mice resorbed more and exhibited wider SZ, mimicking the results obtained with human OC infected with HIV-1. Therefore, it is likely that OC participate in the bone remodeling defects evidenced in Nef Tg mice. Given that these mice express Nef in CD4-positive cells, including T cells, macrophages, OC and dendritic cells, we propose that the observed bone defects are due, at least in part, to OC expressing Nef in addition to disrupted immune responses, which are known to participate in bone homeostasis (6, 19, 46, 66). Although we do not exclude that other viral proteins could play a role (67, 68), our results reveal Nef as an essential mediator of the HIV-1 effect on bones (Fig. 8). It is not clear yet how the virus may benefit from manipulating OC. Although OC are giant cells, they do not produce more viral particles than macrophages and these virions exhibit the same infectivity. In contrast with T cells, the cell viability of infected OC is not affected and we can suspect that these infected cells may survive for a long time in bones. Moreover, drug delivery to bones is limited by the unique anatomical features of this tissue (69). Thus, a putative advantage for the virus could consist in the use of OC as viral reservoirs to hide and survive.

In conclusion, OC are novel host cells for HIV-1 that become more osteolytic as a consequence of larger and more degradative SZ. We propose that infected OC participate in bone disorders encountered in HIV-1 patients and may constitute a reservoir for the virus. The viral protein Nef appears as a key regulator of the bone resorption activity of OC infected by HIV-1. *In toto*, this study provides a better understanding of the underlying causes of bone loss following HIV-1 infection.

Acknowledgements

We greatly acknowledge C. Salon from US006/CREFRE; G. Lugo-Villarino and R. Poincloux for critical reading of the manuscript; M. Dubois, M. Cazabat, M. Requena and J. Izopet from the BSL3 laboratory of the BiVic facility, F. Moreau and C. Berrone from the animal BSL3 facilities at IPBS BS, C. Bordier for help with cytometry experiments, N. Ortega and A. Métais for help in histology and E. Cavaignac for providing synovium samples. The authors acknowledge the TRI imaging facility and ANEXPLO functional exploration facility. This work was supported by the *Centre National de la Recherche Scientifique*, the *Agence Nationale de la Recherche* (ANR 2010-01301, ANR14-CE11-0020-02, ANR16-CE13-0005-01, ANR-11-EQUIPEX-0003), the *Agence Nationale de Recherche sur le Sida et les hépatites virales* (ANRS2014-CI-2, ANRS2014-049), the *Fondation pour la Recherche Médicale* (DEQ2016 0334894), INSERM Plan Cancer, the Human Frontier Science Program (RGP0035/2016), German Science Foundation (DFG) research fellowship (US116-2-1 to SMU), National Institutes of Health (NIH) R01 grant (AI097052 to TRM). LB is supported by grants from the Institut Pasteur International Network and

the Chinese Academy of Sciences. Work in PJo' laboratory was supported by the Canadian Institute of Health Research (CIHR

References

1. Cotter AG & Mallon PW (2014) The effects of untreated and treated HIV infection on bone disease. Curr Opin HIV AIDS 9(1):17-26.
2. Descours B, et al. (2017) CD32a is a marker of a CD4 T-cell HIV reservoir harbouring replication- competent proviruses. Nature.
3. Bruera D, Luna N, David DO, Bergoglio LM, & Zamudio J (2003) Decreased bone mineral density in HIV-infected patients is independent of antiretroviral therapy. Aids 17(13):1917-1923.
4. Gibellini D, et al. (2007) RANKL/OPG/TRAIL plasma levels and bone mass loss evaluation in antiretroviral naive HIV-1-positive men. J Med Virol 79(10):1446-1454.
5. Grijsen ML, et al. (2010) High prevalence of reduced bone mineral density in primary HIV-1- infected men. Aids 24(14):2233-2238.
6. Titanji K, et al. (2014) Dysregulated B cell expression of RANKL and OPG correlates with loss of bone mineral density in HIV infection. PLoS pathogens 10(10):e1004497.
7. Boyle WJ, Simonet WS, & Lacey DL (2003) Osteoclast differentiation and activation. Nature 423(6937):337-342.
8. Prideaux M, et al. (2016) Isolation of osteocytes from human trabecular bone. Bone 88:64-72.
9. Aziz N, Butch AW, Quint JJ, & Detels R (2014) Association of Blood Biomarkers of Bone Turnover in HIV-1 Infected Individuals Receiving Anti-Retroviral Therapy (ART). J AIDS Clin Res 5.
10. Kotani M, et al. (2013) Systemic circulation and bone recruitment of osteoclast precursors tracked by using fluorescent imaging techniques. J Immunol 190(2):605-612.
11. Teitelbaum SL (2011) The osteoclast and its unique cytoskeleton. Ann N Y Acad Sci 1240:14-17.
12. Georgess D, Machuca-Gayet I, Blangy A, & Jurdic P (2014) Podosome organization drives osteoclast-mediated bone resorption. Cell Adh. Migr. 8(3):191-204.
13. Jurdic P, Saltel F, Chabadel A, & Destaing O (2006) Podosome and sealing zone: specificity of the osteoclast model. Eur. J. Cell Biol. 85:195-202.
14. Luxenburg C, Parsons JT, Addadi L, & Geiger B (2006) Involvement of the Src-cortactin pathway in podosome formation and turnover during polarization of cultured osteoclasts. Journal of cell science 119(Pt 23):4878-4888.

15. Soriano P, Montgomery C, Geske R, & Bradley A (1991) Targeted disruption of the c-src proto- oncogene leads to osteopetrosis in mice. Cell 64(4):693-702.

16. Verollet C, et al. (2013) Hck contributes to bone homeostasis by controlling the recruitment of osteoclast precursors. FASEB journal : official publication of the Federation of American Societies for Experimental Biology 27(9):3608-3618.

17. Vives V, et al. (2011) The Rac1 exchange factor Dock5 is essential for bone resorption by osteoclasts. J Bone Miner Res 26(5):1099-1110.

18. de Menezes EG, Machado AA, Barbosa F, Jr., de Paula FJ, & Navarro AM (2016) Bone metabolism dysfunction mediated by the increase of proinflammatory cytokines in chronic HIV infection. J Bone Miner Metab.

19. Vikulina T, et al. (2010) Alterations in the immuno-skeletal interface drive bone destruction in HIV-1 transgenic rats. Proceedings of the National Academy of Sciences of the United States of America 107(31):13848-13853.

20. Gohda J & al. e (2015) HIV-1 replicates in human osteoclasts and enhances their differentiation in vitro. Retrovirology 12:12.

21. Honeycutt JB, et al. (2017) HIV persistence in tissue macrophages of humanized myeloid-only mice during antiretroviral therapy. Nature medicine.

22. Honeycutt JB, et al. (2016) Macrophages sustain HIV replication in vivo independently of T cells. The Journal of clinical investigation 126(4):1353-1366.

23. Sattentau QJ (1988) The role of the CD4 antigen in HIV infection and immune pathogenesis. AIDS 2 Suppl 1:S11-16.

24. Brainard DM, et al. (2009) Induction of robust cellular and humoral virus-specific adaptive immune responses in human immunodeficiency virus-infected humanized BLT mice. Journal of virology 83(14):7305-7321.

25. Murooka TT, et al. (2012) HIV-infected T cells are migratory vehicles for viral dissemination. Nature 490(7419):283-287.

26. Hayder M, et al. (2011) A phosphorus-based dendrimer targets inflammation and osteoclastogenesis in experimental arthritis. Science translational medicine 3(81):81ra35.

27. Casartelli N, et al. (2010) Tetherin restricts productive HIV-1 cell-to-cell transmission. PLoS pathogens 6(6):e1000955.

28. Iwami S, et al. (2015) Cell-to-cell infection by HIV contributes over half of virus infection. eLife 4.

29. Sewald X, et al. (2015) Retroviruses use CD169-mediated trans-infection of permissive lymphocytes to establish infection. Science 350(6260):563-567.

30. Casartelli N (2016) HIV-1 Cell-to-Cell Transmission and Antiviral Strategies: An

Overview. Current drug targets 17(1):65-75.

31. Blavier L & Delaisse JM (1995) Matrix metalloproteinases are obligatory for the migration of preosteoclasts to the developing marrow cavity of primitive long bones. Journal of cell science 108 (Pt 12):3649-3659.

32. Van Goethem E, Poincloux R, Gauffre F, Maridonneau-Parini I, & Le Cabec V (2010) Matrix Architecture Dictates Three-Dimensional Migration Modes of Human Macrophages: Differential Involvement of Proteases and Podosome-Like Structures. J Immunol 184(2):1049-1061.

33. Verollet C, et al. (2015) HIV-1 reprograms the migration of macrophages. Blood 125(10):1611- 1622.

34. Saltel F, Destaing O, Bard F, Eichert D, & Jurdic P (2004) Apatite-mediated actin dynamics in resorbing osteoclasts. Mol. Biol. Cell 15(12):5231-5241.

35. Vaananen HK, Zhao H, Mulari M, & Halleen JM (2000) The cell biology of osteoclast function. Journal of cell science 113 (Pt 3):377-381.

36. Soe K & Delaisse JM (2017) Time-lapse reveals that osteoclasts can move across the bone surface while resorbing. Journal of cell science 130(12):2026-2035.

37. Geblinger D, Addadi L, & Geiger B (2010) Nano-topography sensing by osteoclasts. Journal of cell science 123(Pt 9):1503-1510.

38. Destaing O, et al. (2008) The tyrosine kinase activity of c-Src regulates actin dynamics and organization of podosomes in osteoclasts. Mol Biol Cell 19(1):394-404.

39. Moarefi I, et al. (1997) Activation of the Src-family tyrosine kinase Hck by SH3 domain displacement. Nature 385(6617):650-653.

40. Saksela K (2011) Interactions of the HIV/SIV pathogenicity factor Nef with SH3 domain- containing host cell proteins. Current HIV research 9(7):531-542.

41. Stolp B & Fackler OT (2011) How HIV takes advantage of the cytoskeleton in entry and replication. Viruses 3(4):293-311.

42. Stolp B, et al. (2009) HIV-1 Nef interferes with host cell motility by deregulation of Cofilin. Cell host & microbe 6(2):174-186.

43. Trible RP, Emert-Sedlak L, & Smithgall TE (2006) HIV-1 Nef selectively activates Src family kinases Hck, Lyn, and c-Src through direct SH3 domain interaction. The Journal of biological chemistry 281(37):27029-27038.

44. Nobile C, et al. (2010) HIV-1 Nef inhibits ruffles, induces filopodia, and modulates migration of infected lymphocytes. Journal of virology 84(5):2282-2293.

45. Verollet C, et al. (2010) HIV-1 Nef triggers macrophage fusion in a p61Hck- and

protease- dependent manner. J Immunol 184(12):7030-7039.

46. Hanna Z, et al. (1998) Nef harbors a major determinant of pathogenicity for an AIDS-like disease induced by HIV-1 in transgenic mice. Cell 95(2):163-175.

47. Hanna Z, et al. (2009) Selective expression of human immunodeficiency virus Nef in specific immune cell populations of transgenic mice is associated with distinct AIDS-like phenotypes. Journal of virology 83(19):9743-9758.

48. Dougall WC, et al. (1999) RANK is essential for osteoclast and lymph node development. Genes & development 13(18):2412-2424.

49. Li J, et al. (2000) RANK is the intrinsic hematopoietic cell surface receptor that controls osteoclastogenesis and regulation of bone mass and calcium metabolism. Proceedings of the National Academy of Sciences of the United States of America 97(4):1566-1571.

50. Verollet C, et al. (2013) HIV-1 Nef alters podosomes and promotes the mesenchymal migration in human macrophages. Retrovirology 10:S34-S34.

51. Sattentau QJ & Stevenson M (2016) Macrophages and HIV-1: An Unhealthy Constellation. Cell host & microbe 19(3):304-310.

52. Delobel P, et al. (2005) Persistence of distinct HIV-1 populations in blood monocytes and naive and memory CD4 T cells during prolonged suppressive HAART. AIDS 19(16):1739-1750.

53. Zhu T, et al. (2002) Evidence for human immunodeficiency virus type 1 replication in vivo in CD14(+) monocytes and its potential role as a source of virus in patients on highly active antiretroviral therapy. Journal of virology 76(2):707-716.

54. Law KM, et al. (2016) In Vivo HIV-1 Cell-to-Cell Transmission Promotes Multicopy Micro- compartmentalized Infection. Cell reports 15(12):2771-2783.

55. Russell RA, Martin N, Mitar I, Jones E, & Sattentau QJ (2013) Multiple proviral integration events after virological synapse-mediated HIV-1 spread. Virology 443(1):143-149.

56. Sigal A, et al. (2011) Cell-to-cell spread of HIV permits ongoing replication despite antiretroviral therapy. Nature 477(7362):95-98.

57. Wiesner C, Le-Cabec V, El Azzouzi K, Maridonneau-Parini I, & Linder S (2014) Podosomes in space: Macrophage migration and matrix degradation in 2D and 3D settings. Cell Adh. Migr. 8(3):179-191.

58. Proag A, et al. (2015) Working together: spatial synchrony in the force and actin dynamics of podosome first neighbors. ACS nano 9(4):3800-3813.

59. Stenbeck G & Horton MA (2000) A new specialized cell-matrix interaction in actively resorbing osteoclasts. Journal of cell science 113 (Pt 9):1577-1587.

60. Merrild DM, et al. (2015) Pit- and trench-forming osteoclasts: a distinction that matters. Bone research 3:15032.

61. Panwar P, et al. (2016) A novel approach to inhibit bone resorption: exosite inhibitors against cathepsin K. British journal of pharmacology 173(2):396-410.

62. Vives V, et al. (2015) Pharmacological inhibition of Dock5 prevents osteolysis by affecting osteoclast podosome organization while preserving bone formation. Nature communications 6:6218.

63. Foster JL & Garcia JV (2006) HIV pathogenesis: Nef loses control. Cell 125(6):1034-1035.

64. Stolp B, et al. (2012) HIV-1 Nef interferes with T-lymphocyte circulation through confined environments in vivo. Proceedings of the National Academy of Sciences of the United States of America 109(45):18541-18546.

65. Verollet C, Le Cabec V, & Maridonneau-Parini I (2015) HIV-1 Infection of T Lymphocytes and Macrophages Affects Their Migration via Nef. Frontiers in immunology 6:514.

66. Hanna Z, et al. (2001) The pathogenicity of human immunodeficiency virus (HIV) type 1 Nef in CD4C/HIV transgenic mice is abolished by mutation of its SH3-binding domain, and disease development is delayed in the absence of Hck. Journal of virology 75(19):9378-9392.

67. Chew N, Tan E, Li L, & Lim R (2014) HIV-1 tat and rev upregulates osteoclast bone resorption. J Int AIDS Soc 17(4 Suppl 3):19724.

68. Gibellini D, et al. (2010) HIV-1 Tat protein enhances RANKL/M-CSF-mediated osteoclast differentiation. Biochemical and biophysical research communications 401(3):429-434.

69. Hirabayashi H & Fujisaki J (2003) Bone-specific drug delivery systems: approaches via chemical modification of bone-seeking agents. Clinical pharmacokinetics 42(15):1319-1330.

Figure Legends

Figure 1: Tissue-osteoclasts (OC) are infected by HIV-1 *in vivo* and *ex vivo.* A. HIV-1 infects OC *in vivo* in HIV-1-infected BLT-humanized mice. Two serial sections (3µm between each section, 1-2) of the head of a tibia of HIV-1-BLT mice were stained for TRAP activity (in purple, 1) and with a monoclonal antibody directed towards human viral protein p24 (in brown, 2). Representative sections (n=4 mice, 3 sections of tibia and femur heads). Arrowheads show an infected OC. Scale bar, 50µm. Enlarged frames, X 2 zoom. **B. Human OC are infected by HIV-1 in synovial explants**. Pieces of a non-inflammatory human synovial tissue were cultured with M-CSF and RANKL and infected with HIV-1 (ADA strain). Two weeks post-infection, histological analyses (TRAP activity in purple, p24 and cathepsin K IHC in brown, nuclei in blue) were performed on 3 serial sections (3µm between each section, 1-3). Representative histological sections (n=3 synovial tissues, 4 pieces per tissue). Scale bar, 100µm. Enlarged frames, X 2.3 zoom.

Figure 2. HIV-1 infects human OC and their precursors *in vitro*. A-C. OC are infected by cell- free viruses at different stages of differentiation. (A) Experimental design of infection (ADA strain) at multiplicity of infection (MOI) of 0.1. (B-C) Kinetics of the percentage of p24-positive cells (B, determined by Iimmunofluorescence (IF)) and of p24 release in the supernatants (C, determined by ELISA) in cells maintained in M-CSF plus RANKL (OC, black bars) or M-CSF alone (MDM, blue bars) from the same donor are shown. Results from a representative experiment are expressed as mean +/- SEM (n=5 donors). Day of i: day of infection. **D-F. OC are efficiently infected through viral transmission from HIV-1 infected T cells.** OC have been in contact for 6h with non-infected Jurkat T lymphocytes (left), with HIV-1-infected T lymphocytes (middle) or with cell-free viral particles produced by T cells during 6 hours (right), they were washed then harvested immediately (day 0) or 5 days later (day 5). (D) Representative mosaic of 3X3 confocal fields of original magnification 20X, after staining for p24 (green), F-actin (red) and nuclei (DAPI, blue) at day 5. Scale, 50µm. (E-F) Quantification of the percentage of p24-positive cells evaluated by IF (E) immediately (day 0) or 5 days (day 5) post-infection and of p24 release in the supernatants determined by ELISA after 5 days (day 5) (F) (n=8 donors). (NI: non-infected)

Figure 3. HIV-1 enhances the 3D migration of OC precursors in Matrigel. OC precursors were infected or not at day 1, seeded at day 2 on thick layers of Matrigel polymerized in transwell chambers and migration was recorded 48h later. (A) Representative brightfield images of live cells either at the surface (top) or within the matrix (inside), taken after 48h of migration using an inverted video microscope. Scale bar, 50 µm. (B) The percentage of migrating cells was measured for 7 donors. (NI: non-infected). (C) 3D positions of OC precursors in the matrix and mean distance of migration (d) from a representative experiment are shown using the TopCat software.

Figure 4. HIV-1 enhances the fusion, osteolytic activity and adhesion of OC. A. HIV-1 triggers OC fusion. (A) 10 days post-infection, cells were stained for p24 (green), F-actin

(red) and nuclei (DAPI, blue). Mosaic of 4X4 confocal fields of original magnification 20X. Scale bar, 150 µm. The cell fusion index (nuclei number in multinucleated cells/total nuclei number) and the percentage of area covered by multinucleated cells (area index) were measured for >3,000 cells in each condition, n=6 donors. Results are expressed as mean +/- SEM. **B-G. OC bone resorption is increased by HIV-1 infection.** Day 10-non-infected and HIV-1-infected OC were seeded on cortical bone slides for 48h. Then, OC were removed, the supernatants collected and the bone slices stained with toluidine blue to visualize resorption pits. Data were obtained from 6 independent donors. (B) Representative brightfield images of bone-resorption pits (purple). Scale bar, 20 µm. (C) Representative confocal images of pits. Color codes for the depth of resorption pits (color scale bar, z). Scale bar (x, y), 20 µm. Quantification of the percentage of degradation area (D) and circularity (E) from brightfield images and resorbed volume (F) from confocal images are shown. The degradation area of non-infected OC, normalized as 100%, corresponded to 9% of the total area. (G) The concentration of CTX in the supernatant was measured by ELISA and normalized at 100% for non-infected cells (mean CTX concentration=1790 pg/mL), n= 6 donors. **H-K. Effects of infection on mineral dissolution and extracellular osteolytic enzymes.** (H) Day 10-non-infected and HIV-1-infected OC were seeded on crystalline inorganic calcium phosphate-coated multiwells. The cells were removed and the wells stained with the Von Kossa solution. Scale bar, 50 µm. Graph shows the area covered by mineral dissolution pits from 10 fields per condition and per donor, n=3 donors. (I-K) The supernatants of day 10-non-infected and HIV-1-infected OC seeded on glass were collected. TRAP and cathepsin K (CtsK) expression level (Western blot, I-J) and MMP9 activity (zymography analysis, K) were quantified. Charges have been controlled by Coomassie blue staining, n=4 donors. (NI: non-infected). **L. HIV-1 infection increases OC adhesive properties.** Day 10-non- infected and HIV-1-infected OC were treated with Accutase for 10 min and the percentage of remaining nuclei still present in the plate was quantified. Graph represents average of 5 fields per condition from n=3 donors.

Figure 5. HIV-1 modifies the organization of the SZ and induces Src-kinase activation in human OC. A-E. HIV-1 infection increases the size and F-actin intensity of the SZ. (A) Confocal images of non-infected or HIV-1-infected OC seeded on bone slides. Cells were stained for p24 (green) and F-actin (red). Scale bar, 10 µm. (B) Quantification of the percentage of cells forming SZ (n=4 donors, 300 cells per donor). (C-E) Vertical scatter plots showing for each SZ, the area (C), the ratio of SZ area to cell area (D) and the F-actin intensity (E) (n= 3 donors, >25 SZ). Graphs show individual SZ values and the mean. **F-G. HIV-1 infection increases the size of individual podosomes.** OC seeded on glass were infected with HIV-1 and stained for F-actin. (F) IF images. Scale bar, 10 µm. (G) Automated quantification of the F-actin fluorescence area of individual podosomes. Mean +/- SEM, n=3 donors (>2000 podosomes, 10 cells per donor). **H. HIV-1 infection induces Src-kinase activation.** Whole-cell lysate Western blot using antibodies against phospho-Tyr416-Src kinases, Src and Actin. A representative blot out of 6 independent experiments and the quantification of the phospho-Tyr416 kinase ratio over total Src are shown. Results are expressed as mean ± SEM. n=6 donors. (NI: non-infected).

Figure 6. HIV-1 effects on differentiation and function of OC require the viral protein Nef. A- F. Nef is necessary for HIV-1-induced effects in OC. Human OC precursors (A) or mature OC (B- F) were infected with *wild type* HIV-1 or with a *nef*-deleted HIV-1 (HIV-1*Δnef*) (NI: non-infected). (A) Percentage of migrating OC precursors after 48h measured as in Fig. 3, n= 4 donors. (B) Quantification of Western blot analyses of whole-cell lysate using antibodies against phospho- Tyr416-Src kinases, Src and Actin as in Fig. 5H. Results are expressed as mean +/- SEM, n=6 donors. Quantification of (C) resorbed bone area (n=4), of (D) the percentage of cells forming 26
SZ (n=4 donors, 300 cells per donor), of (E) the fusion index (>3000 cells per condition, n=6 donors) illustrated by mosaics of 4X4 confocal fields (F-actin in red and DAPI in green, scale bar, 150 μm), and of (F) the SZ area of OC seeded on bones and stained for actin (phalloidin). Scale bar, 10 μm, n= 3 donors, >25 SZ. Results are expressed as mean +/- SEM. **G-H. Nef expression in OC.** OC were transfected with Nef_{SF2}-GFP or GFP (control) and stained for F-actin (phalloidin). (G) A fraction of Nef localizes to the SZ. Confocal images of OC expressing Nef_{SF2}-GFP. Arrowheads show co-localization of Nef-GFP with F-actin at the SZ. Scale bar, 10 μm, Inserts, X 2 zoom. (H) Nef expression increases the size of individual podosomes. Automated quantification of the F-actin fluorescence area of individual podosomes. Mean ± SEM, n=4 donors (>2000 podosomes from over 5 cells per donor).

Figure 7. The viral protein Nef induces bone defects *in vivo* and modifications in OC differentiation. **A-B. Nef Tg-mice exhibit bone defects.** (A) Representative histological sections of tibia of 7-week-old mice stained for TRAP to visualize OC (purple), and counterstained with Methyl green and Alcian blue: bone appears in grey, nuclei in green (corresponding to the nuclei of bone marrow cells), and cartilage in blue. Scale bar, 200μm.Enlarged frames: x 4 zoom. (B) Quantification of the surface occupied by trabecular bone and surface occupied by TRAP- positive signal in 3 separate histological sections per mouse (n=3 mice per genotype) are shown. **C-F**. **OC differentiated *ex vivo* from Tg-mice are more osteolytic**. OC were differentiated from bone marrow precursors isolated from Nef Tg- and non Tg-mice and the fusion index (C), the bone resorption area (D) and the F-actin belt thickness (E) were quantified (50 SZ per condition, n=3 mice per genotype). (F) Representative images of belt structures of OC differentiated from non Tg and Tg mice stained for F-actin (red) and vinculin (green). Enlarged frames, x 2 zoom. Scale bar, 10 μm.
Figure 8: Graphical abstract proposed to explain HIV-1-induced bone defects in patients. HIV- 1 infection impacts OC precursor recruitment to bones and the OC differentiation process. These effects, dependent on the viral protein Nef, result in more numerous and more osteolytic OC exhibiting larger and denser SZ.l

Raynaud et al., Figure 1

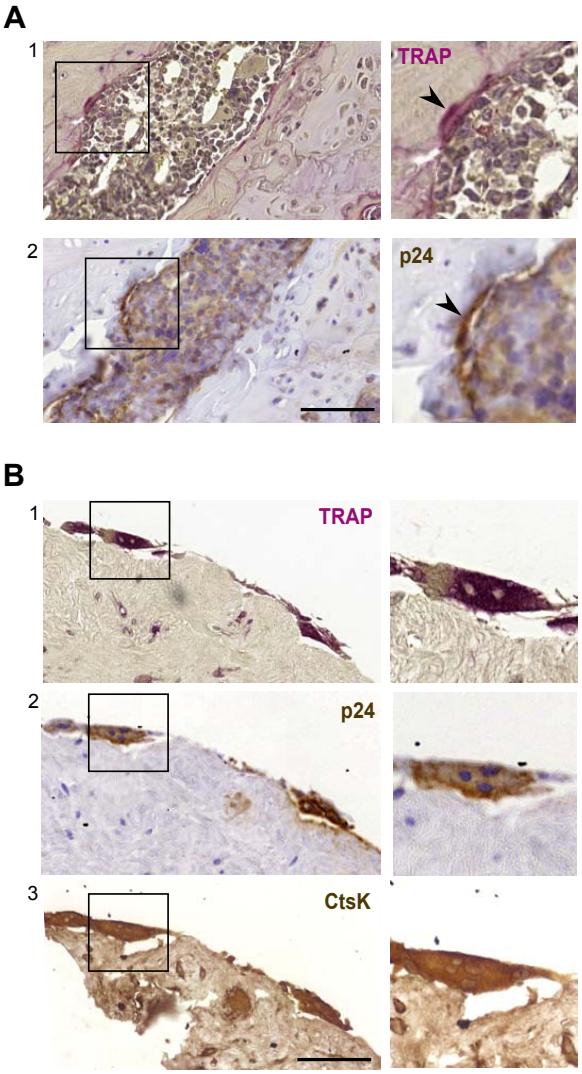

Raynaud et al., Figure 2

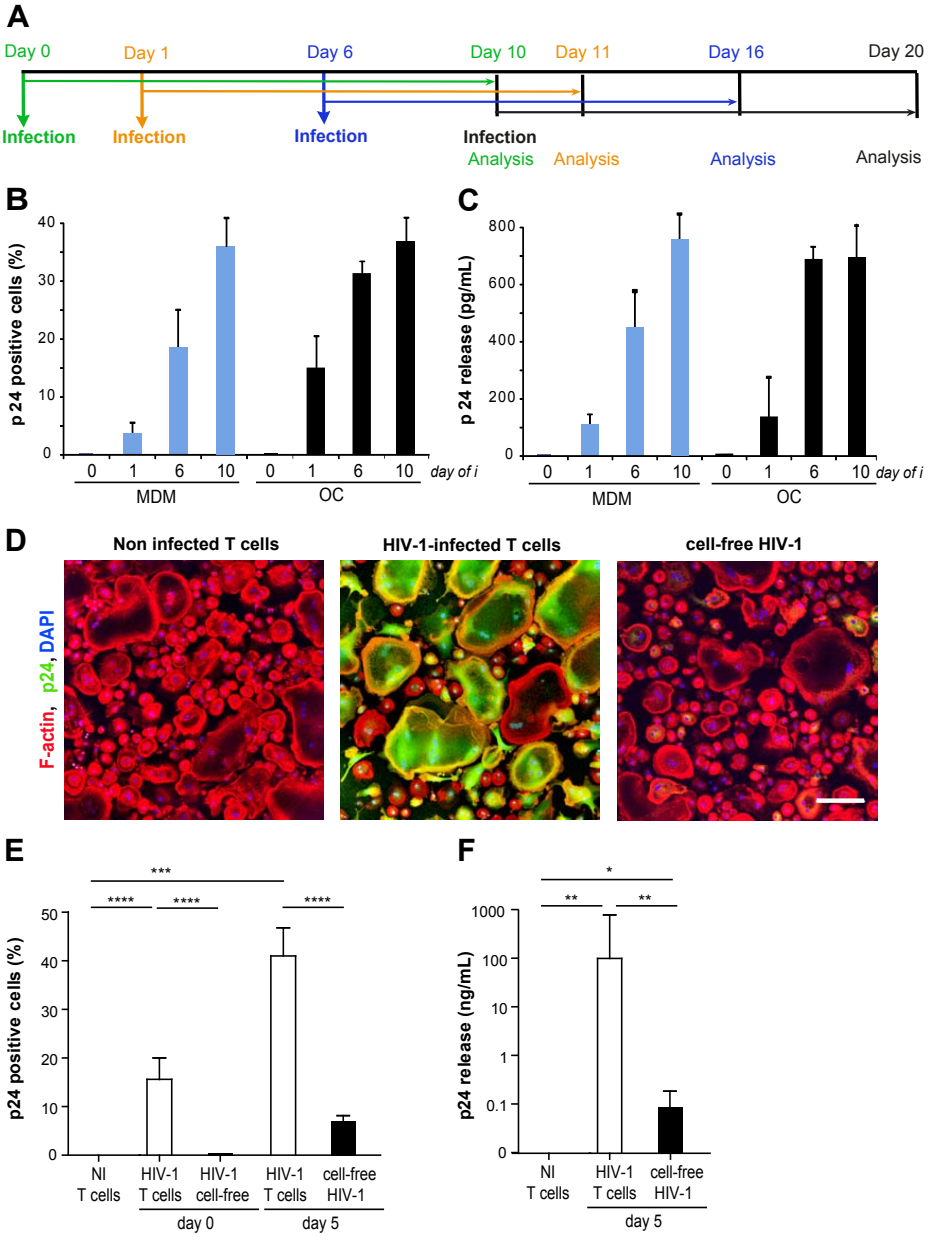

Raynaud et al., Figure 3

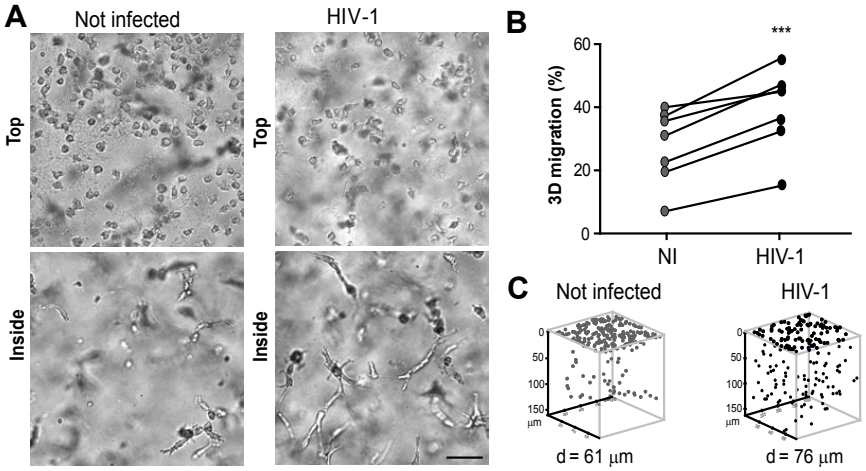

Raynaud et al., Figure 4

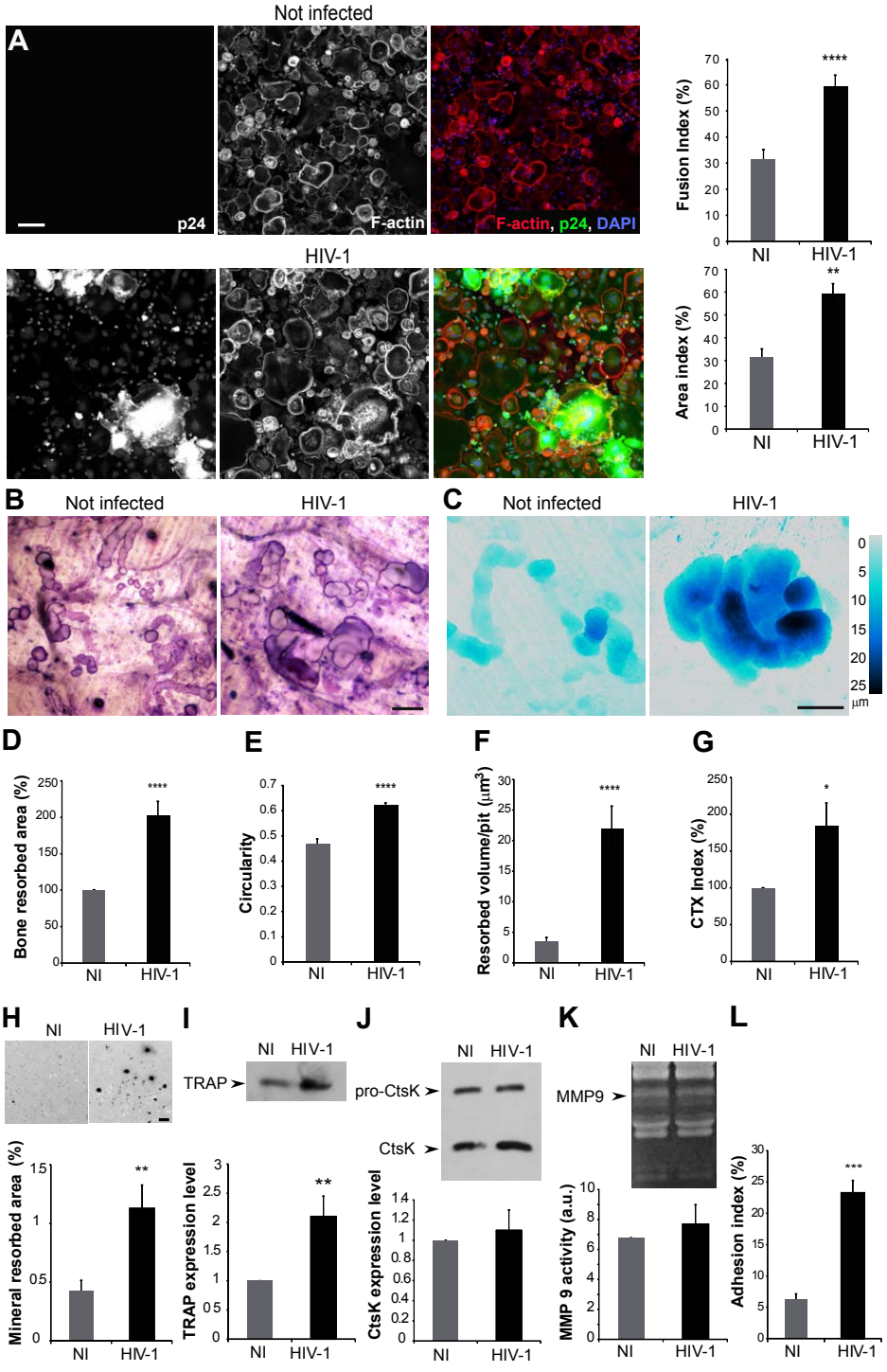

Raynaud et al., Figure 5

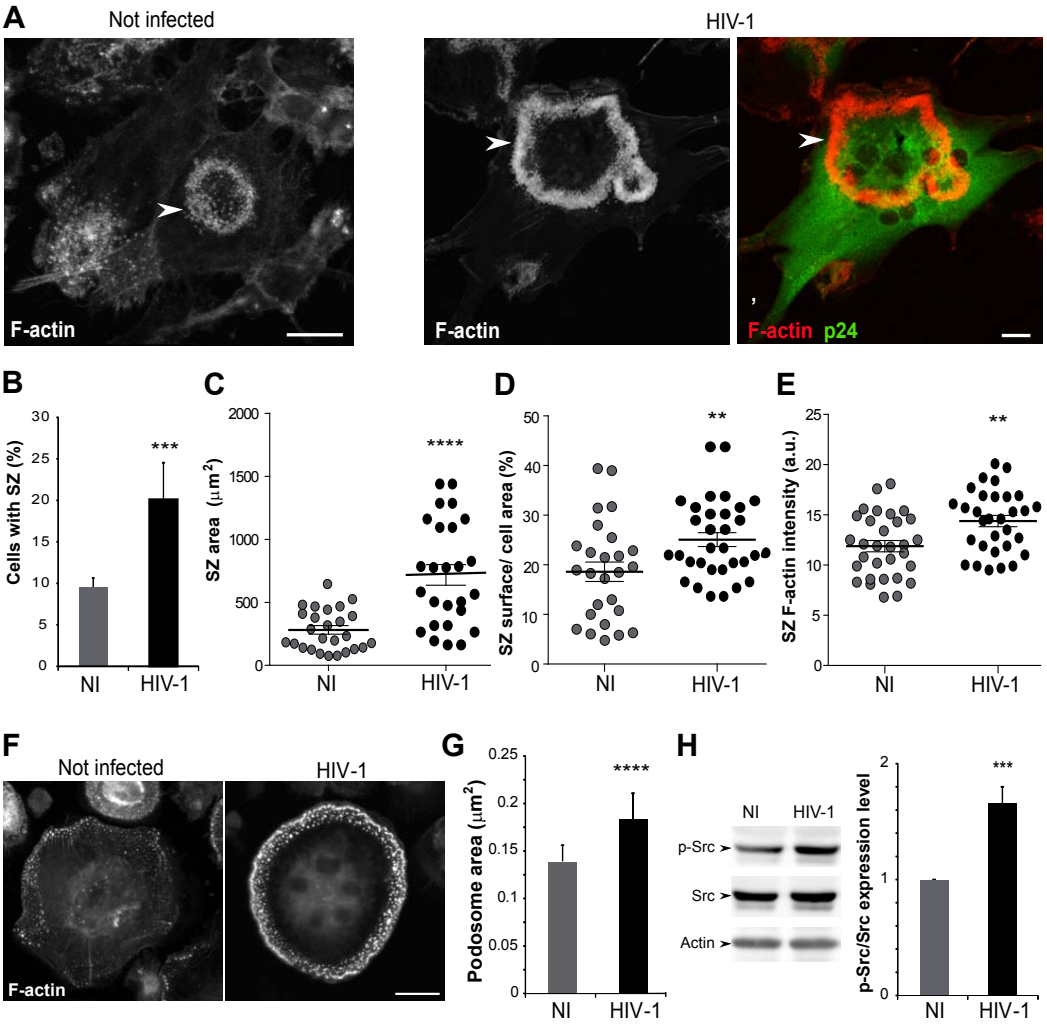

Raynaud et al., Figure 6

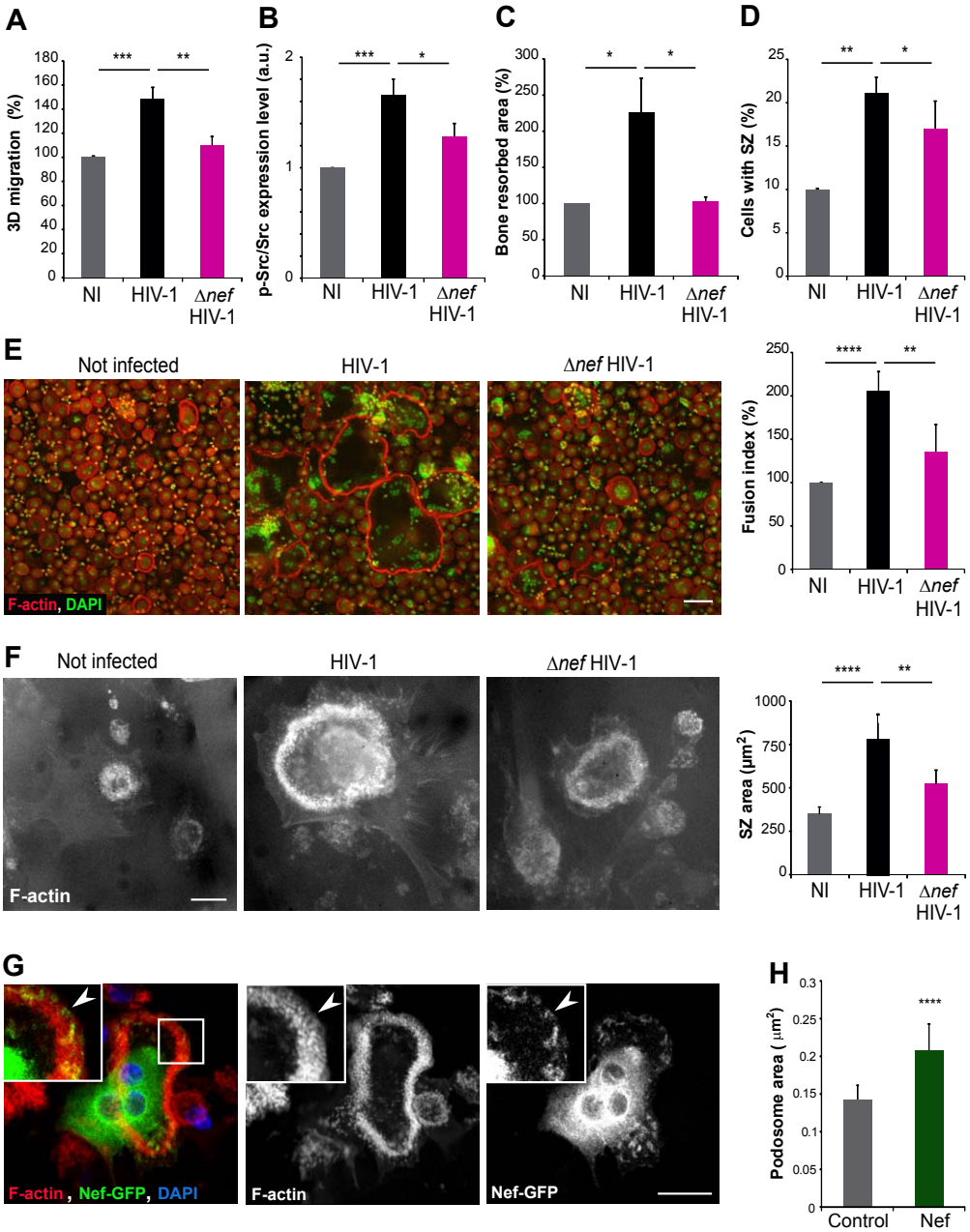

Raynaud et al., Figure 7

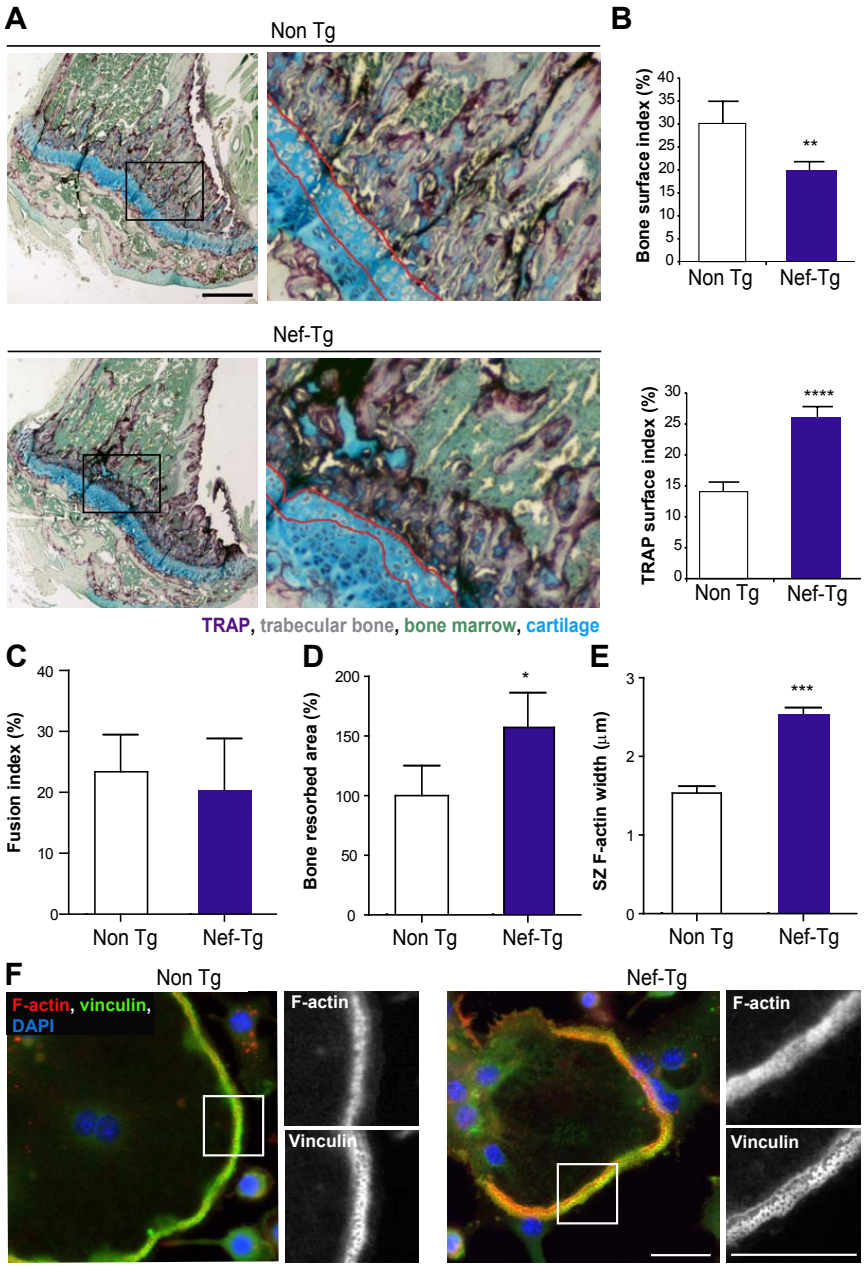

Raynaud et al., Figure 8

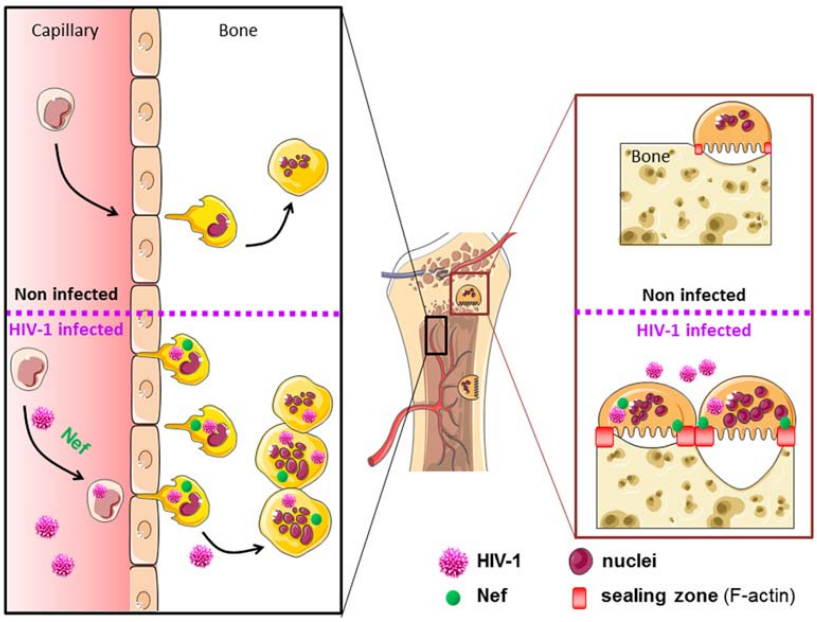

Supplemental informations

Material and Methods

Chemicals and antibodies

Recombinant macrophage colony-stimulating factor (M-CSF) was purchased from Peprotech (London, UK) and Human receptor activator of NF-κB-ligand (RANKL) from Miltenyi Biotec (Germany). Leukocyte acid phosphatase kit for Tartrate Resistant Acid Phosphatase (TRAP) mg/mL) was from BD Biosciences (San Jose, CA). The following antibodies were used: Rabbit anti-Phospho-Src (Tyr416) (Cell Signaling Technology, Ozyme, France), rabbit anti-integrin β3 (Cell Signaling) mouse monoclonal anti-cathepsin K (clone 3F9, ab37259, Abcam) and anti- TRAP antibodies (sc-28204) (Santa Cruz Biotechnologies, TEBU-Bio, France), monoclonal anti- Actin (clone 20-33), anti-β–tubulin (clone B-5-1-2), mouse anti-vinculin (clone hVin-1) (Sigma- Aldrich) and mouse monoclonal anti- human p24 (clone Kal-1) (Dako, Les Ulis, France) or anti- p24-FITC monoclonal antibody clone KC57-FITC (Beckman Coulter). Secondary biotin- conjugated antibodies and avidin-biotin-perodydasecomplex were from Dako (Les Ulis, France) and Vector laboratories (LTP, United Kingdom) and fluorescent secondary antibodies and Texas Red/Alexa Fluor 488-conjugated phalloidins were obtained from Molecular probes (Invitrogen, Cergy Pontoise, France). Maraviroc (Sigma-Aldrich) was used at 10μM, 30 min before infection.

Mice

The CD4C/HIV Nef (previsouly named CD4C/HIV^{MutG})(1) and CD4C/HIV^{GFP} Tg mice[(2)] have been described. Experiments were approved by the Institutional Animal Ethics. Female BLT mice were generated as previsouly described (3). Briefly, NOD/SCID/$\gamma c^{-/-}$ mice 6 to 8 weeks of age ere conditioned with sublethal (2 Gy) whole-body irradiation, and 1mm^3 fragments of human fetal thymus and liver (17 to 19 weeks of gestational age) (Advanced Bioscience Resources) were implanted under the recipient kidney capsules bilaterally. Remaining fetal liver tissue was used to isolate CD34 cells with anti-CD34 microbeads within 6 h.

Intra-vaginal HIV infection

5-7 days before intravaginal infection NSG-BLT humanized mice were subcutaneously injected with 200μg progesterone (Depo-Provera, Pfizer) to synchronize their estrus cycle. Prior to intravaginal inoculation, mice were anesthetized with a mixture Ketamine and that was engineered to express V3 loop from Bal strain thus conferring CCR5 tropism(4). Control group received 10 μl of PBS intravaginally. Plasma viremia was monitored weekly by collecting few drops of blood from facial vein and basis by quantitating plasma viral loads by qPCR. All animal experiments were performed in accordance with guidelines and regulations implemented by the Massachusetts General Hospital (MGH) Institutional Animal Care and Use Committee (IACUC).

Plasma viral loads

Viral RNA was isolated from approximately 50 μl of plasma using the QIAamp viral RNA kit (Qiagen). Quantitative reverse transcription, and PCR was performed using HIV-1 gag

specific primers 5'-AGTGGGGGGACATCAAGCAGCCATGCAAAT-3' and 5'-TGCTATGTCACTTCCCCTTGGTTCTCT-3' by using single step QuantiFast SYBR Green RT-PCR Kit (Qiagen) on Lightcycler 480-II (Roche). Plasma from uninfected BLT mice was used to determine the background signal as described previously (4).

Cell culture and transfection

Human monocytes were isolated from the blood of healthy donors and differentiated as hMDM as described (5). For differentiation to human osteoclasts (OC), monocytes were Memorial Institute medium (RPMI) supplemented with 10% FBS, M-CSF (50 ng/mL) and RANKL (30 ng/mL). The medium was replaced every 3 days with medium containing M-CSF (25 ng/mL) and RANKL (100 ng/mL). hMDM and OC from the same donor were used from day 1 to 6 of differentiation (OC precursors) or at day 10 of differentiation (mature OC). We used a Neon MP 5000 electroporation system (Invitrogen) for transient expression of Nef in GFP have been described (6). Cells were used within 24h (5% transfection efficiency).

Jurkat T cells (RRID:CVCL_DS02) were maintained in RPMI medium containing 10% FBS and 1% penicillin/ streptomycin (Invitrogen). Mouse OC were differentiated from bone marrow (BM) cells isolated from long bones as previously described (7). Briefly, non-adherent cells were cultured in α-MEM supplemented with 30 ng/ml mouse M-CSF (Miltenyi Biotec, Germany) for 48h. Then, OC differentiation was initiated in medium containing 100 ng/ml mouse RANKL (Miltenyi Biotec) and 30 ng/ml plate). Media was changed and cytokines were replenished every 2 days. Cells were maintained in culture for 4–6 days before analyses.

Cell-free infection of macrophages and OC

Macrophages and OC were infected at MOI 0.1 with the macrophage-tropic HIV-1 isolate ADA or HIVΔ*nef*-1, as described (8). Infectivity and replication was assessed by measuring p24- positive cells by immunostaining, p24 level in cell supernatants by ELISA assay (6), and using TZM-bl indicator cells, as previously described (9).

Viral transfer to OC via infected T cells

Jurkat cells (J77 provided by S. Benichou, Institut Cochin, France) were infected with the CCR5- tropic virus (NLAD8) co-expressing VSV-G envelope glycoprotein, to allow efficient infection independently of entry receptors. The cells were infected for 24h at a MOI of 0.5, then washed and cultured for another 24h. At this stage, T cell infection rate was evaluated to at least 50% by flow cytometry. After 3 PBS-washes to remove free-cell viral particles, infected T cells were co-cultured 6h with OC (ratio 2:1). Then, Jurkat cells were eliminated by washing (once with PBS-10 mM EDTA and twice with PBS) and OC were maintained in culture in presence of M- CSF (25 ng/mL) and RANKL (100 ng/mL) for additional 5 days.

FACS analysis

Cells detached by Accutase (Gibco Technology) were incubated for 30 min on ice with the following antibodies and fixed in 4% paraformaldehyde before analysis: Alexa Fluor 488 anti- human CD16, APC anti-human CD4, PE anti-human CCR5, APC anti-human CD61 (β3 integrin) (BD Biosciences) and analyzed with Flow Jo software (TreeStar).

Immunoblotting

Cells were lysed and total proteins were separated through SDS-polyacrylamide gel electrophoresis, transferred and immunoblotted. Quantification of immunoblot intensity for several donors was performed using Image Lab (BioRad). The quantification was reported to tubulin or actin (used as a loading control). Systematic Coommassie blue staining was performed to control the charges of extracellular lysates.

Gelatin zymography

OC cell-conditioned medium was analyzed for Matrix-MetalloProtease-9 (MMP-9) activity by gelatin substrate gel electrophoresis, as in (10).

TRAP staining and IF microscopy

Cells were fixed with PFA 3.7% and stained for TRAP (Sigma-Aldrich), according to the manufacturer's protocols. IF experiments in 2D (on glass coverslips or on bone slices) were 5 performed as described (6, 11). Quantification of OC fusion index (total number of nuclei in multinucleated cells divided by total number of nuclei x 100), number of nuclei per multinucleated cells and surface index (surface covered by multinucleated cells/ total surface x 100) were assessed by using a semi-automatic quantification with a home-made ImageJ macro, allowing the study of more than 3,000 cells per condition in at least 5 independent donors. All images were prepared with Adobe Photoshop software. The number of cells with podosomes and SZ was quantified after phalloidin staining. F-actin fluorescence intensity inside podosomes and inside SZ (3 zones per SZ) was assessed using ImageJ software. Slides were visualized with a Leica DM-RB fluorescence microscope or on a IX71 confocal microscope (Olympus), and the associated softwares. Images were processed with ImageJ and Adobe Photoshop softwares.

Resorption assays

To assess bone resorption activity, mature OC were detached using Accutase treatment (Gibco Technology, ThermoFischer Scientific, Courtaboeuf, France) 10 min, at 37°C, and cultured on bovine cortical bone slices (IDS Nordic Biosciences, Paris, France) for 48h in medium supplemented with M-CSF (25 ng/mL) and RANKL (100 ng/mL). Following complete cell removal by immersion in water and scraping, bone slices were stained with toluidine blue to detect resorption pits under a light microscope (Leica DMIRB, Leica Microsystems). Circularity and the surface of bone degradation areas were quantified manually with ImageJ software. For quantification of the volume of bone degradation, we imaged the resorption pits with a confocal microscope (Olympus LEXT OLS 3100, 50X, z=50 nm). Cross-linked C-telopeptide collagen I (CTX) concentrations were measured using betaCrosslaps assay (Immunodiagnostic System laboratory) in the culture medium of OC grown on bone slices. To assess demineralization activity, OC were differentiated in

multiwell Osteologic Biocoat (Corning,VWR, Fontenay-Sous-Bois, France), fixed, stained with Von Kossa method as described previously(12) and quantified using ImageJ software.

Adhesion assays

OC were differentiated on glass coverslips in 24-well plates, incubated for 10 min at 37°C in Accutase (Gibco Technology) or in a non-enzymatic cell dissociation buffer (Gibco Technology). Cells were washed with PBS, adherent cells were fixed and nuclei were quantified after DAPI staining.

3D migration assays

3D migration assays of OC precursors were performed as described (11) and quantified at 48h. Briefly, pictures of cells were taken automatically with a 10X objective at constant intervals using the motorized stage of an inverted microscope (Leica DMIRB, Leica Microsystems, Deerfield, IL); cells were counted using ImageJ software as described previously (13). The number of cells inside the matrix (% of migration measured after 48h of migration) and the distance of migration were quantified using ImageJ.

Histological analysis of GFP-Tg, Nef-Tg and HIV-1-infected BLT mice

Femurs and tibia from adult mice were fixed in 10% buffered formalin solution (Sigma-Aldrich), decalcified in EDTA and embedded in paraffin. Longitudinal serial sections of the median portion of whole bone were stained for TRAP (Sigma-Aldrich) according to the manufacturer's protocols and counterstained with Fast green or Hematoxylin Gill 3. Stained slides were digitized using Panoramic 250 Flash digital microscope (P250 Flash, 3DHisTech, Hungary). Whole-slides were scanned in brightfield scan mode with a 40X / NA 0.8 Zeiss Plan- Apochromat dry objective, and images were acquired with a 2 megapixels 3CCD color camera (CIS Cam Ref#VCC-F52U25CL, CIS Americas Inc., USA). This objective and camera combination yield a 0.22 µm/pixel resolution in fluorescence scan mode, which corresponds, in conventional microscopy, to 56X magnification at the highest optical resolution. Panoramic Viewer software (RTM 1.15.0.53) was used for viewing, analyzing and quantification of the digital slides. Cortical bone surface and TRAP-positive cells were quantified. Animal groups were composed of 3 mice. Mononucleated and multinucleated TRAP-positive cells were counted on a minimum of 4 serial sections chosen among the most median part of 4 different tibias for each genotype. For histological analysis of GFP-Tg, sections (3 µm) were stained for TRAP activity (Sigma-Aldrich), Hemalum/Eosin, or with a rabbit antibody directed towards GFP (ab6556, Abcam, dilution 1/400, epitope retrieval: citrate buffer pH 6, boiling micro-oven, 2X10 min). For histological analysis of HIV-1-infected BLT mice, serial sections were stained for TRAP activity (Sigma-Aldrich), Hemalum/Eosin, or with a monoclonal antibody directed towards human p24 (clone Kal-1, dilution 1/10, usual epitope retrieval: Tris-EDTA buffer pH 9, 95°C, 40min). In addition to the commonly critical technical issues associated with performing IHC on calcified bone tissue, we need to overcome first, the high background due to the presence of some endogenous mouse Ig (to this end we use of a blocking step, mouse-on - mouse kit, Vector Laboratory, LTP, United Kingdom) and second, the detachment of samples from the slides due to the high temperature required for p24 antigen retrieval (adapted epitope retrieval:

Tris-EDTA buffer pH 9, 70°C, 5h) (14, 15). Animal groups were composed of 4 viremic mice and 3 non infected.

Histological analysis of human synovial tissues

Synovial tissues obtained from arthroplastic surgery of non-arthritic patients were cut into) alone or with M-CSF (50ng/mL) and RANKL (33ng/mL). Explants were infected with the macrophage-tropic HIV-1 isolate ADA for 24 hours, washed free of virus particles and with 10% FBS. Medium was replaced every 3 days with M-CSF (50 ng/mL) and RANKL (100 ng/mL) as described (16). Tissues were then fixed in 10% phosphate-buffered formalin and embedded in paraffin. Sections (3 μm) were stained for TRAP activity (Sigma-Aldrich), Hemalum/Eosin, or with mouse monoclonal antibodies directed towards p24 (clone Kal-1, Dako, Les Ulis, France) and cathepsin K (clone 3F9, ab37259, Abcam, dilution 1/600, epitope retrieval: EDTA buffer 1 mM pH8, boiling 8 min).

Statistical analysis

One-tailed paired or unpaired t-test was applied on data sets with a normal distribution, whereas one-tailed Mann-Whitney (unpaired test) or Wilcoxon (matched-pair test) tests were used otherwise (Prism). * p≤0.05; ** p≤0.01; *** p≤0.001, **** p≤0.0001.

Supplemental Figures

Supplemental Figure 1. A. Kinetics of osteoclast (OC) differentiation. Whole-cell extracts of cells maintained cultured with the osteoclastogenic cytokines during 0, 1, 6 or 10 days were blotted using antibodies against β3 integrin, TRAP, cathepsin K (Ctsk) and tubulin (load control). A representative blot out of 3 independent experiments is shown**. B-E. Characteristics of OC compared to human monocyte-derived macrophages (MDM) at day 10 of differentiation.** MDM (mauve) and OC (grey) from the same donors (n=6) were examined for fusion index by IF (B), cell surface expression of β3-integrin by cytometry (expression in MDM was used as reference), β3-integrin (intracellular) and cathepsin K (extracellular) expression level by Western blot and MMP9 activity by zymography (C). (D) Representative brightfield images of TRAP staining of MDM and OC seeded on glass at day 10. Scale bar, 30 μm. (E) Brightfield images of bone-resorption pits. MDM and OC were seeded on bovine cortical bone slides for 48h and bone resorption pits revealed with toluidine blue. Scale bar, 20 μm. **F. CCR5 cell-surface expression in OC precursors at day 0, 1, 2 and 3 of differentiation.** The kinetics of cell-surface marker expressions in monocytes maintained in M-CSF (mauve) and M-CSF/RANKL (grey) from same donors were determined by the median fluorescent intensity (MFI) (n=5 donors).

Supplemental Figure 2. A-B. HIV-1 enhances OC differentiation. (A) Representative brightfield images of TRAP staining of non-infected OC (left) or HIV-1-infected OC (right) at day 10 post-infection. Scale bar, 30 μm. (B) Quantification of the percentage of multinucleated cells (≥2 nuclei) and of the number of nuclei per multinucleated cells after confocal analysis as in Fig. 4A. **C. Maraviroc abolishes virus production.** Mature (10 days-differentiated) OC were treated with Maraviroc 30 min before infection and fusion index was determined (n= 5 donors). NI: non infected.

Supplemental Figure 3. A. CD4C regulatory elements drive the expression of GFP in OC. Two representative images of histological analyses (GFP IHC in brown and TRAP activity in purple) we performed on 2 serial sections of tibia of CD4/HIV^{GFP} tg-mice (3µm between each section). Representative histological sections (n=3 mice). Arrowheads show GFP-positive OC along bone. Scale bar, 50µm. **B. Nef Tg mice exhibit a low bone density and bone micro- damages.** Representative bone radio-density of non-Tg (left) and Nef-Tg (right) mice. Arrowheads show bone micro-damages in Nef-Tg mice. Scale bar, 0.5 cm.

Supplemental Figure 1

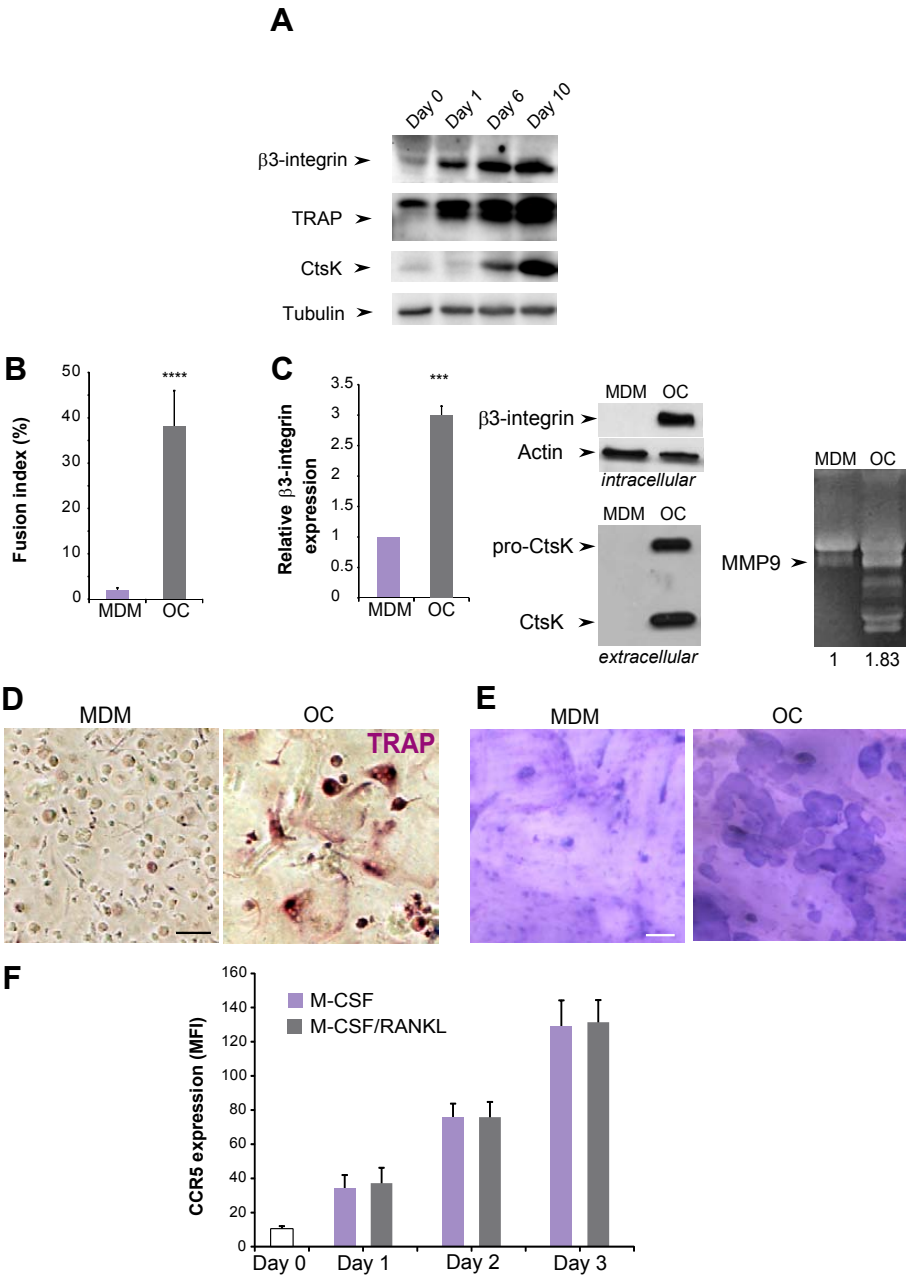

Supplemental Figure 2

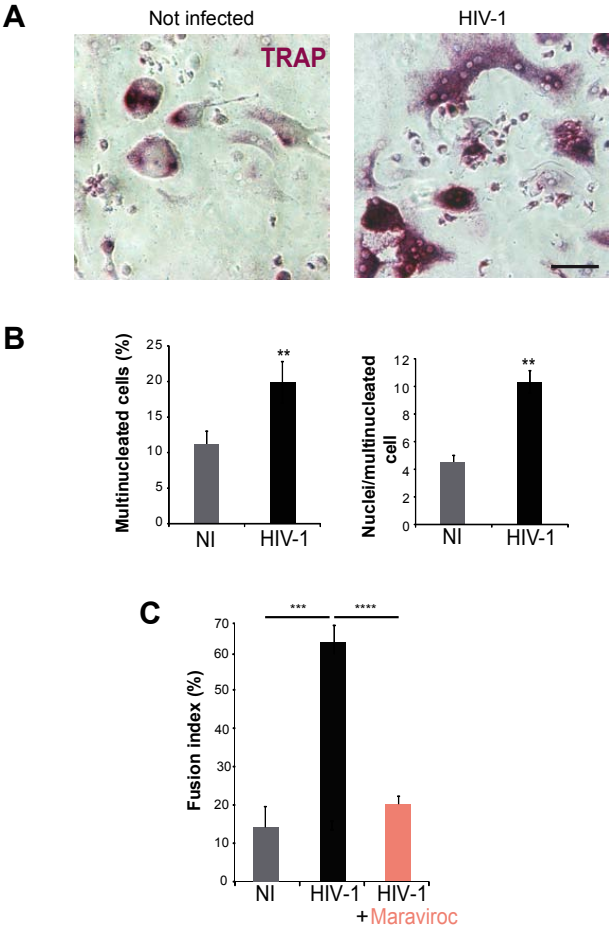

Supplemental Figure 3

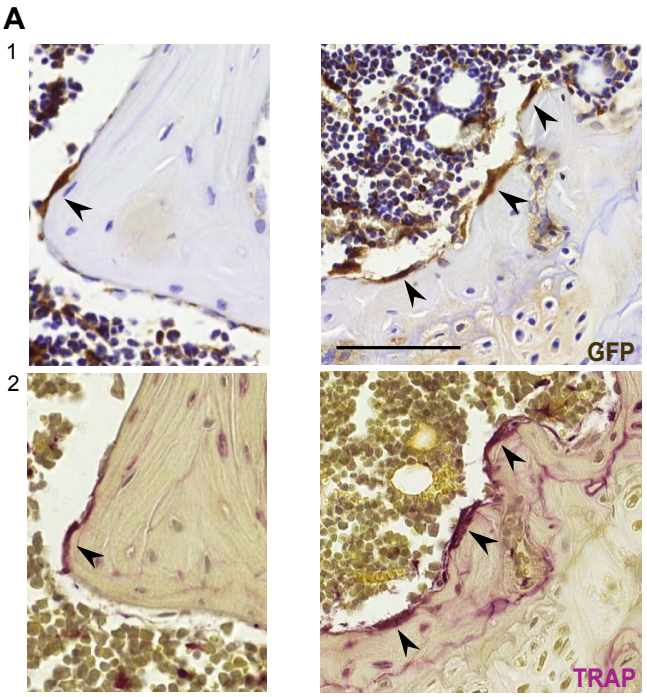

Supplemental references

1. Hanna Z*, et al.* (1998) Nef harbors a major determinant of pathogenicity for an AIDS-like disease induced by HIV-1 in transgenic mice. *Cell* 95(2):163-175.
2. Chrobak P*, et al.* (2014) HIV Nef expression favors the relative preservation of CD4+ T regulatory cells that retain some important suppressive functions. *J Immunol* 192(4):1681-1692.
3. Brainard DM*, et al.* (2009) Induction of robust cellular and humoral virus-specific adaptive immune responses in human immunodeficiency virus-infected humanized BLT mice. *Journal of virology* 83(14):7305-7321.
4. Murooka TT*, et al.* (2012) HIV-infected T cells are migratory vehicles for viral dissemination. *Nature* 490(7419):283-287.
5. Le Cabec V & Maridonneau-Parini I (1995) Complete and reversible inhibition of NADPH oxidase in human neutrophils by phenylarsine oxide at a step distal to membrane translocation of the enzyme subunits. *The Journal of biological chemistry* 270(5):2067-2073.
6. Verollet C*, et al.* (2015) HIV-1 reprograms the migration of macrophages. *Blood* 125(10):1611- 1622.
7. Vives V*, et al.* (2015) Pharmacological inhibition of Dock5 prevents osteolysis by affecting osteoclast podosome organization while preserving bone formation. *Nature communications* 6:6218.
8. Verollet C*, et al.* (2010) HIV-1 Nef triggers macrophage fusion in a p61Hck- and protease-dependent manner. *J Immunol* 184(12):7030-7039.
9. Bertin J, Jalaguier P, Barat C, Roy MA, & Tremblay MJ (2014) Exposure of human astrocytes to leukotriene C4 promotes a CX3CL1/fractalkine-mediated transmigration of HIV-1-infected CD4(+) T cells across an in vitro blood-brain barrier model. *Virology* 454-455:128-138.
10. Cougoule C*, et al.* (2010) Three-dimensional migration of macrophages requires Hck for podosome organization and extracellular matrix proteolysis. *Blood* 115(7):1444-1452.
11. Verollet C*, et al.* (2013) Hck contributes to bone homeostasis by controlling the recruitment of osteoclast precursors. *FASEB journal : official publication of the Federation of American Societies for Experimental Biology* 27(9):3608-3618.
12. Brazier H, Pawlak G, Vives V, & Blangy A (2009) The Rho GTPase Wrch1 regulates osteoclast precursor adhesion and migration. *Int J Biochem Cell Biol* 41(6):1391-1401.
13. Van Goethem E, Poincloux R, Gauffre F, Maridonneau-Parini I, & Le Cabec V (2010) Matrix Architecture Dictates Three-Dimensional Migration Modes of Human Macrophages: Differential Involvement of Proteases and Podosome-Like Structures. *J Immunol* 184(2):1049- 1061.
14. Li S*, et al.* (2015) An effective and practical immunohistochemical protocol for bone specimens characterized by hyaluronidase and pepsin predigestion combined with alkaline phosphatase- mediated chromogenic detection. *Histology and histopathology* 30(3):331-343.
15. Shi SR, Cote RJ, & Taylor CR (1998) Antigen retrieval immunohistochemistry used for routinely processed celloidin-embedded human temporal bone sections: standardization and development. *Auris, nasus, larynx* 25(4):425-443.
16. Hayder M*, et al.* (2011) A phosphorus-based dendrimer targets inflammation and osteoclastogenesis in experimental arthritis. *Science translational medicine* 3(81):81ra35.

4. Conclusions

In this article, we have demonstrated that HIV-1 infects osteoclasts *in vivo*, *ex vivo* and *in vitro*. *In vitro*, osteoclasts can be infected by cell-free viruses or by virus cell-to-cell transfer from infected T cells. This latter process was more efficient than cell-free infection. When infected, the functions of osteoclasts such migration, bone attachment and resorption were impacted, and these mechanisms are dependent of the Nef auxiliary viral protein. My contribution to this work was to investigate cell-to-cell infection of osteoclasts. As observed in macrophages, infected T cells are able to efficiently transmit HIV-1 to osteoclasts for massive and fast transfer and dissemination of the virus in this cell type.

DISCUSSION

The model of HIV-1 cell-to-cell transfer from infected T cells to macrophages described in our first article is a two-step cell-cell fusion process: first, heterologous fusion between infected T cells and macrophages, then fusion between the newly formed lymphocyte/macrophage infected fused cells and surrounding uninfected macrophages. As evidence by fluorescence microscopy, the first step is related to the establishment of contacts with infected T cells leading to the fusion of the infected T cells with macrophages. This cell fusion, dependent of the viral envelope/ CD4 receptor interaction and restricted t CCR5-tropic viral strains, is evidence by a massive and transfer of Gag+ material as well as the presence, in the cytoplasm and at the cell membrane in macrophages, of specific T cells markers (CD3, CD2 and Lck). The newly formed Lymphocyte/Macrophage fused cells are able to fuse with surrounding uninfected macrophages leading to the formation of multinucleated giant cells for efficient viral dissemination. This route of infection may be a major determinant *in vivo* for virus dissemination to macrophages.

1. Relevance of macrophages in HIV-1 infection.

Infected multinucleated giant macrophages have been observed in several different tissues in infected patients as lymphoid tissues (Dargent *et al*, 2000), hyperplastic tonsils and adenoids (Orenstein & Wahl, 1999), lungs (Costiniuk & Jenabian, 2014), colon (Lewin-Smith *et al*, 1999), paratoid glands (Vicandi *et al*, 1999) and especially in brain (Fischer-Smith *et al*, 2008; Geny *et al*, 1991; Koenig *et al*, 1986; Teo *et al*, 1997) where infected macrophages have been proposed to be the major cause of HIV-1-associated neurological disorders. While many publications demonstrated the presence of these infected multinucleated giant cells *in vivo*, the mechanism of their formation was not investigated. The infected multinucleated giant cells observed *in vitro* in our experimental systems after virus transfer from infected T cells are reminiscent of the infected multinucleated giant macrophages detected *in vivo* in lymphoid organs and the CNS of HIV-1-infected patients (Costiniuk & Jenabian, 2014; Dargent *et al*, 2000; Fischer-Smith *et al*, 2008; Geny *et al*, 1991; Koenig *et al*, 1986; Lewin-Smith *et al*, 1999; Orenstein & Wahl, 1999; Teo *et al*, 1997; Vicandi *et al*, 1999) and SIV-infected macaques (Calantone *et al*, 2014; DiNapoli *et al*, 2017; Harbison *et al*, 2014; Soulas *et al*, 2011). We can thus suggest that the mechanisms of HIV-1 cell-to-cell infection of macrophages revealed in our *in vitro* experimental work could be a model for the formation of the HIV-1 infected multinucleated giant cells observed *in vivo*.

Interestingly, Calantone et al reported that in SIV-infected macaques, viral DNA originating from infected T cells could be found in myeloid cells (including macrophages,

monocytes and various subsets of dendritic cells) and also contained rearranged TCR DNA. They hypothesize that the presence of viral and T specific DNA in myeloid cells could come from phagocytosis of infected T cells by resident macrophages (Calantone *et al*, 2014). However, we could also suggest that, in accordance with the model revealed in our work, this presence of viral RNA and DNA originating from infected T cells, as well as the T cell specific markers observed *in vivo* in SIV-infected macaques, could also come from cell-to-cell fusion of infected T cells with macrophage targets.

2. Envelope and co-receptor implication for cell-cell fusion

In our experiment system, the first fusion step between infected T cells and macrophages is dependent of the interaction of the receptor CD4 with the HIV-1 envelope glycoprotein since the presence of fusion inhibitor T20 or neutralizing antibodies targeting gp120 or CD4 during the 6h co-culture between infected T cells and macrophages srtongly inhibit cell-to-cell fusion with macrophages.

We also demonstrated that HIV-1 transfer in macrophages through cell-to-cell fusion with infected T cells is restricted to macrophage-tropic CCR5-using viral strains since no fusion was observed using CXCR4-tropic viruses and that CCR5 antagonist maraviroc inhibited cell-to-cell fusion between infected T cells and macrophages. In contrast, Baxter et al demonstrated that internalization of dying/infected T cells is related to a non-conventional mechanism independent of the viral envelope and co-receptor usage (Baxter *et al*, 2014). In this study, they showed that the NL4.3 CXCR4-tropic viral strain could be internalized by macrophages using GFP-tagged NL4.3 infected T cells as donor cells. However, if internalization was independent of the co-receptor, the infection following engulfment was restricted to CCR5-tropic viral strain. The discrepancy observed could be related to the use of undying infected T cells and untagged wild-type viruses in our experimental system.

We demonstrated that after the first fusion step, the newly formed Lymphocyte/Macrophage fused cells are able to fuse with surrounding uninfected macrophages leading to the formation of multinucleated giant cells. This second fusion step is also dependent of the viral envelope and the co receptor CCR5 since treatment of LMFC with the fusion inhibitor T20, targeting the viral transmembrane gp41 envelope glycoprotein, or CCR5 antagonist significantly decrease the number of nuclei per cell and inhibit viral dissemination in macrophages. Furthermore, electron microscopy experiment

showed that after only 6h of co-culture with infected T cells, some events of assembly and budding of virus particles were already detected at the plasma membrane of macrophages suggesting that lymphocyte/macrophage fused cells expose viral envelope at their surface. Virus assembly and budding were still observed when macrophages were treated with the reverse-transcriptase inhibitor AZT indicating that the viral buds and matured viral particles observed at cell surface of LMFCs are not coming from de novo synthesis but coming from membrane sharing with T cells after cell fusion.

Whether the viral envelope is sufficient or not to induce cell-cell fusion between infected T cells and macrophages or between LMFC and macrophages is still uncertain. To go further in the analysis of this step, we should explore with T cells expressing only the viral envelope whether the envelope is sufficient to induce fusion between T cells and macrophage targets.

Furthermore, the characteristics of the co-receptor usage by the viral envelope in this first cell-cell fusion step needs further investigations. HIV-1 strains were initially classified as syncytia-inducing (SI) or non-syncytia inducing (NSI) strains, referring to their capacity to induce syncytia *in vitro* in human CD4+ T cell-lines (Berger *et al*, 1998), and viral CXCR4-trains strains were considered as syncytia-inducing. In our experimental system, we observed cell fusion with macrophages only when T cells were initially infected with CCR5 viral strains. To investigate the role of cell-tropism and co-receptor usage in this cell fusion process we could use different macrophage-tropic viral strains using either CCR5 or CXCR4 coreceptor as well as dual tropic strains using both coreceptor.

The establishment of infection result from the transmission and subsequent propagation of a single virus termed transmitted/founder (T/F) virus. These viruses use the co receptor CCR5 for viral entry but poorly infect macrophages by cell-free infection suggesting that macrophages infection occurs at late stage after virus transmission. In fact, T/F viruses are CCR5-T tropic and efficiently infect T cells during cell-free infection. However, Baxter et al demonstrated that during cell-to-cell infection, macrophages were productively infected after internalization of T cells infected with T/F viruses (Baxter *et al*, 2014). Thus, infection of macrophages could also occur at early stage after transmission. In our system, we can hypothesize that similarly to Baxter et al, macrophages could be productively infected through cell-cell fusion with T cells infected with T/F virus and thus participate in viral dissemination in early stage of infection.

3. HIV-1 Cell-to-cell infection of macrophages through cell-cell fusion or internalization of infected T cells.

The model of cell fusion deduced from our work is a new model for HIV-1 infection of macrophages through viral cell-to-cell transfer and dissemination by a two-steps cell fusion process. The group of Quentin Sattentau (Baxter *et al*, 2014) also reported that macrophages can be infected by HIV-1 after cell-to-cell transfer from infected T cells. From this work, Baxter et al established a model in which uninfected macrophages can engulf infected T cells for HIV-1 transfer and productive infection of macrophages. The engulfment of infected dead or dying T cells was significantly higher compared to uninfected/healthy cells. This uptake of infected T cells is dependent of cytoskeleton rearrangements, but is independent of interactions between the viral envelope and CD4. In contrast, the productive infection of the macrophage targets after T cell engulfment is restricted to CCR5-tropic viral strains (see 2.4 section – Engulfment of infected T cells by macrophages). We can propose that both models participate in macrophages infection and viral dissemination even if we observed very rare event of phagocytosis in our experimental system.

3.1. Different experimental systems could lead to phagocytosis

The differences observed *in vitro* between our cell fusion model and the phagocytosis/engulfment model proposed by Baxter et al (2014) for the HIV-1 cell-to-cell transfer from infected T cells to macrophage targets could be related to the different experimental systems used to address this question (Baxter *et al*, 2014). First, infection of T cells was different in this two studies. In the Baxter et al study, infection of primary CD4+ T cells were performed using HIV-1_{BAL} or HIV-1_{IIIB} viral strains and were infected for 7 days whereas in our work, in order to prevent HIV-1-induced cell death of infected T cells, we infected primary, CD4+ T cells as well as Jurkat T cells with HIV-1_{NLAD8}, HIV-1_{YU2}, HIV-1_{ADA} or HIV-$1_{NL4.3}$ only during 36 h. We verified that at this time, more that 98% of infected T cells were not apoptotic. Because macrophages are cells specialized in phagocytosis of apoptotic cells (Aderem & Underhill, 1999), the presence of infected/dying cells could indeed favor phagocytosis of infected cells instead of cell-cell fusion observed

with non-apoptotic infected T cells.

Both studies used live-cell imaging and GFP- or mCherry-tagged HIV-1 to visualize cell-to-cell transmission between infected T cells and macrophages. Interestingly, while we did not observe phagocytosis events of infected T cells by macrophages immunofluorescence microscopy analysis on fixed cells using untagged-wildtype viruses, we could visualize some rare event of phagocytosis of infected T cells by the macrophages using GFP tagged CCR5- and CXCR4-tropic strains. Thus, the use of GFP- or mCherry tagged viruses could artificially increases the level of phagocytosis of infected T cells by macrophages compared to WT viruses independently of the co-receptor tropism.

3.2. Phagocytosis and cell-fusion are tightly regulated.

If both phagocytosis of infected T cells or cell-cell fusion led to macrophages infection depending of the experimental system used, we hypothesize that the balance between cell-cell fusion and phagocytosis could be highly regulated. Intriguingly, several molecules shown to be involved in macrophage fusion are also important in phagocytosis. Phagocytosis involves several membrane fusion events, and fusion may represent an alternative process to the engulfment of infected/dying cells. First, phosphatidylserine in the outer leaflet of the plasma membrane is one of the factors involved in the recognition of apoptotic cells by macrophages before subsequent phagocytosis. Interestingly, phosphatidylserine is also re-localized in the outer leaflet during cell-cell fusion of macrophages where it can bind to the CD36 scavenger receptor to induce fusion between macrophages (Helming & Gordon, 2009). Phosphatidylserine recognition via CD36 is thus involved in both macrophage fusion and phagocytosis of apoptotic cells (Helming *et al*, 2009). The involvement of the same cellular actors in both processes suggest that even if fusion and phagocytosis are morphologically and functionally very distinct processes, they share common features and could be tightly regulated (Figure 23).

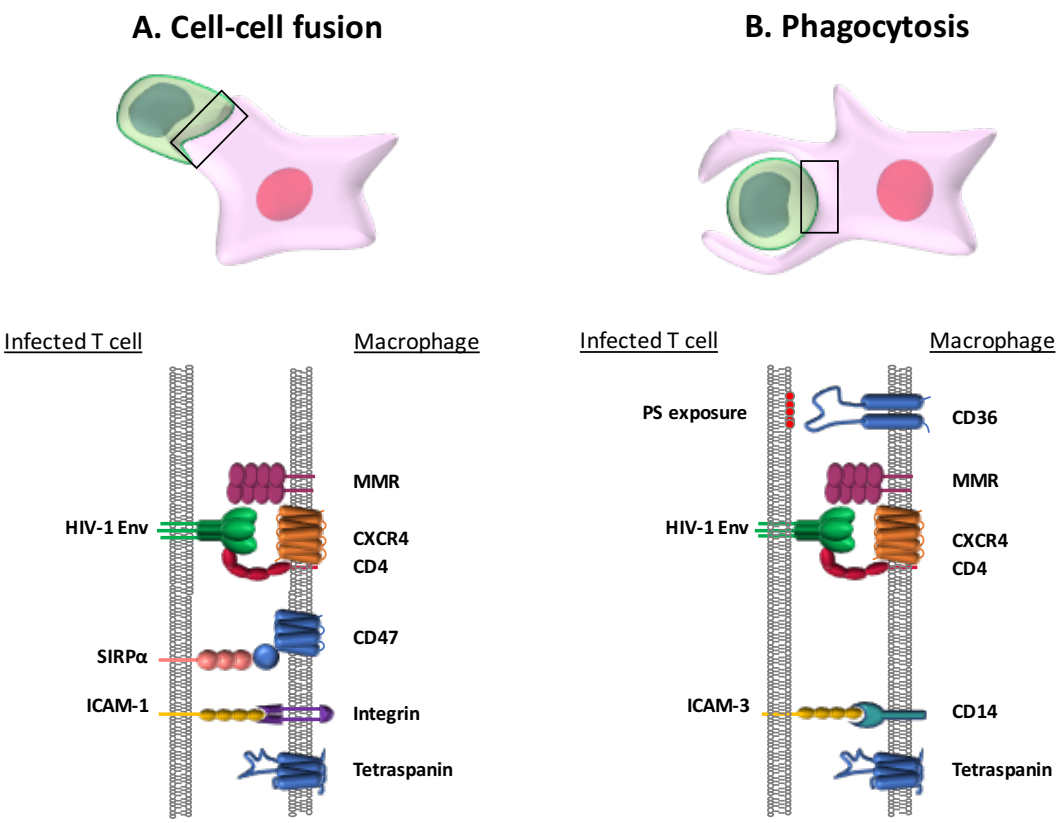

Figure 23: hypothetical regulation of cell-cell fusion and phagocytosis for HIV-1 transfer.
In A) the interaction of CD47 and SIRPα is implicated in cell-cell fusion in macrophages whereas this interaction inhibits phagocytosis. In B) The absence of CD47/SIRPα interaction and the recognition of phosphatidylserine by CD36 induce phagocytosis of the infected T cell.

Helming et al hypothesize that phagocytosis mediated by macrophages should be negatively regulated for successful fusion of macrophages (Helming & Gordon, 2009). Signal regulatory protein α (SIRP-α) and CD47 (also termed integrin-associated protein) are both members of the Ig superfamily, and CD47 can function as a ligand for SIRP-α. CD47/SIRP-α interaction is required for efficient cell-cell fusion and formation of osteoclast and multinucleated giant cells from mononucleated macrophages (Lundberg *et al*, 2007). Whereas the CD47/SIRP-α interaction induces cell-cell fusion in macrophages, this interaction can also inhibit the phagocytosis process (Oldenborg *et al*, 2001). Therefore, these proteins could be essential for both regulation of phagocytosis by macrophages and cell fusion between macrophages. In order to determine their implication in HIV-1 cell-to-cell infection of macrophages from infected T cells and then viral dissemination in macrophages, it could be interesting to block, in our experimental system where we observed cell-cell fusion, the interaction between CD47 and SIRP-α to investigate whether it will induce rather phagocytosis of infected T cells instead of cell-cell fusion (Figure 23).

3.3. Absence of HIV-1 induced cell-cell fusion between T cells.

In our experimental system, we did not observe formation of HIV-1-induced T cell syncytia between infected T cells, either using Jurkats cells or CD4+ primary T cells as virus-donor cells, suggesting that HIV-1 induced cell-cell fusion we observed is restricted to myeloid cell targets, such as macrophages and osteoclast, and inhibited between T cells.

Several proteins or cytokines have been shown to be implicated in the formation of HIV-1-induced T cell syncytia. In addition, the formation of multinucleated giant macrophages has been observed in other physiological (i.e. osteoclast formation) or physiopathological processes (i.e. tuberculosis) (Zhu & Friedland, 2006). Interleukin 4 was well described as a fusion-inducing cytokine involved in the formation of osteoclasts and multinucleated giant macrophages (Helming & Gordon, 2009). However, to our knowledge, no study reported the implication of IL-4 in the formation of T cell syncytia. Interleukin 13, is another cytokine that can also induces cell-cell fusion of macrophages for formation of multinucleated giant cells (DeFife *et al*, 1997). These cytokines (IL-4 and IL-13) promote expression of the macrophage mannose receptor (DeFife *et al*, 1997) which has been shown to induce cell-cell fusion of macrophages (McNally *et al*, 1996). The macrophage mannose receptor, which is not express in T cells, could be one important factor required for induction of cell-cell fusion in macrophages. Interestingly, it was reported that blockage of the macrophage mannose receptor decreased by 80% HIV-1 transmission from infected macrophages to T cells and viral dissemination (Nguyen & Hildreth, 2003). It would be interesting to investigate the role of this receptor in the cell fusion process we described for HIV-1 transfer and dissemination in macrophages (Figure 24).

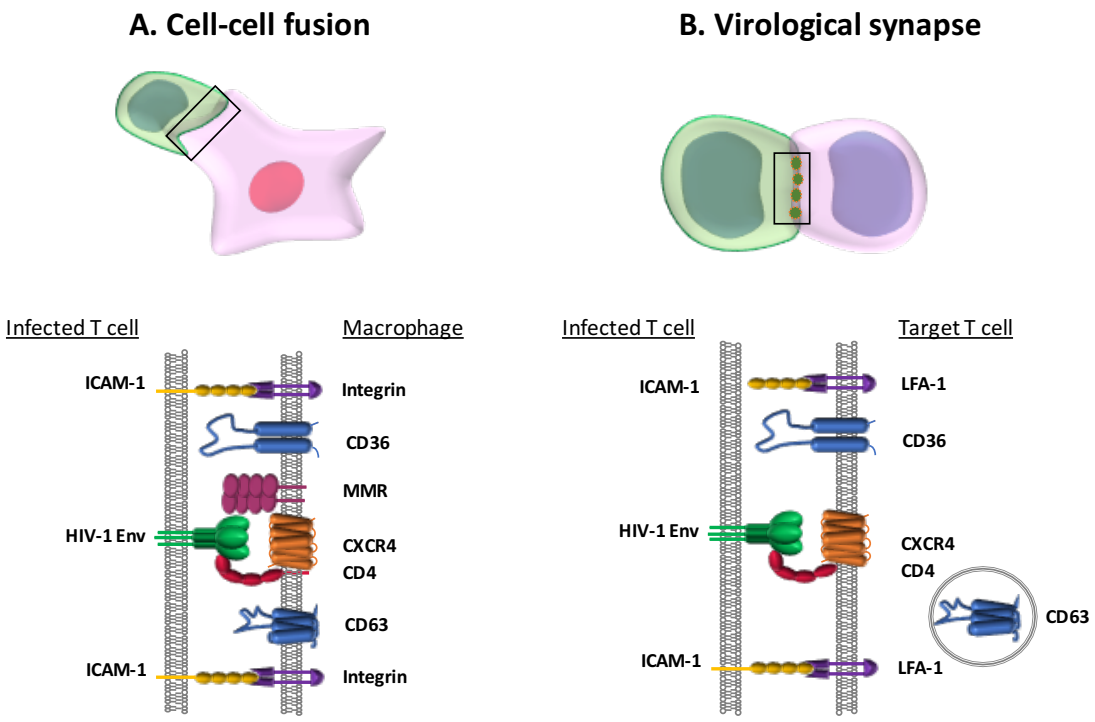

Figure 24: hypothetical regulation of cell-cell fusion for HIV-1 transfer.
In A) the presence of CD63 and the macrophage mannose receptor (MMR) is implicated in cell-cell fusion for HIV-1 transfer in macrophages. In B) The internalization of CD63 by Syntenin-1 and the absence of MMR in T cells prevent cell-cell fusion and lead to virological synapse for HIV-1 transfer between T cells.

In addition, another cellular protein, syntenin-1, a PDZ domain-containing protein, could also have different roles in cell-cell fusion processes depending on the cell type. It was reported that syntenin-1 is a diffuse cytosolic protein, but in HIV-1 infected T cells, syntenin-1 is recruited at the virological synapse formed between T cells (Gordón-Alonso *et al*, 2012). By suppressing or overexpressing this cellular protein, it has been shown that the presence of syntenin-1 at the cell-cell contact zone inhibit the formation of HIV-1-induced syncytia in T cells (Gordón-Alonso *et al*, 2012). In macrophages, there is no report regarding the potential implication of syntenin-1 in cell-cell fusion. However, syntenin-1 is present in tetraspanins-enriched microdomains and directly interacts with the CD63 tetraspanin. CD63 is constitutively internalized from the plasma membrane by endocytosis, but the interaction of Cd63 with syntenin-1 inhibits CD63 internalization leading to high expression of CD63 at the plasma membrane (Latysheva *et al*, 2006). Moreover, the CD63 tetraspanin is directly involved in cell-cell fusion of macrophages (Parthasarathy *et al*, 2009). Indeed, while other tetraspanins such as CD9 or CD81 play an inhibitory function in the formation of multinucleated giant macrophages, CD63 rather promote cell-cell fusion of macrophages (Parthasarathy *et al*, 2009). We can thus hypothesize that whereas syntenin-1 inhibits HIV-1-induced syncytia formation in T cells, it could promote cell-cell fusion in

macrophages through a CD63-dependent mechanism (Figure 24). This could provide one explanation for the different model of HIV-1 cell-to-cell transmission observed between different cell types (Figure 25).

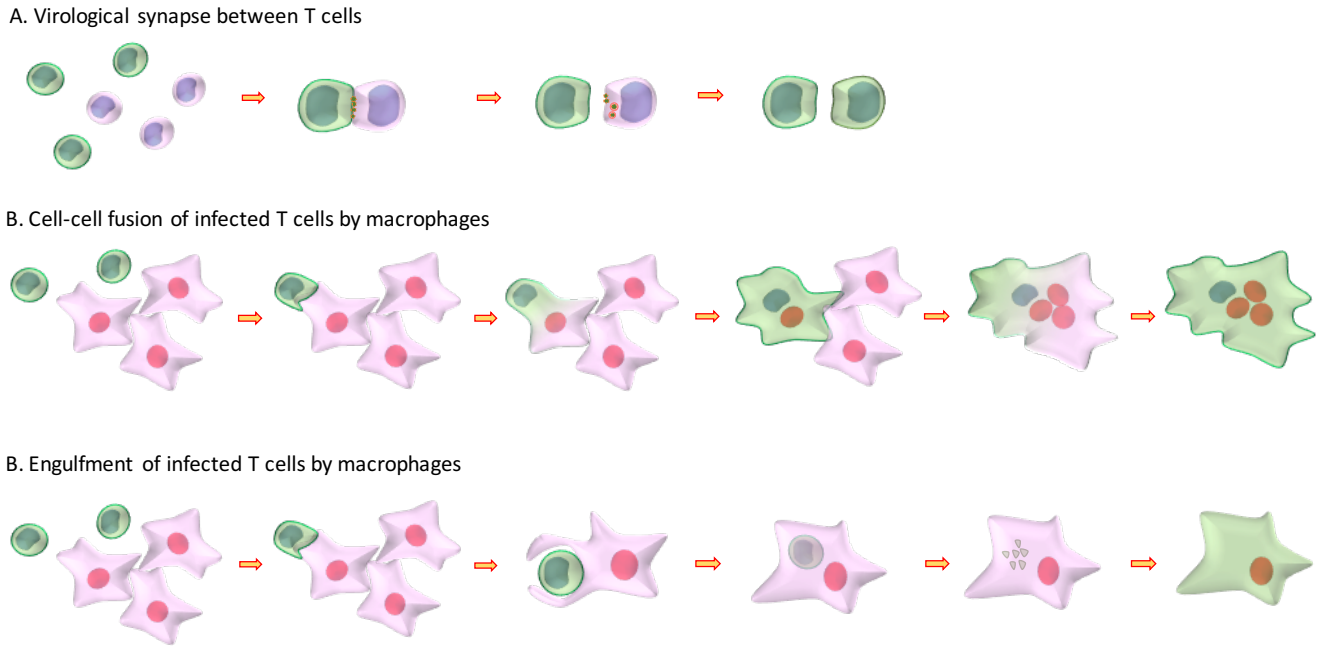

Figure 25: Summary of different model for HIV-1 cell-to-cell transfer.
In A) Infected T cells transmit HIV-1 to uninfected T cells through the virological synapse. In B) Infected T cells fuse with uninfected macrophages for HIV-1 transfer and the newly formed Lymphocyte/macrophage fused cell (LFMC) fuse with surrounding macrophages for HIV-1 dissemination. In C) Uninfected macrophage engulf infected T cells for HIV-1 infection of macrophage.

3.4. Signaling pathways involved in HIV-1 cell-cell fusion.

In the work presented here we demonstrated an efficient cell-to-cell fusion dependent of the viral envelope/CD4 receptor and restricted to CCR5-vrail strains. However, whether other factors are required for this two-step fusion or not is still unknown. Several pathways have already been described for the formation of osteoclasts or multinucleated giant macrophages in absence of HIV-1.

Macrophages fusion can be induced by different factors such as RANKL and M-CSF for osteoclast formation and various cytokines including IL4, for the formation of multinucleated giant cells. After binding to IL4-receptor present at the cell surface of macrophages, IL4 trigger different signaling pathways, including activation of gene transcription through the signal transducer and activator or transcription (STAT6). The

activation of STAT6 lead to the upregulation of the fusion mediators E-cadherin and dendritic cell-specific transmembrane protein (DC-STAMP). In addition, activation of the signaling adaptor DNAX activating protein (DAP12) lead to the recruitment and activation of the SYK and ZAP70 tyrosine kinase and mediate transcription of fusion mediators such as DC-STAMP, E-cadherin and MMP9 (Helming & Gordon, 2009). Thus, these signaling pathways leads to a fusion competent state of macrophages by promoting the expression of several proteins directly involved in the fusion process, such as E-cadherin, DC-STAMP but also CD36, and the CD9 and CD81 tetraspanins. Cell-cell contacts and fusion with infected T cells could also induce this fusion-competent state in LMFCs and upregulate expression of these proteins involved in macrophage fusion for efficient fusion between lymphocyte/Macrophages fused cells and surrounding macrophages and HIV-1 dissemination. Our preliminary data show that the fusion proteins E-cadherin, CD9 and CD81 are upregulated at the cell surface of LMFCs one day after the co-culture of macrophages with infected T cells (Additional Figure A1). Thus, other factors could be involved in the fusion between lymphocyte/Macrophages fused cells and surrounding macrophages for HIV-1 dissemination.

3.5. HIV-1 Cell-cell fusion of macrophages

The formation of multinucleated giant cells was reporter when macrophages were infected with cell-free viruses (Kadiu *et al*, 2007; Vérollet *et al*, 2010), but their formation requires much more time compared to cell-cell infection of macrophages demonstrated in this study. In our experimental system, after 6 h of co-culture between infected T cells and macrophages, more than 80% of the newly formed Lymphocyte/Macrophage fused cells contain more than 3 nuclei with an average of 5 nuclei per cell. More than 80% of Gag+ multinucleated cells contain only one nucleus coming from the first step fusion with infected T cells, indicating that other nuclei are coming from fusion with surrounding macrophages as soon as 6 h of co-culture. In contrast, in the cell-free infection model, Verollet et al reported that 8 days post-infection, 45% of infected cells contained more than 3 nuclei (Vérollet *et al*, 2010) compared to 80% after only 6h co-culture with infected T cells in our system. This high difference regarding the kinetic of formation of MGCs when they are infected by cell-free viruses or viral cell-to-cell transfer from infected T cells indicate that the cell-to-cell fusion process is largely more efficient and more rapid, since it takes place in a few hours (i.e. 6 h) compared to cell-free infection. As demonstrated by our electron microscopy experiment, assembly and budding of viral particles take place in

macrophages after only 6h co-culture with infected T cells, suggesting that lymphocyte/macrophage fused cells expose viral envelope at their surface. The expression of viral envelope at the cell surface of macrophages after only 6h, compared to several days during cell-free infection, could be determinant for this fast and massive process of fusion during cell-to-cell infection of macrophage through cell-cell fusion with infected T cells.

CONCLUSIONS

During this PhD work, we have characterized new mechanisms of cell-to-cell transfer of HIV-1 from infected CD4+ T cells for subsequent virus dissemination in macrophage targets. From these results, we propose a new model of HIV-1 cell-to-cell transmission where HIV-1 infected T cells transfer viruses to macrophages through a two-step fusion process (Figure 23).

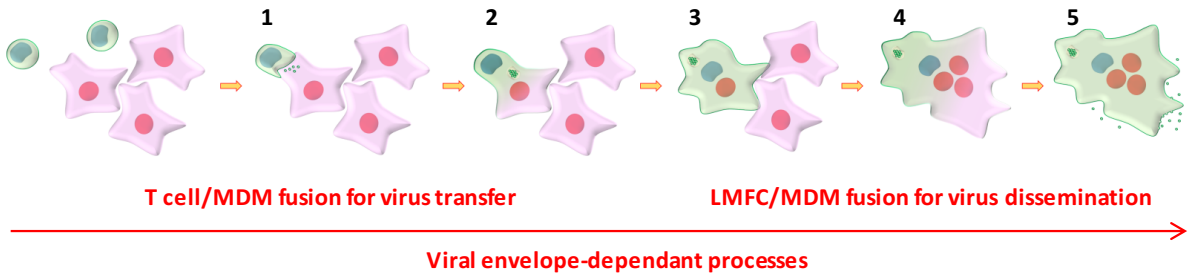

Figure 26. Model for virus cell-to-cell transfer from infected T cells to MDMs and virus spreading between MDMs.
Initial virus transfer and subsequent virus spreading are mediated by a two-step cell fusion process. In a first step, infected T cells establish contacts, initially discharge viral material to MDMs [1], and then fuse with MDM targets [2] with accumulation of viruses in intracytoplasmic compartments and virus assembly and budding at the cell surface. Gag+ newly formed LMFCs [3] then acquire the ability to fuse with surrounding uninfected MDMs leading to the formation of Gag+ multinucleated giant cells [4] that could survive for a long time to produce infectious viruses [5].

In the first article, we demonstrated that infected CD4+ T cells efficiently transmit HIV-1 to macrophages leading to productive infection and viral spreading in macrophages through a two-step cell-cell fusion process. First, infected T cells interact with macrophages and fuse together for massive and fast transfer of viral material. Then, the newly formed lymphocyte/macrophage fused cells fuse with surrounding uninfected macrophages for HIV-1 spreading. Both cell fusion steps are mediated by viral envelope-receptor interactions at the cell surface of T cells and MDMs, and are completed in less than 2 h of co-culture since Gag+ multinucleated MDMs were already detected at this time. If the fusion between infected Lymphocyte/macrophage fused cells and surrounding macrophages is dependent of the viral envelope, other mechanisms could be involved and increase the fusogenic activity in macrophages. Furthermore, auxiliary proteins which are known to be essential for viral replication in cell-free infected macrophages, could have no effect on viral replication and dissemination after cell-to-cell transfer from infected T cells. We thus would like to investigate how cell-to-cell transfer is able to overcome the requirement of the auxiliary proteins observed when macrophages are infected with cell-free viruses. This route of infection may be a major determinant *in vivo* for virus dissemination to macrophages.

In collaboration with team of Isabel Maridonneau-Parini, we also investigated the HIV-1 cell-to-cell transmission and dissemination between infected T cells and osteoclast targets. Osteoclasts can be infected by HIV-1 cell-free viruses but cell-to-cell infection by infected T cells leads to efficient productive infection of osteoclast much more efficient than cell-free viruses. We showed that similarly to macrophages, cell-to-cell transfer between infected T cells and osteoclasts is dependent of the viral envelope glycoprotein and is restricted to CCR-tropic viral strains. Cell-to-cell transfer could be determinant for HIV-1 infection of osteoclasts which is important for physiopathology of AIDS since they could contribute to bone loss frequently observed in HIV-1 infected patients.

The mechanisms of these new cell-to-cell models we proposed from our works for HIV-1 infection of macrophages and osteoclast open new avenues for further investigations. Macrophages fusion is already described for the formation of osteoclast and several proteins involved in the formation of osteoclasts and multinucleated giant cells could also be involved in HIV-1-induced cell fusion processes for viral dissemination. In addition, Verollet et al (2011) already demonstrated that macrophages infected with cell-free viruses have the ability to fuse together and that the auxiliary protein Nef is involved in this cell fusion process. Our preliminary results showed that auxiliary protein Vpr, Vif an Vpu could have no effect on cell-to-cell infection of macrophages. Thus, the implication of fusion protein and auxiliary proteins in cell-to-cell transfer needs further investigations.

In our experimental model, we did not observe cell-fusion between infected CD4+ T cells. We suggest that HIV-1 cell-cell fusion is restricted to myeloid cells and is highly regulated. It could be interesting to investigate the roles of different factors specific of T cells or macrophages such as macrophage mannose receptor specific of macrophages and involve in cell-cell fusion and whether they can restrict cell-fusion in T cells or induce it in macrophages.

Only one other study from group of Quentin Sattentau investigated HIV-1 cell-to-cell transfer between infected T cells and macrophages, and reported that macrophages can engulf infected T cells for HIV-1 productive infection. We can propose that both models of virus cell-to-cell transfer and dissemination could co-exist during the natural infection *in vivo*, since both processes are tightly regulated by common features involving common cellular effectors in macrophages. In conclusion, further investigations are needed for analysis of the implication of these effector in this regulation to determine the implication of both process in HIV-1 dissemination in macrophages.

REFERENCES

Abbas W, Tariq M, Iqbal M, Kumar A & Herbein G (2015) Eradication of HIV-1 from the macrophage reservoir: an uncertain goal? *Viruses* **7:** 1578–1598

Abela IA, Berlinger L, Schanz M, Reynell L, Günthard HF, Rusert P & Trkola A (2012) Cell-cell transmission enables HIV-1 to evade inhibition by potent CD4bs directed antibodies. *PLoS Pathog.* **8:** e1002634

Abraham L & Fackler OT (2012) HIV-1 Nef: a multifaceted modulator of T cell receptor signaling. *Cell Commun. Signal. CCS* **10:** 39

Aderem A & Underhill DM (1999) Mechanisms of phagocytosis in macrophages. *Annu. Rev. Immunol.* **17:** 593–623

Aggarwal A, Iemma TL, Shih I, Newsome TP, McAllery S, Cunningham AL & Turville SG (2012) Mobilization of HIV spread by diaphanous 2 dependent filopodia in infected dendritic cells. *PLoS Pathog.* **8:** e1002762

Agosto LM, Uchil PD & Mothes W (2015) HIV cell-to-cell transmission: effects on pathogenesis and antiretroviral therapy. *Trends Microbiol.* **23:** 289–295

Agosto LM, Zhong P, Munro J & Mothes W (2014) Highly active antiretroviral therapies are effective against HIV-1 cell-to-cell transmission. *PLoS Pathog.* **10:** e1003982

Ahr B, Robert-Hebmann V, Devaux C & Biard-Piechaczyk M (2004) Apoptosis of uninfected cells induced by HIV envelope glycoproteins. *Retrovirology* **1:** 12

Alkhatib G (2009) The biology of CCR5 and CXCR4. *Curr. Opin. HIV AIDS* **4:** 96–103

Alvarez RA, Barría MI & Chen BK (2014) Unique features of HIV-1 spread through T cell virological synapses. *PLoS Pathog.* **10:** e1004513

Ambrose Z & Aiken C (2014) HIV-1 Uncoating: Connection to Nuclear Entry and Regulation by Host Proteins. *Virology* **0:** 371–379

Aucher A, Puigdomènech I, Joly E, Clotet B, Hudrisier D & Blanco J (2010) Could CD4 Capture by T Cells Play a Role in HIV Spreading? *BioMed Res. Int.* **2010:** e907371

Aziz N, Butch AW, Quint JJ & Detels R (2014) Association of Blood Biomarkers of Bone Turnover in HIV-1 Infected Individuals Receiving Anti-Retroviral Therapy (ART). *J. AIDS Clin. Res.* **5:**

Azzam R, Kedzierska K, Leeansyah E, Chan H, Doischer D, Gorry PR, Cunningham AL, Crowe SM & Jaworowski A (2006) Impaired complement-mediated phagocytosis by HIV type-1-infected human monocyte-derived macrophages involves a cAMP-dependent mechanism. *AIDS Res. Hum. Retroviruses* **22:** 619–629

Baldauf H-M, Pan X, Erikson E, Schmidt S, Daddacha W, Burggraf M, Schenkova K, Ambiel I, Wabnitz G, Gramberg T, Panitz S, Flory E, Landau NR, Sertel S, Rutsch F, Lasitschka F, Kim B, König R, Fackler OT & Keppler OT (2012) SAMHD1 restricts HIV-1 infection in resting CD4(+) T cells. *Nat. Med.* **18:** 1682–1687

Basmaciogullari S & Pizzato M (2014) The activity of Nef on HIV-1 infectivity. *Front. Microbiol.* **5:** 232

Baxter AE, Russell RA, Duncan CJA, Moore MD, Willberg CB, Pablos JL, Finzi A,

Kaufmann DE, Ochsenbauer C, Kappes JC, Groot F & Sattentau QJ (2014) Macrophage Infection via Selective Capture of HIV-1-Infected CD4+ T Cells. *Cell Host Microbe* **16:** 711–721

Bennett AE, Narayan K, Shi D, Hartnell LM, Gousset K, He H, Lowekamp BC, Yoo TS, Bliss D, Freed EO & Subramaniam S (2009) Ion-abrasion scanning electron microscopy reveals surface-connected tubular conduits in HIV-infected macrophages. *PLoS Pathog.* **5:** e1000591

Berger EA, Doms RW, Fenyö EM, Korber BT, Littman DR, Moore JP, Sattentau QJ, Schuitemaker H, Sodroski J & Weiss RA (1998) A new classification for HIV-1. *Nature* **391:** 240

Biggs BA, Hewish M, Kent S, Hayes K & Crowe SM (1995) HIV-1 infection of human macrophages impairs phagocytosis and killing of Toxoplasma gondii. *J. Immunol. Baltim. Md 1950* **154:** 6132–6139

Blanchard N, Di Bartolo V & Hivroz C (2002) In the immune synapse, ZAP-70 controls T cell polarization and recruitment of signaling proteins but not formation of the synaptic pattern. *Immunity* **17:** 389–399

Blanco J, Bosch B, Fernández-Figueras MT, Barretina J, Clotet B & Esté JA (2004) High Level of Coreceptor-independent HIV Transfer Induced by Contacts between Primary CD4 T Cells. *J. Biol. Chem.* **279:** 51305–51314

Bosch B, Grigorov B, Senserrich J, Clotet B, Darlix J-L, Muriaux D & Este JA (2008) A clathrin-dynamin-dependent endocytic pathway for the uptake of HIV-1 by direct T cell-T cell transmission. *Antiviral Res.* **80:** 185–193

Bouchet J, Del Río-Iñiguez I, Lasserre R, Agüera-Gonzalez S, Cuche C, Danckaert A, McCaffrey MW, Di Bartolo V & Alcover A (2016) Rac1-Rab11-FIP3 regulatory hub coordinates vesicle traffic with actin remodeling and T-cell activation. *EMBO J.*

Brew BJ, Corbeil J, Pemberton L, Evans L, Saito K, Penny R, Cooper DA & Heyes MP (1995) Quinolinic acid production is related to macrophage tropic isolates of HIV-1. *J. Neurovirol.* **1:** 369–374

Bruera D, Luna N, David DO, Bergoglio LM & Zamudio J (2003) Decreased bone mineral density in HIV-infected patients is independent of antiretroviral therapy. *AIDS Lond. Engl.* **17:** 1917–1923

Burdo TH, Lackner A & Williams KC (2013) Monocyte/macrophages and their role in HIV neuropathogenesis. *Immunol. Rev.* **254:** 102–113

Calantone N, Wu F, Klase Z, Deleage C, Perkins M, Matsuda K, Thompson EA, Ortiz AM, Vinton CL, Ourmanov I, Loré K, Douek DC, Estes JD, Hirsch VM & Brenchley JM (2014) Tissue myeloid cells in SIV-infected primates acquire viral DNA through phagocytosis of infected T cells. *Immunity* **41:** 493–502

Carr JM, Hocking H, Li P & Burrell CJ (1999) Rapid and efficient cell-to-cell transmission of human immunodeficiency virus infection from monocyte-derived macrophages to peripheral blood lymphocytes. *Virology* **265:** 319–329

Carter CA & Ehrlich LS (2008) Cell biology of HIV-1 infection of macrophages. *Annu. Rev. Microbiol.* **62:** 425–443

Casartelli N, Sourisseau M, Feldmann J, Guivel-Benhassine F, Mallet A, Marcelin A-G, Guatelli J & Schwartz O (2010) Tetherin restricts productive HIV-1 cell-to-cell transmission. *PLoS Pathog.* **6:** e1000955

Caumartin J, LeMaoult J & Carosella ED (2006) Intercellular exchanges of membrane patches (trogocytosis) highlight the next level of immune plasticity. *Transpl. Immunol.* **17:** 20–22

Chen P, Hübner W, Spinelli MA & Chen BK (2007) Predominant mode of human immunodeficiency virus transfer between T cells is mediated by sustained Env-dependent neutralization-resistant virological synapses. *J. Virol.* **81:** 12582–12595

Chen R, Rouzic EL, Kearney JA, Mansky LM & Benichou S (2004) Vpr-mediated Incorporation of UNG2 into HIV-1 Particles Is Required to Modulate the Virus Mutation Rate and for Replication in Macrophages. *J. Biol. Chem.* **279:** 28419–28425

Chertova E, Bess JW, Crise BJ, Sowder II RC, Schaden TM, Hilburn JM, Hoxie JA, Benveniste RE, Lifson JD, Henderson LE & Arthur LO (2002) Envelope glycoprotein incorporation, not shedding of surface envelope glycoprotein (gp120/SU), Is the primary determinant of SU content of purified human immunodeficiency virus type 1 and simian immunodeficiency virus. *J. Virol.* **76:** 5315–5325

Chinnery HR, Pearlman E & McMenamin PG (2008) Cutting edge: Membrane nanotubes in vivo: a feature of MHC class II+ cells in the mouse cornea. *J. Immunol. Baltim. Md 1950* **180:** 5779–5783

Chowdhury IH, Chao W, Potash MJ, Sova P, Gendelman HE & Volsky DJ (1996) vif-negative human immunodeficiency virus type 1 persistently replicates in primary macrophages, producing attenuated progeny virus. *J. Virol.* **70:** 5336–5345

Chu H, Wang J-J, Qi M, Yoon J-J, Chen X, Wen X, Hammonds J, Ding L & Spearman P (2012) Tetherin/BST-2 is essential for the formation of the intracellular virus-containing compartment in HIV-infected macrophages. *Cell Host Microbe* **12:** 360–372

Chutiwitoonchai N, Hiyoshi M, Hiyoshi-Yoshidomi Y, Hashimoto M, Tokunaga K & Suzu S (2013) Characteristics of IFITM, the newly identified IFN-inducible anti-HIV-1 family proteins. *Microbes Infect.* **15:** 280–290

Connor RI, Sheridan KE, Ceradini D, Choe S & Landau NR (1997) Change in coreceptor use correlates with disease progression in HIV-1--infected individuals. *J. Exp. Med.* **185:** 621–628

Cosson P (1996) Direct interaction between the envelope and matrix proteins of HIV-1. *EMBO J.* **15:** 5783–5788

Costiniuk CT & Jenabian M-A (2014) The lungs as anatomical reservoirs of HIV infection. *Rev. Med. Virol.* **24:** 35–54

Crowe SM, Vardaxis NJ, Kent SJ, Maerz AL, Hewish MJ, McGrath MS & Mills J (1994) HIV infection of monocyte-derived macrophages in vitro reduces phagocytosis of Candida albicans. *J. Leukoc. Biol.* **56:** 318–327

Dale BM, Alvarez RA & Chen BK (2013) Mechanisms of enhanced HIV spread through T-cell virological synapses. *Immunol. Rev.* **251:** 113–124

Dale BM, McNerney GP, Thompson DL, Hubner W, de los Reyes K, Chuang FYS, Huser T & Chen BK (2011) Cell-to-Cell Transfer of HIV-1 via Virological Synapses Leads to Endosomal Virion Maturation that Activates Viral Membrane Fusion. *Cell Host Microbe* **10:** 551–562

Dargent JL, Lespagnard L, Kornreich A, Hermans P, Clumeck N & Verhest A (2000) HIV-associated multinucleated giant cells in lymphoid tissue of the Waldeyer's ring: a detailed study. *Mod. Pathol. Off. J. U. S. Can. Acad. Pathol. Inc* **13:** 1293–1299

Debaisieux S, Lachambre S, Gross A, Mettling C, Besteiro S, Yezid H, Henaff D, Chopard C, Mesnard J-M & Beaumelle B (2015) HIV-1 Tat inhibits phagocytosis by preventing the recruitment of Cdc42 to the phagocytic cup. *Nat. Commun.* **6:** 6211

DeFife KM, Jenney CR, McNally AK, Colton E & Anderson JM (1997) Interleukin-13 induces human monocyte/macrophage fusion and macrophage mannose receptor expression. *J. Immunol. Baltim. Md 1950* **158:** 3385–3390

Deneka M, Pelchen-Matthews A, Byland R, Ruiz-Mateos E & Marsh M (2007) In macrophages, HIV-1 assembles into an intracellular plasma membrane domain containing the tetraspanins CD81, CD9, and CD53. *J. Cell Biol.* **177:** 329–341

Dimitrov DS, Willey RL, Sato H, Chang LJ, Blumenthal R & Martin MA (1993) Quantitation of human immunodeficiency virus type 1 infection kinetics. *J. Virol.* **67:** 2182–2190

DiNapoli SR, Ortiz AM, Wu F, Matsuda K, Twigg HL, Hirsch VM, Knox K & Brenchley JM (2017) Tissue-resident macrophages can contain replication-competent virus in antiretroviral-naive, SIV-infected Asian macaques. *JCI Insight* **2:** e91214

Dong C, Janas AM, Wang J-H, Olson WJ & Wu L (2007) Characterization of human immunodeficiency virus type 1 replication in immature and mature dendritic cells reveals dissociable cis- and trans-infection. *J. Virol.* **81:** 11352–11362

Duncan CJA, Williams JP, Schiffner T, Gärtner K, Ochsenbauer C, Kappes J, Russell RA, Frater J & Sattentau QJ (2014) High-Multiplicity HIV-1 Infection and Neutralizing Antibody Evasion Mediated by the Macrophage-T Cell Virological Synapse. *J. Virol.* **88:** 2025–2034

Durham ND, Yewdall AW, Chen P, Lee R, Zony C, Robinson JE & Chen BK (2012) Neutralization Resistance of Virological Synapse-Mediated HIV-1 Infection Is Regulated by the gp41 Cytoplasmic Tail. *J. Virol.* **86:** 7484–7495

Dutartre H, Clavière M, Journo C & Mahieux R (2016) Cell-Free versus Cell-to-Cell Infection by Human Immunodeficiency Virus Type 1 and Human T-Lymphotropic Virus Type 1: Exploring the Link among Viral Source, Viral Trafficking, and Viral Replication. *J. Virol.* **90:** 7607–7617

Eugenin EA, Gaskill PJ & Berman JW (2009) Tunneling nanotubes (TNT) are induced by HIV-infection of macrophages. *Cell. Immunol.* **254:** 142–148

Fassati A (2006) HIV infection of non-dividing cells: a divisive problem. *Retrovirology* **3:** 74

Felts RL, Narayan K, Estes JD, Shi D, Trubey CM, Fu J, Hartnell LM, Ruthel GT, Schneider DK, Nagashima K, Bess JW, Bavari S, Lowekamp BC, Bliss D, Lifson JD & Subramaniam S (2010) 3D visualization of HIV transfer at the virological synapse between dendritic cells and T cells. *Proc. Natl. Acad. Sci.* **107:** 13336–13341

Fischer-Smith T, Bell C, Croul S, Lewis M & Rappaport J (2008) Monocyte/macrophage trafficking in acquired immunodeficiency syndrome encephalitis: Lessons from human and nonhuman primate studies. *J. Neurovirol.* **14:** 318–326

Frank I, Stoiber H, Godar S, Stockinger H, Steindl F, Katinger HW & Dierich MP (1996) Acquisition of host cell-surface-derived molecules by HIV-1. *AIDS Lond. Engl.* **10:** 1611–1620

Frankel SS, Wenig BM, Burke AP, Mannan P, Thompson LD, Abbondanzo SL, Nelson AM, Pope M & Steinman RM (1996) Replication of HIV-1 in dendritic cell-derived syncytia at the mucosal surface of the adenoid. *Science* **272:** 115–117

Freed EO (2001) HIV-1 replication. *Somat. Cell Mol. Genet.* **26:** 13–33

Freed EO, Englund G & Martin MA (1995) Role of the basic domain of human immunodeficiency virus type 1 matrix in macrophage infection. *J. Virol.* **69:** 3949–3954

Freed EO & Martin MA (1995) The Role of Human Immunodeficiency Virus Type 1 Envelope Glycoproteins in Virus Infection. *J. Biol. Chem.* **270:** 23883–23886

Ganser-Pornillos BK, Yeager M & Sundquist WI (2008) The structural biology of HIV assembly. *Curr. Opin. Struct. Biol.* **18:** 203–217

Geijtenbeek TBH, Kwon DS, Torensma R, van Vliet SJ, van Duijnhoven GCF, Middel J, Cornelissen ILMHA, Nottet HSLM, KewalRamani VN, Littman DR, Figdor CG & van Kooyk Y (2000) DC-SIGN, a Dendritic Cell–Specific HIV-1-Binding Protein that Enhances trans-Infection of T Cells. *Cell* **100:** 587–597

Gendelman HE, Genis P, Jett M, Zhai QH & Nottet HS (1994) An experimental model system for HIV-1-induced brain injury. *Adv. Neuroimmunol.* **4:** 189–193

Geny C, Gherardi R, Boudes P, Lionnet F, Cesaro P & Gray F (1991) Multifocal multinucleated giant cell myelitis in an AIDS patient. *Neuropathol. Appl. Neurobiol.* **17:** 157–162

Gibellini D, Borderi M, De Crignis E, Cicola R, Vescini F, Caudarella R, Chiodo F & Re MC (2007) RANKL/OPG/TRAIL plasma levels and bone mass loss evaluation in antiretroviral naive HIV-1-positive men. *J. Med. Virol.* **79:** 1446–1454

Giese S & Marsh M (2014) Tetherin Can Restrict Cell-Free and Cell-Cell Transmission of HIV from Primary Macrophages to T Cells. *PLoS Pathog.* **10:** e1004189

Gilbert PB, McKeague IW, Eisen G, Mullins C, Guéye-NDiaye A, Mboup S & Kanki PJ (2003) Comparison of HIV-1 and HIV-2 infectivity from a prospective cohort study in Senegal. *Stat. Med.* **22:** 573–593

Giulian D, Vaca K & Noonan CA (1990) Secretion of neurotoxins by mononuclear phagocytes infected with HIV-1. *Science* **250:** 1593–1596

Gohda J, Ma Y, Huang Y, Zhang Y, Gu L, Han Y, Li T, Gao B, Gao GF, Inoue J-I, Iwamoto A & Ishida T (2015) HIV-1 replicates in human osteoclasts and enhances their differentiation in vitro. *Retrovirology* **12:** 12

Gordon S & Martinez-Pomares L (2017) Physiological roles of macrophages. *Pflugers Arch.* **469:** 365–374

Gordón-Alonso M, Rocha-Perugini V, Álvarez S, Moreno-Gonzalo O, Ursa A, López-Martín S, Izquierdo-Useros N, Martínez-Picado J, Muñoz-Fernández MÁ, Yáñez-Mó M & Sánchez-Madrid F (2012) The PDZ-adaptor protein syntenin-1 regulates HIV-1 entry. *Mol. Biol. Cell* **23:** 2253–2263

Gorry PR, Francella N, Lewin SR & Collman RG (2014) HIV-1 envelope–receptor interactions required for macrophage infection and implications for current HIV-1 cure strategies. *J. Leukoc. Biol.* **95:** 71–81

Gousset K, Ablan SD, Coren LV, Ono A, Soheilian F, Nagashima K, Ott DE & Freed EO (2008) Real-time visualization of HIV-1 GAG trafficking in infected macrophages. *PLoS Pathog.* **4:** e1000015

Gras G & Kaul M (2010) Molecular mechanisms of neuroinvasion by monocytes-macrophages in HIV-1 infection. *Retrovirology* **7:** 30

Grijsen ML, Vrouenraets SME, Steingrover R, Lips P, Reiss P, Wit FWNM & Prins JM (2010) High prevalence of reduced bone mineral density in primary HIV-1-infected men. *AIDS Lond. Engl.* **24:** 2233–2238

Groot F, Welsch S & Sattentau QJ (2008) Efficient HIV-1 transmission from macrophages to T cells across transient virological synapses. *Blood* **111:** 4660–4663

Guenzel CA, Herate C & Benichou S (2014) HIV-1 Vpr—a still 'enigmatic multitasker'. *Virology* **5:** 127

Haldar M & Murphy KM (2014) Origin, development, and homeostasis of tissue-resident macrophages. *Immunol. Rev.* **262:** 25–35

Harbison C, Zhuang K, Gettie A, Blanchard J, Knight H, Didier P, Cheng-Mayer C & Westmoreland S (2014) Giant cell encephalitis and microglial infection with mucosally transmitted simian-human immunodeficiency virus SHIVSF162P3N in rhesus macaques. *J. Neurovirol.* **20:** 62–72

Hashimoto M, Bhuyan F, Hiyoshi M, Noyori O, Nasser H, Miyazaki M, Saito T, Kondoh Y, Osada H, Kimura S, Hase K, Ohno H & Suzu S (2016) Potential Role of the Formation of Tunneling Nanotubes in HIV-1 Spread in Macrophages. *J. Immunol.* **196:** 1832–1841

Helming L & Gordon S (2009) Molecular mediators of macrophage fusion. *Trends Cell Biol.* **19:** 514–522

Helming L, Tomasello E, Kyriakides TR, Martinez FO, Takai T, Gordon S & Vivier E (2008) Essential role of DAP12 signaling in macrophage programming into a fusion-competent state. *Sci. Signal.* **1:** ra11

Helming L, Winter J & Gordon S (2009) The scavenger receptor CD36 plays a role in cytokine-induced macrophage fusion. *J. Cell Sci.* **122:** 453–459

Herate C, Vigne C, Guenzel CA, Lambele M, Rouyez M-C & Benichou S (2016) Uracil DNA glycosylase interacts with the p32 subunit of the replication protein A complex to modulate HIV-1 reverse transcription for optimal virus dissemination. *Retrovirology* **13:** 26

Hildreth JE & Orentas RJ (1989) Involvement of a leukocyte adhesion receptor (LFA-1) in HIV-induced syncytium formation. *Science* **244:** 1075–1078

Honeycutt JB, Thayer WO, Baker CE, Ribeiro RM, Lada SM, Cao Y, Cleary RA, Hudgens MG, Richman DD & Garcia JV (2017) HIV persistence in tissue macrophages of humanized myeloid-only mice during antiretroviral therapy. *Nat. Med.*

Honeycutt JB, Wahl A, Baker C, Spagnuolo RA, Foster J, Zakharova O, Wietgrefe S, Caro-Vegas C, Madden V, Sharpe G, Haase AT, Eron JJ & Garcia JV (2016) Macrophages sustain HIV replication in vivo independently of T cells. *J. Clin. Invest.* **126:** 1353

Hrecka K, Hao C, Gierszewska M, Swanson SK, Kesik-Brodacka M, Srivastava S, Florens L, Washburn MP & Skowronski J (2011) Vpx relieves inhibition of HIV-1 infection of macrophages mediated by the SAMHD1 protein. *Nature* **474:** 658–661

Hübner W, McNerney GP, Chen P, Dale BM, Gordon RE, Chuang FYS, Li X-D, Asmuth DM, Huser T & Chen BK (2009) Quantitative 3D video microscopy of HIV transfer across T cell virological synapses. *Science* **323:** 1743–1747

Huppa JB & Davis MM (2003) T-cell-antigen recognition and the immunological synapse. *Nat. Rev. Immunol.* **3:** 973–983

Igakura T, Stinchcombe JC, Goon PKC, Taylor GP, Weber JN, Griffiths GM, Tanaka Y, Osame M & Bangham CRM (2003) Spread of HTLV-I between lymphocytes by virus-induced polarization of the cytoskeleton. *Science* **299:** 1713–1716

Iwami S, Takeuchi JS, Nakaoka S, Mammano F, Clavel F, Inaba H, Kobayashi T, Misawa N, Aihara K, Koyanagi Y & Sato K (2015) Cell-to-cell infection by HIV contributes over half of virus infection. *eLife* **4:**

Izquierdo-Useros N, Lorizate M, Contreras F-X, Rodriguez-Plata MT, Glass B, Erkizia I, Prado JG, Casas J, Fabriàs G, Kräusslich H-G & Martinez-Picado J (2012) Sialyllactose in viral membrane gangliosides is a novel molecular recognition pattern for mature dendritic cell capture of HIV-1. *PLoS Biol.* **10:** e1001315

Jacque J-M & Stevenson M (2006) The inner-nuclear-envelope protein emerin regulates HIV-1 infectivity. *Nature* **441:** 641–645

Jambo KC, Banda DH, Kankwatira AM, Sukumar N, Allain TJ, Heyderman RS, Russell DG & Mwandumba HC (2014) Small alveolar macrophages are infected preferentially by HIV and exhibit impaired phagocytic function. *Mucosal Immunol.* **7:** 1116–1126

Janeway CA (1992) The immune system evolved to discriminate infectious nonself from noninfectious self. *Immunol. Today* **13:** 11–16

Jolly C, Kashefi K, Hollinshead M & Sattentau QJ (2004) HIV-1 Cell to Cell Transfer across an Env-induced, Actin-dependent Synapse. *J. Exp. Med.* **199:** 283–293

Jolly C, Mitar I & Sattentau QJ (2007a) Requirement for an Intact T-Cell Actin and Tubulin Cytoskeleton for Efficient Assembly and Spread of Human Immunodeficiency Virus Type 1. *J. Virol.* **81:** 5547–5560

Jolly C, Mitar I & Sattentau QJ (2007b) Adhesion Molecule Interactions Facilitate Human Immunodeficiency Virus Type 1-Induced Virological Synapse Formation between T Cells. *J. Virol.* **81:** 13916–13921

Jolly C & Sattentau QJ (2004) Retroviral Spread by Induction of Virological Synapses. *Traffic* **5:** 643–650

Jolly C & Sattentau QJ (2005) Human Immunodeficiency Virus Type 1 Virological Synapse Formation in T Cells Requires Lipid Raft Integrity. *J. Virol.* **79:** 12088–12094

Jolly C, Welsch S, Michor S & Sattentau QJ (2011) The regulated secretory pathway in CD4(+) T cells contributes to human immunodeficiency virus type-1 cell-to-cell spread at the virological synapse. *PLoS Pathog.* **7:** e1002226

Joly E & Hudrisier D (2003) What is trogocytosis and what is its purpose? *Nat. Immunol.* **4:** 815

Jónsson SR & Andrésdóttir V (2013) Host restriction of lentiviruses and viral countermeasures: APOBEC3 and Vif. *Viruses* **5:** 1934–1947

Jouve M, Sol-Foulon N, Watson S, Schwartz O & Benaroch P (2007) HIV-1 buds and accumulates in 'nonacidic' endosomes of macrophages. *Cell Host Microbe* **2:** 85–95

Kadiu I, Ricardo-Dukelow M, Ciborowski P & Gendelman HE (2007) Cytoskeletal Protein Transformation in HIV-1-Infected Macrophage Giant Cells. *J. Immunol.* **178:** 6404–6415

Kaul M, Garden GA & Lipton SA (2001) Pathways to neuronal injury and apoptosis in HIV-associated dementia. *Nature* **410:** 988–994

Kedzierska K, Ellery P, Mak J, Lewin SR, Crowe SM & Jaworowski A (2002) HIV-1 Down-Modulates γ Signaling Chain of FcγR in Human Macrophages: A Possible Mechanism for Inhibition of Phagocytosis. *J. Immunol.* **168:** 2895–2903

Kimura S, Hase K & Ohno H (2013) The molecular basis of induction and formation of tunneling nanotubes. *Cell Tissue Res.* **352:** 67–76

Klatzmann D, Champagne E, Chamaret S, Gruest J, Guetard D, Hercend T, Gluckman JC &

Montagnier L (1984) T-lymphocyte T4 molecule behaves as the receptor for human retrovirus LAV. *Nature* **312:** 767–768

Koenig S, Gendelman HE, Orenstein JM, Dal Canto MC, Pezeshkpour GH, Yungbluth M, Janotta F, Aksamit A, Martin MA & Fauci AS (1986) Detection of AIDS virus in macrophages in brain tissue from AIDS patients with encephalopathy. *Science* **233:** 1089–1093

Koppensteiner H, Banning C, Schneider C, Hohenberg H & Schindler M (2012) Macrophage Internal HIV-1 Is Protected from Neutralizing Antibodies. *J. Virol.* **86:** 2826–2836

Kuhl BD, Sloan RD, Donahue DA, Bar-Magen T, Liang C & Wainberg MA (2010) Tetherin restricts direct cell-to-cell infection of HIV-1. *Retrovirology* **7:** 115

Kumar A & Herbein G (2014) The macrophage: a therapeutic target in HIV-1 infection. *Mol. Cell. Ther.* **2:** 10

Laguette N, Sobhian B, Casartelli N, Ringeard M, Chable-Bessia C, Ségéral E, Yatim A, Emiliani S, Schwartz O & Benkirane M (2011) SAMHD1 is the dendritic- and myeloid-cell-specific HIV-1 restriction factor counteracted by Vpx. *Nature* **474:** 654–657

Lahouassa H, Daddacha W, Hofmann H, Ayinde D, Logue EC, Dragin L, Bloch N, Maudet C, Bertrand M, Gramberg T, Pancino G, Priet S, Canard B, Laguette N, Benkirane M, Transy C, Landau NR, Kim B & Margottin-Goguet F (2012) SAMHD1 restricts the replication of human immunodeficiency virus type 1 by depleting the intracellular pool of deoxynucleoside triphosphates. *Nat. Immunol.* **13:** 223–228

Latysheva N, Muratov G, Rajesh S, Padgett M, Hotchin NA, Overduin M & Berditchevski F (2006) Syntenin-1 is a new component of tetraspanin-enriched microdomains: mechanisms and consequences of the interaction of syntenin-1 with CD63. *Mol. Cell. Biol.* **26:** 7707–7718

Law KM, Komarova NL, Yewdall AW, Lee RK, Herrera OL, Wodarz D & Chen BK (2016) In Vivo HIV-1 Cell-to-Cell Transmission Promotes Multicopy Micro-compartmentalized Infection. *Cell Rep.* **15:** 2771–2783

Leeansyah E, Wines BD, Crowe SM & Jaworowski A (2007) The mechanism underlying defective Fcgamma receptor-mediated phagocytosis by HIV-1-infected human monocyte-derived macrophages. *J. Immunol. Baltim. Md 1950* **178:** 1096–1104

Lehmann MJ, Sherer NM, Marks CB, Pypaert M & Mothes W (2005) Actin- and myosin-driven movement of viruses along filopodia precedes their entry into cells. *J. Cell Biol.* **170:** 317–325

Lewin-Smith M, Wahl SM & Orenstein JM (1999) Human immunodeficiency virus-rich multinucleated giant cells in the colon: a case report with transmission electron microscopy, immunohistochemistry, and in situ hybridization. *Mod. Pathol. Off. J. U. S. Can. Acad. Pathol. Inc* **12:** 75–81

Li L, Li HS, Pauza CD, Bukrinsky M & Zhao RY (2005) Roles of HIV-1 auxiliary proteins in viral pathogenesis and host-pathogen interactions. *Cell Res.* **15:** 923–934

Lichterfeld M, Mou D, Cung TDH, Williams KL, Waring MT, Huang J, Pereyra F, Trocha A, Freeman GJ, Rosenberg ES, Walker BD & Yu XG (2008) Telomerase activity of HIV-1-specific CD8+ T cells: constitutive up-regulation in controllers and selective increase by blockade of PD ligand 1 in progressors. *Blood* **112:** 3679–3687

Llano M, Saenz DT, Meehan A, Wongthida P, Peretz M, Walker WH, Teo W & Poeschla EM (2006) An essential role for LEDGF/p75 in HIV integration. *Science* **314:** 461–464

Llewellyn GN, Hogue IB, Grover JR & Ono A (2010) Nucleocapsid promotes localization of HIV-1 gag to uropods that participate in virological synapses between T cells. *PLoS Pathog.* **6:** e1001167

Lou E, Fujisawa S, Morozov A, Barlas A, Romin Y, Dogan Y, Gholami S, Moreira AL, Manova-Todorova K & Moore MAS (2012) Tunneling nanotubes provide a unique conduit for intercellular transfer of cellular contents in human malignant pleural mesothelioma. *PloS One* **7:** e33093

Lundberg P, Koskinen C, Baldock PA, Löthgren H, Stenberg A, Lerner UH & Oldenborg P-A (2007) Osteoclast formation is strongly reduced both in vivo and in vitro in the absence of CD47/SIRPalpha-interaction. *Biochem. Biophys. Res. Commun.* **352:** 444–448

Malbec M, Sourisseau M, Guivel-Benhassine F, Porrot F, Blanchet F, Schwartz O & Casartelli N (2013) HIV-1 Nef promotes the localization of Gag to the cell membrane and facilitates viral cell-to-cell transfer. *Retrovirology* **10:** 80

Malim MH & Emerman M (2008) HIV-1 accessory proteins--ensuring viral survival in a hostile environment. *Cell Host Microbe* **3:** 388–398

Mantegazza AR, Magalhaes JG, Amigorena S & Marks MS (2013) Presentation of phagocytosed antigens by MHC class I and II. *Traffic Cph. Den.* **14:** 135–152

Martin N & Sattentau Q (2009) Cell-to-cell HIV-1 spread and its implications for immune evasion. *Curr. Opin. HIV AIDS* **4:** 143–149

Martin N, Welsch S, Jolly C, Briggs JAG, Vaux D & Sattentau QJ (2010) Virological Synapse-Mediated Spread of Human Immunodeficiency Virus Type 1 between T Cells Is Sensitive to Entry Inhibition. *J. Virol.* **84:** 3516–3527

Marzo L, Gousset K & Zurzolo C (2012) Multifaceted roles of tunneling nanotubes in intercellular communication. *Front. Physiol.* **3:** 72

Massanella M, Puigdomènech I, Cabrera C, Fernandez-Figueras MT, Aucher A, Gaibelet G, Hudrisier D, García E, Bofill M, Clotet B & Blanco J (2009) Antigp41 antibodies fail to block early events of virological synapses but inhibit HIV spread between T cells. *AIDS Lond. Engl.* **23:** 183–188

Mazzolini J, Herit F, Bouchet J, Benmerah A, Benichou S & Niedergang F (2010) Inhibition of phagocytosis in HIV-1–infected macrophages relies on Nef-dependent alteration of focal delivery of recycling compartments. *Blood* **115:** 4226–4236

McCune JM (2001) The dynamics of CD4+ T-cell depletion in HIV disease. *Nature* **410:**

974–979

McDonald D (2010) Dendritic Cells and HIV-1 Trans-Infection. *Viruses* **2:** 1704–1717

McDonald D, Wu L, Bohks SM, KewalRamani VN, Unutmaz D & Hope TJ (2003) Recruitment of HIV and Its Receptors to Dendritic Cell-T Cell Junctions. *Science* **300:** 1295–1297

McIlroy D, Autran B, Cheynier R, Wain-Hobson S, Clauvel JP, Oksenhendler E, Debré P & Hosmalin A (1995) Infection frequency of dendritic cells and CD4+ T lymphocytes in spleens of human immunodeficiency virus-positive patients. *J. Virol.* **69:** 4737–4745

McNally AK, DeFife KM & Anderson JM (1996) Interleukin-4-induced macrophage fusion is prevented by inhibitors of mannose receptor activity. *Am. J. Pathol.* **149:** 975–985

Ménager MM & Littman DR (2016) Actin Dynamics Regulates Dendritic Cell-Mediated Transfer of HIV-1 to T Cells. *Cell* **164:** 695–709

Meucci O, Fatatis A, Simen AA, Bushell TJ, Gray PW & Miller RJ (1998) Chemokines regulate hippocampal neuronal signaling and gp120 neurotoxicity. *Proc. Natl. Acad. Sci. U. S. A.* **95:** 14500–14505

Miyauchi K, Kim Y, Latinovic O, Morozov V & Melikyan GB (2009) HIV enters cells via endocytosis and dynamin-dependent fusion with endosomes. *Cell* **137:** 433–444

Moore JP & Ho DD (1995) HIV-1 neutralization: the consequences of viral adaptation to growth on transformed T cells. *AIDS Lond. Engl.* **9 Suppl A:** S117-136

Moreno JL, Mikhailenko I, Tondravi MM & Keegan AD (2007) IL-4 promotes the formation of multinucleated giant cells from macrophage precursors by a STAT6-dependent, homotypic mechanism: contribution of E-cadherin. *J. Leukoc. Biol.* **82:** 1542–1553

Münk C, Jensen B-EO, Zielonka J, Häussinger D & Kamp C (2012) Running loose or getting lost: how HIV-1 counters and capitalizes on APOBEC3-induced mutagenesis through its Vif protein. *Viruses* **4:** 3132–3161

Murooka TT, Deruaz M, Marangoni F, Vrbanac VD, Seung E, von Andrian UH, Tager AM, Luster AD & Mempel TR (2012) HIV-infected T cells are migratory vehicles for viral dissemination. *Nature* **490:** 283–287

Murray PJ & Wynn TA (2011) Protective and pathogenic functions of macrophage subsets. *Nat. Rev. Immunol.* **11:** 723–737

Nardacci R, Antinori A, Kroemer G & Piacentini M (2005) Cell death mechanisms in HIV-associated dementia: the involvement of syncytia. *Cell Death Differ.* **12 Suppl 1:** 855–858

Nguyen DG & Hildreth JEK (2003) Involvement of macrophage mannose receptor in the binding and transmission of HIV by macrophages. *Eur. J. Immunol.* **33:** 483–493

Novack DV & Teitelbaum SL (2008) The osteoclast: friend or foe? *Annu. Rev. Pathol.* **3:** 457–484

Ojeda D, López-Costa JJ, Sede M, López EM, Berria MI & Quarleri J (2014) Increased in vitro glial fibrillary acidic protein expression, telomerase activity, and telomere length after productive human immunodeficiency virus-1 infection in murine astrocytes. *J. Neurosci. Res.* **92:** 267–274

Oldenborg PA, Gresham HD & Lindberg FP (2001) CD47-signal regulatory protein alpha (SIRPalpha) regulates Fcgamma and complement receptor-mediated phagocytosis. *J. Exp. Med.* **193:** 855–862

Onfelt B, Nedvetzki S, Yanagi K & Davis DM (2004) Cutting edge: Membrane nanotubes connect immune cells. *J. Immunol. Baltim. Md 1950* **173:** 1511–1513

Ono A & Freed EO (2004) Cell-type-dependent targeting of human immunodeficiency virus type 1 assembly to the plasma membrane and the multivesicular body. *J. Virol.* **78:** 1552–1563

Opi S, Kao S, Goila-Gaur R, Khan MA, Miyagi E, Takeuchi H & Strebel K (2007) Human immunodeficiency virus type 1 Vif inhibits packaging and antiviral activity of a degradation-resistant APOBEC3G variant. *J. Virol.* **81:** 8236–8246

Orenstein JM (2000) In vivo cytolysis and fusion of human immunodeficiency virus type 1-infected lymphocytes in lymphoid tissue. *J. Infect. Dis.* **182:** 338–342

Orenstein JM (2001) The Macrophage in HIV Infection. *Immunobiology* **204:** 598–602

Orenstein JM, Meltzer MS, Phipps T & Gendelman HE (1988) Cytoplasmic assembly and accumulation of human immunodeficiency virus types 1 and 2 in recombinant human colony-stimulating factor-1-treated human monocytes: an ultrastructural study. *J. Virol.* **62:** 2578–2586

Orenstein JM & Wahl SM (1999) The macrophage origin of the HIV-expressing multinucleated giant cells in hyperplastic tonsils and adenoids. *Ultrastruct. Pathol.* **23:** 79–91

Pantaleo G, Demarest JF, Vaccarezza M, Graziosi C, Bansal GP, Koenig S & Fauci AS (1995) Effect of anti-V3 antibodies on cell-free and cell-to-cell human immunodeficiency virus transmission. *Eur. J. Immunol.* **25:** 226–231

Pantaleo G, Graziosi C & Fauci AS (1993) The role of lymphoid organs in the pathogenesis of HIV infection. *Semin. Immunol.* **5:** 157–163

Parthasarathy V, Martin F, Higginbottom A, Murray H, Moseley GW, Read RC, Mal G, Hulme R, Monk PN & Partridge LJ (2009) Distinct roles for tetraspanins CD9, CD63 and CD81 in the formation of multinucleated giant cells. *Immunology* **127:** 237–248

Pasquier J, Guerrouahen BS, Al Thawadi H, Ghiabi P, Maleki M, Abu-Kaoud N, Jacob A, Mirshahi M, Galas L, Rafii S, Le Foll F & Rafii A (2013) Preferential transfer of mitochondria from endothelial to cancer cells through tunneling nanotubes modulates chemoresistance. *J. Transl. Med.* **11:** 94

Pelchen-Matthews A, Kramer B & Marsh M (2003) Infectious HIV-1 assembles in late endosomes in primary macrophages. *J. Cell Biol.* **162:** 443–455

Peng G, Greenwell-Wild T, Nares S, Jin W, Lei KJ, Rangel ZG, Munson PJ & Wahl SM (2007) Myeloid differentiation and susceptibility to HIV-1 are linked to APOBEC3 expression. *Blood* **110:** 393–400

Perelson AS, Neumann AU, Markowitz M, Leonard JM & Ho DD (1996) HIV-1 dynamics in vivo: virion clearance rate, infected cell life-span, and viral generation time. *Science* **271:** 1582–1586

Permanyer M, Ballana E, Ruiz A, Badia R, Riveira-Munoz E, Gonzalo E, Clotet B & Esté JA (2012) Antiretroviral Agents Effectively Block HIV Replication after Cell-to-Cell Transfer. *J. Virol.* **86:** 8773–8780

Phillips DM (1994) The role of cell-to-cell transmission in HIV infection. *AIDS Lond. Engl.* **8:** 719–731

Piguet V & Steinman RM (2007) The interaction of HIV with dendritic cells: outcomes and pathways. *Trends Immunol.* **28:** 503–510

Pope M, Betjes MG, Romani N, Hirmand H, Cameron PU, Hoffman L, Gezelter S, Schuler G & Steinman RM (1994) Conjugates of dendritic cells and memory T lymphocytes from skin facilitate productive infection with HIV-1. *Cell* **78:** 389–398

Puigdomènech I, Massanella M, Cabrera C, Clotet B & Blanco J (2009) On the steps of cell-to-cell HIV transmission between CD4 T cells. *Retrovirology* **6:** 89

Puigdomènech I, Massanella M, Izquierdo-Useros N, Ruiz-Hernandez R, Curriu M, Bofill M, Martinez-Picado J, Juan M, Clotet B & Blanco J (2008) HIV transfer between CD4 T cells does not require LFA-1 binding to ICAM-1 and is governed by the interaction of HIV envelope glycoprotein with CD4. *Retrovirology* **5:** 32

Reynoso R, Wieser M, Ojeda D, Bönisch M, Kühnel H, Bolcic F, Quendler H, Grillari J, Grillari-Voglauer R & Quarleri J (2012) HIV-1 Induces Telomerase Activity in Monocyte-Derived Macrophages, Possibly Safeguarding One of Its Reservoirs. *J. Virol.* **86:** 10327–10337

Rinaldo CR (2013) HIV-1 Trans Infection of CD4+ T Cells by Professional Antigen Presenting Cells. *Scientifica* **2013:** Available at: http://www.ncbi.nlm.nih.gov/pmc/articles/PMC3820354/ [Accessed June 2, 2015]

Rodriguez-Plata MT, Puigdomènech I, Izquierdo-Useros N, Puertas MC, Carrillo J, Erkizia I, Clotet B, Blanco J & Martinez-Picado J (2013) The infectious synapse formed between mature dendritic cells and CD4+ T cells is independent of the presence of the HIV-1 envelope glycoprotein. *Retrovirology* **10:** 42

Rosa A, Chande A, Ziglio S, De Sanctis V, Bertorelli R, Goh SL, McCauley SM, Nowosielska A, Antonarakis SE, Luban J, Santoni FA & Pizzato M (2015) HIV-1 Nef promotes infection by excluding SERINC5 from virion incorporation. *Nature* **526:** 212–217

Roy N, Pacini G, Berlioz-Torrent C & Janvier K (2014) Mechanisms underlying HIV-1 Vpu-mediated viral egress. *Front. Microbiol.* **5:** 177

Rudnicka D, Feldmann J, Porrot F, Wietgrefe S, Guadagnini S, Prévost M-C, Estaquier J, Haase AT, Sol-Foulon N & Schwartz O (2009) Simultaneous Cell-to-Cell Transmission of Human Immunodeficiency Virus to Multiple Targets through Polysynapses. *J. Virol.* **83:** 6234–6246

Ruggiero E, Bona R, Muratori C & Federico M (2008) Virological consequences of early events following cell-cell contact between human immunodeficiency virus type 1-infected and uninfected CD4+ cells. *J. Virol.* **82:** 7773–7789

Rustom A, Saffrich R, Markovic I, Walther P & Gerdes H-H (2004) Nanotubular Highways for Intercellular Organelle Transport. *Science* **303:** 1007–1010

Ryzhova EV, Crino P, Shawver L, Westmoreland SV, Lackner AA & González-Scarano F (2002) Simian immunodeficiency virus encephalitis: analysis of envelope sequences from individual brain multinucleated giant cells and tissue samples. *Virology* **297:** 57–67

Sagar M, Akiyama H, Etemad B, Ramirez N, Freitas I & Gummuluru S (2012) Transmembrane domain membrane proximal external region but not surface unit-directed broadly neutralizing HIV-1 antibodies can restrict dendritic cell-mediated HIV-1 trans-infection. *J. Infect. Dis.* **205:** 1248–1257

Sastry K & Ezekowitz RA (1993) Collectins: pattern recognition molecules involved in first line host defense. *Curr. Opin. Immunol.* **5:** 59–66

Sattentau Q (2008) Avoiding the void: cell-to-cell spread of human viruses. *Nat. Rev. Microbiol.* **6:** 815–826

Sattentau QJ (2010) Cell-to-Cell Spread of Retroviruses. *Viruses* **2:** 1306–1321

Scarlatti G, Tresoldi E, Björndal A, Fredriksson R, Colognesi C, Deng HK, Malnati MS, Plebani A, Siccardi AG, Littman DR, Fenyö EM & Lusso P (1997) In vivo evolution of HIV-1 co-receptor usage and sensitivity to chemokine-mediated suppression. *Nat. Med.* **3:** 1259–1265

Schiffner T, Sattentau QJ & Duncan CJA (2013) Cell-to-cell spread of HIV-1 and evasion of neutralizing antibodies. *Vaccine* **31:** 5789–5797

Schindelin J, Arganda-Carreras I, Frise E, Kaynig V, Longair M, Pietzsch T, Preibisch S, Rueden C, Saalfeld S, Schmid B, Tinevez J-Y, White DJ, Hartenstein V, Eliceiri K, Tomancak P & Cardona A (2012) Fiji: an open-source platform for biological-image analysis. *Nat. Methods* **9:** 676–682

Schols D, Pauwels R, Baba M, Desmyter J & De Clercq E (1989) Syncytium formation and destruction of bystander CD4+ cells cocultured with T cells persistently infected with human immunodeficiency virus as demonstrated by flow cytometry. *J. Gen. Virol.* **70 (Pt 9):** 2397–2408

Sewald X, Gonzalez DG, Haberman AM & Mothes W (2012) In vivo imaging of virological synapses. *Nat. Commun.* **3:** 1320

Seyed-Razavi Y, Hickey MJ, Kuffová L, McMenamin PG & Chinnery HR (2013) Membrane

nanotubes in myeloid cells in the adult mouse cornea represent a novel mode of immune cell interaction. *Immunol. Cell Biol.* **91:** 89–95

Sheehy AM, Gaddis NC, Choi JD & Malim MH (2002) Isolation of a human gene that inhibits HIV-1 infection and is suppressed by the viral Vif protein. *Nature* **418:** 646–650

Sherer NM, Lehmann MJ, Jimenez-Soto LF, Horensavitz C, Pypaert M & Mothes W (2007) Retroviruses can establish filopodial bridges for efficient cell-to-cell transmission. *Nat. Cell Biol.* **9:** 310–315

Shun M-C, Daigle JE, Vandegraaff N & Engelman A (2007) Wild-type levels of human immunodeficiency virus type 1 infectivity in the absence of cellular emerin protein. *J. Virol.* **81:** 166–172

Sigal A, Kim JT, Balazs AB, Dekel E, Mayo A, Milo R & Baltimore D (2011) Cell-to-cell spread of HIV permits ongoing replication despite antiretroviral therapy. *Nature* **477:** 95–98

Sloan RD, Kuhl BD, Mesplède T, Münch J, Donahue DA & Wainberg MA (2013) Productive entry of HIV-1 during cell-to-cell transmission via dynamin-dependent endocytosis. *J. Virol.* **87:** 8110–8123

Smith BA, Gartner S, Liu Y, Perelson AS, Stilianakis NI, Keele BF, Kerkering TM, Ferreira-Gonzalez A, Szakal AK, Tew JG & Burton GF (2001) Persistence of infectious HIV on follicular dendritic cells. *J. Immunol. Baltim. Md 1950* **166:** 690–696

Sol-Foulon N, Sourisseau M, Porrot F, Thoulouze M-I, Trouillet C, Nobile C, Blanchet F, di Bartolo V, Noraz N, Taylor N, Alcover A, Hivroz C & Schwartz O (2007) ZAP-70 kinase regulates HIV cell-to-cell spread and virological synapse formation. *EMBO J.* **26:** 516–526

Sood C, Marin M, Chande A, Pizzato M & Melikyan GB (2017) SERINC5 Inhibits HIV-1 Fusion Pore Formation by Promoting Functional Inactivation of Envelope Glycoproteins. *J. Biol. Chem.***:** jbc.M117.777714

Soulas C, Conerly C, Kim W-K, Burdo TH, Alvarez X, Lackner AA & Williams KC (2011) Recently infiltrating MAC387(+) monocytes/macrophages a third macrophage population involved in SIV and HIV encephalitic lesion formation. *Am. J. Pathol.* **178:** 2121–2135

Sourisseau M, Sol-Foulon N, Porrot F, Blanchet F & Schwartz O (2007) Inefficient Human Immunodeficiency Virus Replication in Mobile Lymphocytes. *J. Virol.* **81:** 1000–1012

Sowinski S, Jolly C, Berninghausen O, Purbhoo MA, Chauveau A, Köhler K, Oddos S, Eissmann P, Brodsky FM, Hopkins C, Onfelt B, Sattentau Q & Davis DM (2008) Membrane nanotubes physically connect T cells over long distances presenting a novel route for HIV-1 transmission. *Nat. Cell Biol.* **10:** 211–219

Stahl PD & Ezekowitz RA (1998) The mannose receptor is a pattern recognition receptor involved in host defense. *Curr. Opin. Immunol.* **10:** 50–55

Starling S & Jolly C (2016) LFA-1 Engagement Triggers T Cell Polarization at the HIV-1 Virological Synapse. *J. Virol.* **90:** 9841–9854

Strebel K (2013) HIV accessory proteins versus host restriction factors. *Curr. Opin. Virol.* **3:** 692–699

Swingler S, Mann AM, Zhou J, Swingler C & Stevenson M (2007) Apoptotic killing of HIV-1-infected macrophages is subverted by the viral envelope glycoprotein. *PLoS Pathog.* **3:** 1281–1290

Sylwester A, Murphy S, Shutt D & Soll DR (1997) HIV-induced T cell syncytia are self-perpetuating and the primary cause of T cell death in culture. *J. Immunol. Baltim. Md 1950* **158:** 3996–4007

Sylwester A, Wessels D, Anderson SA, Warren RQ, Shutt DC, Kennedy RC & Soll DR (1993) HIV-induced syncytia of a T cell line form single giant pseudopods and are motile. *J. Cell Sci.* **106 (Pt 3):** 941–953

Symeonides M, Murooka TT, Bellfy LN, Roy NH, Mempel TR & Thali M (2015) HIV-1-Induced Small T Cell Syncytia Can Transfer Virus Particles to Target Cells through Transient Contacts. *Viruses* **7:** 6590–6603

Takeda Y, Tachibana I, Miyado K, Kobayashi M, Miyazaki T, Funakoshi T, Kimura H, Yamane H, Saito Y, Goto H, Yoneda T, Yoshida M, Kumagai T, Osaki T, Hayashi S, Kawase I & Mekada E (2003) Tetraspanins CD9 and CD81 function to prevent the fusion of mononuclear phagocytes. *J. Cell Biol.* **161:** 945–956

Tan J & Sattentau QJ (2013) The HIV-1-containing macrophage compartment: a perfect cellular niche? *Trends Microbiol.* **21:** 405–412

Tartour K, Appourchaux R, Gaillard J, Nguyen X-N, Durand S, Turpin J, Beaumont E, Roch E, Berger G, Mahieux R, Brand D, Roingeard P & Cimarelli A (2014) IFITM proteins are incorporated onto HIV-1 virion particles and negatively imprint their infectivity. *Retrovirology* **11:** 103

Tebit DM & Arts EJ (2011) Tracking a century of global expansion and evolution of HIV to drive understanding and to combat disease. *Lancet Infect. Dis.* **11:** 45–56

Teo I, Veryard C, Barnes H, An SF, Jones M, Lantos PL, Luthert P & Shaunak S (1997) Circular forms of unintegrated human immunodeficiency virus type 1 DNA and high levels of viral protein expression: association with dementia and multinucleated giant cells in the brains of patients with AIDS. *J. Virol.* **71:** 2928–2933

Titanji K, Vunnava A, Sheth AN, Delille C, Lennox JL, Sanford SE, Foster A, Knezevic A, Easley KA, Weitzmann MN & Ofotokun I (2014) Dysregulated B cell expression of RANKL and OPG correlates with loss of bone mineral density in HIV infection. *PLoS Pathog.* **10:** e1004497

Tokarev A & Guatelli J (2011) Misdirection of membrane trafficking by HIV-1 Vpu and Nef: Keys to viral virulence and persistence. *Cell. Logist.* **1:** 90–102

Usami Y, Wu Y & Göttlinger HG (2015) SERINC3 and SERINC5 restrict HIV-1 infectivity

and are counteracted by Nef. *Nature* **526:** 218–223

Van Damme N, Goff D, Katsura C, Jorgenson RL, Mitchell R, Johnson MC, Stephens EB & Guatelli J (2008) The interferon-induced protein BST-2 restricts HIV-1 release and is downregulated from the cell surface by the viral Vpu protein. *Cell Host Microbe* **3:** 245–252

Vasiliver-Shamis G, Cho MW, Hioe CE & Dustin ML (2009) Human Immunodeficiency Virus Type 1 Envelope gp120-Induced Partial T-Cell Receptor Signaling Creates an F-Actin-Depleted Zone in the Virological Synapse. *J. Virol.* **83:** 11341–11355

Vérollet C, Souriant S, Bonnaud E, Jolicoeur P, Raynaud-Messina B, Kinnaer C, Fourquaux I, Imle A, Benichou S, Fackler OT, Poincloux R & Maridonneau-Parini I (2015) HIV-1 reprograms the migration of macrophages. *Blood* **125:** 1611–1622

Vérollet C, Zhang YM, Cabec VL, Mazzolini J, Charrière G, Labrousse A, Bouchet J, Medina I, Biessen E, Niedergang F, Bénichou S & Maridonneau-Parini I (2010) HIV-1 Nef Triggers Macrophage Fusion in a p61Hck- and Protease-Dependent Manner. *J. Immunol.* **184:** 7030–7039

Vicandi B, Jiménez-Heffernan JA, López-Ferrer P, Patrón M, Gamallo C, Colmenero C & Viguer JM (1999) HIV-1 (p24)-positive multinucleated giant cells in HIV-associated lymphoepithelial lesion of the parotid gland. A report of two cases. *Acta Cytol.* **43:** 247–251

Waki K & Freed EO (2010) Macrophages and Cell-Cell Spread of HIV-1. *Viruses* **2:** 1603–1620

Wang L, Eng ET, Law K, Gordon RE, Rice WJ & Chen BK (2017) Visualization of HIV T Cell Virological Synapses and Virus-Containing Compartments by Three-Dimensional Correlative Light and Electron Microscopy. *J. Virol.* **91:**

Watters SA, Mlcochova P & Gupta RK (2013) Macrophages: the neglected barrier to eradication. *Curr. Opin. Infect. Dis.* **26:** 561–566

Welsch S, Keppler OT, Habermann A, Allespach I, Krijnse-Locker J & Kräusslich H-G (2007) HIV-1 Buds Predominantly at the Plasma Membrane of Primary Human Macrophages. *PLoS Pathog* **3:** e36

Weng J, Krementsov DN, Khurana S, Roy NH & Thali M (2009) Formation of syncytia is repressed by tetraspanins in human immunodeficiency virus type 1-producing cells. *J. Virol.* **83:** 7467–7474

White TA, Bartesaghi A, Borgnia MJ, Meyerson JR, Cruz MJV de la, Bess JW, Nandwani R, Hoxie JA, Lifson JD, Milne JLS & Subramaniam S (2010) Molecular Architectures of Trimeric SIV and HIV-1 Envelope Glycoproteins on Intact Viruses: Strain-Dependent Variation in Quaternary Structure. *PLOS Pathog.* **6:** e1001249

Wilen CB, Tilton JC & Doms RW (2012) HIV: cell binding and entry. *Cold Spring Harb. Perspect. Med.* **2:**

Wissing S, Galloway NLK & Greene WC (2010) HIV-1 Vif versus the APOBEC3 cytidine

deaminases: an intracellular duel between pathogen and host restriction factors. *Mol. Aspects Med.* **31:** 383–397

Wu L & KewalRamani VN (2006) Dendritic-cell interactions with HIV: infection and viral dissemination. *Nat. Rev. Immunol.* **6:** 859–868

Yagi M, Ninomiya K, Fujita N, Suzuki T, Iwasaki R, Morita K, Hosogane N, Matsuo K, Toyama Y, Suda T & Miyamoto T (2007) Induction of DC-STAMP by alternative activation and downstream signaling mechanisms. *J. Bone Miner. Res. Off. J. Am. Soc. Bone Miner. Res.* **22:** 992–1001

Yeh MW, Kaul M, Zheng J, Nottet HS, Thylin M, Gendelman HE & Lipton SA (2000) Cytokine-stimulated, but not HIV-infected, human monocyte-derived macrophages produce neurotoxic levels of l -cysteine. *J. Immunol. Baltim. Md 1950* **164:** 4265–4270

Yu Q, König R, Pillai S, Chiles K, Kearney M, Palmer S, Richman D, Coffin JM & Landau NR (2004) Single-strand specificity of APOBEC3G accounts for minus-strand deamination of the HIV genome. *Nat. Struct. Mol. Biol.* **11:** 435–442

Zheng L, Yang Y, Guocai L, Pauza CD & Salvato MS (2007) HIV Tat protein increases Bcl-2 expression in monocytes which inhibits monocyte apoptosis induced by tumor necrosis factor-alpha-related apoptosis-induced ligand. *Intervirology* **50:** 224–228

Zhong P, Agosto LM, Ilinskaya A, Dorjbal B, Truong R, Derse D, Uchil PD, Heidecker G & Mothes W (2013) Cell-to-Cell Transmission Can Overcome Multiple Donor and Target Cell Barriers Imposed on Cell-Free HIV. *PLoS ONE* **8:** Available at: http://www.ncbi.nlm.nih.gov/pmc/articles/PMC3538641/ [Accessed September 5, 2017]

Zhu XW & Friedland JS (2006) Multinucleate giant cells and the control of chemokine secretion in response to Mycobacterium tuberculosis. *Clin. Immunol.* **120:** 10–20

APPENDIX

AMERICAN SOCIETY FOR MICROBIOLOGY | Journal of Virology

The Glycosylphosphatidylinositol-Anchored Variable Region of Llama Heavy Chain-Only Antibody JM4 Efficiently Blocks both Cell-Free and T Cell-T Cell Transmission of Human Immunodeficiency Virus Type 1

Lihong Liu,[a] Weiming Wang,[a] Julie Matz,[b] Chaobaihui Ye,[a] Lucie Bracq,[b] Jerome Delon,[b] Jason T. Kimata,[c] Zhiwei Chen,[d] Serge Benichou,[b] Paul Zhou[a]

Unit of Anti-Viral Immunity and Genetic Therapy, Key Laboratory of Molecular Virology and Immunology, Institut Pasteur of Shanghai, Chinese Academy of Sciences, Shanghai, China[a]; Institut Cochin-INSERM U1016-CNRS UMR 8104-University Paris Descartes, Paris, France[b]; Department of Molecular Virology and Microbiology, Baylor College of Medicine, Houston, Texas, USA[c]; HKU-AIDS Institute, Department of Microbiology, Research Center of Infection and Immunology, The University of Hong Kong, Hong Kong Special Administrative Region, China[d]

ABSTRACT

The variable regions (VHHs) of two heavy chain-only antibodies, JM2 and JM4, from llamas that have been immunized with a trimeric gp140 bound to a CD4 mimic have been recently isolated (here referred to as VHH JM2 and VHH JM4, respectively). JM2 binds the CD4-binding site of gp120 and neutralizes HIV-1 strains from subtypes B, C, and G. JM4 binds gp120 and neutralizes HIV-1 strains from subtypes A, B, C, A/E, and G in a CD4-dependent manner. In the present study, we constructed glycosylphosphatidylinositol (GPI)-anchored VHH JM2 and JM4 along with an E4 control and transduced them into human CD4$^+$ cell lines and primary CD4 T cells. We report that by genetically linking the VHHs with a GPI attachment signal, VHHs are targeted to the lipid rafts of the plasma membranes. Expression of GPI-VHH JM4, but not GPI-VHH E4 and JM2, on the surface of transduced TZM.bl cells potently neutralizes multiple subtypes of HIV-1 isolates, including tier 2 or 3 strains, transmitted founders, quasispecies, and soluble single domain antibody (sdAb) JM4-resistant viruses. Moreover, transduction of CEMss-CCR5 cells with GPI-VHH JM4, but not with GPI-VHH E4, confers resistance to both cell-free and T cell-T cell transmission of HIV-1 and HIV-1 envelope-mediated fusion. Finally, GPI-VHH JM4-transduced human primary CD4 T cells efficiently resist both cell-free and T cell-T cell transmission of HIV-1. Thus, we conclude that VHH JM4, when targeted to the lipid rafts of the plasma membrane, efficiently neutralizes HIV-1 infection via both cell-free and T cell-T cell transmission. Our findings should have important implications for GPI-anchored antibody-based therapy against HIV-1.

IMPORTANCE

Lipid rafts are specialized dynamic microdomains of the plasma membrane and have been shown to be gateways for HIV-1 budding as well as entry into T cells and macrophages. In nature, many glycosylphosphatidylinositol (GPI)-anchored proteins localize in the lipid rafts. In the present study, we developed GPI-anchored variable regions (VHHs) of two heavy chain-only antibodies, JM2 and JM4, from immunized llamas. We show that by genetically linking the VHHs with a GPI attachment signal, VHHs are targeted to the lipid rafts of the plasma membranes. GPI-VHH JM4, but not GPI-VHH JM2, in transduced CD4$^+$ cell lines and human primary CD4 T cells not only efficiently blocks diverse HIV-1 strains, including tier 2 or 3 strains, transmitted founders, quasispecies, and soluble sdAb JM4-resistant strains, but also efficiently interferes T cell-T cell transmissions of HIV-1 and HIV-1 envelope-mediated fusion. Our findings should have important implications in GPI-anchored antibody-based therapy against HIV-1.

Llamas naturally produce heavy chain-only antibodies. The variable regions (VHHs) of these heavy chain-only antibodies exhibit antigen-specific binding affinity comparable to that of conventional immunoglobulins (1). Previously, using trimeric gp140 bound to a CD4 mimic as immunogens in llamas, we isolated a panel of broadly neutralizing VHHs of heavy chain-only antibodies. Among these antibodies, JM2 binds the CD4-binding site (CD4BS) of gp120 and neutralizes human immunodeficiency virus type 1 (HIV-1) strains from subtypes B, C, and G, and JM4 binds gp120 and neutralizes HIV-1 strains from subtypes A, B, C, A/E, and G in a CD4-dependent manner (2). A recent crystal structure of JM4 in the complex of HIV-1 Yu2 gp120 core and a CD4 mimic shows that JM4 binds to an epitope spanning the gp120 bridge sheet, V3 loop, β19 strand, the CD4-binding loop, and the glycan at residue Asn386 (3). The JM4 epitope overlaps the b12 epitope in the CD4BS and the 17b, 48d, X5, and 412d epitopes in the coreceptor-binding site (CRBS) of gp120 (3). Thus, consistent with what was found with binding and mutagenesis analyses (2), JM4 targets a hybrid epitope on gp120 that com-

Received 8 August 2016 **Accepted** 7 September 2016

Accepted manuscript posted online 21 September 2016

Citation Liu L, Wang W, Matz J, Ye C, Bracq L, Delon J, Kimata JT, Chen Z, Benichou S, Zhou P. 2016. The glycosylphosphatidylinositol-anchored variable region of llama heavy chain-only antibody JM4 efficiently blocks both cell-free and T cell-T cell transmission of human immunodeficiency virus type 1. J Virol 90:10642–10659. doi:10.1128/JVI.01559-16.

Editor: G. Silvestri, Emory University

Address correspondence to Serge Benichou, serge.benichou@inserm.fr, or Paul Zhou, blzhou@sibs.ac.cn.

L.L. and W.W. contributed equally to this article.

bines elements from both the CD4-binding and coreceptor-binding sites.

HIV-1 infects cells by both cell-free and cell-cell mechanisms. Viral transmission from infected to uninfected cells occurs via formation of virological and infectious synapses, nanotubes, and filopodia (4, 5). The formation of such structures allows the coordination of viral assembly with viral entry at sites of cell-cell contacts (6). As a result, HIV-1 infection of T cells *in vitro* by cell-cell transmission has been found to be 100- to 1,000-fold more efficient for spreading virus than cell-free transmission (7, 8). While the relative impact of cell-free and cell-cell transmission *in vivo* remains to be defined, in a bone marrow-liver-thymus (BLT) humanized mouse model, HIV-1-infected T cells in lymph nodes were found to be mobile and to form virological synapses and syncytia. Of note, a sphingosine 1-phosphate receptor 1 (S1PR1) antagonist, FTY720, blocks the egress of migratory T cells from the lymph nodes into efferent lymph vessels, thereby interrupting T cell recirculation. When used at the onset of HIV-1 infection, it limited HIV-1 dissemination and reduced plasma viremia (9), indicating that the cell-cell transmission of HIV-1 could be important in the establishment of systemic HIV-1 infection.

Neutralizing antibodies and entry inhibitors effectively block cell-free HIV-1. But with few exceptions, they are much less capable of blocking cell-cell viral transmission (7, 8, 10–14). In T cell-T cell coculture, neutralization was demonstrated only when virus-infected donor T cells were pretreated with antibodies before being added to target T cells (7, 8, 10–14). In dendritic cell (DC)-CD4 T cell cocultures, due to variations in assay systems used by different laboratories, the results were quite variable, sometimes even controversial (15–19). For example, Su et al. showed that both anti-gp120 and anti-gp41 antibodies block the *trans*-infection (15), whereas Sagar et al. showed that only anti-gp41, but not anti-gp120, antibodies could block the *trans*-infection (19). Moreover, van Montfort et al. showed that HIV-1 bound to antibodies 2F5, 4E10, and 10E8, but not those bound to b12, NIH45-46, and VRC01, could still be captured by DCs and subsequently infect CD4 T cells (17, 18). Finally, Reh et al. recently tested a panel of 16 broadly neutralizing antibodies against 11 HIV-1 strains during both cell-free and cell-cell transmissions and concluded that the capacity of broadly neutralizing antibodies to inhibit cell-cell transmission of HIV-1 is not only strain and epitope dependent but also dependent on the window of action during the entry process (11). Thus, entry inhibitors that can efficiently block both cell-free and cell-cell transmissions of HIV-1 are urgently needed.

Lipid rafts are specialized dynamic microdomains of the plasma membrane that have been shown to be gateways for HIV-1 budding (20, 21), as well as for HIV-1 entry into T cells and macrophages (21). CD4, the receptor for HIV-1 entry, is located in lipid rafts of the plasma membrane (22–24). Previously, we showed that by genetically linking single-chain Fv (scFv) or third-heavy-chain complementarity-determining region (HCDR3) of human anti-HIV-1 envelope antibodies with a glycosylphosphatidylinositol (GPI) attachment signal from decay-accelerating factor (DAF) (25), scFvs and HCDR3s are targeted into lipid rafts of the plasma membrane. GPI-scFv X5 and 48d and GPI-HCDR3s PG9 and PG16 on the surface of transduced human $CD4^+$ cell lines exhibit potent neutralization against diverse cell-free HIV-1 strains (26, 27). Recently, we showed that trimerization of GPI-HCDR3s PG9 and PG16 further improves anti-HIV-1 neutralizing activity (28). However, so far no studies on the effect of GPI-anchored antibody derivatives on human primary CD4 T cells and on HIV-1 transmission from infected T cells to uninfected T cells have been reported.

In the present study, we constructed fusion genes in which sequences encoding the VHH domains of JM2, JM4, or E4 (here referred to as VHH JM2, VHH JM4, and VHH E4, respectively) and a IgG3 hinge region and histidine (his) tag were genetically linked with or without the sequence encoding the GPI attachment signal of DAF (25). VHH E4, originally isolated from a phage display library, recognizes the Trf2 telomeric protein (J. Matz and S. Benichou, unpublished results) and was used as a negative control. These constructs were used to transduce human $CD4^+$ cell lines and human primary CD4 T cells to investigate whether GPI-VHH JM2 or JM4 would confer broad and potent protection against HIV-1. We report here that transduction of human $CD4^+$ cell lines and primary CD4 T cells with GPI-VHH JM4 confers broad and potent neutralization of HIV-1 via both cell-free and T cell-T cell transmission.

MATERIALS AND METHODS

Gene constructs. Fusion genes encoding VHH E4, JM2, or JM4, the IgG3 hinge, and the his tag, with or without a GPI attachment signal (C-terminal 34 amino acid residues of DAF), were generated by overlapping PCR, ligated into the TA vector system (Invitrogen Life Technologies, San Diego, CA), and sequenced as described previously (29). The fusion genes with the correct sequences were ligated between the BamHI and SalI sites of a third-generation lentiviral transfer vector, pRRLsin-18.PPT.hPGK.Wpre (30). The resulting lentiviral transfer constructs were designated pRRL-VHH E4, JM2, or JM4/hinge/his-tag/DAF and pRRL-VHH E4, JM2, or JM4/hinge/his-tag, respectively.

Fusion genes encoding GPI-VHH E4 or JM4 were generated by PCR and ligated between the BamHI and SalI sites of a third-generation lentiviral transfer vector, pRRLsin-18.PPT.EF1α.2A.GFP.Wpre (31). The resulting lentiviral transfer constructs were designated pRRL-GPI-VHH E4 or JM4-2A-GFP.

The gene encoding rhesus TRIM5α (rhTRIM5α) was also amplified by PCR using pLPCX-rhTRIM5αvector (32) as a template and a pair of primers (5′-GGACTAGTTCCACCATGGCTTCTGGAATCCTGCTTAATGT-3′ and 5′-CCGCTCGAGTCAAGCGTAGTCTGGGACGTCGTATGGGTA-3′, where the underlined sequences are those recognized by restriction enzymes SpeI and XhoI, respectively), ligated into the SpeI and XhoI sites of the lentiviral transfer vector pTRIP-MND-NeffinB6-IRES-GFP (33), and sequenced. The resulting lentiviral transfer construct was designated pTRIP-rhTRIM5α-IRES-GFP. The lentiviral transfer vector containing the correct rhTRIM5α sequence was used to generate recombinant lentiviruses.

The genes encoding soluble VHH E4 and JM4 were amplified using pRRL-VHH E4 or JM4/hinge/his-tag/DAF as templates and a pair of primers (5′-CGGGATCCGAGGTGCAGCTGGTGGAGTC-3′ and 5′-GGCTCGAGCTAGCTCCCATGGTGATGGTGGT-3′, where the underlined sequences are those recognized by two restriction enzymes, BamHI and XhoI, respectively) and ligated into BamHI and XhoI sites of bacterial expression vector pET28b in frame with a his tag coding sequence and sequenced. The pET28E vectors containing the correct VHH E4 and JM4 sequences were used to transform bacterial strain BL21(DE3) (Invitrogen).

Cell lines and human primary CD4 T cells. The packaging cell line 293FT was purchased from Invitrogen Life Technologies and was maintained in complete Dulbecco's modified Eagle's medium (DMEM) (i.e., high-glucose DMEM supplemented with 10% fetal bovine serum [FBS], 2 mM L-glutamine, 1 mM sodium pyruvate, penicillin [100 U/ml], and streptomycin [100 μg/ml]) plus G418 (500 μg/ml) (Invitrogen Life Technologies). The human CD4 T cell lines CEMss-CCR5 and Jurkat-CCR5 were generated as described previously (27). TZM.bl cells were obtained from the NIH AIDS Research and Reference Reagent Program (ARRRP;

Germantown, MD), contributed by J. Kappes and X. Wu (23, 34–37). CEMss-CCR5, Jurkat-CCR5, and TZM.bl cells were maintained in complete DMEM.

Human peripheral blood mononuclear cells (PBMCs) were obtained from healthy donors through the blood bank of the Changhai Hospital, Shanghai, China. Human primary CD4 T cells were enriched from PBMCs by negatively selecting magnetic beads according to the manufacturer's instructions (Thermo Fisher Scientific) and resuspended in the complete RPMI 1640 medium (i.e., RPMI 1640 medium supplemented with 15% FBS, 2 mM L-glutamine, 1 mM sodium pyruvate, penicillin [100 U/ml], and streptomycin [100 μg/ml]) supplemented with human recombinant interleukin 2 (rIL-2; 100 IU/ml; R&D Systems) before being activated and transduced with recombinant lentiviral vectors.

Generation of recombinant lentiviruses. Recombinant lentiviruses were generated as described previously (38). Briefly, 4×10^6 293FT cells were seeded onto a P-100 dish in 10 ml of complete DMEM. After culturing overnight, cells were cotransfected with 20 μg of transfer construct (pRRL-VHH E4, JM2, or JM4/hinge/his-tag/DAF, pRRL-VHH E4, JM2, or JM4/hinge/his-tag, pRRL-GPI-VHH E4 or JM4-2A-GFP, or pTRIP-rhTRIM5α-IRES-GFP), 10 μg of packaging construct encoding HIV-1 Gag/Pol (pLP1), 7.5 μg of plasmids encoding the vesicular stomatitis virus G protein (VSV-G) envelope (pLP/VSV-G), and 7.5 μg of HIV-1 Rev protein (pLP2; Invitrogen), using a calcium phosphate precipitation method. Sixteen hours later, culture supernatants were removed and replaced with fresh complete DMEM plus 1 mM sodium butyrate (Sigma). Eight hours later, supernatants were again removed and replaced with fresh DMEM plus 4% FBS. After another 20 h, the culture supernatants were harvested and concentrated by ultracentrifugation as described previously (38). The vector pellets were resuspended in a small volume of DMEM and stored in aliquots in a −80°C freezer. Vector titers were determined as previously described (38). The amount of HIV-1 Gag p24 in concentrated vector stocks was determined by an enzyme-linked immunosorbent assay (ELISA).

Generation of stably transduced $CD4^+$ cell lines and human primary CD4 T cells. To generate stably transduced TZM.bl cell lines, 5×10^4 TZM.bl cells per well were seeded onto a 24-well plate. After overnight culture, 2×10^6 transducing units (TU) of one of the recombinant lentiviral viruses (expressing VHH E4, JM2, or JM4/hinge/his-tag/DAF or pRRL-VHH E4, JM2, or JM4/hinge/his-tag fusion genes) was added onto a 24-well tissue culture plate in the presence of 8 μg/ml of Polybrene. Twenty-four hours later, cells were extensively washed and cultured in complete DMEM. The expressions of pRRL-VHH E4, JM2, or JM4/hinge/his-tag/DAF and pRRL-VHH E4, JM2, or JM4/hinge/his-tag constructs were measured by fluorescence-activated cell sorter (FACS) analysis and/or Western blot analysis. We usually found that after a single round of transduction, over 98% of cells express transgenes (data not shown). After transduced cells were generated, cells were continuously cultured in complete DMEM and split every 3 or 4 days. Periodically, the expression of transgenes was measured. We found that the level of transgene expression was very stable in the stably transduced cell lines (data not shown).

To generate a stably transduced CEMss-CCR5-rhTRIM5α/GFP cell line, 1×10^5 CEMss-CCR5 cells and 2×10^6 TU of the recombinant lentiviruses containing pTRIP-rhTRIM5α-IRES-GFP were added to a 24-well tissue culture plate in the presence of 8 μg/ml of Polybrene (Sigma). Twenty-four hours later, cells were extensively washed and cultured in complete DMEM. The expression of fusion gene rhTRIM5α-IRES-GFP was analyzed by Western blotting.

To transduce CEMss-CCR5 or CEMss-CCR5-rhTRIM5α/GFP cells, 1×10^5 CEMss-CCR5 or CEMss-CCR5-rhTRIM5α/GFP cells and 2×10^6 TU of one of the recombinant lentiviruses containing pRRL-GPI-VHH E4 or JM4 were added to a 24-well tissue culture plate in the presence of 8 μg/ml of Polybrene (Sigma). Twenty-four hours later, cells were extensively washed and cultured in complete DMEM. The expression of fusion genes rhTRIM5α-IRES-GFP and pRRL-GPI-VHH E4 or JM4 was detected by FACS analysis.

To transduce human primary CD4 T cells, CD4 T cells were enriched from human PBMCs by negatively selecting magnetic beads (Thermo Fisher Scientific). A total of 2.5×10^5 enriched human CD4 T cells per well were activated by mixing with anti-CD3/CD28 antibody-coated microbeads (Thermo Fisher Scientific) at a 1:1 ratio in 500 μl of complete RPMI 1640 medium supplemented with human rIL-2 (100 IU/ml) in 48-well plates. After 24 h, 5×10^6 TU of pseudotyped virions containing pRRL-GPI-VHH E4 or JM4-2A-GFP in complete RPMI 1640 supplemented with human rIL-2 (100 IU/ml) and 8 μg/ml of Polybrene were added into cell suspension at a final volume of 750 μl and a multiplicity of infection (MOI) of 20. The plates were centrifuged at 1,500 × *g* and 37°C for 2 h to facilitate transduction. After overnight incubation at 37°C, 500 μl of supernatant was removed and 750 μl of fresh complete RPMI 1640 medium supplemented with human rIL-2 (100 IU/ml) were added into cells. The anti-CD3/CD28 antibody-coated microbeads in human CD4 T cells were removed by DynaMag magnet after 4 days of activation. Transduced human CD4 T cells were resuspended in 2 ml of complete RPMI 1640 supplemented with human rIL-2 (100 IU/ml) and cultured in 24-well plates for additional 2 days. The transduction efficiency and CD4, CCR5, and CXCR4 gene expression were estimated by antibody staining followed by FACS analysis before transduced human CD4 T cells were challenged with cell-free HIV-1 and used as recipient cells in T cell-T cell transmission of HIV-1.

The generation of soluble VHH JM4 and E4 and CD4. To produce soluble VHH JM4 and E4, bacterial strain BL21(DE3) containing the pET28-VHH E4 or JM4 plasmid was cultured in LB medium until the optical density at 600 nm (OD_{600}) reached 0.6 to 0.7. Then 0.4 mM isopropyl-β-D-thiogalactopyranoside (IPTG) was added and bacteria were incubated for another 8 h at 18°C. Bacteria were lysed and VHH JM4 and E4 proteins were purified from the soluble fraction of the bacterial lysates using the nickel-nitrilotriacetic acid (Ni-NTA) purification system according to the manufacturer's instructions (Invitrogen). Soluble CD4 (sCD4) used in this study was generated as before (27). We purified soluble CD4 and VHH E4 and JM4.

Western blot analysis. To detect transgene expression, 1×10^6 TZM.bl cells that were mock transduced or transduced with pRRL-VHH E4, JM2, or JM4/hinge/his-tag or pRRL-VHH E4, JM2, or JM4/hinge/his-tag/DAF were grown in DMEM plus 1% FBS on a 6-well plate for 48 h. Cells and supernatant were harvested. Cells were lysed with lysis buffer (100 mM Tris-HCl [pH 8.0], 1% NP-40) in the presence of a protease inhibitor cocktail (Calbiochem). Proteins in supernatant were precipitated by trichloroacetic acid (TCA) and dissolved in a volume of lysis buffer equal to that of the lysed cell pellet. Samples were separated by 12% SDS–PAGE, transferred onto a polyvinylidene difluoride (PVDF) membrane, and detected by mouse anti-his tag antibody (Sigma) and mouse anti-human glyceraldehyde-3-phosphate dehydrogenase (GAPDH) antibody as a control.

To detect the expression of rhTRIM5α/GFP fusion gene, 1×10^6 mock- and rhTRIM5α/GFP fusion gene-transduced CEMss-CCR5 cells were grown in DMEM plus 1% FBS on a 12-well plate for 24 h. Cells were harvested, lysed using lysis buffer in the presence of protease inhibitor cocktail, separated by 12% SDS-PAGE, transferred onto a PVDF membrane (Millipore), and detected by mouse anti-hemagglutinin (anti-HA) tag antibody (Sigma) and mouse anti-GAPDH antibody (Sigma) as a control.

FACS analysis. To measure green fluorescent protein (GFP) expression, 1×10^5 mock-, rhTRIM5α/GFP-, or GPI-VHH E4- or JM4-2A-GFP-transduced CEMss-CCR5 cells were collected 4 days after transduction (see above), washed twice with FACS buffer (phosphate-buffered saline [PBS] containing 1% bovine serum albumin [BSA] and 0.02% NaN_3), and fixed with 1% formaldehyde in 0.5 ml of FACS buffer. FACS analysis was performed with a BD LSRII flow cytometer (BD Biosciences).

To measure the cell surface expression of GPI-VHH E4, JM2, or JM4, 2×10^5 mock- and VHH E4, JM2, or JM4/hinge/his-tag/DAF-transduced TZM.bl cells, mock- and VHH E4- or JM4/hinge/his-tag/DAF-trans-

duced CEMss-CCR5 cells, or mock- and GPI-VHH E4- or JM4-2A-GFP-transduced human primary CD4 T cells were incubated with a mouse anti-his tag antibody for 45 min on ice. Cells were then washed twice with FACS buffer and stained with phycoerythrin (PE)-conjugated goat anti-mouse IgG antibody (Sigma) for another 45 min on ice. Cells then were washed twice with FACS buffer and fixed with 1% formaldehyde in 0.5 ml of FACS buffer. FACS analysis was performed with a BD LSRII flow cytometer.

To determine whether the expression of GPI-VHH E4, JM2, or JM4 is truly targeted through a GPI anchor, 8×10^5 mock- and VHH E4-, JM2-, or JM4/hinge/his-tag/DAF-transduced TZM.bl cells were first incubated with or without 6 U/ml of phosphatidylinositol-specific phospholipase C (PI-PLC; Invitrogen) in 0.5 ml of 1× PBS and rocked at 4°C for 20 min. After incubation, cells were washed twice to remove the remaining PI-PLC and then stained with a mouse anti-his tag antibody as described above.

To determine whether the expression of Sec-VHH or GPI-VHH E4, JM2, or JM4 could alter the cell surface expression of CD4, CCR5, and CXCR4, 2×10^5 mock- and GPI-VHH E4-, JM2-, or JM4- or Sec-VHH E4-, JM2-, or JM4-transduced TZM.bl cells, mock- and GPI-VHH E4- or JM4-transduced CEMss-CCR5 cells, or mock- and pRRL-VHH E4- or JM4-2A-GFP-transduced human primary CD4 T cells were incubated with allophycocyanin (APC)-conjugated anti-human CD4 (Miltenyi), PE-conjugated anti-human CCR5 (BD Science), or PE-conjugated anti-human CXCR4 (BD Science) antibodies for 45 min on ice. Cells were then washed twice with FACS buffer and fixed with 1% formaldehyde in 0.5 ml of FACS buffer. FACS analysis was performed with a BD LSRII flow cytometer.

Intracellular HIV-1 Gag p24 was stained as described before (15). Briefly, at the desired intervals after HIV-1 infection, small portions of cells were harvested, washed with 1 ml of FACS buffer, and fixed and permeabilized with a Cytofix/Cytoperm kit (Becton Dickinson). Cells were resuspended in 50 μl of Perm/Wash buffer with 0.8 μl of PE-conjugated anti-Gag p24 antibody (KC57; Beckman Coulter) and incubated for 30 min on ice. After being washed twice with 1 ml of Perm/Wash buffer, the cells were resuspended in 400 μl of FACS buffer and analyzed by FACS Fortessa (BD Biosciences) using FlowJo and GraphPad Prism software.

Immunofluorescence staining and confocal analysis. Mock- and GPI-VHH E4-, JM2-, or JM4-transduced TZM.bl cells were seeded (5,000 cells per well) onto a tissue culture-treated glass slide (BD Biosciences) and incubated at 37°C in 5% CO_2 for 2 days. Cells were then washed twice with 500 μl of PBS and fixed with fixation buffer (4% formaldehyde in PBS plus 1% BSA) for 15 min. Cells were washed twice with 500 μl of PBS and blocked with blocking buffer (5% goat serum in PBS plus 1% BSA) for 1 h. Cells were stained with Alexa 555-conjugated cholera toxin subunit B (CtxB; Invitrogen Life Technologies) at 4°C for 45 min. After being washed 3 times with PBS, cells were stained with mouse anti-his tag antibody at 4°C for 45 min and then stained with Alexa 488-conjugated goat anti-mouse IgG antibody (Invitrogen) at 4°C. After cells were washed 3 times with PBS, cells were stained with 4′,6-diamidino-2-phenylindole (DAPI) in permeabilization buffer (blocking buffer plus 0.5% saponin) for 5 min. The slides were mounted before being analyzed under a confocal fluorescence microscope (Zeiss model LSM 510).

Chemotaxis assay. The chemotaxis response of GPI-VHH E4 or JM4-transduced CEMss-CCR5 cells was assessed using Transwell filters (5-μm pore size; Corning) with 100 ng/ml of SDF1α (Peprotech) used as a chemoattractant. While 3×10^5 cells were resuspended in 300 μl of RPMI 1640 in the upper chamber, 600 μl of RPMI 1640 medium with or without 100 ng/ml of SDF1α was added to the lower chamber. Chemotaxis assays were performed at 37°C in 5% CO_2 for 3 h. The filter was then removed, and the number of cells in the lower chamber was determined by flow cytometry (Accuri C6).

Capping assay. To analyze the capping of the CXCR4 coreceptor, mock- and GPI-VHH-JM4- or E4-transduced CEMss-CCR5 cells were stimulated with 100 ng/ml of SDF1α for 10 min and then fixed with 4% paraformaldehyde (PFA) in PBS. Cells were then plated onto coverslips coated with poly-L-lysine (0.002%, wt/vol; Sigma) in H_2O_2 for 2 min and stained with anti-CXCR4 antibody (R&D Systems; MAB172 at 10 μg/ml) for 30 min and Alexa 488-conjugated anti-mouse IgG Fc antibody (Invitrogen) for 30 min. Cells were then permeabilized in PBS containing 1% BSA and 0.15% Triton X-100 and stained with Alexa 647-conjugated phalloidin (Invitrogen). Coverslips were washed with PBS and mounted using 10 μl of Fluoromount media containing DAPI (Sigma). Images were acquired on a spinning-disk (CSU-X1M1; Yokogawa) inverted microscope (DMI6000, Leica) equipped with a CoolSnap HQ2 camera (Photometrics) with a 63× oil objective using Metamorph software (v7.7.5 Molecular Devices) and processed using Fiji (ImageJ; NIH).

Generation of HIV-1 pseudotypes and viruses. To generate HIV-1 pseudotypes, 4×10^6 293FT packaging cells were cotransfected with 10 μg of an HIV-1–luciferase transfer vector and 1 μg of a DNA plasmid encoding one of several HIV-1 envelopes (Q168, Q461ENVe2, Yu2, AD8, JRFL, SF162, HxBc2, consensus B and C, PVO.4, QH0692.42, CNE3, CNE5, CNE8, CNE11, CNE15, CNE50, CNE55, 92BR025.9, 93TH966.8, and 92UG975.10) or control VSV-G using a calcium phosphate precipitation method. The pseudotype-containing supernatants were harvested and stored in aliquots in a freezer at −80°C. Titers of pseudotyped virions were determined as previously described (38).

To generate infectious HIV-1, 4×10^6 293FT packaging cells were transfected with 10 μg of one of infectious HIV-1 molecular clones Bru-3, Yu2, AD8, JRCSF, and PBRGX, one of molecular clones of HIV-1 transmitted founder viruses WITO, CH040, THRO, REJO, CH077, and CH106 (39), or a molecular clone of simian immunodeficiency virus (SIV) strain SIVMne027 (40) using a calcium phosphate precipitation method. The virus-containing supernatants were harvested and stored in aliquots in a freezer at −80°C. Virus titers were determined as previously described (27). The amount of HIV-1 p24 in collected supernatants was measured by the RETROtek HIV-1 p24 antigen ELISA (Zeptometrix Corporation).

Single-cycle infectivity assay. In a single-cycle assay, 1×10^4 TZM.bl cells mock transduced or transduced with pRRL-VHH E4, JM2, or JM4/hinge/his-tag/DAF-, and pRRL-VHH E4, JM2, or JM4/hinge/his-tag were transduced with HIV-1 or 10A1 pseudotype-containing supernatants equivalent to a relative luciferase activity (RLA) of 100,000 to 500,000 overnight or infected with HIV-1 strains Bru-3, Bru-Yu2, AD8, JRCSF, and PBRGX, HIV-1 transmitted founder viruses WITO, CH040, THRO, REJO, CH077, and CH106, and SIV strain SIVMne027 as a control at an MOI of 2 in a final volume of 0.2 ml overnight. Cells were then washed twice with PBS and cultured in complete DMEM for 2 days. Cells were then washed once with PBS and lysed in 100 μl of Glo-lysis buffer. The luciferase activity in 50-μl cell suspensions was measured by a BrightGlo luciferase assay according to the manufacturer's instructions (Promega).

Cell-free HIV-1 infection and p24 assay. To test the effect of GPI-VHH JM4 on cell-free HIV-1 infection, 1×10^6 GPI-VHH JM4- or E4-transduced CEMss-CCR5 cells were infected with HIV-1 strains Bru-3, Bru-Yu2, JRCSF, AD8, THRO.c, and Mj4 at an MOI of 0.01 in a final volume of 0.5 ml overnight. Cells were then extensively washed with Hanks' balanced salt solution (HBSS), resuspended in 6 ml of complete DMEM, and cultured for 30 days. Every 3 days, 4.5 ml of cell suspensions was harvested and replaced with fresh medium. The supernatants were then collected. HIV-1 Gag p24 in the supernatants was measured by ELISA (Zeptometrix Corporation) according to the manufacturer's instructions.

To test the effect of GPI-VHH JM4 on cell-free HIV-1 infection in transduced human primary CD4 T cells, 1×10^6 human primary CD4 T cells transduced with GPI-VHH E4 or JM4-2A-GFP (see above) were infected with HIV-1 Bru-3 and AD8 at an MOI of 0.01 in a final volume of 0.5 ml overnight. Cells were then extensively washed with HBSS, resuspended in 2 ml of complete RPMI 1640 supplemented with 100 IU/ml of human rIL-2, and cultured on 24-well plates for 9 days. Every 3 days, small portions of cells were harvested and replaced with fresh RPMI 1640 supplemented with 100 IU/ml of human rIL-2. HIV-1 infection was measured by intracellular Gag p24 staining at 3, 6, and 9 days postinfection (see above).

Measurement of T cell-T cell transmission of HIV-1. To establish HIV-1-infected donor cells, CEMss-CCR5 cells were incubated with HIV-1 JRCSF and Jurkat-CCR5 cells were incubated with HIV-1 Bru-3 or AD8 overnight at an MOI of 5 and washed twice with RPMI 1640. Infected CEMss-CCR5 and Jurkat-CCR5 cells were then cultured for 4 days at 37°C and the percentage of infected cells was assessed by intracellular Gag p24 staining (see above).

To assess the effect of GPI-VHH JM4 on cell-cell transmission of HIV-1 in transduced human $CD4^+$ T cell lines, 1×10^5 HIV-1 JRCSF-infected or uninfected CEMss-CCR5 cells (see above) were cocultured with 5×10^5 CEMss-CCR5-rhTRIM5α/GFP cells transduced with lentiviral vectors expressing VHH E4 or JM4/hinge/his-tag/DAF. Infection was monitored for 12 days after coculture by measuring intracellular Gag p24 protein expression in the target cell population as described in the section on FACS analysis (see above). For the comparison, 1×10^5 HIV-1 JRCSF-infected or uninfected CEMss-CCR5 cells cocultured with 5×10^5 CEMss-CCR5-rhTRIM5α/GFP cells in the presence of 10 or 40 μg/ml of soluble VHH E4 or JM4 were also monitored for 12 days post coculture. The cell-cell transmission of HIV-1, as measured by intracellular Gag p24 staining in target cells and Gag p24 in coculture supernatants, was assessed every other day postcoculture. Percent inhibition was determined by the equation $100 - 100 \times$ [percent infected cells in coculture between HIV-1-infected CEMss-CCR5 cells and CEMss-CCR5-rhTRIM5α/GFP cells transduced with lentiviral vector expressing VHH E4/hinge/his-tag/DAF]/[percent infected cells in coculture between HIV-1-infected CEMss-CCR5 cells and CEMss-CCR5-rhTRIM5α/GFP cells transduced with lentiviral vector expressing VHH JM4/hinge/his-tag/DAF].

For the comparison, JRCSF-infected donor cells and uninfected CEMss-CCR5-rhTRIM5α/GFP cells or CEMss-CCR5-rhTRIM5α/GFP cells transduced with pRRL-VHH E4 or JM4/hinge/his-tag/DAF were also cocultured in Transwell chambers (12-well 0.4-mm polyester-membrane dishes; Corning Life Sciences, Corning, NY), in which JRCSF-infected donor cells added to the Transwell insert and uninfected CEMss-CCR5-rhTRIM5α/GFP cells or CEMss-CCR5-rhTRIM5α/GFP cells transduced with pRRL-VHH E4 or JM4/hinge/his-tag/DAF were seeded as target cells in the bottom chamber. Intracellular Gag p24 staining was performed as described above.

To assess the effect of GPI-VHH JM4 on cell-cell transmission of HIV-1 in transduced human primary CD4 T cells, 1×10^5 HIV-1 AD8- or Bru-3-infected or uninfected Jurkat-CCR5 cells (see above) were cocultured with 4×10^5 GPI-VHH E4- or JM4.2A.eGFP-transduced human primary CD4 T cells in 2 ml of complete RPMI 1640 supplemented with human rIL-2 (100 IU/ml). After 3, 6, and 9 days of coculture at 37°C, the infectivity in transduced human primary CD4 T cells was assessed by intracellular Gag p24 staining (see above).

Cell-cell fusion experiment. A total of 1×10^5 HIV-1 Bru-3 and JRCSF-infected or uninfected CEMss-CCR5 cells (see above) were cocultured with 5×10^5 CEMss-CCR5-rhTRIM5α/GFP cells transduced with lentiviral vectors expressing VHH E4 and JM4/hinge/his-tag/DAF on a 12-well plate at 37°C and 5% CO_2. As controls, 1×10^5 HIV-1 Bru-3- or JRCSF-infected or uninfected CEMss-CCR5 cells were cocultured with 5×10^5 CEMss-CCR5-rhTRIM5α/GFP cells in the presence of 10 or 40 μg/ml of soluble VHH E4 or JM4. Cell-cell fusion was monitored by light microscopy at various intervals and recorded by a charge-coupled-device (CCD) digital camera (Leica DM IRB). The syncytia (3 pictures per coculture sample) were counted manually.

RESULTS

Targeting VHH JM2, JM4, and E4 to the lipid rafts of the plasma membrane through a GPI anchor. To generate GPI-anchored and secreted VHH, the sequences encoding VHH from the heavy chain-only antibodies E4, JM2, and JM4 were genetically linked with the sequence encoding a his-tagged IgG3 hinge region and with or without the sequence encoding a GPI attachment signal of DAF. The VHH/hinge/his-tag/DAF and the VHH/hinge/his-tag fusion genes were inserted into a third-generation lentiviral vector, pRRLsin-18.PPT.hPGK.Wpre (Fig. 1A). The recombinant viruses were then generated and used to transduce TZM.bl, CEMss-CCR5, and CEMss-CCR5-rhTRIM5α/GFP cells (see below).

Figure 1B shows the expression of VHH/hinge/his-tag/DAF and VHH/hinge/his-tag fusion genes in cell lysates and culture supernatants of transduced TZM.bl cells by Western blotting using anti-his tag and anti-GAPDH antibodies. As expected, without a GPI attachment signal, VHHs were detected in both culture supernatants and cell lysates, with a majority in supernatants (right side). In contrast, with a GPI attachment signal VHH were detected only in cell lysates and not in culture supernatants (left side), indicating that inclusion of a GPI attachment signal allows for cell association and prevents secretion of the VHH.

To determine if VHH/hinge/his-tag/DAF was expressed on the cell surface through a GPI anchor, VHH/hinge/his-tag/DAF E4, JM2, and JM4-transduced TZM.bl cells were treated or not with phosphatidylinositol phospholipase C (PI-PLC) and stained with anti-his tag antibody, followed by FACS analysis. Figure 1C shows that VHH/hinge/his-tag/DAFs were highly expressed at the cell surface and their expression was significantly reduced with PI-PLC treatment, indicating that VHH/hinge/his-tag/DAF is attached to the cell surface through a GPI anchor. Thus, we refer to the VHH/hinge/his-tag/DAF and VHH/hinge/his-tag as GPI-VHH and Sec-VHH, respectively.

To localize GPI-VHH, mock- and GPI-VHH E4-, JM2-, or JM4-transduced TZM.bl cells were seeded onto a glass slide and costained with (i) anti-his tag antibody followed by Alexa 488-conjugated anti-mouse IgG antibody, (ii) Alexa 555-conjugated cholera toxin subunit B (CtxB), and (iii) DAPI. CtxB interacts with GM1 (a lipid raft marker). Figure 1D shows that GPI-VHH E4, JM2, or JM4 is colocalized with GM1 on cell surface, indicating that it is located in the lipid rafts of the plasma membrane.

GPI-VHH JM4 in transduced TZM.bl cells exhibits a remarkable degree of breadth and potency against HIV-1. Next, we compared CD4, CCR5, and CXCR4 expression in Sec-VHH- and GPI-VHH E4-, JM2-, or JM4-transduced TZM.bl cells by flow cytometry and found that there was no significant difference in their expression compared to that in mock-transduced TZM.bl cells, suggesting that the expression of transgenes does not alter the expression of the receptor and the coreceptors for HIV-1 in the transduced cells (Fig. 2A). Nor did we find that the expression of the transgenes alters the cell growth (data not shown).

To test neutralization activity of Sec-VHH and GPI-VHH E4, JM2, and JM4 against cell-free HIV-1, a panel of 21 HIV-1 pseudotypes and a VSV-G pseudotype control were used to infect transduced TZM.bl cells in a single-round infectivity assay (38). The 21 HIV-1 pseudotypes consist of HIV-1 envelopes derived from subtype A (Q168 and Q461ENVe2), subtype B (Yu2, AD8, JRFL, SF162, HxBc2, consensus B, PVO.4, and QH0692.42), subtype B′ (CNE11), subtype C (consensus C and 92BR025.9), CRF07_B′C recombinant (CNE15 and CNE50), CRF01_AE recombinants (CNE3, CNE5, CNE8, CNE55, and 93TH966.8), and subtype G (92UG975.10). Of note, Q168, Q461ENV2e, Yu2, AD8, JRFL, QH0692.42, CNE5, CNE8, CNE11, CNE15, CNE55, and 92BR025.9 are tier 2 strains and PVO.4 is a tier 3 strain. 93TH966.8 and 92UG975.10 are two soluble sdAb JM4-resistant strains (2). Figure 2B shows that while mock-transduced TZM.bl cells and TZM.bl cells transduced with Sec-VHH E4, JM2, or JM4 and with GPI-VHH E4 or JM2 did not

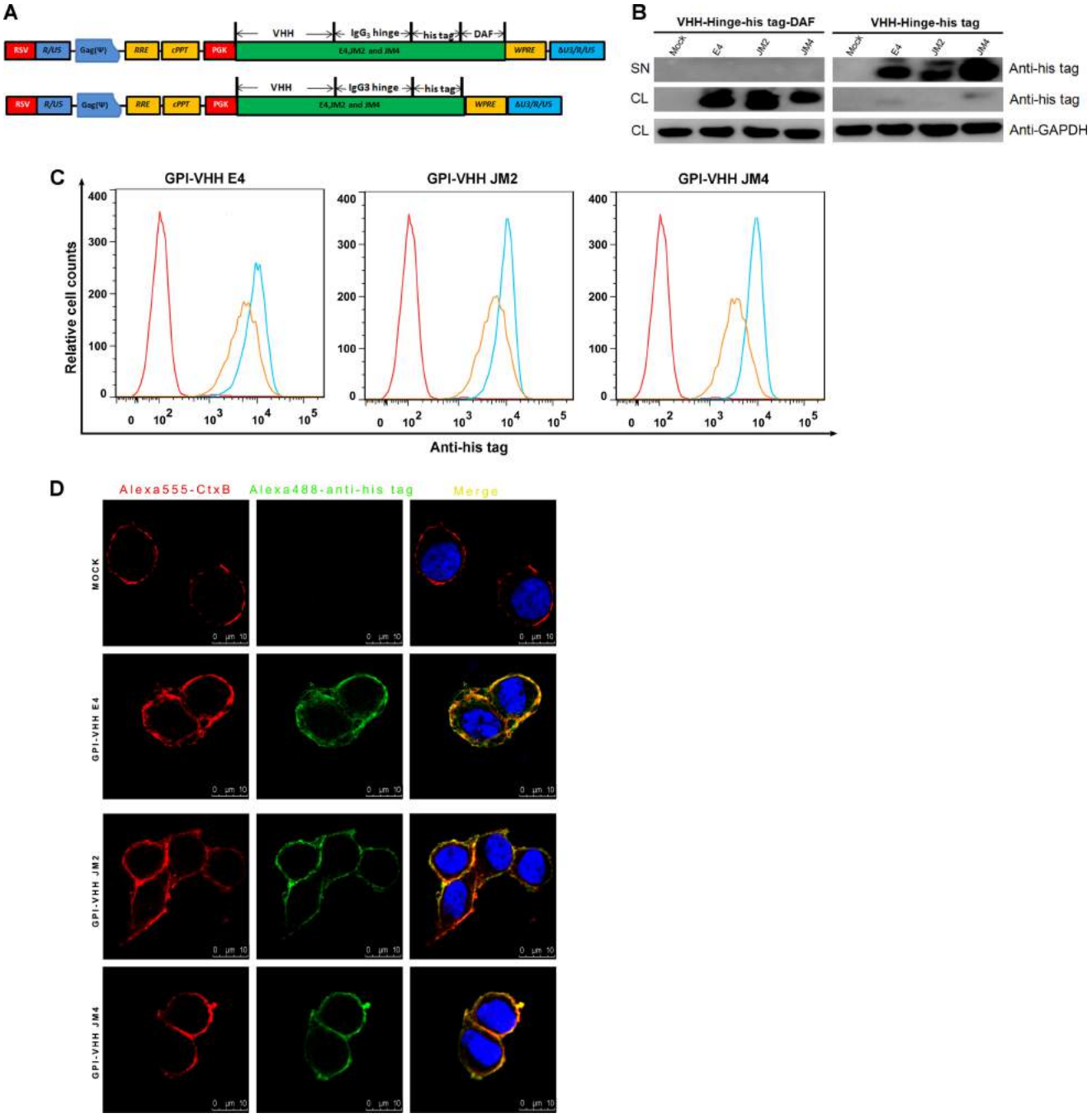

FIG 1 Expression of GPI-VHH and Sec-VHH in transduced TZM.bl cells. (A) Schematic diagram of the lentiviral vectors pRRL-VHH/hinge/his-tag and pRRL-VHH/hinge/his-tag/DAF. VHHs were derived from llama heavy chain-only antibodies E4, JM2, and JM4. Hinge, a human IgG3 hinge region; his-tag: a 6-histidine residue tag; DAF, the C-terminal 34 amino acid residues of decay-accelerating factor. (B) Western blot analysis of VHH E4, JM2, and JM4 in TZM.bl cells transduced with VHH/hinge/his-tag and VHH/hinge/his-tag/DAF. GPI-VHH, GPI-anchored VHH; Sec-VHH, secreted VHH; anti-his, anti-his tag antibody; SN, supernatants; CL, cell lysates. (C) FACS analysis of cell surface expression of GPI-VHH E4, JM2, and JM4 in mock- or VHH/hinge/his-tag/DAF-transduced TZM.bl cells with or without PI-PLC treatment. Red, mock-transduced cells stained with anti-his tag antibody; blue, VHH E4, JM2, or JM4/hinge/his-tag/DAF-transduced cells without PI-PLC treatment stained with anti-his tag antibody; yellow, VHH E4, JM2, or JM4/hinge/his-tag/DAF-transduced cells with PI-PLC treatment stained with anti-his tag antibody. (D) Confocal analysis of mock or pRRL-VHH/hinge/his-tag/DAF-transduced TZM.bl cells. CtxB, cells were stained with Alexa 555-conjugated cholera toxin B subunit; anti-his, cells were stained with mouse anti-his tag antibody followed by Alexa 488-conjugated goat anti-mouse IgG antibody. Scale bar: 10 μm.

neutralize any of 21 HIV-1 pseudotypes tested, TZM.bl cells transduced with GPI-VHH JM4 had a high degree of potency and breadth against all 21 HIV-1 pseudotypes. Except for 89.4 and 93.5% neutralization activity against HIV-1 92UG975.10 and Q461ENV2e pseudotypes, respectively, over 99% neutralization activity was detected against all other 19 HIV-1 pseudotypes. For the comparison, none of the transduced TZM.bl cells neutralized the VSV-G pseudotype control.

A

	CD4		CCR5		CXCR4	
	Mean	Median	Mean	Median	Mean	Median
Mock unstained	112	104	168	159	78	74
Mock	7622	6743	3016	2482	293	169
GPI-VHH E4	8779	7672	2874	2512	444	277
GPI-VHH JM2	8924	7875	2782	2361	461	314
GPI-VHH JM4	9936	8792	3515	2918	346	225
Sec.-VHH E4	8691	7460	3850	3197	398	224
Sec.-VHH JM2	8028	6847	4299	3661	421	229
Sec.-VHH JM4	8143	6895	3830	3125	488	250

B

Pseudotype viruses	Tier	TZM-bl-GPI anchored-VHH			TZM-bl-Secretory-VHH		
		E4	JM2	JM4	E4	JM2	JM4
VSVG	Non	3	0	0	17	14	11
Q168(A,R5)	2	41	0	99.2	0	0	0
Q461ENVe2(A,R5)	2	12	0	93.5	0	0	0
YU2(B,R5)	2	34	18	99.9	1	10	0
AD8(B,R5)	2	27	6	99.8	4	34	27
JR-FL(B,R5)	2	11	27	99.8	15	34	21
SF162(B,R5)	1A	10	24	99.9	5	0	0
Consensus B(B,R5)	-	35	0	99.8	0	0	0
HxBc2(B,X4)	1B	33	0	99.1	0	0	0
PVO.4(B,R5)	3	34	0	100	0	0	0
QH0692.42(B,R5)	2	36	0	100	0	0	0
CNE11(B',R5)	2	18	0	99.8	0	0	0
CNE15(B'C,R5)	2	17	9	99.8	7	18	4
CNE50(B'C,R5)	-	2	0	99.8	0	0	0
Consensus C(C,R5)	-	0	0	100	0	0	0
92BR025.9(C,R5)	2	22	0	100	0	0	0
CNE3(AE,R5)	-	0	0	99.7	0	0	0
CNE8(AE,R5)	2	26	0	100	0	0	0
93TH966.8 (AE,R5)	-	11	ND	100	ND	ND	ND
CNE5(AE,R5)	2	1	0	99	0	0	0
CNE55(AE,R5)	2	34	0	100	0	0	0
92UG975.10(G,R5)	-	17	ND	89.4	ND	ND	ND

C

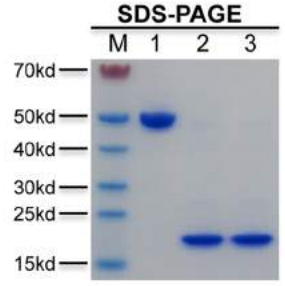

D

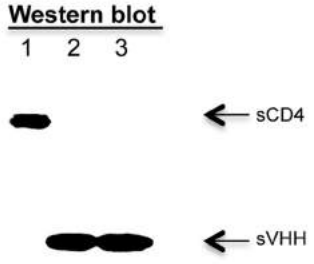

E

	1.25ug/ml	0.625ug/ml	0.3125ug/ml	0.15625ug/ml	0.078125ug/ml	0.0390625ug/ml	Without CD4	Mock
VSVG	529955±3845	545780±67402	625671±66189	598654±61256	738365±25734	754398±61216	716952±57857	
HxBc(B,R5)	20084±3400	97731±15614	298266±9957	519041±64839	583205±28073	546225±73450	530383±64076	
YU2(B,R5)	39928±803	119068±232	238696±31090	325874±18161	327233±11229	389920±19689	292483±31475	5151±618
93TH966.8 (A/E,R5)	116987±6001	130709±13478	127584±6822	131391±10643	124040±10720	138145±1578	128704±2275	
92UG975.10 (G,R5)	16167±935	54874±6163	81540±5729	92682±5822	113909±5087	113295±2255	108241±7362	

F

Heavy chain variable region		VHH-JM4						VHH-E4					
VHH concentration(μg/ml)		40	13	4.4	1.5	0.5	0.2	40	13	4.4	1.48	0.49	0.2
10A1	W/O CD4	0	0	0	0	0	0	0	0	0	0	0	0
	With CD4	0	0	0	0	0	0	0	0	0	0	7.5	0
YU2	W/O CD4	92	49	2.7	0	0	0	0	0	0	0	0	0
	With CD4	96	66	32	0	0	0	0	0	0	0	0	0
HxBc2	W/O CD4	100	100	100	90	27	0	0	0	0	0	0	0
	With CD4	100	100	100	89	26	0	0	0	0	0	0	0
93TH966.8	W/O CD4	0	0	0	3.6	0	0	0	0	0	0	2.4	0
	With CD4	0	0	0	0	0	0	0	0	0	0	0	0
92UG975.10	W/O CD4	0	0	1.8	0	0	0	0	0	0	3.2	4	0
	With CD4	0	4	3.6	2.3	0.6	3.4	0	0	0.5	0	0	3.4

FIG 2 Neutralization by GPI-VHH and Sec-VHH JM2 and JM4 in transduced TZM.bl cells against HIV-1 or VSV-G pseudotypes using a single-cycle infectivity assay. (A) Summary of mean and median fluorescence intensities of CD4, CCR5, and CXCR4 expression in mock-transduced and GPI-VHH and Sec-VHH E4-, JM2-, and JM4-transduced TZM.bl cells. (B) Neutralization by GPI-VHH and Sec-VHH E4, JM2, and JM4 against HIV-1 and VSV-G pseudotypes. The numbers represent the percent inhibition, which was calculated as follows: (RLA in virus alone to a given transduced cell − RLA in no virus to the same transduced cell)/(RLA in virus alone to parental cells − RLA in no virus to parental cell). (C and D) Purified soluble CD4 (sCD4) and soluble VHH (sVHH) JM4 (lane 2) and E4 (lane 3) revealed by SDS-PAGE followed by Coomassie blue staining (C) or Western blotting (D). (E) Determination of the highest concentrations of sCD4 that did not have an inhibitory effect by itself on a given HIV-1 strain (highlighted in red). These sCD4 concentrations were used in the coculture assay with sVHH JM4 and E4. (F) The neutralization activity of various indicated concentrations of sVHH JM2 and JM4 in the presence or absence of sCD4 on infectivity of HIV-1 and VSV-G pseudotypes. The numbers represent the percent inhibition, based on the calculation described above.

TABLE 1 Neutralization activities of GPI-VHH and Sec-VHH E4, JM2, and JM4 against replication-competent HIV-1[a]

Replication competent viruses		TZM-bl-GPI-VHH			TZM-bl-Sec-VHH		
		E4	JM2	JM4	E4	JM2	JM4
Lab-adapted viruses	SIVmne027	0	0	0	10	0	0
	Bru3(B,R5)	12	55	100	18	66	51
	Bru-Yu(B,R5)	0	8	99.9	0	0	0
	JR-CSF(B,R5)	0	0	99.2	4	9	1
	AD8(B,R5)	10	0	99.9	0	0	0
	Mj4(C,R5)	4	56	99.9	10	65	54
	pBRGX(BC,R5)	16	40	99.9	0	28	45
T/F viruses	WITO.c(B,R5)	22	43	99.7	15	44	48
	REJO.c(B,R5)	17	19	99.6	12	31	42
	THRO.c(B,R5)	25	58	99.7	12	59	59
	CH040.c(B,R5)	12	41	99.8	13	56	54
	CH077.t (B,R5)	11	79	99.8	26	80	81
	CH106.c(B,R5)	21	25	99.7	12	38	41
Quasispecies	HKU1721(B)	10	19	100	0	23	0
	HKU004(C)	15	17	100	0	0	0
	HKU1447(AE)	8	15	100	0	0	33

[a] Red indicates over 99% neutralization activity; green indicates from 50% to 89% neutralization activity.

To confirm that 93TH966.8 and 92UG975.10 are indeed sdAb JM4-resistant strains (2), the Yu2, HxBc2, 93TH966.8, and 92UG975.10 pseudotypes, along with 10A1 as a pseudotype control, were incubated with various concentrations (ranging from 0.2 to 40 μg/ml) of sVHH JM4 or E4 in the presence of indicated concentrations of soluble CD4 (sCD4) (Fig. 2C to E). Figure 2F shows that while the Yu2 and HxBc2 pseudotypes were efficiently neutralized by high doses of sVHH JM4, the 93TH966.8 and 92UG975.10 pseudotypes indeed were totally resistant to neutralization by sVHH JM4 in the presence or absence of sCD4.

To test if GPI-VHH JM4-transduced TZM.bl cells are resistant to replication competent HIV-1 infection, GPI-VHH- and Sec-VHH E4-, JM2-, or JM4-transduced TZM.bl cells were infected with HIV-1 strains Yu2, AD8, ADA, JRCSF, and PBRGX, transmitted founder viruses WITO, CH040, THRO, REJO, CH077, and CH106, and quasispecies HKU1721, HKU004, and HKU1447 along with an SIV control, SIVMne027 (40), in a single-round infectivity assay. Table 1 shows that although all transduced TZM.bl cells were equally infected with SIVmne027, TZM.bl cells transduced with GPI-VHH JM4 neutralized all HIV-1 variants tested at a level of >99%. In contrast, TZM.bl cells transduced with GPI-VHH E4 or Sec-VHH E4 had no significant neutralization activity. Interestingly, TZM.bl cells transduced with GPI-VHH JM2 or Sec-VHH JM2 and JM4 exhibited moderate neutralization (ranging from 51 to 81% inhibition) against a few HIV-1 strains (Bru-3, Mj4, THRO, CH040, and CH077). Thus, taken together, these results clearly show that TZM.bl cells transduced with GPI-VHH JM4 exhibit remarkable degrees of breadth and potency against both HIV-1 pseudotypes and replication-competent HIV-1, including tier 2 or 3 strains and strains that are resistant to soluble sdAb JM4.

GPI-VHH JM4-transduced CEMss-CCR5 cells completely resist cell-free HIV-1 infection. While TZM.bl cells, which were engineered with an HIV-1 long terminal repeat (LTR)-driven reporter gene, have been widely used in antibody neutralization assays (23, 34–37), they are of epithelial origin (23). Therefore, we transduced cells of the human $CD4^+$ T cell line CEMss-CCR5 with lentiviral vectors expressing GPI-VHH E4 or JM4. Importantly, both GPI-VHH E4 and JM4 are expressed at high levels on transduced CEMss-CCR5 cells (Fig. 3A and B), and no significant difference in CD4, CCR5, and CXCR4 expression was observed in GPI-VHH E4- and JM4-transduced CEMss-CCR5 cells compared to that in mock-transduced CEMss-CCR5 cells (Fig. 3C). Importantly, when stimulated with 100 ng/ml of SDF1α, mock- and GPI-VHH E4- and JM4-transduced CEMss-CCR5 cells exhibited comparable levels of migration (chemotaxis) (Fig. 3D) as well as capping activities (Fig. 3E), indicating that the functions of CXCR4 coreceptor are not impaired due to the lipid raft expression of GPI-VHHs.

Mock- and GPI-VHH E4- and JM4-transduced CEMss-CCR5 cells were then infected with HIV-1 strains Bru-3, Yu2, JRCSF, AD8, THRO.c, and Mj4 using an MOI of 0.01 as described before (26) and cultured in complete DMEM for 30 days or longer. As shown in Fig. 3F, the replication of all 6 HIV-1 strains was completely inhibited in CEMss-CCR5 cells transduced with GPI-VHH JM4 throughout the experiments. In contrast, robust replication of all 6 HIV-1 strains was observed in mock- and GPI-VHH E4-transduced CEMss-CCR5 cells. Thus, we concluded that GPI-VHH JM4 expression in CEMss-CCR5 cells completely blocks viral replication.

GPI-VHH JM4-transduced CEMss-CCR5 cells resist T cell-T cell HIV-1 transmission. HIV-1 infection is potently restricted by rhesus TRIM5α (rhTRIM5α) at postentry steps preceding integration (41). Notably, this restriction inhibits infection only by cell-free HIV-1 and not virus by cell-cell transmission (42). Thus, before we examined if GPI-VHH JM4 could block T cell-T cell transmission of HIV-1, we generated CEMss-CCR5 cells stably expressing rhTRIM5α and GFP from a bicistronic expression vector (Fig. 4A). Figure 4B shows that in rhTRIM5α/GFP-transduced CEMss-CCR5 cells, both GFP- and HA-tagged rhTRIM5α was expressed well (lane 2) compared to expression in mock-transduced CEMss-CCR5 cells (lane 1). We then tested the effect of rhTRIM5α on cell-free and cell-cell transmission of HIV-1. Clearly, although the expression of rhTRIM5α does not alter CD4,

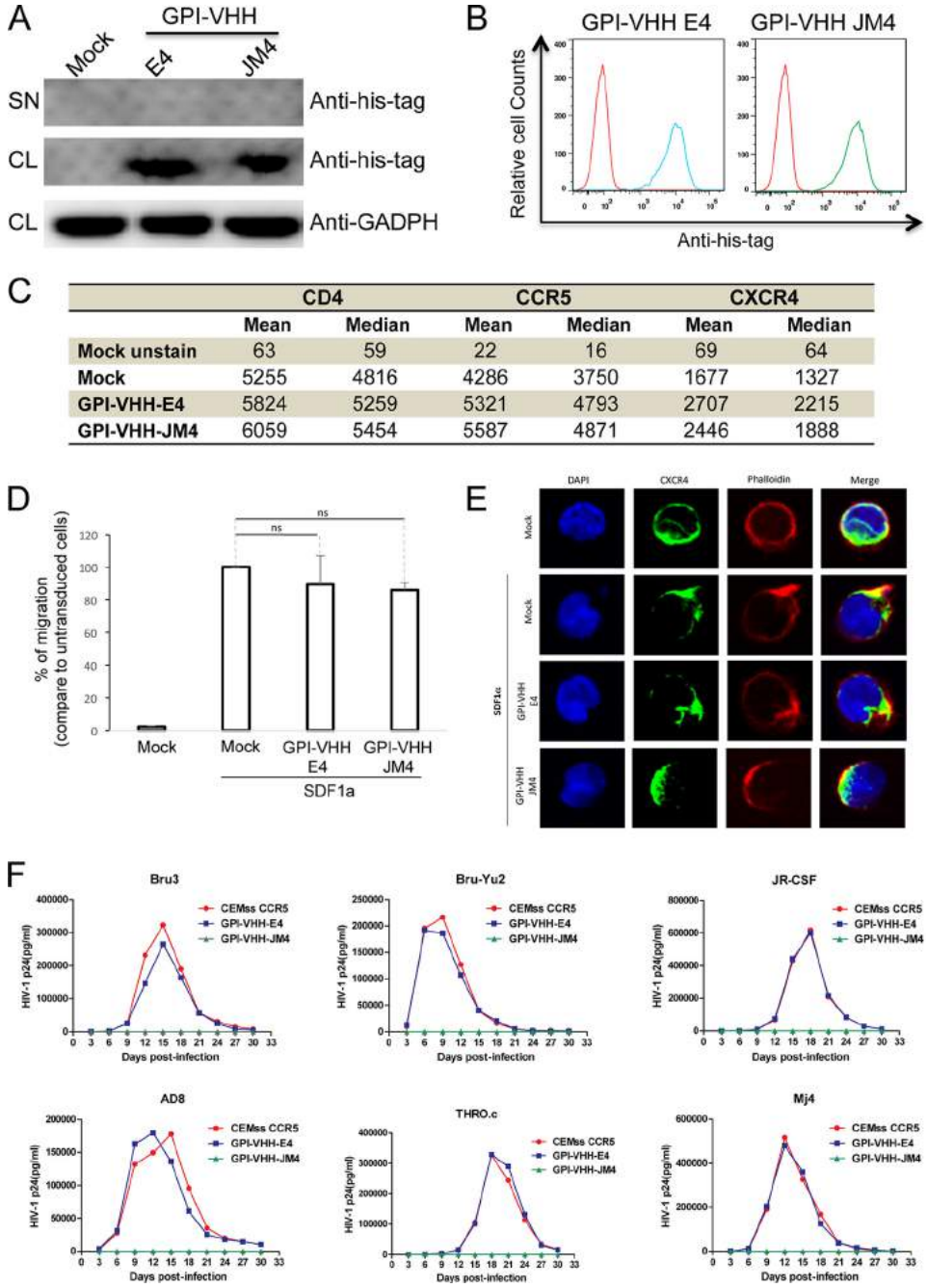

	CD4		CCR5		CXCR4	
	Mean	Median	Mean	Median	Mean	Median
Mock unstain	63	59	22	16	69	64
Mock	5255	4816	4286	3750	1677	1327
GPI-VHH-E4	5824	5259	5321	4793	2707	2215
GPI-VHH-JM4	6059	5454	5587	4871	2446	1888

FIG 3 Neutralization activity of GPI-VHH JM4 in transduced CEMss-CCR5 cells to replication-competent HIV-1. (A) Western blot analysis of mock- and GPI-VHH E4 or JM4-transduced CEMss-CCR5 cells. Anti-his tag, anti-his tag antibody; anti-GAPDH, anti-GAPDH antibody; SN, supernatants; CL, cell lysates. (B) Expression of GPI-VHH E4 and JM4 on the surface of transduced CEMss-CCR5 cells. (Left) Mock- and GPI-VHH E4-transduced CEMss-CCR5 cells; (right) mock- and GPI-VHH JM4-transduced CEMss-CCR5 cells. (C) Summary of mean and median fluorescence intensities of CD4, CCR5, and CXCR4 expression in mock- and GPI-VHH E4- and JM4-transduced CEMss-CCR5 cells. (D) Chemotaxis of mock- and GPI-VHH E4- or JM4-transduced CEMss-CCR5 cells to SDF1α. Cells were loaded onto the upper chamber of a 5-μm Transwell filter, whereas medium containing SDF1α was added in the lower chamber. After 3 h of incubation, the filter was removed and the cell number in the lower chamber was determined by flow cytometry. (E) CXCR4 coreceptor capping of mock- or GPI-VHH E4- or JM4-transduced CEMss-CCR5 cells after stimulation with SDF1α for 10 min followed by stained using anti-CXCR4 antibody, phalloidin, and DAPI and analysis by confocal microscopy. (F) GPI-VHH JM4 confers long-term resistance to HIV-1 Bru-3, Bru-YU2, JRCSF, AD8, THRO.c, and Mj4 in transduced CEMss-CCR5 cells. Mock, mock-transduced CEMss-CCR5 cells; GPI-VHH E4, GPI-VHH E4-transduced CEMss-CCR5 cells; GPI-VHH JM4, GPI-VHH JM4-transduced CEMss-CCR5 cells.

CCR5, and CXCR4 expression (Fig. 4C), it significantly blocks cell-free HIV-1 (Fig. 4D) but not cell-cell transmission of HIV-1 (Fig. 4E and F). These data are consistent with previous studies (42).

To test if GPI-VHH JM4 blocks T cell-T cell transmission of HIV-1, CEMss-CCR5-rhTRIM5α/GFP cells were transduced with lentiviral vectors expressing GPI-VHH E4 or JM4. Figure 4B shows that both GPI-VHH E4 (lane 3) and JM4 (lane 4) are well

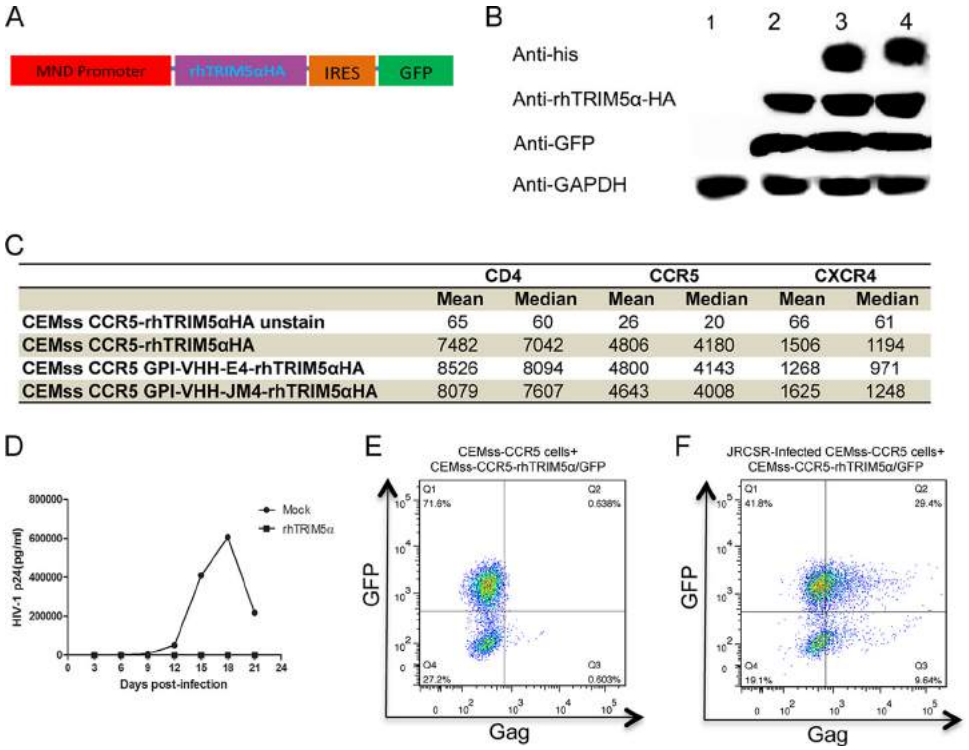

	CD4		CCR5		CXCR4	
	Mean	Median	Mean	Median	Mean	Median
CEMss CCR5-rhTRIM5αHA unstain	65	60	26	20	66	61
CEMss CCR5-rhTRIM5αHA	7482	7042	4806	4180	1506	1194
CEMss CCR5 GPI-VHH-E4-rhTRIM5αHA	8526	8094	4800	4143	1268	971
CEMss CCR5 GPI-VHH-JM4-rhTRIM5αHA	8079	7607	4643	4008	1625	1248

FIG 4 Effect of rhesus TRIM5α on cell-free and cell-cell transmission of HIV-1. (A) Schematic diagram of the lentiviral vector MND-rhTRIM5α-IRES-GFP. In this vector the rhTRIM5α-IRES-GFP was driven by an internal MND promoter. (B) Western blot analysis of mock- and rhTRIM5α-IRES-GFP-transduced CEMss-CCR5 cells (lanes 1 and 2) as well as GPI-VHH E4 or JM4-transduced CEMss-CCR5-rhTRIM5α-IRES-GFP cells (lanes 3 and 4). Anti-his, anti-his tag antibody; anti-rhTRIM5α-HA, anti-HA tag antibody to detect HA-tagged rhTRIM5α; anti-GFP, anti-GFP antibody; anti-GAPDH, anti-GAPDH antibody. (C) Summary of mean and median fluorescence intensities of CD4, CCR5, and CXCR4 expression in CEMss-CCR5-rhTRIM5α/GFP cells and CEMss-CCR5-rhTRIM5α/GFP cells transduced with GPI-VHH E4 or JM4. (D) rhTRIM5α/GFP-transduced CEMss-CCR5 cells are resistant to cell-free HIV-1 JRCSF infection measured by HIV-1 Gag p24 in culture supernatants. (E and F) rhTRIM5α/GFP-transduced CEMss-CCR5 cells are susceptible to the cell-cell transmission of HIV-1 JRCSF measured by GFP^+ Gag^+ cells. (E) GFP^+ Gag^+ cells in coculture between uninfected CEMss-CCR5 cells and rhTRIM5α/GFP-transduced CEMss-CCR5 cells. (F) GFP^+ Gag^+ cells in coculture between HIV-1 JRCSF-infected CEMss-CCR5 cells and rhTRIM5α/GFP-transduced CEMss-CCR5 cells.

expressed. No significant difference in CD4, CCR5, and CXCR4 expression was observed in CEMss-CCR5-rhTRIM5/GFP-GPI-VHH E4 and JM4 cells compared to CEMss-CCR5-rhTRIM5α/GFP cells (Fig. 4C). GPI-VHH E4- or JM4-transduced CEMss-CCR5-rhTRIM5α/GFP cells were then cocultured with HIV-1 JRCSF-infected or uninfected CEMss-CCR5 cells in a regular 24-well plate. For comparison, mock- and GPI-VHH E4- or JM4-transduced CEMss-CCR5-rhTRIM5α/GFP cells were also cocultured with HIV-1 JRCSF-infected CEMss-CCR5 cells in a 24-well Transwell plate. Every 2 days postcoculture, small aliquots of culture supernatants were collected for measuring HIV-1 Gag p24 for a total of 12 days. At 2 and 12 days postcoculture, small aliquots of cells were also harvested, permeabilized, and stained with PE-conjugated anti-HIV-1 Gag p24 antibody. Figure 5A shows the cell-cell transmission of HIV-1 as measured by GFP^+ Gag^+ cells at 2 days postcoculture. Compared to the coculture between mock-transduced CEMss-CCR5-rhTRIM5α/GFP cells and uninfected donor cells (0.4%) (leftmost image), significant HIV-1 transmission (41.6% or 35.4%, respectively) was observed in the coculture between mock- or GFP-GPI-VHH E4-transduced CEMss-CCR5-rhTRIM5α/GFP cells and HIV-1 JRCSF-infected cells (middle left and middle right images). In contrast, a significant reduction in HIV-1 transmission (5.6%) was found in GFP-GPI-VHH JM4-transduced CEMss-CCR5-rhTRIM5α/GFP cells and HIV-1 JRCSF-infected donor cells (rightmost image). As expected, no cell-cell HIV-1 transmission was observed in coculture between mock-, GFP-GPI-VHH E4-, or JM4-transduced CEMss-CCR5-rhTRIM5α/GFP and HIV-1 JRCSF-infected cells in a Transwell plate (Fig. 5B). A similar pattern of cell-cell HIV-1 transmission was observed at 12 days postcoculture (Fig. 5C).

For comparison, we also did intracellular Gag staining in coculture between CEMss-CCR5-rhTRIM5α/GFP cells and JRCSF-infected CEMss-CCR5 donor cells in the presence of 10 or 40 μg/ml of soluble VHH E4 and JM4. Figure 5D shows that in the presence of 10 or 40 μg/ml of soluble VHH E4, significant HIV-1 transmission (36.2% or 42.6%, respectively) occurred in the coculture between CEMss-CCR5-rhTRIM5α/GFP cells and HIV-1 JRCSF-infected cells (middle left and leftmost images), whereas in the presence of 10 or 40 μg/ml of soluble VHH JM4, HIV-1 transmission was moderately reduced, to 28.7% and 14.2%, respectively, in coculture between JRCSF-infected CEMss-CCR5 donor cells and CEMss-CCR5-rhTRIM5α/GFP cells (rightmost and middle right images). The experiment was repeated three times, with similar results. Thus, taken together, these results indicate that GPI-VHH JM4 effectively blocks T cell-T cell transmission of HIV-1, whereas soluble VHH JM4 has only a moderate effect.

The results of intracellular Gag staining shown above correlate well with Gag in culture supernatants. Robust HIV-1 replication

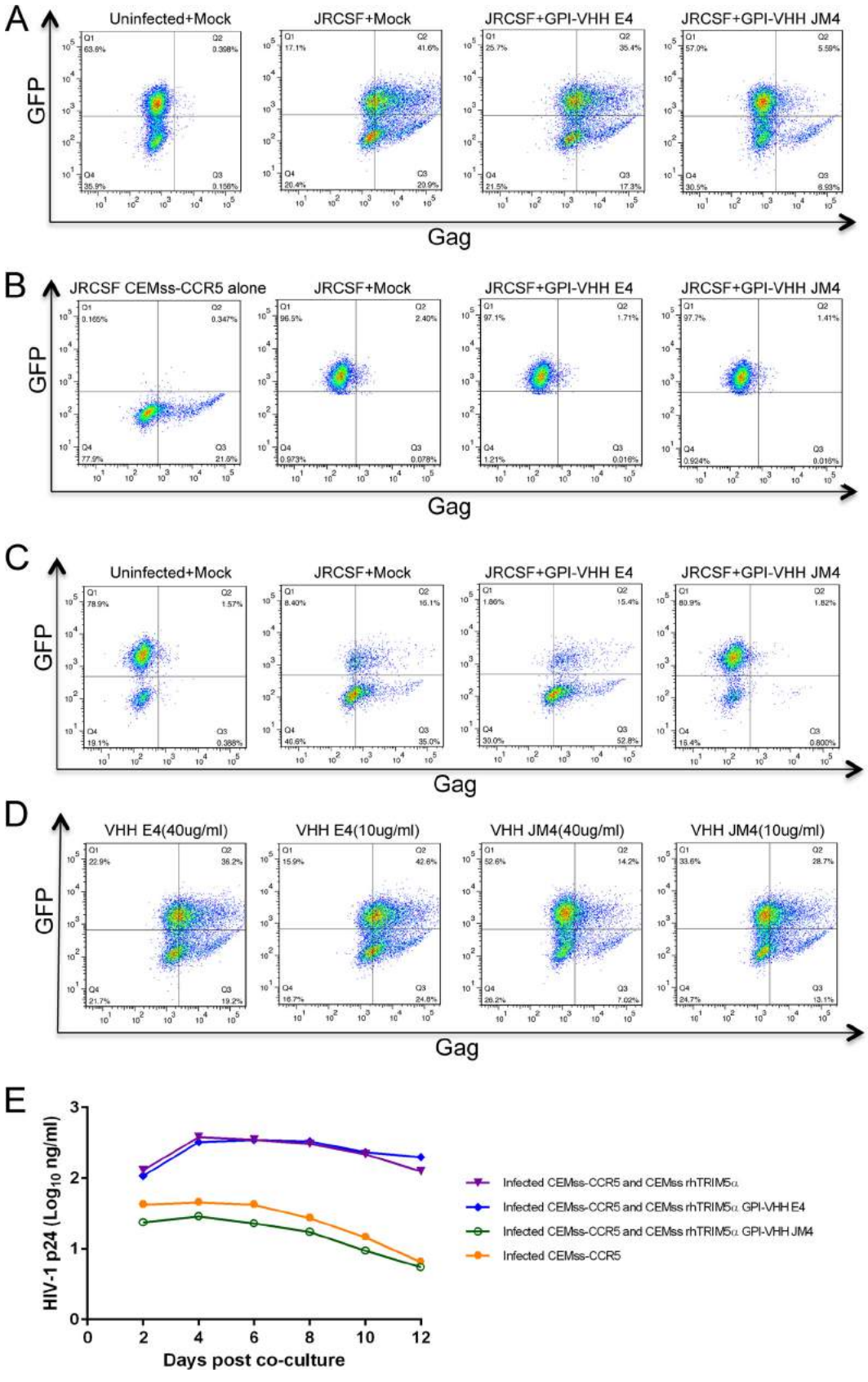
A
Uninfected+Mock
JRCSF+Mock
JRCSF+GPI-VHH E4
JRCSF+GPI-VHH JM4
GFP
Gag
B
JRCSF CEMss-CCR5 alone
JRCSF+Mock
JRCSF+GPI-VHH E4
JRCSF+GPI-VHH JM4
GFP
Gag
C
Uninfected+Mock
JRCSF+Mock
JRCSF+GPI-VHH E4
JRCSF+GPI-VHH JM4
GFP
Gag
D
VHH E4(40ug/ml)
VHH E4(10ug/ml)
VHH JM4(40ug/ml)
VHH JM4(10ug/ml)
GFP
Gag
E
HIV-1 p24 (Log10 ng/ml)
Days post co-culture
Infected CEMss-CCR5 and CEMss rhTRIM5α
Infected CEMss-CCR5 and CEMss rhTRIM5α GPI-VHH E4
Infected CEMss-CCR5 and CEMss rhTRIM5α GPI-VHH JM4
Infected CEMss-CCR5

as measured by Gag in culture supernatants was detected in cocultures between mock- or GPI-VHH E4-transduced CEMss-CCR5-rhTRIM5α/GFP cells and HIV-1 JRCSF-infected donor cells. In contrast, HIV-1 replication in cocultures between GPI-VHH JM4-transduced CEMss-CCR5-rhTRIM5α/GFP cells and HIV-1 JRCSF-infected donor cells was significantly lower, similar to the case with HIV-1 JRCSF-infected donor cells alone (Fig. 5E).

GPI-VHH JM4 completely blocks HIV-1 envelope-mediated cell-cell fusion. Figure 6A and D show the HIV-1 envelope-mediated cell-cell fusion as measured by syncytium formation at 2 days postcoculture. Compared to the cocultures between CEMss-CCR5-rhTRIM5α/GFP cells and uninfected donor cells (Fig. 6A, leftmost image), significant HIV-1 envelope-mediated cell-cell fusion (on average, there were 40 and 41 syncytia per picture, respectively) was observed in cocultures between CEMss-CCR5-rhTRIM5α/GFP or CEMss-CCR5-rhTRIM5α/GFP-GPI-VHH E4 cells and HIV-1 JRCSF-infected cells (Fig. 6A and D, middle left and middle right images). In contrast, no HIV-1 envelope-mediated cell-cell fusion was observed in cocultures between GPI-VHH JM4-transduced CEMss-CCR5-rhTRIM5α/GFP cells and HIV-1 JRCSF-infected donor cells (Fig. 6A and D, rightmost image). As expected, no cell-cell fusion was observed in coculture between CEMss-CCR5-rhTRIM5α/GFP cells and HIV-1 JRCSF-infected cells in a Transwell plate (Fig. 6B).

For comparison, we also recorded cell-cell fusion in coculture between CEMss-CCR5-rhTRIM5α/GFP cells and JRCSF-infected CEMss-CCR5 donor cells in the presence of 10 or 40 μg/ml of sVHH E4 and JM4 (Fig. 6C and D). Coculture between JRCSF-infected CEMss-CCR5 donor cells and CEMss-CCR5-rhTRIM5α/GFP cells in the presence of 10 and 40 μg/ml of sVHH E4 did not have any inhibitory effect on HIV-1 envelope-mediated cell-cell fusion of HIV-1 (with average numbers of syncytia of 43 and 44, respectively) (Fig. 6C and D, leftmost and middle left images). In contrast, coculture between JRCSF-infected CEMss-CCR5 donor cells and CEMss-CCR5-rhTRIM5α/GFP cells in the presence of 10 or 40 μg/ml of soluble VHH JM4 resulted in moderate reduction in cell-cell transmission of HIV-1 (with average numbers of syncytia of 35 and 28, respectively) (Fig. 6C and D, middle right and rightmost images). The experiment was repeated three times, with similar results. Thus, taken together, these results indicate that GPI-VHH JM4 completely blocks HIV-1 envelope-mediated cell-cell fusion, whereas high concentrations of soluble VHH JM4 have only a moderate effect.

GPI-VHH JM4 in transduced human primary CD4 T cells blocks both cell-free and T cell-T cell transmission of HIV-1. Having demonstrated that GPI-VHH JM4 in transduced CEMss-CCR5 cells potently blocks both cell-free and T cell-T cell transmission of HIV-1, we went on to test if human primary CD4 T cells could be efficiently transduced with GPI-VHH JM4 or E4 and, if so, whether GPI-VHH JM4-transduced human primary CD4 T cells could efficiently resist cell-free and T cell-T cell transmission of HIV-1. To facilitate monitoring of transduced human primary CD4 T cells, we inserted genes encoding GPI-VHH JM4 or E4 into the pRRLsin-18.PPT.EF1α0.2A.GFP.Wpre (31). The resulting pRRL-GPI-VHH JM4 or E4-2A-GFP transfer vectors (Fig. 7A) were used to produce recombinant lentiviruses. The latter were used to transduce human primary CD4 T cells. Figure 7B shows that after a single round of transduction, over 80% of human primary CD4 T cells became transgene positive as measured by GFP and GPI-VHH JM4 (left image) or E4 (right image) expression.

To measure the resistance or susceptibility of GPI-VHH JM4 or E4-transduced human primary CD4 T cells to cell-free HIV-1 infection, at 6 days posttransduction, cells were infected with HIV-1 AD8 or Bru-3 at an MOI of 0.1. After infection, HIV-1 replication in transduced human primary CD4 T cells as measured by intracellular Gag staining was monitored for 9 days. Figure 7C shows representative gating of GFP^+ Gag^+ cells in GPI-VHH JM4- or GPI-VHH E4-transduced primary CD4 T cells 6 days after HIV-1 Bru-3 infection along with the uninfected CEMss-CCR5 cell control (top image). Of human primary CD4 T cells transduced with GPI-VHH E4 control 39.6% were GFP^+ Gag^+ (middle image), whereas of cells transduced with GPI-VHH JM4, less than 0.1% were GFP^+ Gag^+ (bottom image). Figure 7D summarizes the percentage of GFP^+ Gag^+ cells in GPI-VHH E4- or JM4-transduced human CD4 T cells from all three donors at 3, 6, and 9 days after HIV-1 AD8 (left image) or Bru-3 (right image) infection. Clearly, while robust replication of HIV-1 AD8 and Bru-3 was seen in GPI-VHH E4-transduced human primary CD4 T cells from all three donors, GPI-VHH JM4-transduced human primary CD4 T cells were completely resistant to cell-free HIV-1 AD8 or Bru-3 infection.

To measure the resistance or susceptibility of GPI-VHH JM4- or E4-transduced human primary CD4 T cells to T cell-T cell transmission of HIV-1, transduced cells 6 days postransduction were cocultured with HIV-1 AD8- or Bru-3-infected Jurkat-CCR5 cells (Fig. 8A). Figure 8B shows representative gating on GFP^+ Gag^+ cells in GPI-VHH JM4- or E4-transduced primary CD4 T cells 6 days after GPI-VHH JM4- or E4-transduced cells were cocultured with HIV-1 Bru-3-infected Jurkat-CCR5 cells along with an uninfected CEMss-CCR5 cell control (left image). Of human primary CD4 T cells transduced with the GPI-VHH E4 control, 36% were GFP^+ Gag^+ (middle image), whereas of cells transduced with GPI-VHH JM4, less than 0.3% were GFP^+ Gag^+ (right image). Figure 8C summarizes the percentage of GFP^+ Gag^+ cells in GPI-VHH E4- or JM4-transduced human CD4 T cells from all three donors at 3, 6, and 9 days after transduced cells were cocultured with HIV-1 AD8-infected (left image) or Bru-3-infected (right image) Jurkat-CCR5

FIG 5 GPI-VHH-JM4-transduced CEMss-CCR5-rhTRIMα/GFP cells are resistant to T cell-T cell transmission of HIV-1. (A) GFP^+ Gag^+ cells in day 2 coculture using regular culture plates between uninfected CEMss-CCR5 and rhTRIM5α/GFP-transduced CEMss-CCR5 cells (far left), GFP^+ Gag^+ cells in coculture between HIV-1 JRCSF-infected CEMss-CCR5 and rhTRIM5α/GFP-transduced CEMss-CCR5 cells (left middle), GFP^+ Gag^+ cells in coculture between HIV-1 JRCSF-infected CEMss-CCR5 and GPI-VHH E4-transduced CEMss-CCR5-rhTRIM5α/GFP cells (middle right), and GFP^+ Gag^+ cells in coculture between HIV-1 JRCSF-infected CEMss-CCR5 and GPI-VHH JM4-transduced CEMss-CCR5-rhTRIM5α/GFP cells (far right). (B) Same coculture as in panel A but using Transwell plates. (C) Same coculture as in panel A but with day 12 coculture samples. (D) GFP^+ Gag^+ cells in coculture between HIV-1 JRCSF-infected CEMss-CCR5 and rhTRIM5α/GFP-transduced CEMss-CCR5 cells in the presence of 40 and 10 μg/ml of sVHH E4 (far left and middle left) and GFP^+ Gag^+ cells in coculture between HIV-1 JRCSF-infected CEMss-CCR5 and rhTRIM5α/GFP-transduced CEMss-CCR5 cells in the presence of 40 and 10 μg/ml of soluble JM4 (middle right and far right). (E) HIV-1 replication measured by Gag p24 in coculture supernatants between HIV-1 JRCSF-infected CEMss-CCR5 and rhTRIM5α/GFP-transduced CEMss-CCR5 cells and between HIV-1 JRCSF-infected CEMss-CCR5 and GPI-VHH E4- or JM4-transduced CEMss-CCR5-rhTRIM5α/GFP cells, along with HIV-1 JRCSF-infected CEMss-CCR5 alone.

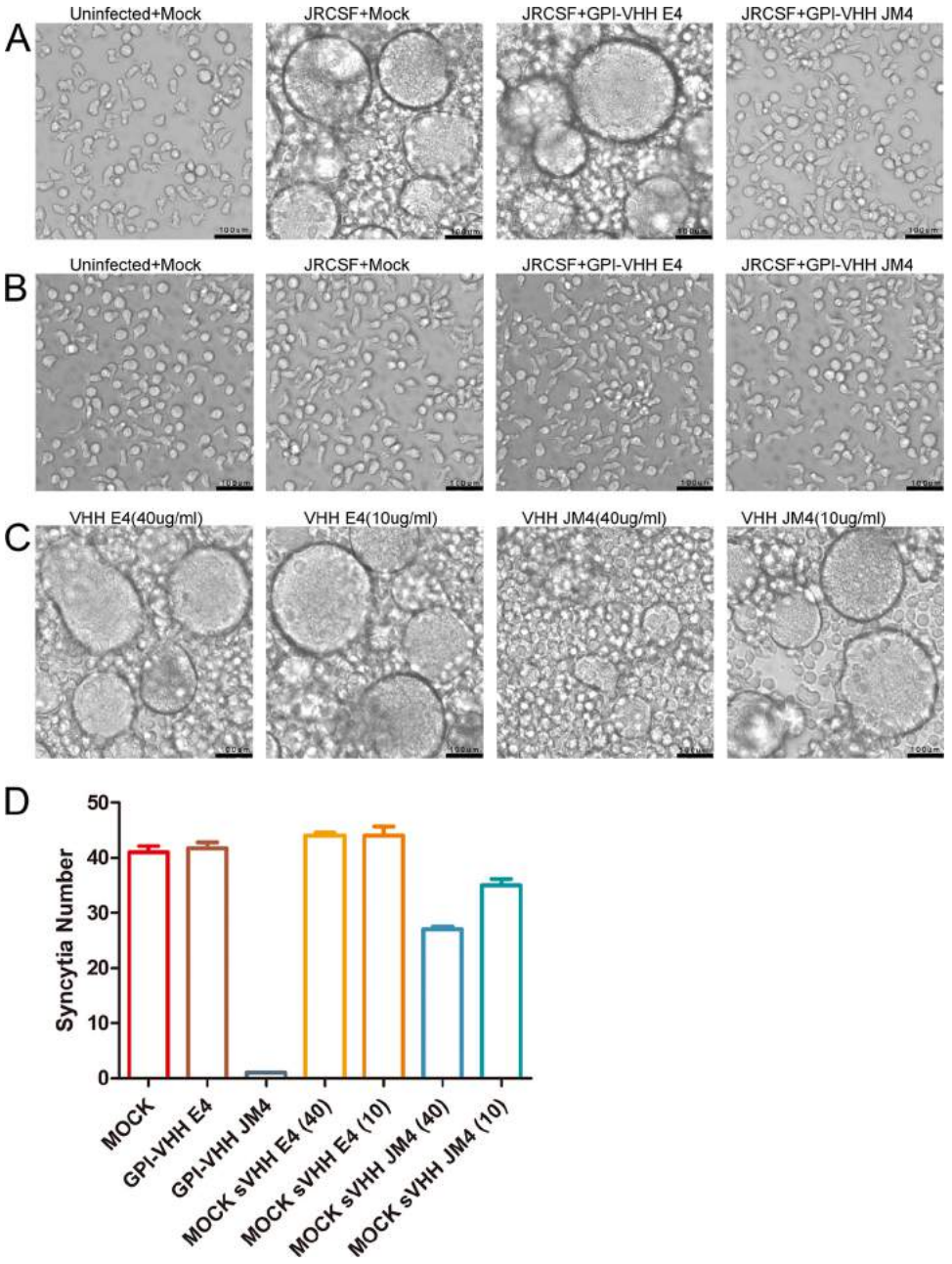

FIG 6 GPI-VHH JM4-transduced CEMss-CCR5-rhTRIMα/GFP are resistant to HIV-1 envelope-mediated cell-cell fusion. (A) Absence of cell-cell fusion in coculture between uninfected CEMss-CCR5 and rhTRIM5α/GFP-transduced CEMss-CCR5 cells (far left), dramatic cell-cell fusion in coculture between HIV-1 JRCSF-infected CEMss-CCR5 and rhTRIM5α/GFP-transduced CEMss-CCR5 cells (middle left), dramatic cell-cell fusion in coculture between HIV-1 JRCSF-infected CEMss-CCR5 and GPI-VHH E4-transduced CEMss-CCR5-rhTRIM5α/GFP cells (middle right), and absence of cell-cell fusion in coculture between HIV-1 JRCSF-infected CEMss-CCR5 and GPI-VHH JM4-transduced CEMss-CCR5-rhTRIM5α/GFP cells (far right). (B) Same fusion assay as in panel A but using Transwell plates. (C) Dramatic cell-cell fusion in coculture between HIV-1 JRCSF-infected CEMss-CCR5 and rhTRIM5α/GFP-transduced CEMss-CCR5 cells in the presence of 40 and 10 μg/ml of sVHH E4 (far left and middle left) and moderate reduction in cell-cell fusion in coculture between HIV-1 JRCSF-infected CEMss-CCR5 and rhTRIM5α/GFP-transduced CEMss-CCR5 cells in the presence of 40 and 10 μg/ml of soluble JM4 (middle right and far right). (D) Mean and standard deviation (SD) of the number of syncytia in coculture between HIV-1 JRCSF-infected CEMss-CCR5 and mock-transduced CEMss-CCR5-rhTRIM5α/GFP cells (red bar), between HIV-1 JRCSF-infected CEMss-CCR5 and GPI-VHH E4-transduced CEMss-CCR5-rhTRIM5α/GFP cells (brown bar); between HIV-1 JRCSF-infected CEMss-CCR5 and GPI-VHH JM4-transduced CEMss-CCR5-rhTRIM5α/GFP cells (gray bar), between HIV-1 JRCSF-infected CEMss-CCR5 and rhTRIM5α/GFP-transduced CEMss-CCR5 cells in the presence of 40 μg/ml of sVHH E4 (yellow bar), between HIV-1 JRCSF-infected CEMss-CCR5 and rhTRIM5α/GFP-transduced CEMss-CCR5 cells in the presence of 10 μg/ml of sVHH E4 (orange bar), between HIV-1 JRCSF-infected CEMss-CCR5 and rhTRIM5α/GFP-transduced CEMss-CCR5 cells in the presence of 40 μg/ml of sVHH JM4 (blue bar), and between HIV-1 JRCSF-infected CEMss-CCR5 and rhTRIM5α/GFP-transduced CEMss-CCR5 cells in the presence of 10 μg/ml of sVHH JM4 (green bar).

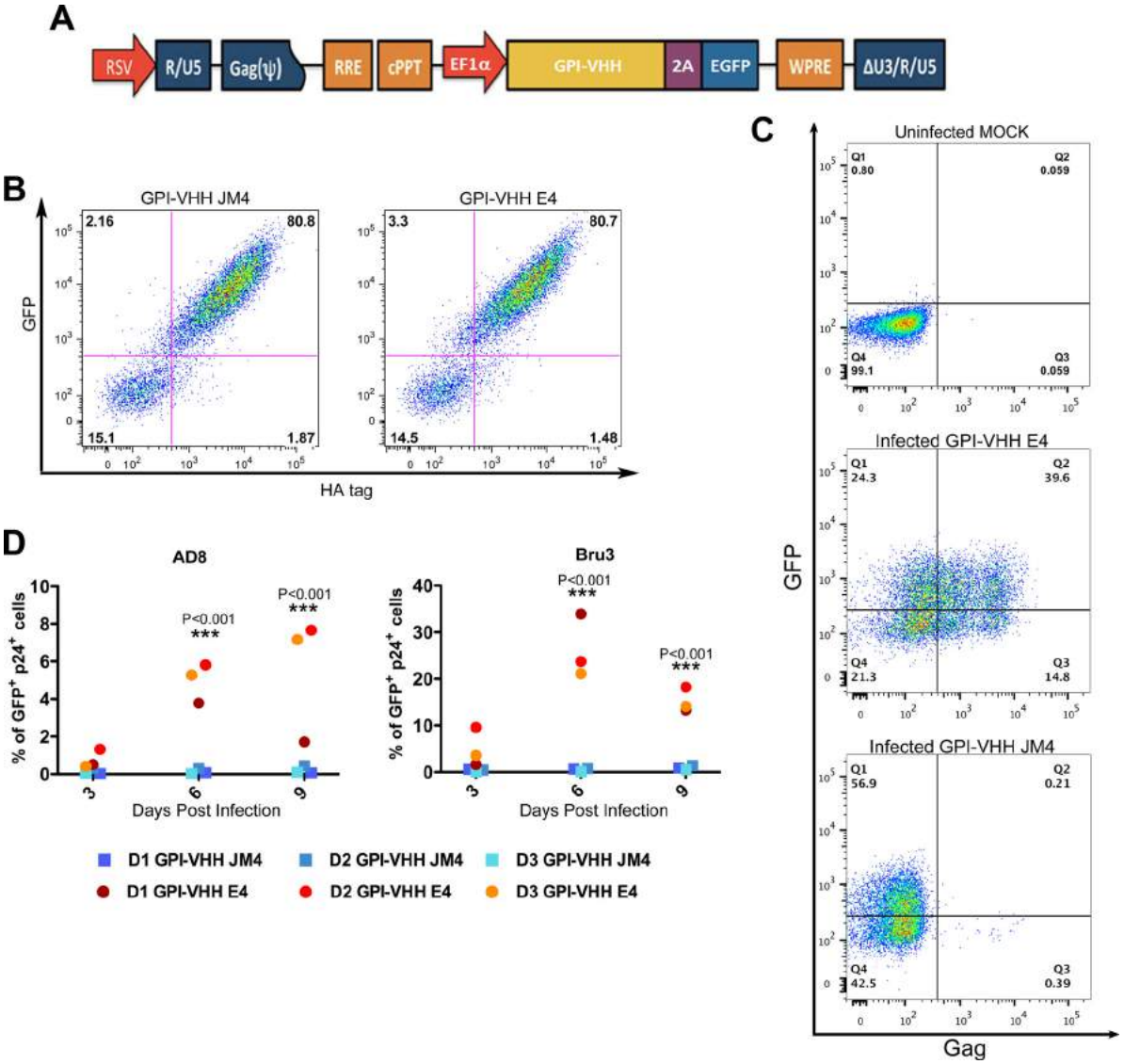

FIG 7 GPI-VHH JM4-transduced human primary CD4 T cells are resistant to cell-free HIV-1 infection. (A) Schematic diagram of lentiviral transfer vector pRRL-GPI-VHH E4 or JM4-2A-GFP. RRE, Rev response element; cPPT, central polypurine tract; EF1α, promoter derived from elongating factor 1α; GFP, green fluorescent protein. (B) Expression of GFP and GPI-VHH JM4 (left) or E4 (right) in human primary CD4 T cells transduced with recombinant lentiviral vectors containing pRRL-GPI-VHH JM4 or E4-2A-GFP, respectively, after a single round of transduction. (C) Representative gating of Gag^+ GFP^+ cells in human primary CD4 T cells transduced with recombinant lentiviral vectors containing GPI-VHH JM4 (bottom) or E4 (middle) infected with HIV-1 Bru-3 at 6 days postculture, along with an uninfected mock-transduced control (top). (D) Summary of percentages of Gag^+ GFP^+ cells at 3, 6, and 9 days postinfection of culture of GPI-VHH E4- or JM4-transduced human CD4 T cells from all three donors infected with HIV-1 AD8 (left) and Bru-3 (right).

cells. Clearly, GPI-VHH JM4-transduced human primary CD4 T cells from the first two donors were almost completely resistant to T cell-T cell transmission of both AD8 and Bru-3 HIV-1. GPI-VHH JM4-transduced human primary CD4 T cells from the third donor were almost completely resistant to T cell-T cell transmission of HIV-1 AD8 but significantly reduced T cell-T cell transmission of HIV-1 Bru-3. Thus, we concluded that GPI-VHH JM4 in transduced human primary CD4 T cells substantially blocks both cell-free and T cell-T cell transmission of HIV-1.

DISCUSSION

To date, llamas are an only animal species in which immunization has elicited broadly neutralizing antibodies against HIV-1 (1, 2). The broadly neutralizing antibodies elicited in llamas are heavy chain-only antibodies, and their VHHs exhibit antigen-specific binding affinity comparable to that of conventional immunoglobulins (1). Due to their high-level expression in yeasts and bacteria as well as extreme thermal and pH stability, VHHs have been developed as microbicides against HIV-1 both in gels and in commensal bacteria (43). In the present study, we developed GPI-anchored VHH JM2 and JM4 from two heavy chain-only antibodies isolated from immunized llamas (2). We demonstrated that by genetically linking the VHHs with a GPI attachment signal, VHHs are targeted to the lipid rafts of the plasma membranes through a GPI anchor (Fig. 1). GPI-VHH JM4, but not GPI-VHH JM2, efficiently blocks cell-free HIV-1 infection in transduced $CD4^+$ cell

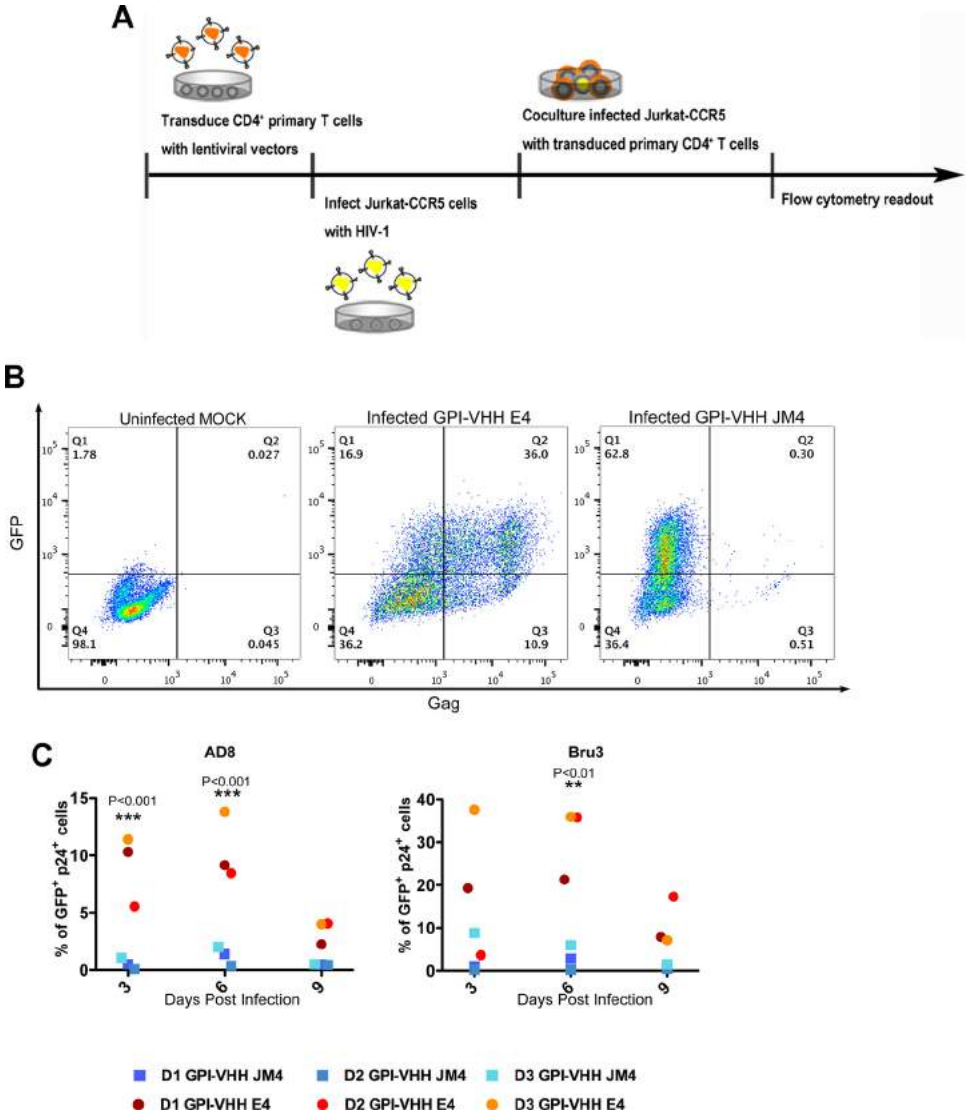

FIG 8 GPI-VHH JM4-transduced human primary CD4 T cells are resistant to cell-cell transmission of HIV-1. (A) Schematic diagram of transducing human CD4 T cells with lentiviral vectors expressing GPI-VHH E4 or JM4, establishing HIV-1 AD8- or Bru-3-infected Jurkat cells; coculture between infected or uninfected Jurkat cells, and GPI-VHH JM4- or E4-transduced human primary CD4 T cells. (B) Representative gating of Gag^+ GFP^+ cells in human primary CD4 T cells transduced with GPI-VHH JM4 (right) or E4 (middle) cocultured with HIV-1 Bru-3-infected Jurkat cells at 6 days postcoculture along with uninfected mock-transduced control cells (left). (C) Summary of percentages of Gag^+ GFP^+ cells at 3, 6, and 9 days postinfection of coculture between GPI-VHH E4- or JM4-transduced human CD4 T cells from all three donors and HIV-1 AD8-infected (left) and Bru-3-infected (right) human T cells.

lines and human primary CD4 T cells (Fig. 2, 3, and 7 and Table 1). HIV-1 viruses neutralized by GPI-VHH JM4 include diverse strains of various subtypes, including tier 2 and 3 strains, transmitted founders, and quasispecies as well as strains resistant to neutralization by sVHH JM4 plus sCD4 (Fig. 2 and Table 1). Thus, GPI-VHH JM4 is truly a much more potent and broader entry inhibitor than sVHH JM4.

Increasing evidence indicates that the cell-cell transmission of retroviruses plays an important role in the establishment of systemic infection as well as in virus spread within lymphoid tissues *in vivo* (9). For example, in a BLT humanized mouse model, Murooka et al. showed that HIV-1-infected T cells in lymph nodes form virological synapses and block the egress of T cells from the lymph nodes into efferent lymph vessels at the onset of limited systemic HIV-1 infection (9). Sewald et al. showed that in secondary lymph tissues, HIV-1 and murine leukemia virus (MLV) are captured by sinus-lining macrophages via CD169. MLV-captured by macrophages can then *trans*-infect B-1 cells. Infected B-1 cells then migrate into the lymph node to spread the infection through virological synapses (44). HIV-1 transmission from infected T cells to uninfected T cells occurs via virological synapses (4). The formation of such structures allows the coordination of viral assembly with viral entry at sites of cell-cell contacts, resulting in a high local concentration and high rate of transmission of HIV-1 (6). As a result, T cell-T cell transmission of HIV-1 is much more efficient for spreading virus and is much less susceptible to neutralizing antibodies and entry inhibitors than cell-free HIV-1 (7, 8, 10–14). In the present study, we demonstrated that GPI-VHH

TABLE 2 Breadth and the potency of GPI-anchored antibody derivatives (scFv, HCDR3, and VHH) and soluble IgG or scFv and sdAb of various human monoclonal antibodies[a]

Epitopes	Antibodies	GPI-scFv	GPI-HCDR3	GPI-VHH	IgG or scFv	sdAb
CD4BS	VRC01	ND	1/17	ND	173/190	ND
	b12	ND	2/24	ND	78/190	ND
	JM2	ND	ND	0/21	ND	5/11
CD4BS/CRBS	JM4	ND	ND	21/21	ND	18/30
CRBS	X5	11/11	ND	ND	11/33	ND
	E51	ND	24/24	ND	5/6	ND
V1/V2	PG9	ND	24/24	ND	128/162	ND
	PG16	ND	24/24	ND	120/162	ND
C helix	TG15	8/12	ND	ND	0/5	ND
MPER	4E10	11/11	ND	ND	177/181	ND

[a] Neutralization breadth is presented as the number of HIV-1 strains neutralized per number of HIV-1 strains tested. Colors represent the neutralization potency. For GPI-anchored antibody derivatives, red stands for an average inhibition of ≥98%, green an average inhibition between 50 and 80%, and gray an average inhibition between 0 and 50%. For soluble IgG, scFv, or VHH, red stands for a median 50% inhibitory concentration (IC_{50}) of <1 μg/ml, yellow an IC_{50} between 1 and 10 μg/ml, green an IC_{50} between >10 and 50 μg/ml, and gray an IC_{50} of >50 μg/ml or no neutralization. ND, not done.

JM4 in transduced CEMss-CCR5 cells exerts a potent block on T cell-T cell transmission of HIV-1 (Fig. 5) and HIV-1 envelope protein-mediated cell-cell fusion (Fig. 6). GPI-VHH JM4-transduced human primary CD4 T cells are resistant to T cell-T cell transmission of HIV-1 (Fig. 8).

The potent neutralization of cell-cell transmission of HIV-1 by GPI-VHH JM4 is likely due to the high local concentration of GPI-VHH JM4 in the lipid rafts of the cell plasma membrane. When viral transmission from infected T cells to uninfected T cells and HIV-1 envelope-mediated cell-cell fusion occur at sites of cell-cell contacts, GPI-VHH JM4 is able to capture its CD4-induced epitope. This may block further conformational change of the HIV-1 envelope protein, thereby preventing HIV-1 envelope-mediated membrane fusion and virus entry.

Table 2 summarizes neutralization breadth and potency of GPI-anchored antibody derivatives (scFv, HCDR3, and VHH) that we have developed in this study or previous studies (26–28) compared to those of soluble whole antibodies, scFvs and VHHs, that serve as sources for GPI-anchored antibody derivatives (2, 45–50). GPI-anchored antibody derivatives that we have tested include CD4BS, coreceptor-binding site (CRBS), V1/V2 loop, C-helix, and MPER antibodies. Interestingly, GPI-VHH JM2, like other anti-CD4BSs (GPI-scFv VRC01, and GPI-HCDR3 b12) that we tested previously, has no or very limited neutralization activity, whereas the soluble whole antibodies VRC01, b12, and JM2 exhibit various potencies and breadths of neutralization activity (2, 45, 46). In contrast, GPI-VHH JM4, like the other anti-CRBSs GPI-scFv X5 and E51, has extremely potent and broad neutralization activity, whereas the soluble whole antibodies, scFv and VHH, of these anti-CRBS antibodies have lower or little neutralization activity or breadth (26, 27, 47, 49). Moreover, anti-V1/V2 loop GPI-HCDR3 PG9 and PG16 have potent and broad neutralization activities similar to those of the soluble whole antibodies PG9 and PG16 (26, 28, 46). Furthermore, anti-C-helix GPI-scFv TG15 exhibited moderate neutralization against 8 out of 12 HIV-1 strains tested, whereas soluble whole antibody TG15, which was originally defined as a nonneutralizing antibody, does not have any neutralization activity (27, 48). Finally, anti-MPER GPI-scFv 4E10 significantly increases neutralization potency compared to that of soluble whole antibody 4E10 (27, 46, 50). Thus, it appears that the broad and the potent neutralization by GPI-anchored antibody derivatives is epitope specific and only partially overlaps those of soluble broadly neutralizing antibodies.

Finally, GPI-VHH JM4, with such remarkable neutralization breadth and potency against both cell-free and T cell-T cell transmission of HIV-1, should have the potential to be developed into an anti-HIV-1 agent either alone or in combination with other anti-HIV-1 gene constructs. For example, GPI-VHH JM4 could be delivered or codelivered with trimeric GPI-HCDR3 PG16 (28) into autologous hematopoietic progenitor cells or $CD4^+$ T cells of HIV-1 patients *ex vivo* using lentiviral vectors. The modified cells could then be transfused into the patients as recently described by DiGiusto et al. (51) or by Tebas et al. (52). However, before being tested in HIV-1-infected individuals, the safety, immunogenicity, potential "toxicity" of GPI-anchored antibody expression on the surface of CD4 cells or its impact on CD4 T cell functions, immune reconstitution, and therapeutic potential of the GPI-VHH JM4-transduced primary $CD4^+$ T cells and/or hematopoietic progenitor cells should first be tested in relevant animal models, such as the simian-human immunodeficiency virus (SHIV) rhesus macaque infection model or HIV-1 humanized mouse infection model.

ACKNOWLEDGMENTS

We thank L. Naldini at the University of Torino Medical School, Turin, Italy, for lentiviral transfer vector, B. H. Hahn at the University of Pennsylvania for DNA plasmids encoding consensus B and C HIV-1 envelope proteins, and Linqi Zhang at Tsinghua University for DNA plasmid encoding CNE3, CNE5, CNE8, CNE11, CNE15, CNE50, and CNE55. Cell

line TZM.bl, molecular clones of HIV-1 Bru-3, AD8, Mj4, and Yu2, transmitted founder viruses WITO, CH040, THRO, REJO, and CH077, pNL4-3.luc.R-E- transfer vector, and DNA plasmids encoding Q168, Q461ENVe2, Yu2, AD8, JRFL, SF162, HxBc2, PVO.4, QH0692.42, 92BR025.9, 93TH966.8, and 92UG975.10 envelope proteins were obtained through the AIDS Research and Reference Reagent Program, Division of AIDS, National Institute of Allergy and Infectious Diseases, National Institutes of Health, Germantown, MD. The relevant reagents were originally developed and contributed by J. Kappes, X. Wu, N. Landau, R. Risser, J. Overbaugh, E. Freed, A. Adachi, M. A. Martin, I. R. Chen, G. W. Shaw, and B. H. Hahn.

This work was supported by research grants from the Chinese National Natural Science Foundation (number 31170871) and the National Science and Technology Major Project (number 2014ZX10001-001) to P.Z.; by research grants from the National Institutes of Health (R56 AI108467 to J.T.K.) and the Baylor-UTHouston CFAR (P30AI036211); by a Chinese National Natural Science Foundation-National Institutes of Health joint grant (number 81361120406-R01 AI106574) to P.Z. and J.T.K.; by a Chinese National Natural Science Foundation-Hong Kong RGC joint grant (number 81161160569-N_HKU709/11) to P.Z. and Z.C.; and by research grants from the French National Agency for AIDS Research to S.B. S.B. obtained a Visiting Professorship from the Chinese Academy of Sciences (number 2012T1S0024 and number 2016VBA062).

FUNDING INFORMATION

This work, including the efforts of Jason T. Kimata, was funded by HHS | National Institutes of Health (NIH) (R56 AI108467, P30AI036211, and R01 AI106574). This work, including the efforts of Paul Zhou, was funded by National Natural Science Foundation of China (NSFC) (31170871, 81361120406, and 81161160569). This work, including the efforts of Serge Benichou, was funded by Chinese Academy of Sciences (CAS) (2012T1S0024 and 2016VBA062). This work, including the efforts of Zhiwei Chen, was funded by Research Grants Council, University Grants Committee (RGC, UGC) (N_HKU709/11). This work, including the efforts of Paul Zhou, was funded by Ministry of Science and Technology of the People's Republic of China (MOST) (2014ZX10001-001).

The funders had no role in study design, data collection and interpretation, or the decision to submit the work for publication.

REFERENCES

1. **McCoy LE, Quigley AF, Strokappe NM, Bulmer-Thomas B, Seaman MS, Mortier D, Rutten L, Chander N, Edwards CJ, Ketteler R, Davis D, Verrips T, Weiss RA.** 2012. Potent and broad neutralization of HIV-1 by a llama antibody elicited by immunization. J Exp Med **209:**1091–1103. http://dx.doi.org/10.1084/jem.20112655.
2. **Matz J, Kessler P, Bouchet J, Combes O, Ramos OH, Barin F, Baty D, Martin L, Benichou S, Chames P.** 2013. Straightforward selection of broadly neutralizing single-domain antibodies targeting the conserved CD4 and coreceptor binding sites of HIV-1 gp120. J Virol **87:**1137–1149. http://dx.doi.org/10.1128/JVI.00461-12.
3. **Acharya P, Luongo TS, Georgiev IS, Matz J, Schmidt SD, Louder MK, Kessler P, Yang Y, McKee K, O'Dell S, Chen L, Baty D, Chames P, Martin L, Mascola JR, Kwong PD.** 2013. Heavy chain-only IgG2b llama antibody effects near-pan HIV-1 neutralization by recognizing a CD4-induced epitope that includes elements of coreceptor- and CD4-binding sites. J Virol **87:**10173–10181. http://dx.doi.org/10.1128/JVI.01332-13.
4. **Schiffner T, Sattentau QJ, Duncan CJ.** 2013. Cell-to-cell spread of HIV-1 and evasion of neutralizing antibodies. Vaccine **31:**5789–5797. http://dx.doi.org/10.1016/j.vaccine.2013.10.020.
5. **Rudnicka D, Feldmann J, Porrot F, Wietgrefe S, Guadagnini S, Prevost MC, Estaquier J, Haase AT, Sol-Foulon N, Schwartz O.** 2009. Simultaneous cell-to-cell transmission of human immunodeficiency virus to multiple targets through polysynapses. J Virol **83:**6234–6246. http://dx.doi.org/10.1128/JVI.00282-09.
6. **Hübner W, McNerney GP, Chen P, Dale BM, Gordon RE, Chuang FYS, Li X-D, Asmuth DM, Huser T, Chen BK.** 2009. Quantitative 3D video microscopy of HIV transfer across T cell virological synapses. Science **323:**1743–1747. http://dx.doi.org/10.1126/science.1167525.
7. **Malbec M, Porrot F, Rua R, Horwitz J, Klein F, Halper-Stromberg A, Scheid JF, Eden C, Mouquet H, Nussenzweig MC, Schwartz O.** 2013. Broadly neutralizing antibodies that inhibit HIV-1 cell to cell transmission. J Exp Med **210:**2813–2821. http://dx.doi.org/10.1084/jem.20131244.
8. **Abela IA, Berlinger L, Schanz M, Reynell L, Gunthard HF, Rusert P, Trkola A.** 2012. Cell-cell transmission enables HIV-1 to evade inhibition by potent CD4bs directed antibodies. PLoS Pathog **8:**e1002634. http://dx.doi.org/10.1371/journal.ppat.1002634.
9. **Murooka TT, Deruaz M, Marangoni F, Vrbanac VD, Seung E, von Andrian UH, Tager AM, Luster AD, Mempel TR.** 2012. HIV-infected T cells are migratory vehicles for viral dissemination. Nature **490:**283–287. http://dx.doi.org/10.1038/nature11398.
10. **Chen P, Hubner W, Spinelli MA, Chen BK.** 2007. Predominant mode of human immunodeficiency virus transfer between T cells is mediated by sustained Env-dependent neutralization-resistant virological synapses. J Virol **81:**12582–12595. http://dx.doi.org/10.1128/JVI.00381-07.
11. **Reh L, Magnus C, Schanz M, Weber J, Uhr T, Rusert P, Trkola A.** 2015. Capacity of broadly neutralizing antibodies to inhibit HIV-1 cell-cell transmission is strain- and epitope-dependent. PLoS Pathog **11:**e1004966. http://dx.doi.org/10.1371/journal.ppat.1004966.
12. **Durham ND, Yewdall AW, Chen P, Lee R, Zony C, Robinson JE, Chen BK.** 2012. Neutralization resistance of virological synapse-mediated HIV-1 infection is regulated by the gp41 cytoplasmic tail. J Virol **86:**7484–7495. http://dx.doi.org/10.1128/JVI.00230-12.
13. **Martin N, Welsch S, Jolly C, Briggs JA, Vaux D, Sattentau QJ.** 2010. Virological synapse-mediated spread of human immunodeficiency virus type 1 between T cells is sensitive to entry inhibition. J Virol **84:**3516–3527. http://dx.doi.org/10.1128/JVI.02651-09.
14. **Massanella M, Puigdomenech I, Cabrera C, Fernandez-Figueras MT, Aucher A, Gaibelet G, Hudrisier D, Garcia E, Bofill M, Clotet B, Blanco J.** 2009. Antigp41 antibodies fail to block early events of virological synapses but inhibit HIV spread between T cells. AIDS **23:**183–188. http://dx.doi.org/10.1097/QAD.0b013e32831ef1a3.
15. **Su B, Xu K, Lederle A, Peressin M, Biedma ME, Laumond G, Schmidt S, Decoville T, Proust A, Lambotin M, Holl V, Moog C.** 2012. Neutralizing antibodies inhibit HIV-1 transfer from primary dendritic cells to autologous CD4 T lymphocytes. Blood **120:**3708–3717. http://dx.doi.org/10.1182/blood-2012-03-418913.
16. **Frankel SS, Steinman RM, Michael NL, Kim SR, Bhardwaj N, Pope M, Louder MK, Ehrenberg PK, Parren PW, Burton DR, Katinger H, VanCott TC, Robb ML, Birx DL, Mascola JR.** 1998. Neutralizing monoclonal antibodies block human immunodeficiency virus type 1 infection of dendritic cells and transmission to T cells. J Virol **72:**9788–9794.
17. **van Montfort T, Nabatov AA, Geijtenbeek TBH, Pollakis G, Paxton WA.** 2007. Efficient capture of antibody neutralized HIV-1 by cells expressing DC-SIGN and transfer to CD4+ T lymphocytes. J Immunol **178:**3177–3185. http://dx.doi.org/10.4049/jimmunol.178.5.3177.
18. **van Montfort T, Thomas AAM, Pollakis G, Paxton WA.** 2008. Dendritic cells preferentially transfer CXCR4-using human immunodeficiency virus type 1 variants to CD4+ T lymphocytes in trans. J Virol **82:**7886–7896. http://dx.doi.org/10.1128/JVI.00245-08.
19. **Sagar M, Akiyama H, Etemad B, Ramirez N, Freitas I, Gummuluru S.** 2012. Transmembrane domain membrane proximal external region but not surface unit-directed broadly neutralizing HIV-1 antibodies can restrict dendritic cell-mediated HIV-1 trans-infection. J Infect Dis **205:**1248–1257. http://dx.doi.org/10.1093/infdis/jis183.
20. **Liao Z, Cimakasky LM, Hampton R, Nguyen DH, Hildreth JE.** 2001. Lipid rafts and HIV pathogenesis: host membrane cholesterol is required for infection by HIV type 1. AIDS Res Hum Retroviruses **17:**1009–1019. http://dx.doi.org/10.1089/088922201300343690.
21. **Chazal N, Gerlier D.** 2003. Virus entry, assembly, budding, and membrane rafts. Microbiol Mol Biol Rev **67:**226–237. http://dx.doi.org/10.1128/MMBR.67.2.226-237.2003.
22. **Popik W, Alce TM, Au WC.** 2002. Human immunodeficiency virus type 1 uses lipid raft-colocalized CD4 and chemokine receptors for productive entry into CD4(+) T cells. J Virol **76:**4709–4722. http://dx.doi.org/10.1128/JVI.76.10.4709-4722.2002.
23. **Platt EJ, Wehrly K, Kuhmann SE, Chesebro B, Kabat D.** 1998. Effects of CCR5 and CD4 cell surface concentrations on infections by macrophagetropic isolates of human immunodeficiency virus type 1. J Virol **72:**2855–2864.
24. **Carter GC, Bernstone L, Sangani D, Bee JW, Harder T, James W.** 2009.

HIV entry in macrophages is dependent on intact lipid rafts. Virology **386:**192–202. http://dx.doi.org/10.1016/j.virol.2008.12.031.

25. **Medof ME, Kinoshita T, Nussenzweig V.** 1984. Inhibition of complement activation on the surface of cells after incorporation of decay-accelerating factor (DAF) into their membranes. J Exp Med **160:**1558–1578. http://dx.doi.org/10.1084/jem.160.5.1558.
26. **Liu L, Wen M, Wang W, Wang S, Yang L, Liu Y, Qian M, Zhang L, Shao Y, Kimata JT, Zhou P.** 2011. Potent and broad anti-HIV-1 activity exhibited by a glycosyl-phosphatidylinositol-anchored peptide derived from the CDR H3 of broadly neutralizing antibody PG16. J Virol **85:**8467–8476. http://dx.doi.org/10.1128/JVI.00520-11.
27. **Wen M, Arora R, Wang H, Liu L, Kimata JT, Zhou P.** 2010. GPI-anchored single chain Fv–an effective way to capture transiently-exposed neutralization epitopes on HIV-1 envelope spike. Retrovirology **7:**79. http://dx.doi.org/10.1186/1742-4690-7-79.
28. **Liu L, Wang W, Yang L, Ren H, Kimata JT, Zhou P.** 2013. Trimeric glycosylphosphatidylinositol-anchored HCDR3 of broadly neutralizing antibody PG16 is a potent HIV-1 entry inhibitor. J Virol **87:**1899–1905. http://dx.doi.org/10.1128/JVI.01038-12.
29. **Zhou P, Cao H, Smart M, David C.** 1993. Molecular basis of genetic polymorphism in major histocompatibility complex-linked proteasome gene (Lmp-2). Proc Natl Acad Sci U S A **90:**2681–2684. http://dx.doi.org/10.1073/pnas.90.7.2681.
30. **Follenzi A, Ailles LE, Bakovic S, Geuna M, Naldini L.** 2000. Gene transfer by lentiviral vectors is limited by nuclear translocation and rescued by HIV-1 pol sequences. Nat Genet **25:**217–222. http://dx.doi.org/10.1038/76095.
31. **Wang W, Ye C, Liu J, Zhang D, Kimata JT, Zhou P.** 2014. CCR5 gene disruption via lentiviral vectors expressing Cas9 and single guided RNA renders cells resistant to HIV-1 infection. PLoS One **9:**e115987. http://dx.doi.org/10.1371/journal.pone.0115987.
32. **Thippeshappa R, Polacino P, Yu Kimata MT, Siwak EB, Anderson D, Wang W, Sherwood L, Arora R, Wen M, Zhou P, Hu SL, Kimata JT.** 2011. Vif substitution enables persistent infection of pig-tailed macaques by human immunodeficiency virus type 1. J Virol **85:**3767–3779. http://dx.doi.org/10.1128/JVI.02438-10.
33. **Sirven A, Ravet E, Charneau P, Zennou V, Coulombel L, Guetard D, Pflumio F, Dubart-Kupperschmitt A.** 2001. Enhanced transgene expression in cord blood CD34(+)-derived hematopoietic cells, including developing T cells and NOD/SCID mouse repopulating cells, following transduction with modified trip lentiviral vectors. Mol Ther **3:**438–448. http://dx.doi.org/10.1006/mthe.2001.0282.
34. **Wei X, Decker JM, Liu H, Zhang Z, Arani RB, Kilby JM, Saag MS, Wu X, Shaw GM, Kappes JC.** 2002. Emergence of resistant human immunodeficiency virus type 1 in patients receiving fusion inhibitor (T-20) monotherapy. Antimicrob Agents Chemother **46:**1896–1905. http://dx.doi.org/10.1128/AAC.46.6.1896-1905.2002.
35. **Takeuchi Y, McClure MO, Pizzato M.** 2008. Identification of gammaretroviruses constitutively released from cell lines used for human immunodeficiency virus research. J Virol **82:**12585–12588. http://dx.doi.org/10.1128/JVI.01726-08.
36. **Derdeyn CA, Decker JM, Sfakianos JN, Wu X, O'Brien WA, Ratner L, Kappes JC, Shaw GM, Hunter E.** 2000. Sensitivity of human immunodeficiency virus type 1 to the fusion inhibitor T-20 is modulated by coreceptor specificity defined by the V3 loop of gp120. J Virol **74:**8358–8367. http://dx.doi.org/10.1128/JVI.74.18.8358-8367.2000.
37. **Platt EJ, Bilska M, Kozak SL, Kabat D, Montefiori DC.** 2009. Evidence that ecotropic murine leukemia virus contamination in TZM-bl cells does not affect the outcome of neutralizing antibody assays with human immunodeficiency virus type 1. J Virol **83:**8289–8292. http://dx.doi.org/10.1128/JVI.00709-09.
38. **Tsai C, Caillet C, Hu H, Zhou F, Ding H, Zhang G, Zhou B, Wang S, Lu S, Buchy P, Deubel V, Vogel FR, Zhou P.** 2009. Measurement of neutralizing antibody responses against H5N1 clades in immunized mice and ferrets using pseudotypes expressing influenza hemagglutinin and neuraminidase. Vaccine **27:**6777–6790. http://dx.doi.org/10.1016/j.vaccine.2009.08.056.
39. **Parrish NF, Gao F, Li H, Giorgi EE, Barbian HJ, Parrish EH, Zajic L, Iyer SS, Decker JM, Kumar A, Hora B, Berg A, Cai F, Hopper J, Denny TN, Ding H, Ochsenbauer C, Kappes JC, Galimidi RP, West AP, Jr, Bjorkman PJ, Wilen CB, Doms RW, O'Brien M, Bhardwaj N, Borrow P, Haynes BF, Muldoon M, Theiler JP, Korber B, Shaw GM, Hahn BH.** 2013. Phenotypic properties of transmitted founder HIV-1. Proc Natl Acad Sci U S A **110:**6626–6633. http://dx.doi.org/10.1073/pnas.1304288110.
40. **Kimata JT, Kuller L, Anderson DB, Dailey P, Overbaugh J.** 1999. Emerging cytopathic and antigenic simian immunodeficiency virus variants influence AIDS progression. Nat Med **5:**535–541. http://dx.doi.org/10.1038/8414.
41. **Stremlau M, Owens CM, Perron MJ, Kiessling M, Autissier P, Sodroski J.** 2004. The cytoplasmic body component TRIM5alpha restricts HIV-1 infection in Old World monkeys. Nature **427:**848–853. http://dx.doi.org/10.1038/nature02343.
42. **Richardson MW, Carroll RG, Stremlau M, Korokhov N, Humeau LM, Silvestri G, Sodroski J, Riley JL.** 2008. Mode of transmission affects the sensitivity of human immunodeficiency virus type 1 to restriction by rhesus TRIM5alpha. J Virol **82:**11117–11128. http://dx.doi.org/10.1128/JVI.01046-08.
43. **Gorlani A, Brouwers J, McConville C, van der Bijl P, Malcolm K, Augustijns P, Quigley AF, Weiss R, De Haard H, Verrips T.** 2012. Llama antibody fragments have good potential for application as HIV type 1 topical microbicides. AIDS Res Hum Retroviruses **28:**198–205. http://dx.doi.org/10.1089/aid.2011.0133.
44. **Sewald X, Ladinsky MS, Uchil PD, Beloor J, Pi R, Herrmann C, Motamedi N, Murooka TT, Brehm MA, Greiner DL, Shultz LD, Mempel TR, Bjorkman PJ, Kumar P, Mothes W.** 2015. Retroviruses use CD169-mediated trans-infection of permissive lymphocytes to establish infection. Science **350:**563–567. http://dx.doi.org/10.1126/science.aab2749.
45. **Wu X, Yang ZY, Li Y, Hogerkorp CM, Schief WR, Seaman MS, Zhou T, Schmidt SD, Wu L, Xu L, Longo NS, McKee K, O'Dell S, Louder MK, Wycuff DL, Feng Y, Nason M, Doria-Rose N, Connors M, Kwong PD, Roederer M, Wyatt RT, Nabel GJ, Mascola JR.** 2010. Rational design of envelope identifies broadly neutralizing human monoclonal antibodies to HIV-1. Science **329:**856–861. http://dx.doi.org/10.1126/science.1187659.
46. **Walker LM, Phogat SK, Chan-Hui PY, Wagner D, Phung P, Goss JL, Wrin T, Simek MD, Fling S, Mitcham JL, Lehrman JK, Priddy FH, Olsen OA, Frey SM, Hammond PW, Protocol GPI, Kaminsky S, Zamb T, Moyle M, Koff WC, Poignard P, Burton DR.** 2009. Broad and potent neutralizing antibodies from an African donor reveal a new HIV-1 vaccine target. Science **326:**285–289. http://dx.doi.org/10.1126/science.1178746.
47. **Dorfman T, Moore MJ, Guth AC, Choe H, Farzan M.** 2006. A tyrosine-sulfated peptide derived from the heavy-chain CDR3 region of an HIV-1-neutralizing antibody binds gp120 and inhibits HIV-1 infection. J Biol Chem **281:**28529–28535. http://dx.doi.org/10.1074/jbc.M602732200.
48. **Takeda S, Dorfman NA, Robert-Guroff M, Notkins AL, Rando RF.** 1995. Two-phase approach for the expression of high-affinity human anti-human immunodeficiency virus immunoglobulin Fab domains in Escherichia coli. Hybridoma **14:**9–18. http://dx.doi.org/10.1089/hyb.1995.14.9.
49. **Zhang MY, Shu Y, Rudolph D, Prabakaran P, Labrijn AF, Zwick MB, Lal RB, Dimitrov DS.** 2004. Improved breadth and potency of an HIV-1-neutralizing human single-chain antibody by random mutagenesis and sequential antigen panning. J Mol Biol **335:**209–219. http://dx.doi.org/10.1016/j.jmb.2003.09.055.
50. **Huang J, Ofek G, Laub L, Louder MK, Doria-Rose NA, Longo NS, Imamichi H, Bailer RT, Chakrabarti B, Sharma SK, Alam SM, Wang T, Yang Y, Zhang B, Migueles SA, Wyatt R, Haynes BF, Kwong PD, Mascola JR, Connors M.** 2012. Broad and potent neutralization of HIV-1 by a gp41-specific human antibody. Nature **491:**406–412. http://dx.doi.org/10.1038/nature11544.
51. **DiGiusto DL, Krishnan A, Li L, Li H, Li S, Rao A, Mi S, Yam P, Stinson S, Kalos M, Alvarnas J, Lacey SF, Yee JK, Li M, Couture L, Hsu D, Forman SJ, Rossi JJ, Zaia JA.** 2010. RNA-based gene therapy for HIV with lentiviral vector-modified CD34(+) cells in patients undergoing transplantation for AIDS-related lymphoma. Sci Transl Med **2:**36ra43.
52. **Tebas P, Stein D, Tang WW, Frank I, Wang SQ, Lee G, Spratt SK, Surosky RT, Giedlin MA, Nichol G, Holmes MC, Gregory PD, Ando DG, Kalos M, Collman RG, Binder-Scholl G, Plesa G, Hwang WT, Levine BL, June CH.** 2014. Gene editing of CCR5 in autologous CD4 T cells of persons infected with HIV. N Engl J Med **370:**901–910. http://dx.doi.org/10.1056/NEJMoa1300662.